



**THESE DE DOCTORAT DE L'ETABLISSEMENT  
UNIVERSITE BOURGOGNE FRANCHE-COMTE PREPAREE A  
L'INSTITUT DE CHIMIE MOLÉCULAIRE DE L'UNIVERSITÉ DE BOURGOGNE**

Ecole doctorale n°553  
École Doctorale Carnot-Pasteur

Doctorat de Chimie

Par

**M. Jian Yang**

**Synthesis of porous materials based on cobalt corroles for  
carbon monoxide detection**

Soutenu à Dijon, le 11 octobre 2022

Composition du Jury :

France	M. Marcel Bouvet	Professeur des Universités Université de Bourgogne	Président
France	Mme Véronique Bulach	Professeure des Universités Université de Strasbourg	Rapporteur
France	M. Zakaria Halime	Chargé de Recherche CNRS Université Paris-Saclay	Rapporteur
France	Mme Alexandra Fateeva	Maître de conférences Université Claude Bernard Lyon 1	Examinatrice
France	M. Claude Gros	Professeur des Universités Université de Bourgogne	Directeur de thèse
France	M. Nicolas Desbois	Maître de conférences Université de Bourgogne	Co-directeur de thèse
France	Mme Laurie André	Chargée de Recherche CNRS Université de Bourgogne	Membre invité



# Acknowledgments

This thesis work was carried out at the *Institut de Chimie Moléculaire de l'Université de Bourgogne* (ICMUB, UMR 6302), team *Polyamines, Porphyrines, Développements et Applications* (P2DA).

First of all, I would like to sincerely thanks Prof. Véronique Bulach, Dr. Zakaria Halime, Prof. Marcel Bouvet and Dr. Alexandra Fateeva to have kindly accepted to evaluate and to be part of my PhD defense.

I would like to thank my thesis director, Pr. Claude Gros, as well as my co-director of thesis, Dr. Nicolas Desbois, for instruction and assistance during my PhD thesis and also my life in France and who gave me the material means necessary to carry out this project. And great thanks to Pr. Claude Gros and Dr. Nicolas Desbois who supervise and encourage me practically and emotionally.

I would also like to warmly thank Dr. Stéphane Brandès and Dr. Laurie André, aspecially for the long period to characterize the COF materials and analysis of experimental results. I am thinking in particular of Dr. Laurie André for many conversation that apply COF materials to sensor application and development of other new and interesting structure COFs.

I would also like to warmly thank Dr. Valentin Quesneau and Dr. Léo Bucher who gave many helps for corrole chemistry as well as many manipulations I never learned before. They are also my best friend and we have many communications during the time they were in Lab. I would also like to warmly thank our technician Sandrine Pacquelet for her very kind assistance about corrole work. I would also like to thank every member in team P2DA, I am very proud of studying and working here for the whole PhD.

I also would like to thank my parents and wife, they supported me to have further study in France.



# Table of content

<b>Abbreviation</b> .....	<b>7</b>
<b>Chapter 1: General introduction</b> .....	<b>11</b>
<b>1.1 Carbon monoxide: a societal issue</b> .....	<b>11</b>
<b>1.2 Carbon monoxide sensors</b> .....	<b>14</b>
1.2.1 Metal Oxide Semiconductor (MOS).....	14
1.2.2 Electrochemical sensors .....	15
1.2.4 SAW sensors .....	17
<b>1.3 Corrole and cobalt complex for CO adsorption</b> .....	<b>20</b>
1.3.1 Synthesis of Corrole.....	20
1.3.2 Metalation of corrole .....	23
1.3.3 Cobalt corrole .....	24
<b>1.4 Porous materials</b> .....	<b>27</b>
1.4.1 Covalent Organic Frameworks (COF).....	28
1.4.1.1 Design principles of COFs.....	32
1.4.1.2 Bond formation for COFs synthesis .....	35
1) Boron-based COFs.....	39
2) Imine-based COFs .....	43
3) Azine-based COFs.....	44
4) Ketoenamine-based COFs .....	46
5) Imide-based COFs .....	47
1.4.1.3 Application of COFs.....	48
1) Gas adsorption.....	48
2) Heterogeneous catalysis .....	49
3) Photoelectric application .....	50
4) Energy storage .....	51
1.4.1.4 COFs based on corroles.....	52
1.4.1.5 Conclusion and Perspectives .....	53
1.4.2 Porous organic polymers .....	53
1.4.3 Metal-Organic Frameworks .....	56
<b>1.5 Objectives of the thesis</b> .....	<b>59</b>
<b>References</b> .....	<b>61</b>
<b>Chapter 2: Synthesis of precursors for porous materials</b> .....	<b>91</b>
<b>2.1 Precursors for COFs</b> .....	<b>91</b>
2.1.1 Synthesis of corroles.....	91
2.1.1.1 Synthesis of aldehyde-functionalized corroles (refer to bis-CHO-corrole) .....	92
1) Synthesis of acetal dipyrromethane .....	93
2) Synthesis of bis-CHO-corrole .....	95
2.1.1.2 Synthesis of amino-functionalized corrole (refer to bis-NH <sub>2</sub> -corrole) .....	96
1) Synthesis of nitrodipyrromethane .....	96
2) Synthesis of bis-amino-corrole .....	97
2.1.2 Synthesis of platforms .....	98
2.1.2.1 Synthesis of amino-platform .....	98
2.1.2.2 Synthesis of aldehyde- platforms .....	99
<b>2.2 Precursors for MOFs</b> .....	<b>101</b>
2.2.1 Corroles precursors for MOFs .....	101
2.2.2 Precursors for MOFs functionalization .....	105

2.2.2.1 Porphyrin precursor for MOF construction .....	105
2.2.2.2 Corroles precursors for further MOF functionalization .....	106
<b>2.3 Precursors for POPs .....</b>	<b>109</b>
2.3.1 Synthesis of the corrole precursor .....	109
2.3.2 Synthesis of the adamantane precursor.....	111
<b>2.4 Conclusion.....</b>	<b>111</b>
<b>References .....</b>	<b>113</b>
<b>Chapter 3: Synthesis of COFs based on cobalt corroles .....</b>	<b>119</b>
<b>3.1 Design of COFs for this project.....</b>	<b>119</b>
3.1.1 Synthetic methods for the preparation of COFs.....	121
<b>3.2 Synthesis of COFs from aldehyde-corrole.....</b>	<b>121</b>
<b>3.3 Synthesis of COFs from amino- corrole .....</b>	<b>125</b>
3.3.1 Synthesis of 3D-COF-Cor based on amino corrole.....	125
3.3.2 Synthesis of 2D-COF-Cor based on amino corrole.....	127
3.3.3 Characterization of 2D/3D-COF-Cor and its cobalt complexes.....	130
3.3.3.1 <sup>1</sup> H NMR Spectroscopy .....	130
3.3.3.2 Infrared Spectroscopy.....	131
3.3.3.3 Powder X-ray diffraction.....	135
3.3.3.4 Scanning electron microscopy .....	138
3.3.3.5 Energy dispersive X-ray spectroscopy.....	140
3.3.3.6 Thermogravimetric analysis.....	143
3.3.3.7 Gas sorption analysis .....	144
3.3.3.8 CO adsorption analysis .....	147
3.3.4 Synthesis of COFs based on other platforms.....	154
3.3.4.1 Synthesis of COFs based on 2,4,6-trihydroxy-1,3,5-benzenetricarbaldehyde.....	154
3.3.4.2 Synthesis of COFs based on truxene .....	155
3.3.4.3 Synthesis of COFs based on adamantane .....	157
<b>3.4 Conclusion.....</b>	<b>158</b>
<b>References .....</b>	<b>159</b>
<b>General conclusion and perspectives.....</b>	<b>165</b>
<b>Experimental Section .....</b>	<b>169</b>
<b>Reference.....</b>	<b>233</b>
<b>Communications .....</b>	<b>237</b>

# Abbreviation

AcOH	Acetic acid
APTES	(3-Aminopropyl)triethoxysilane
BET	Brunauer-Emmett-Teller
CD <sub>3</sub> OD	Deuterated methanol
CDCl <sub>3</sub>	Deuterated Chloroform
COF	Covalent Organic Framework
COHb	Carboxyhemoglobin
CHCl <sub>3</sub>	Chloroform
DCC	Dynamic Covalent Chemistry
DCM	Dichloromethane
DDQ	2,3-dichloro-5,6-dicyano-1,4-benzoquinone
DMF	Dimethylformamide
DMSO	Dimethyl sulfoxide
DMSO- <i>d</i> <sub>6</sub>	Deuterated Dimethyl sulfoxide
EA	Element Analysis
EDS	Energy Dispersive Spectroscopy
EtOH	Ethanol
eq	equivalent
FTIR	Fourier Transform Infrared spectroscopy
HCl	Hydrochloric Acid
HRMS	High Resolution Mass Spectrometry
ICP	Inductively Coupled Plasma
IDT	input impedance transducer
MALDI-TOF	Matrix Assisted Laser Desorption Ionization - Time of Flight
MeOH	Methanol
MOF	Metal-Organic Framework
MOS	Metal Oxide Semiconductor
<i>n</i> -BuOH	1-butanol
NMR	Nuclear Magnetic Resonance
<i>o</i> -DCB	1,2-Dichlorobenzene
O <sub>2</sub> Hb	oxyhemoglobin
POP	Porous Organic Polymer

ppb	part per billion
ppm	part per million
Pd/C	Palladium/carbon
Py	Pyridine
RED	Rotation Electron Diffraction
RT	room temperature
PXRD	Powder X-ray Diffraction
SAW	Surface Acoustic Wave
SEM	Scanning Electron Microscopy
SXRD	Single Crystal X-ray Diffraction
TEA	Triethylamine
TFA	Trifluoroacetic acid
TGA	Thermogravimetric analysis
THF	Tetrahydrofuran
TLC	Thin Layer Chromatography
°C	Degree

# Chapter 1

## General introduction



# Chapter 1: General introduction

## 1.1 Carbon monoxide: a societal issue

Carbon monoxide (CO) is a colorless, odorless, tasteless, toxic gas resulting from the incomplete combustion of fuels (Fig. 1).<sup>1</sup> As reference, the Earth's lower atmosphere contains approximately 50-100 ppb of CO.<sup>2</sup> Indoor ambient levels typically range from 0.5 to 5 ppm, and may reach higher values up to 5-15 ppm near gas ovens or near other point of sources, and even higher levels (up to 30 ppm) if the combustion is inefficient.<sup>3,4</sup> The safety guidelines given by the World Health Organization (WHO) for exposure to CO gas are <10 ppm for 8 h and 90 ppm for periods not exceeding 15 min.<sup>2</sup> Carbon monoxide has a great negative impact on the human body (and mammals, pets). When you inhale carbon monoxide at excessive levels, symptoms that commonly occur include headache, dizziness, weakness, vomiting, chest pain, and confusion.<sup>5</sup> Long time exposures, or exposure to a large excess of CO can result in loss of consciousness, arrhythmias, seizures, or even death. The relationship between the concentration(ppm) of CO in air and symptoms are shown in Table 1.

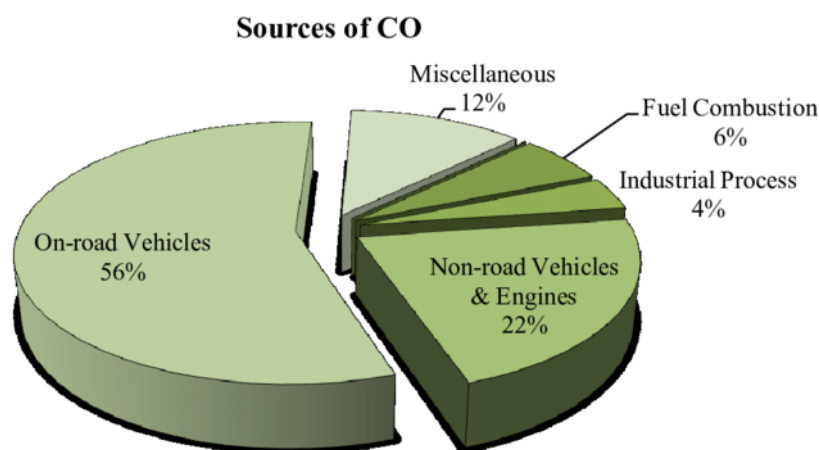
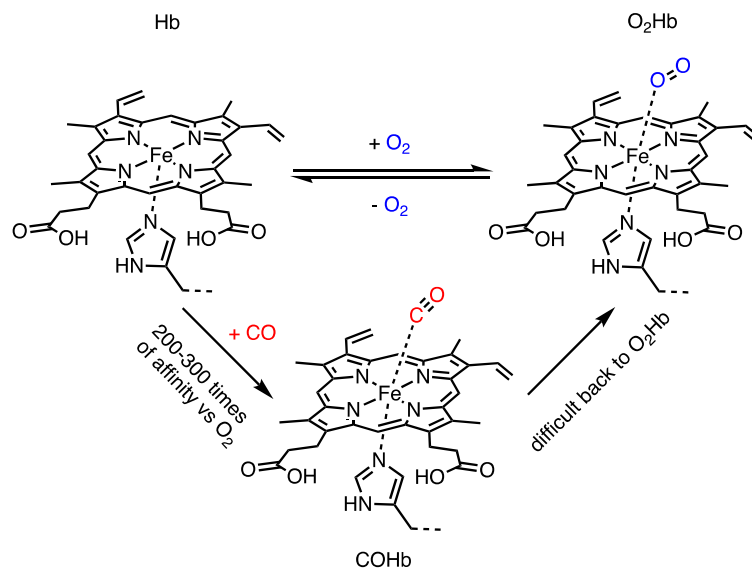


Figure 1. Source of carbon monoxide (CO) emission.<sup>6</sup>

Table 1. Relationship between the concentration(ppm) of CO in air and symptoms.<sup>7</sup>

CO concentration	COHb level	Signs and symptoms
35 ppm	<10%	Headache and dizziness within 6 to 8 h of constant exposure
100 ppm	>10%	Slight headache in 2 to 3 h
200 ppm	20%	Slight headache within 2 to 3 h; loss of judgment
400 ppm	25%	Frontal headache within 1 to 2 h
800 ppm	30%	Dizziness, nausea, convulsions within 45 min; insensible within 2 h
1600 ppm	40%	Headache, tachycardia, dizziness, nausea within 20 min; death in less than 2 h
3200 ppm	50%	Headache, dizziness, nausea in 5 to 10 min; death within 30 min
6400 ppm	60%	Headache and dizziness in 1 to 2 min; convulsions, respiratory arrest, and death in less than 20 min
12800 ppm	>70%	Death in less than 3 min

The mechanism of carbon monoxide poisoning was revealed by the work of Claude Bernard and Felix Hoppe-Seyler who independently published the mechanism in 1857.<sup>8</sup> Hemoglobin is a tetramer with 4 oxygen binding sites. However, the affinity for carbon monoxide to the site of the tetramer receptor site is 200-300 times greater than for the oxygen molecule.<sup>9</sup> When inhaled, CO competes with O<sub>2</sub> for the heme-binding sites of hemoglobin with much higher affinity. Hemes are most commonly considered as the most important component of hemoglobin. It is a coordination complex which is composed of an iron metal center coordinated to a porphyrin, and with one or two axial ligands. Partial occupation of carbon monoxide binding sites in hemoglobin result in the release of O<sub>2</sub> from the remaining heme groups, causing the dissociation curve of O<sub>2</sub> and the formation of carboxyhemoglobin (COHb) instead of oxyhemoglobin(O<sub>2</sub>Hb).<sup>10</sup> The binding reactions of dioxygen and carbon monoxide are shown in Scheme 1.



Scheme 1. Binding reactions of hemoglobin for dioxygen and carbon monoxide.

Thus, the transport and delivery of  $\text{O}_2$  to the tissues interfere with the binding of CO to hemoglobin, leading to tissue hypoxia and asphyxiation (Fig. 2).<sup>11</sup> Inhalation of CO, at high concentrations, in rodent models causes apoptosis of tissues, particularly in brain regions, associated with CO poisoning and tissue injury.<sup>12</sup> Therefore, it is very important to detect the concentration of CO rapidly and accurately. Nowadays, carbon monoxide detectors have been developed to help reduce the incidence and prevalence of unintentional exposures to CO.<sup>13</sup>

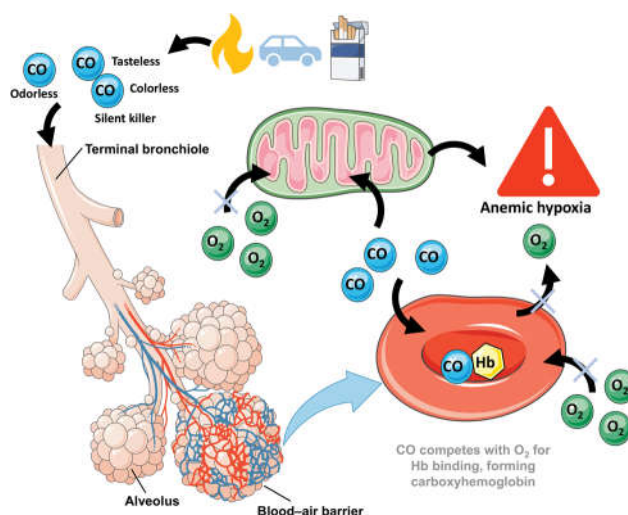


Figure 2. Toxic mechanisms of carbon monoxide (CO) with hemoglobin in human body.<sup>14</sup>

## 1.2 Carbon monoxide sensors

For the detection of carbon monoxide, various technologies and sensors have been developed such as metal oxide semiconductor,<sup>15</sup> electrochemical sensors,<sup>16</sup> In this part, the different sensors designed for carbon monoxide detection will be detailed.

### 1.2.1 Metal Oxide Semiconductor (MOS)

Since Brattain and Bardeen discovered that gas absorption changes the conductivity of semiconductor material in 1953,<sup>17</sup> a great amount of research was carried out to produce commercial semiconductor sensors. In 1962, MOS sensors were first proposed by Seiyama *et al.*<sup>18</sup> and patented by Taguchi.<sup>19</sup> Subsequently, this type of sensors has been investigated worldwide for gas sensing and other applications. Researchers have contributed a lot to the understanding of basic information about general sensing method and mechanisms. In recent years, the priority was oriented towards the development of gas sensor devices optimized for their sensitivity and selectivity towards a specific target gas molecule. MOS gas sensors stand out amongst others because of their simplicity and low cost.<sup>20</sup> MOS are used to detect various gases such as carbon monoxide (CO),<sup>21</sup> carbon dioxide (CO<sub>2</sub>),<sup>22</sup> hydrogen (H<sub>2</sub>),<sup>23</sup> ammonia (NH<sub>3</sub>),<sup>24</sup> hydrogen sulfide (H<sub>2</sub>S),<sup>25</sup> and nitrogen dioxide (NO<sub>2</sub>),<sup>26</sup> because of their distinctive characteristics, especially by making use of the gases reactivity with different metals.

Concerning our main objective, the introduction of carbon monoxide sensors based on MOS will be presented hereafter. Up to this day, there have been many metal oxide semiconductors developed to detect carbon monoxide. They are capable of CO detection with appropriate selectivity and high sensitivity.<sup>27</sup> Generally, MOS such as SnO<sub>2</sub>,<sup>28</sup> ZnO,<sup>29</sup> In<sub>2</sub>O<sub>3</sub>,<sup>30</sup> TiO<sub>2</sub>,<sup>31</sup> CeO<sub>2</sub>,<sup>32</sup> Fe<sub>2</sub>O<sub>3</sub>,<sup>33</sup> WO<sub>3</sub>,<sup>34</sup> CdO,<sup>35</sup> CuO,<sup>36</sup> composite oxides,<sup>37</sup> and yttria-stabilized zirconia (YSZ)<sup>38</sup> are preferred for CO gas sensing. Among these sensor materials, as things currently stand the best MOS material for the detection of carbon monoxide is SnO<sub>2</sub>. The mechanism for detecting CO on SnO<sub>2</sub> is shown in Fig. 3. The carbon monoxide which is considered as reducing gas react with the chemisorbed oxygen atoms on the SnO<sub>2</sub> surface forming into CO<sub>2</sub>, and injecting immobilized electrons back into SnO<sub>2</sub>. As a result, it reduces the depletion region and releases the band bending, which leads to a decrease in resistance.

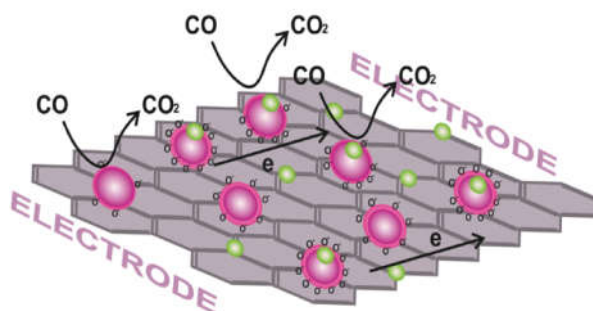


Figure 3. CO-sensing mechanism illustration of the SnO<sub>2</sub> composite.<sup>13</sup>

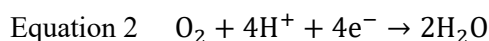
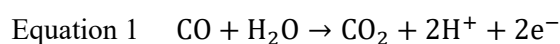
Such sensors have been demonstrated to have higher responses to carbon monoxide at lower concentrations than with infrared gas analyzer,<sup>21</sup> and as a result they show great promise for cheaper air quality measurement. But the use of high operating temperatures limits the application of such sensors for domestic use, e.g. in houses, which implies that it is still desirable to minimize the operating temperatures. Furthermore, the selectivity towards CO is not very high, interferences such as acetone, ethanol, hydrogen, and ammonia still show a response to SnO<sub>2</sub> sensors, even if the response is low. Also, the stability of the sensors should be considered since they will be used over a long period of time, over which they must keep providing an accurate measurement. This entails a maintenance of the detection abilities, which the sensitivity, selectivity, response time, and recovery time. The ideal gas sensor should have high sensitivity, selectivity, stability, low operating temperature, low response and recovery time, low power consumption, and low manufacturing cost. The performance of gas sensors is highly dependent on the sensor material used to manufacture the sensor. As of now, the disadvantages limiting the development of MOS is mainly the high operating temperature and poor selectivity for similar type of gases (reducing or oxidizing).

### 1.2.2 Electrochemical sensors

Electrochemical gas sensors, a well-known technology that was developed from the 1950s, was first applied to oxygen monitoring. A glucose biosensor was one of the earliest applications of this technology and it was used to monitor the depletion of oxygen in glucose. Over the following decades, advanced developments were made for the technology, allowing the expansion of the application to a wide variety of target gases for the sensors. Generally,

electrochemical gas sensors refer to electrochemical analyzers or detectors, which are designed to monitor or measure the concentration of gases outdoors. An electrochemical gas sensor is generally composed of a working (also named sensing), counter, and reference electrodes, all of those are included in a small device fitted with a membrane allowing the gas to go through. Electrochemical sensors are based on an electrical signal which is produced by the reaction between gases and an electrode. Most of the electrochemical gas sensors are amperometric sensors. They monitor the target gas by generating a current which possesses a linearly proportional relationship to the gas concentration. The principle of electrochemical sensors is to measure the potential difference between working and reference electrode.

The mechanism for electrochemical sensors monitoring carbon monoxide is based on the measurement of current generated between working and reference electrode, where the oxidation and reduction reaction take place at the same time (see Fig. 4).<sup>39, 40</sup> For the sensing process, carbon monoxide are oxidized (Eq. 1) after going through the membrane on the surface of the working electrode giving electrons.<sup>41</sup> On the working electrode, with the oxidation of carbon monoxide, oxygen (O<sub>2</sub>) is reduced to water on the counter electrode according to the Eq. 2:



Reactions on the working and counter electrodes cause the different potential between the two electrodes. Electrons move under the certain voltage to generate current. In certain range, after calibration of current and gas concentration, the dependence of concentrations is linear.<sup>42</sup> During the development of electrochemical gas sensors, there is a limitation: the measurement process can be influenced by interfering substances in the analyzed gas.<sup>43</sup> In the case of positive interference with reducing gases like NH<sub>3</sub>, SO<sub>2</sub> and H<sub>2</sub>, the readings are higher than the real values, while negative interference happens, the results are underestimated due to oxidizing gases like NO<sub>2</sub>.<sup>44</sup> It has to be noted also that some electrochemical CO sensors are very sensitive to the presence of hydrogen in the atmosphere.

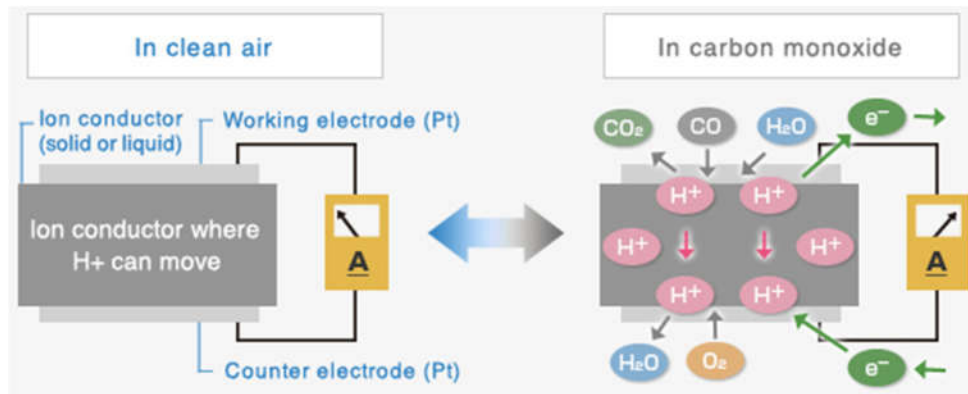


Figure 4. Mechanism of electrochemical gas sensors for the detection of CO.<sup>45</sup>

Except interference gases, accuracy of electrochemical sensors decreases with time going on. There are several factors that contribute to the performance deterioration of sensors such as excessive temperature and humidity. Firstly, temperature is a common factor to reduce the lifespan of sensors. Long time exposure to a temperature higher than 50°C or lower than 0°C, the baseline reading and sensors response can be affected. Secondly, humidity possesses the greatest negative effect on the lifespan of sensors. The appropriate condition for operating electrochemical gas sensors is at a relative humidity around 60 %. A much higher or lower ambient humidity than 60 % change the concentration of the electrolyte inside the sensor, affecting the response time and accuracy. The usual methods to solve those problem is to recalibrate it before using it again, or to replace it, and both are quite costly.

#### 1.2.4 SAW sensors

Surface Acoustic Wave (SAW) sensors consist of a class of microelectromechanical systems that is based on the modulation of surface acoustic waves to detect a physical phenomenon. The structure of a basic SAW sensor is illustrated in Fig. 5. The basic surface acoustic wave device is composed by a piezoelectric substrate with an input impedance transducer (IDT) and an output IDT on the two sides of the substrate part. During the measurement, the surface acoustic waves propagate across the substrate area which is also named delay line. On delay line, the mechanical waves move slower than associated electromagnetic form, making a measurable delay. The operating mechanism of a SAW sensor is converting an electrical input signal into a mechanical wave (direct piezoelectric effect), which can be easily affected by a physical phenomenon. The interfered mechanical wave will be received and translated into an electrical output (indirect piezoelectric effect). Because of the high sensitivity of the mechanical wave, any changes about phase, time delay, amplitude or

frequency between input and output signal can be interpreted to determine the concentration of target gas.

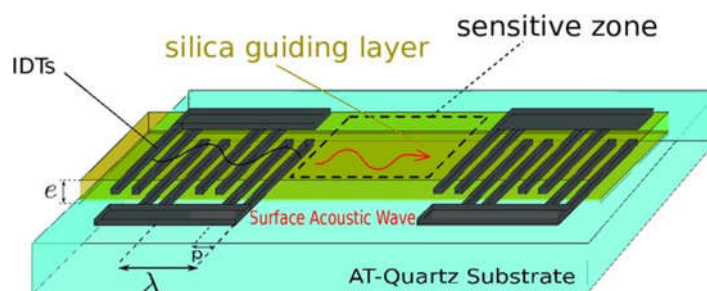


Figure 5. Structure of the SAW device used as a signal conditioner.<sup>46</sup>

Wohltjen and Dessy introduced SAW technology for chemical sensing applications in 1979.<sup>47</sup> Since 1979, a great attention has been paid to SAW sensors and continuous researches have been carried on it. SAW sensors possess several advantages which make them favored by researchers, such as their small size, low cost, planar structure, manufacturing technology, ultra-high sensitivity, excellent response time, possibility to be used in wired and wireless mode.<sup>48-53</sup> In addition, with an appropriate selection of the sensing layer, piezoelectric substrates and IDTs, these sensors show good properties such as ultra-high selectivity, reversibility, stability, linearity and fast response time.<sup>54, 55</sup> Furthermore, SAW sensors usually serve as carriers for sensing probe instead of direct probes for targets.<sup>52, 56</sup> A ZnO nanorods based wireless SAW sensor has also been reported for the detection of CO,<sup>57</sup> but the concentration dependency was not established.

Our team, in collaboration with the Femto-ST institute in Besançon (UBFC) proposed a new type of carbon monoxide sensor relying on a sensitive layer composed of cobalt corrole that shows great affinity toward CO.<sup>58</sup> We have firstly reported experimental data to attest the efficiency of cobalt corrole to trap CO molecules with high selectivity, and secondly, we have established the capability of a Surface Acoustic Wave (SAW) device to probe the mechanical properties of the corroles layer to reveal the adsorption of the target gas (Fig. 6). A cobalt corrole complex, named [5,10,15-tris(2,6-dichlorophenyl)corrole]cobalt(III), was chosen because of its ability to ensure the selective trapping of CO and their ease of synthesis: as already described in previous work.<sup>59-61</sup>

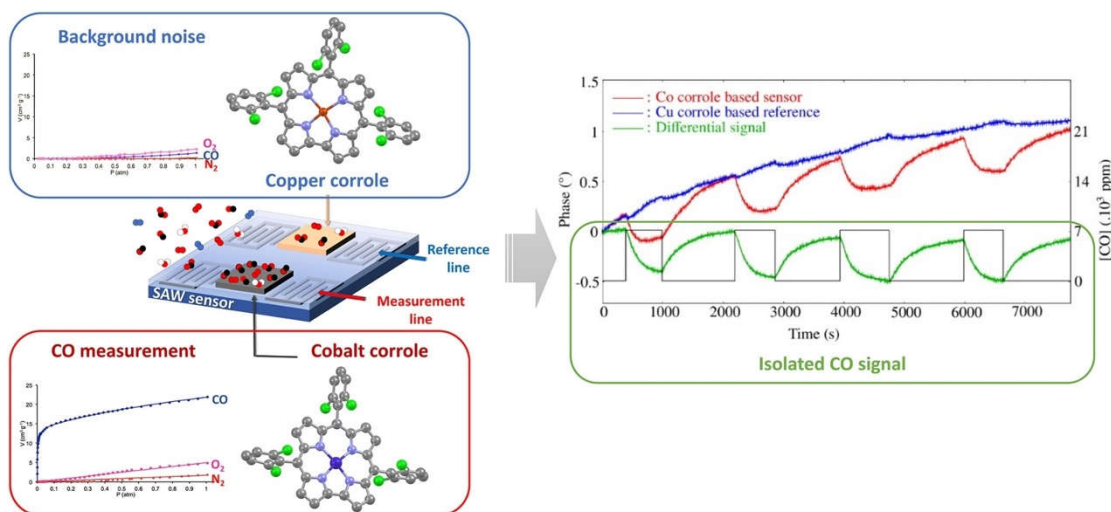


Figure 6. SAW sensor based on cobalt corrole for carbon monoxide detection.<sup>58</sup>

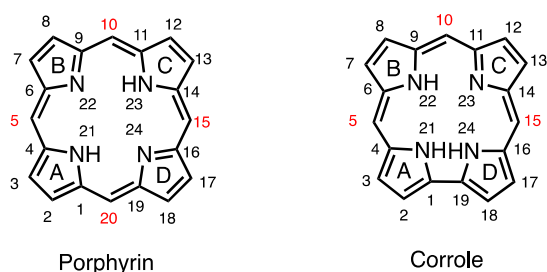
We have proposed a differential configuration for the sensor to overcome the sensitivity to outer parameters and interfering gases. For this purpose, a reference device based on copper corrole (that does not react with CO) was implemented as part of the sensor. Measurements of carbon monoxide concentration in the 100 - 7,000 ppm range in the presence of major interferents such as O<sub>2</sub>, CO<sub>2</sub> and H<sub>2</sub>O (humidity) were achieved. The impact of these interferents on the sensor's sensitivity was estimated. The results demonstrate a very high selectivity for the studied CO/N<sub>2</sub> or CO/O<sub>2</sub> binary mixtures at 298 K, whatever the applied pressure. Indeed, the selectivity varies from 35,000 to 21,000 for CO/N<sub>2</sub> and from 12,000 to 6,000 for CO/O<sub>2</sub> between 0 and 1 atm, respectively. These outcomes point out that the use of cobalt corrole can be considered as an appealing way to build sensible SAW device for CO sensing.

## 1.3 Corrole and cobalt complex for CO adsorption

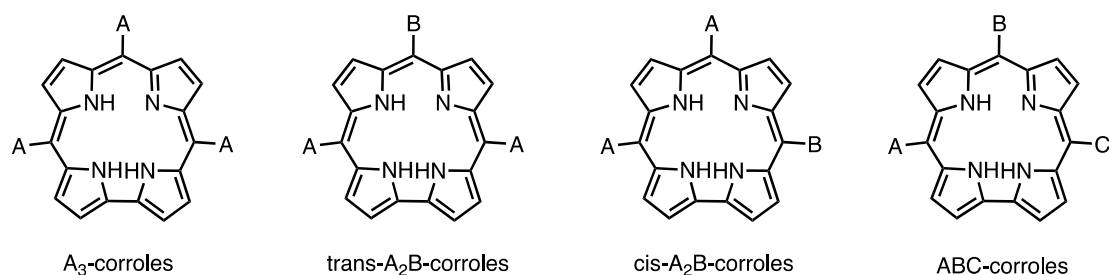
### 1.3.1 Synthesis of Corrole

Porphyrins and corroles are among the most prominent examples in the sub-class of tetrapyrrolic macrocycles.<sup>62</sup> They have a very similar chemical structure, which principally only differs from each other by one carbon atom and the fact that corroles show a higher degree of saturation. This is the main reason why corroles are usually described as analogues of porphyrins lacking one *meso*-carbon and having one direct pyrrole-pyrrole linkage instead.

The numbering and nomenclature of the corroles are derivated from porphyrins and by analogy we designate the  $\alpha$ - and  $\beta$ -pyrrolic positions for the different sites of the four pyrrole rings, and *meso*-positions for atoms 5, 10 and 15 (Scheme 2). Consequently, corroles that are substituted at the *meso*-positions are described by the term of *meso*-substituted corroles. In order to facilitate assignment, the missing *meso*-carbon at position 20 is just omitted, so that the inner nitrogen atoms have equal numbers in the porphyrin and corrole systems. The description of corroles bearing different *meso*-substituents is also reported like porphyrins. They are named by  $A_3$ , *trans*- $A_2B$ , *cis*- $A_2B$  and  $ABC$  corroles (Scheme 3), according to the fact that the corresponding two different substituents are arranged on opposite position or side-by-side. Likewise, during the development of corrole, the same terminology is used. The *trans*-derivatives are more easily accessible by the modern synthetic routes, so this type of corroles are more common. Nevertheless, rational syntheses for the *cis*-products exist, but are of minor practical importance and less interesting to researchers because they are more difficult and time consuming to prepare.



Scheme 2. Structure and nomenclature of porphyrin and corrole.<sup>63</sup>



Scheme 3. Structure of A<sub>3</sub>-, trans-A<sub>2</sub>B-, cis-A<sub>2</sub>B- and ABC-corroles.<sup>64</sup>

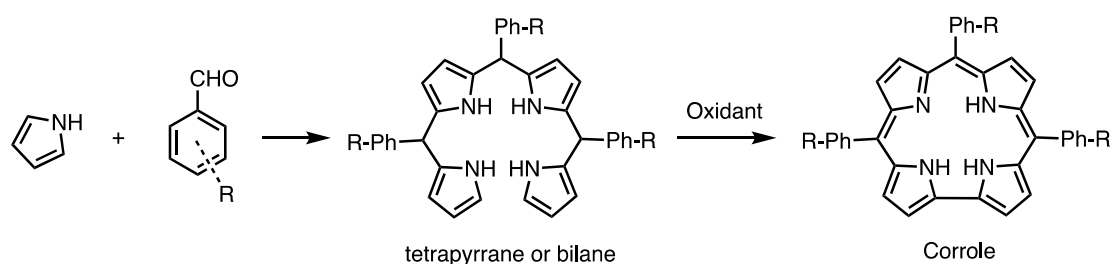
Corroles, possessing three pyrrole-like and one imine-like nitrogen donors, are stronger acids than porphyrins. In addition, because of the four nitrogen atoms working as electron-pair donors, tetrapyrrole ligands in general are interesting partners for metal coordination; there are tri-anions for corroles and di-anions for porphyrins. Then, corroles can stabilize metal ions in a higher oxidation state, having a unique reactivity for low valence metallocorroles.<sup>65</sup>

Although known since 1964,<sup>66</sup> a facile ‘one-pot’ synthesis of corroles was reported separately by two groups.<sup>67, 68</sup> After 1999, there was a dramatic increase in the literature about the number of reported corroles. For example, the methodology for obtaining corrole A<sub>3</sub> is described below (Scheme 4 where A is the substituent at the 5, 10 and 15-positions, see also Schemes 2 and 3) through a two-step synthesis. The first step involved is the reaction between pyrrole and benzaldehyde. According to a nucleophilic substitution reaction. This step is catalyzed by an acid (usually TFA or HCl). The reaction leads to a mixture of polymers which have various lengths. The second step involves an oxidation reaction related to the ring closure of the polymers (pyrrole-pyrrole coupling). The desired polymer chain for the synthesis of corrole is composed of the condensation of four pyrrole and three aldehyde subunits (called a bilane or tetrapyrane).<sup>69</sup> There may be many methodologies to synthesize corrole in one-pot in the first step, but the second step is almost the same and was detailed by the introduction of an oxidant such as 2,3-dichloro-5,6-dicyano-1,4-benzoquinone (DDQ) or tetrachloro-1,4-benzoquinone (*p*-chloranil) in an organic solvent such as dichloromethane or chloroform. Due to the production of numerous polymers, the yields for target corrole are usually quite low (5–15 %).<sup>67, 68, 70, 71</sup>

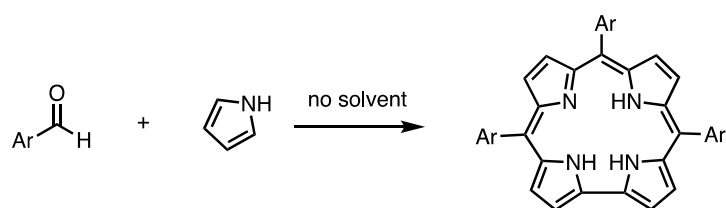
One of the most efficient methodology was reported by Koszarna and Gryko to synthesize *meso*-substituted corroles with a water / methanol mixture and catalyzed by HCl.<sup>69</sup> The method takes advantage of a difference of solubility between the starting materials and the bilane

product. During the reaction, the bilane tends to precipitate because of low solubility in the water / methanol mixture. So, the reaction was effectively stopped at the bilane stage. Then the first step, which aims to obtain the bilane, reduces the formation of porphyrin and other side-products. For next step, it's very convenient to isolate the bilane and oxidize it into a corrole macrocycle. According to reported yields, the use of *p*-chloranil rather than DDQ is better to increase the yields of the corroles' synthesis (between 13 % and 56 %).

Gross and co-workers<sup>68</sup> have also developed a solvent-free method with a solid support (florisil, alumina or silica) to synthesize A<sub>3</sub> corroles (Scheme 5).<sup>71</sup> The reaction successfully yielded the desired corroles which contain electron-withdrawing substituents (like fluorine and other halogens) increasing the electrophilic properties of the aldehyde, making  $\alpha$ -position of the pyrrole more reactive. Yields are generally between 8 % and 11 %.



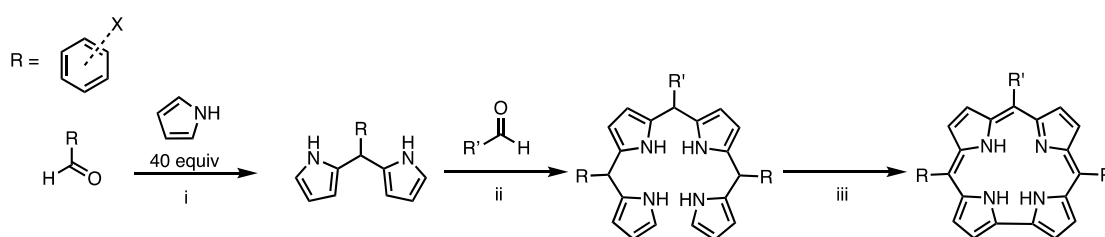
Scheme 4. Synthetic route to corroles from aldehydes and pyrrole.<sup>72</sup>



Scheme 5. Solvent-free synthesis to A<sub>3</sub> corrole.<sup>71</sup>

Koszarna and Gryko have proposed an easier method to obtain corrole in high yields. Unlike the one-pot synthesis method, their approach starts from the synthesis of a dipyrromethane. Dipyrromethanes are synthesized from pyrrole and aldehyde derivatives catalyzed by a small amount of acid, and the most often used acid is trifluoroacetic acid (TFA). During the development of corrole chemistry, dipyrromethanes have been considered to be an important intermediate in the synthesis of corroles.<sup>69, 73, 74</sup>

The first step synthesis of dipyrromethanes requires a large excess of pyrrole (typically 40 equivalents of pyrrole for one aldehyde). With a short reaction time (around 15 minutes) and room temperature, the formation of pyrrole polymerization or oligomers were successfully minimized with a wide range of catalyst, resulting in a high yield of dipyrromethane (usually better than 50 %). The large excess of pyrrole is employed to reduce the continued reaction leading to linear and cyclic oligomers or pyrrole-polymers.<sup>75</sup> When applied to corrole synthesis, two dipyrromethane units will condensate with an aldehyde derivative under acidic conditions to yield bilane and the followed oxidation of bilane produces a corrole A<sub>3</sub> (R = R') or *trans* A<sub>2</sub>B (R ≠ R') (Scheme 6).<sup>69, 73, 76</sup>



Scheme 6. Synthetic route to corroles from dipyrromethane. (i) cat. TFA, 15 min; (ii) CH<sub>3</sub>OH:H<sub>2</sub>O = 1:1, cat. HCl (iii) *p*-chloranil (1 eq).<sup>72</sup>

### 1.3.2 Metalation of corrole

Over the first two decades of the new century, various corrole derivatives have been applied to many fields, and simple synthetic methodologies to prepare metalated corroles have been developed.<sup>77-80</sup> Among the derivatives of corrole, corrole metal complexes take up an important position. The pioneering utilization of metallocorroles in several disciplines, ranging from medicine to chemical sensors, is a result of both synthetic availability and understanding of their characteristics and physical properties. Nowadays, the list of metals coordinated to a corrole ring is extensive, showing an interesting versatility for a wide application of metallocorroles.<sup>81</sup> The dramatic increase of the metal coordination possibilities makes it possible to compete with the more famous porphyrin and phthalocyanine rings. However, because of the unusual and unique characteristics of this contracted ligand, the production of novel metallocorroles remains a subject of rising interest for researchers. Considering the researches on corrole coordination chemistry, it is possible to give the list of all possible metallocorroles according to the periodic table (Table 2). In the recent years, some more

positions of the “periodic table” of metallocorroles have been filled, welcoming new components, such as Silicon,<sup>82, 83</sup> Technetium,<sup>84</sup> Tantalum,<sup>85</sup> Cerium and Lutetium.<sup>86</sup>

The development of metal corrole complex chemistry is very close to that of metalloporphyrins. For early time of the coordination chemistry, much of the work on metallocorroles were focused on some transition metals like Mn, Fe, Co, and Cu due to their stable coordination and biological applications.<sup>77, 87-93</sup> Novel synthetic strategies, for example for Platinum<sup>94</sup> and Manganese,<sup>95</sup> have been finely tuned, and a significant number of functionalized corrole complexes have been reported, to satisfy the requirements needed to fit different application fields, ranging from catalysis through antitumor therapeutics to optical sensors.<sup>65, 90, 96-98</sup> Our group has done a lot of research on cobalt corrole complexes and their applications<sup>58, 61, 99-101</sup> and this will help us to our research project because it is precisely the cobalt complexes that coordinate the carbon monoxide.

Table 2. Periodic table of metallocorroles. The shaded elements indicate specific corroles that have so far been electrochemically examined.<sup>102</sup>

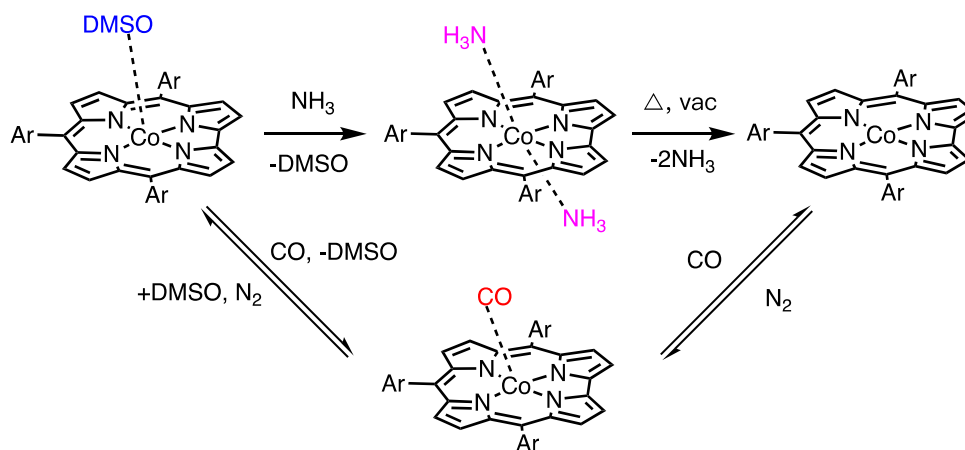
1																		18							
H	2																								He
Li	Be											B	C	N	O	F	Ne								
Na	Mg	3	4	5	6	7	8	9	10	11	12	Al	Si	P	S	Cl	Ar								
K	Ca	Sc	Ti	V	Cr	Mn	Fe	Co	Ni	Cu	Zn	Ga	Ge	As	Se	Br	Kr								
Rb	Sr	Y	Zr	Nb	Mo	Tc	Ru	Rh	Pd	Ag	Cd	In	Sn	Sb	Te	I	Xe								
Cs	Ba	La	Hf	Ta	W	Re	Os	Ir	Pt	Au	Hg	Tl	Pb	Bi	Po	At	Rn								
Fr	Ra																								
Lanthanides		Ce	Pr	Nd	Pm	Sm	Eu	Gd	Tb	Dy	Ho	Er	Tm	Yb	Lu										
Actinides		Th	Pa	U	Np	Pu	Am	Cm	Bk	Cf	Es	Fm	Md	No	Lr										

### 1.3.3 Cobalt corrole

Cobalt complexes of corrole and porphyrin macrocycles were both studied and compared, and it was demonstrated that porphyrins tend to stabilize the (+II) oxidation state of cobalt, while corrole generally stabilize the cobalt metal center at the (+III) oxidation state.<sup>103, 104</sup> It was revealed that in both theoretical and experimental studies, the cobalt-corrole complex is a tetra-coordination system which was characterized as an intermediate-spin Co(III) (S=1) center

coordinated with a corrole 3- ligand in the square planar molecule.<sup>105, 106</sup> In general, there are 4 unpaired electrons for  $\text{Co}^{3+}$ , after the coordination to the tri-anionic corrole, there is unpaired spin density transferred from the paramagnetic Co(III) ion to the  $\pi$  orbitals of the corrole ligand. The electronic configuration of four coordination system (Co(III)) was proposed as  $(d_{xy})^2(d_z^2)^2(d_{xy}, d_{yz})^2$  which is similar to earlier found for isoelectronic  $S = 1$  Fe (II) porphyrins.<sup>105</sup> The system leads to the unoccupied orbitals binding to various axial ligands, such as dimethyl sulfoxide (DMSO), pyridine (Py), triphenylphosphine ( $\text{PPh}_3$ ), cyano ( $\text{CN}^-$ ), and amine ( $\text{NH}_3$ ).<sup>105, 107-110</sup> The coordination property of Co(III) makes it distinguished from porphyrins. For instance, Co(III) corroles are capable of binding carbon monoxide,<sup>60</sup> while Fe(II) porphyrins have shown little response to CO.<sup>111</sup> It was reported that the different ligands and coordination methods cause different oxidation state of cobalt center in corrole. One part of complexes show hexacoordination and the cobalt was kept at Co(III) state.<sup>61</sup> But on the other hand, some cobalt complexes show pentacoordination and the cobalt is kept at the Co(II) oxidation state which is noninnocent.<sup>106, 112, 113</sup> Considering the present PhD project, cobalt porphyrin derivatives are not applicable to CO sensing purposes. Thus, cobalt corroles become one of the most popular corrole complexes among the corrole metal complex chemistry.

Synthetic methods for preparing corrole complexes are often similar to their porphyrin analogs, by the reactions between the free-base ligand in solution and a simple metal halide or acetate salt, with or without heating. The complexes can be easily isolated by column chromatography. Generally, the cobalt corrole was obtained by heating the free-base corrole with cobalt salt ( $\text{Co}(\text{OAc})_2 \cdot n\text{H}_2\text{O}$ ). Among metal and corrole systems, axial ligands also play an important role which is associated with the electron configuration, stability, and application of the complexes by electronic effects. During the study of ligands on the cobalt center in corrole, triphenylphosphine and pyridine have been reported to be the most popular ligands.<sup>106, 112, 114, 115</sup> Furthermore, it is very surprising that the intermediates, five-coordinate Co-corrole with pyridine as ligand,  $\text{Co}[\text{Cor}](\text{py})$ , remains poorly characterized except from Co corrole triphenylphosphine complexes which are stable and can be fully characterized.<sup>106, 116, 117</sup>



Scheme 7. The coordination of CO, DMSO and NH<sub>3</sub> to cobalt corrole and the reactions between each complexes.<sup>61</sup>

For cobalt corroles, ligands such as dimethyl sulfoxide (DMSO), pyridine and gas molecules like CO and NH<sub>3</sub> can strongly coordinate to the cobalt center, resulting in variations in electron density at the metal ion and oxidation state of metal and ligands (Scheme 7).<sup>106</sup> Furthermore, the moieties (electron-withdrawing or donating groups) anchored to the periphery of the corrole will also influence the magnitude and degree of axial coordination.<sup>69</sup> Our lab has reported the synthesis and spectroscopic and e-chem characterizations of various cobalt corroles in great detail including the coordination of cobalt corroles with a single DMSO or two NH<sub>3</sub> axial ligands in stable forms.<sup>61</sup> Examined by DFT computational study, five coordination with one DMSO ligand and six coordination with two NH<sub>3</sub> ligands were proposed.<sup>61</sup> It is difficult to remove the DMSO ligand, and getting the complex into a tetra-coordination requires heating under vacuum. However, it should be noted that ammonia can easily replace the DMSO ligand by forming a hexa-coordination with two NH<sub>3</sub> on the cobalt center. Furthermore, the NH<sub>3</sub> ligands can be easily removed under vacuum at 80°C and the tetra-coordinated form of cobalt corroles (the active species) allows the detection of CO with high sensitivity and selectivity.<sup>118</sup> Thus, tetra-coordinated cobalt corrole can be more easily obtained by the route shown in Scheme 7, and are of great interest for the application of Surface Acoustic Wave (SAW) sensors to detect trace amounts of carbon monoxide at sub-ppm level in the atmosphere.<sup>119</sup> Very recently, our team in collaboration with Femto-ST institute have described a Surface Acoustic Wave (SAW) device, functionalized with cobalt corrole for the selective detection of CO against N<sub>2</sub>, O<sub>2</sub>, CO<sub>2</sub> and humidity (which are all known to be major interferents for SAW sensors applied to CO sensing).<sup>58</sup> At a very low relative pressure, we note a very high affinity for CO, which is called chemisorption. (blue line in Fig. 7). At higher pressure the isotherms

adsorption of CO showed a chemical-physical adsorption profile. The gas selectivity analysis showed the high selectivity for CO against N<sub>2</sub> and O<sub>2</sub> and a wide detection range of 100 - 7000 ppm. This SAW sensor based on cobalt corrole displays potential to detect CO. However, when applied to a SAW sensor surface, the powder of cobalt corrole can be easily removed because of the weak interaction between the corrole and the sensor surface. So, the application of cobalt corrole to sensors still remains to be improved. Enlightened by the 2D and 3D structure of porous materials, we expect to develop a material composed of cobalt corrole to overcome this weakness of cobalt corrole during the CO detection. In the present work, we were interested in the incorporation of corrole inside such porous structures in order to overcome also the pi-stacking of corroles, and benefit from the large pores of the materials to enhance the gas adsorption of the final sensing materials and sensors.

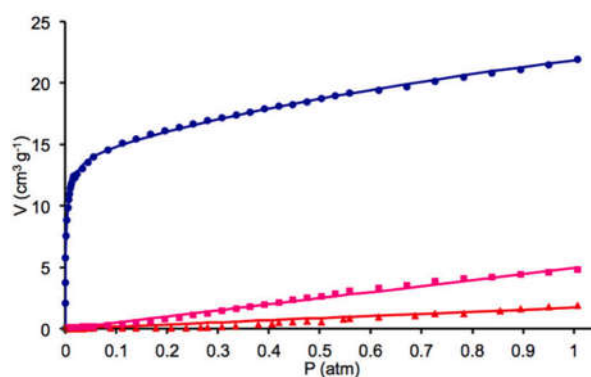


Figure 7. Isotherms adsorption of CO, N<sub>2</sub> and O<sub>2</sub> for 5,10,15-tris(2,6-dichlorophenyl)corrolato]cobalt at 298K. Adsorption isotherms of CO (blue circles), O<sub>2</sub> (pink squares) and N<sub>2</sub> (red triangles) for cobalt corrole recorded at 298 K. Solid lines represent the fitting curves using a triple-site Langmuir model for CO and a single one for O<sub>2</sub> and N<sub>2</sub>.<sup>58</sup>

## 1.4 Porous materials

Porous materials display porosity through three or two dimension networks avoiding molecular packing.<sup>120-122</sup> For example, COFs are organic amorphous 2D or 3D structures which can be built from corroles and specific platforms. On another hand, metal-organic frameworks (MOFs) are composed of metal ions or clusters connected to each other by organic ligands to

form highly crystalline 1D, 2D or 3D structures. The present work will also consider using MOFs as porous support for further corroles insertion.

Porous organic materials are great for the adsorption of greenhouse gases such as methane and carbon dioxide.<sup>123-129</sup> Porous organic materials can also be productively applied to catalysis,<sup>130, 131</sup> proton conduction,<sup>132, 133</sup> gas separation,<sup>134, 135</sup> energy storage,<sup>136, 137</sup> photoenergy conversion in solar cells,<sup>138</sup> semiconduction,<sup>139, 140</sup> photocatalysis and photoluminescence,<sup>141, 142</sup> enantioseparation,<sup>143, 144</sup> drug delivery and release,<sup>145</sup> iodine adsorption,<sup>146</sup> detection and removal of pollutants/contaminants from water/other liquids,<sup>147, 148</sup> along with other essential applications.

According to the IUPAC recommendations,<sup>149</sup> the definition of open pores was given such as pores should have continuous connection pathways with the outer surfaces of the porous structure. In contrast, pores that are separated from other pores are called closed pores. With the exception for practical applications, porous materials with open pores tend to be more interesting. Furthermore, porous materials are also categorized by the IUPAC according to pore size whose pore widths are assigned to less than 2 nm (microporous), between 2 and 50 nm (mesoporous) and greater than 50 nm (macroporous).<sup>149, 150</sup> On the basic state of porous materials, the major types can be classified as covalent organic frameworks (COFs), metal-organic frameworks (MOFs), porous organic polymers (POPs). In general, MOFs are built through coordination between metal ions and organic ligands. COFs and POPs are similarly constructed by organic reactions. However, COFs and POPs are literally different from each other. When it comes to COFs, reversible organic linkages and crystallinity are considered important characters. But, irreversible reactions are applied to POPs which show nothing about crystallinity. In this manuscript, my work mainly focuses on COFs along with extension work of MOFs and POPs. The following part will give the detailed introduction to COFs, MOFs and POPs.

#### 1.4.1 Covalent Organic Frameworks (COF)

With the development of new synthetic and design strategies, more and more COFs materials with different chemical functions, structures and properties have been reported.<sup>151, 152</sup> Due to the diversity together with other advantages such as tunable pore size and functionality,

COF materials show great potential in various applications for gas adsorption, storage and separation, sensing, catalysis and biomedicine.<sup>153-155</sup> Recently, COFs with various functionality have been widely reported in analytic chemistry.<sup>156, 157</sup> For instance, in the field of biomedicine, some COFs have been developed as novel solid carrier or sorbent for the immobilization of enzymes or the capture of target analytes including peptides and other small molecules in complex samples, respectively.<sup>158, 159</sup> Some COFs-based composites have been synthesized as novel stationary phases for separation and detection of important analytes such as isomers and drug molecules.<sup>160, 161</sup>

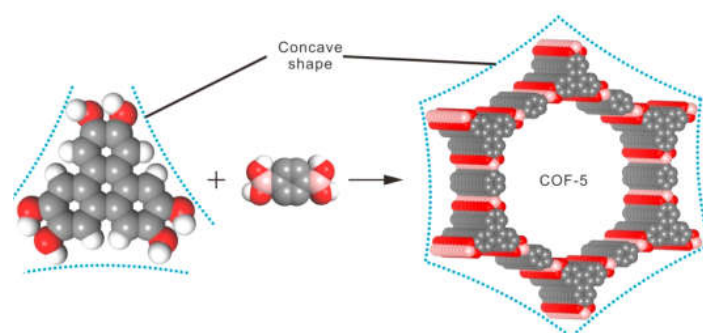


Figure 8. Typical porous organic material, namely, COF-5 formed from molecular building blocks.<sup>162</sup>

Covalent organic frameworks (COFs), as an emerging new type of porous materials, is two- or three-dimensional (2D or 3D) crystalline porous structures constructed by strong covalent bonds between organic subunits.<sup>145, 163</sup> Since the first two 2D COFs materials were tactfully constructed by Yaghi and co-workers in 2005 (Fig. 8) *via* the dehydration reactions of 1,4-benzenediboronic acid itself (COF-1) or with hexahydroxytriphenylene (COF-5), respectively, COFs chemistry has been developed rapidly and making great progress in the past decade.<sup>164-166</sup> In comparison with traditional crystalline porous materials, the COFs consisting of organic building units with different groups by covalent bonding possess many unique advantages including large surface areas, good chemical and thermal stability, tunable porous structure and low density.<sup>167-170</sup> These advantages together with the highly ordered pore structures make the COFs attract intensive interest of researchers.<sup>130, 140, 171</sup>

To efficiently obtain COFs with high crystallinity and in large scale production, many research groups have explored the synthetic possibility in different ways such as solvothermal,<sup>172, 173</sup> ionothermal,<sup>174, 175</sup> mechanochemical,<sup>176</sup> and microwave synthesis.<sup>177, 178</sup> In addition, the different reversible reactions containing the dehydration reaction of boronic acid itself or with catechol, the nitrile cyclotrimerization reaction, and the condensation of aldehyde

with amine or hydrazide have been developed to construct novel COFs that mainly include boron-based COFs, triazine-based COFs, imine-based COFs, respectively, and thus expand many types of COFs.<sup>179, 180</sup>

The synthesis and applications of COFs have evolved considerably over the past 20 years (Fig. 9). Respectively, in 2005 and 2007, extended crystalline 2D COFs (COF-1 and COF-5)<sup>164</sup> and 3D COFs (COF-102, COF-103, COF-105 and COF-108)<sup>166</sup> were synthesized using reversible covalent bonds (cyclotrimerization of boronic acids and dehydration reaction of boronic acid with catechol). Since these COFs are composed of strong covalent bonds, they are expected to possess high stability and easy modification of structures. Furthermore, their intrinsic porosity as well as their chemical robustness together make it possible to possess high permanent porosities.

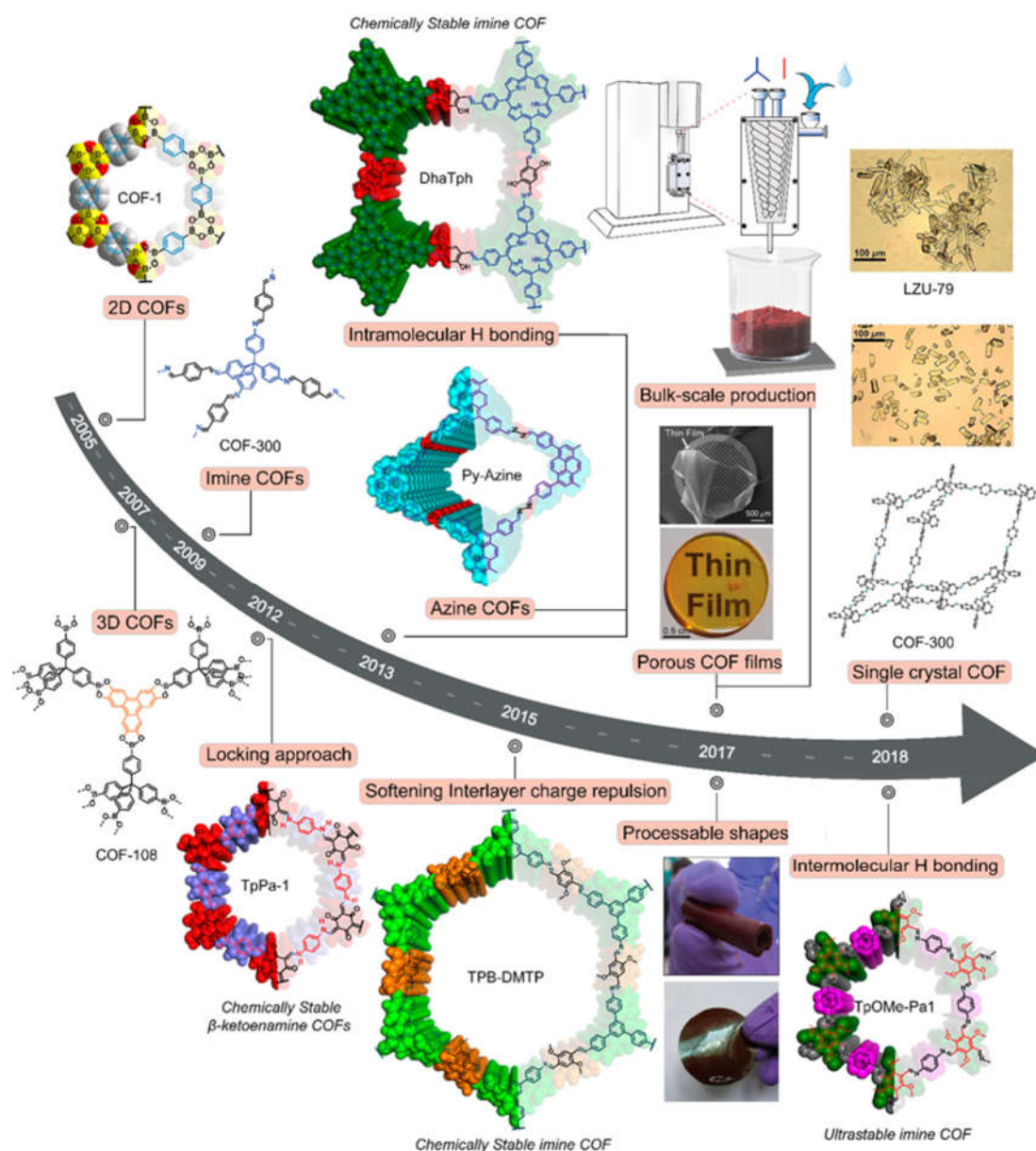


Figure 9. Evolution of the covalent organic framework chemistry.<sup>181</sup>

Over the past decades, a great improvement in the crystallinity of COFs has been achieved. There were two major breakthroughs in 2013 where single crystal structure of COFs could be obtained. Yaghi and co-workers succeeded to synthesize COF-320 with crystal size up to 200 nm. With this size, it is big enough to be solved by using Rotation Electron Diffraction (RED).<sup>182</sup> Independently, Wuest and co-workers successfully obtained crystals of nitroso polymer networks suitable for Single Crystal X-ray Diffraction (SXRD) analysis.<sup>183</sup> After that, a woven COF was firstly reported by Yaghi group in 2016 during the development of COFs (Fig. 10).<sup>184</sup> This class of COF materials were made from molecular weaving of distinct threads. After removing the metal, the crossing networks are completely composed of strong covalent bonds, making these materials essentially COFs. Moreover, 3D-Electron Diffraction

Tomography (3D-EDT) could be applied to solve the single crystal structures of these. Finally, in 2018, ultimate control was reached, with the synthesis of 3D COF crystals of up to 60 mm, linked by strong imine bonds.<sup>185</sup>

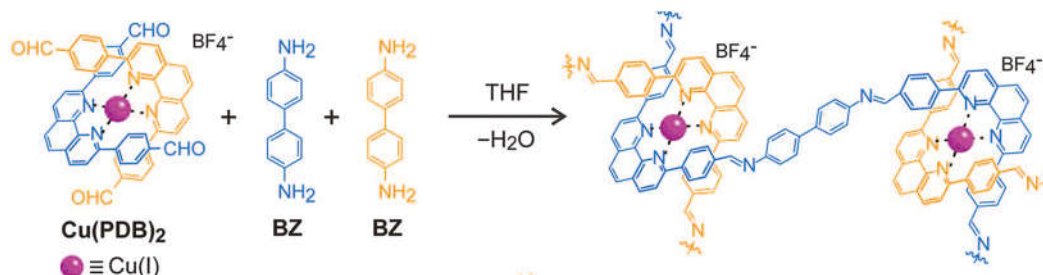


Figure 10. A general strategy for the design and synthesis of weaving structures (COF-505).<sup>184</sup>

#### 1.4.1.1 Design principles of COFs

During the development of COFs, numerous approaches have been developed to synthesize COFs with different topologies and with a wide variety of building blocks. Theoretically, according to the dimension and geometry of the building blocks, the topologies of the target COFs can be pre-determined. Compared to other porous materials, especially pure organic polymers, this property of COFs which allows to pre-design the skeleton of the structures is unique, and also helps to analyze and understand the crystal structure of COFs. This exceptional ability allows the construction of complex geometries with highly ordered structures, rather than primary-ordered structures.<sup>186-188</sup> The diagram of topology shown in Fig. 11 provides a systematic solution to obtain porous polymers through the combination of building blocks to form organic frameworks yielding crystalline networks with alternately placed linkers and knots.<sup>189, 190</sup> Depending on the geometries and dimensions of the knots and linkers,<sup>186</sup> the shape of the formed polygonal skeletons show great variety. Generally, COFs are classified into two categories: 2D and 3D. Based on their geometries, all monomers used to design 2D COFs are categorized into  $C_1$ ,  $C_2$ ,  $C_3$ ,  $C_4$  and  $C_6$  symmetries (Fig. 11). On the other hand, 3D COFs are pre-designed with a  $T_d$  symmetric moiety or an orthogonal unit as the knot which will be combined with the different linkers. In the following part, an overview of most often reported principles for the design of COFs is presented.

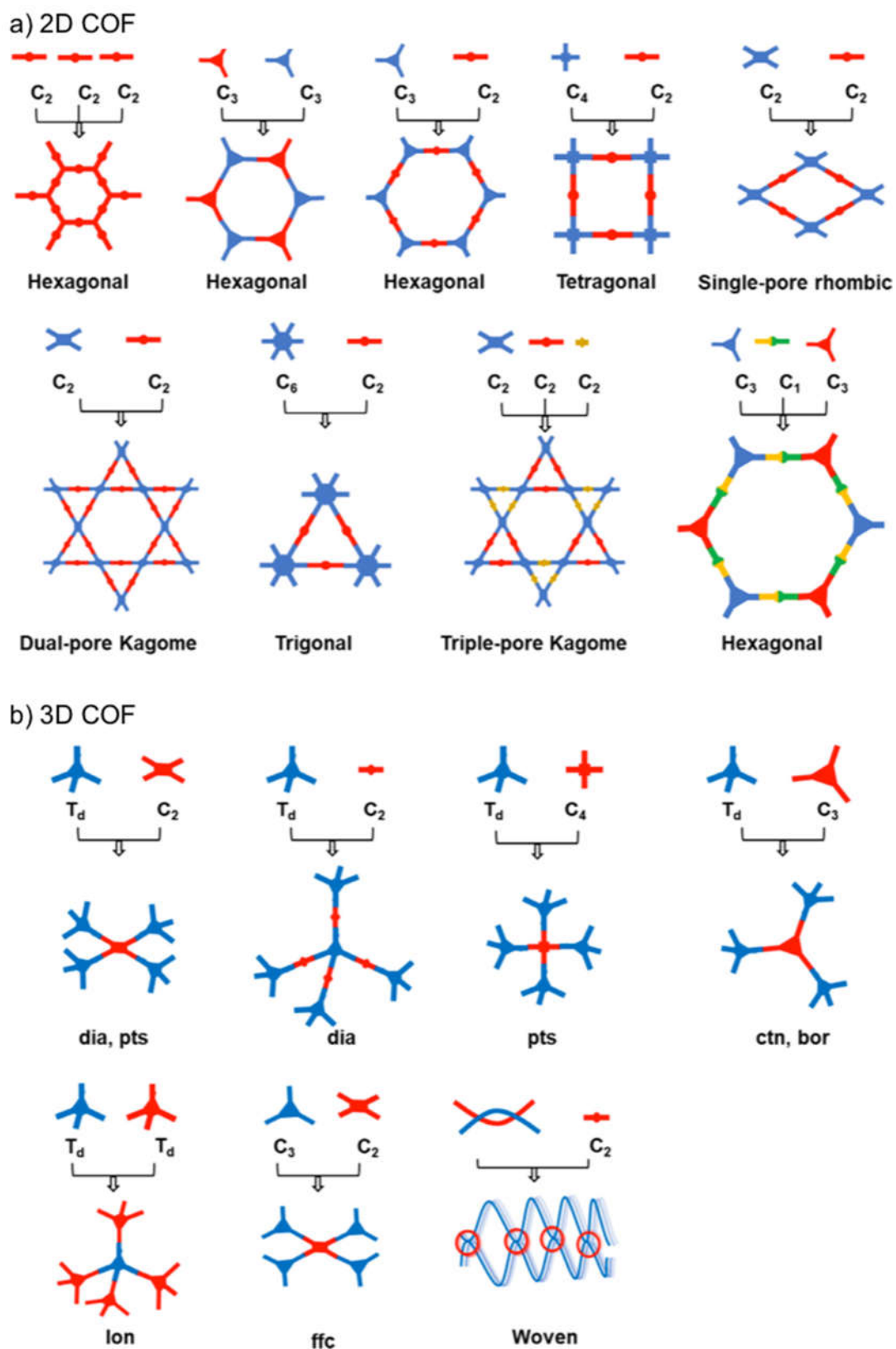


Figure 11. Topology diagrams representing a general basis for COF design and construction of (A) 2D COFs and (B) 3D COFs.<sup>191</sup>

For 2D COFs (Fig. 11a), the hexagonal topology is the most often reported and usually consists of  $(C_2 + C_2 + C_2)$  or  $(C_3 + C_2)$  or  $(C_3 + C_3)$  but with different pore sizes and  $\pi$ -orderings. For example, reported by Côté and co-workers, the condensation of a  $C_3$  symmetry with a  $C_2$  linear linker  $(C_3 + C_2)$  yields an hexagonal COF.<sup>164, 192</sup> A self-condensation of the  $C_2$ -symmetric unit could also provide a hexagonal COF,<sup>140, 164, 193</sup> as well as the reaction of two building units having a trigonal planar  $C_3 + C_3$  geometry.<sup>194-198</sup> Besides the hexagonal topology, tetragonal topology is also very popular among 2D COFs. With the combination of  $(C_4 + C_2)$  the produced sheets, of planar material, feature tetragonal pores.<sup>199, 200</sup> It is worthy to note that tetragonal COFs are usually composed of porphyrin derivatives because of their unique  $C_4$ -symmetry. Among  $C_2$  symmetries, there are platforms also featuring four coupling functions such as 4,4',4'',4'''-(Pyrene-1,3,6,8-tetrayl)-tetraaniline or 4,4',4'',4'''-(Ethene-1,1,2,2-tetrayl)-tetraaniline (Scheme 8) which is used to produce either a single-pore rhombic structure or a dual-pore kagome structure.<sup>187, 201, 202</sup> The kagome network consists of two types of pores in which each hexagonal pore is surrounded by six trigonal pores, while there is only one type of pore in the rhombic network. And finally, the  $(C_6 + C_2)$  combination produces a trigonal topology.<sup>203</sup> The trigonal, tetragonal, rhombic and hexagonal topologies are the major forms of 2D COFs. Besides those common topologies, the combination of three different monomers with appropriate symmetries have been developed to produce complex 2D COFs bearing multi pores.<sup>204</sup> However, all of the 2D COFs have in common that they generate extended one-dimensional (1D) channels through stacked layers.<sup>205, 206</sup>



4,4',4'',4'''-(Pyrene-1,3,6,8-tetrayl) tetraaniline

4,4',4'',4'''-(Ethene-1,1,2,2-tetrayl) tetraaniline

Scheme 8. Structures of  $C_2$  symmetries for single-pore rhombic or dual-pore kagome structures.<sup>187, 202</sup>

In contrast with 2D COFs that require planar building blocks, 3D COFs usually contain at least one knot having a  $T_d$  or orthogonal geometry to support the extension of covalently linked 3D network. For this, there are different possible combinations of  $T_d$ , or orthogonal, knot with  $C_1$ ,  $C_2$ ,  $C_3$ ,  $C_4$  or  $T_d$  symmetry to form skeletons and pores (Fig. 11b).<sup>207, 208</sup> 3D COFs can be categorized among different types of topologies, including **dia**, **pts**, **ctn**, **bor**, **lon**, and **ffc**.<sup>191</sup>

Up to now, the largest number of 3D COFs have been developed using a ( $C_2 + T_d$ ) geometry system, which yields **dia** topology networks.<sup>145, 209, 210</sup> By changing the  $C_2$ -symmetric monomers, a great deal of new 3D COF based on **dia** topology can be obtained easily. Furthermore, the different topology networks can be achieved by replacing the  $C_2$ -symmetric monomers with monomers presenting a different symmetry. For example, the **ctn** or **bor** network can be obtained by the ( $C_3 + T_d$ ) combination with large surface areas without interpenetration inside the skeleton.<sup>166, 211, 212</sup> The **lon** network can be designed through ( $T_d + T_d$ ).<sup>166</sup> On the basis of the ( $C_2 + T_d$ ) and ( $C_4 + T_d$ ) combinations, the **pts** nets are obtained in a two-fold interpenetrated form.<sup>213, 214</sup> For **pts** net, the engaged  $C_2$ - or  $C_4$ -symmetric units are required to have four reactive functions. The ( $C_3 + C_2$ ) topology has been used to prepare rare examples of 3D COF having an ffc net.<sup>208, 215</sup> Interestingly, in 2016, a woven 3D-COF (Fig. 10), named COF-505, has been constructed using helical organic threads by the simple imine polycondensation of benzidine (BZ) with copper(I)-bisphenanthroline tetrafluoroborate ( $Cu(PDB)_2(BF_4)$ ) which possess four aldehyde groups.<sup>184</sup> The topology diagram in Fig. 11 can be considered as the general basis for the construction and design of COFs. The high design ability of COFs is a unique feature which is difficult to obtain in other porous materials. Thus, COFs are taken into consideration as attractive materials that have diverse structures and functions.

#### 1.4.1.2 Bond formation for COFs synthesis

In the previous part, a topology diagram was discussed as the key point to design the COFs structures. Now, we need to note that the synthesis of COF material is mainly influenced by diverse reversible reactions. The synthesis of polymeric materials has generally been dominated by kinetically controlled reactions, which is irreversible reactions, leading to a difficulty to obtain crystalline organic polymers.<sup>216</sup> In order to prevent the formation of disordered kinetic products that are amorphous, it's very important to involve reversible reactions in the synthesis of COF. The reversibility of the bond-forming reaction, together with the help of dynamic covalent chemistry (DCC),<sup>217</sup> in covalent bond formation, allows error correction during the crystallization of COFs which helps the material to attain a higher crystallinity (Fig. 12). In contrast to kinetically controlled reactions, DCC requires a high temperature to give high activation energies to enable the thermal reversibility. Furthermore, a specific agent (water) was used to maintain the reversibility during the covalent bond formation.<sup>164</sup> Therefore, during the COF synthesis, the conditions of reaction are usually dominated by high temperature and

catalytic amount of water. Generally, COF is one of the porous organic polymers (POPs), but according to crystallinity, POPs are divided into crystalline and amorphous. The crystalline one is called COF, the other is amorphous POP. The POPs mentioned in the rest part refers to amorphous one.

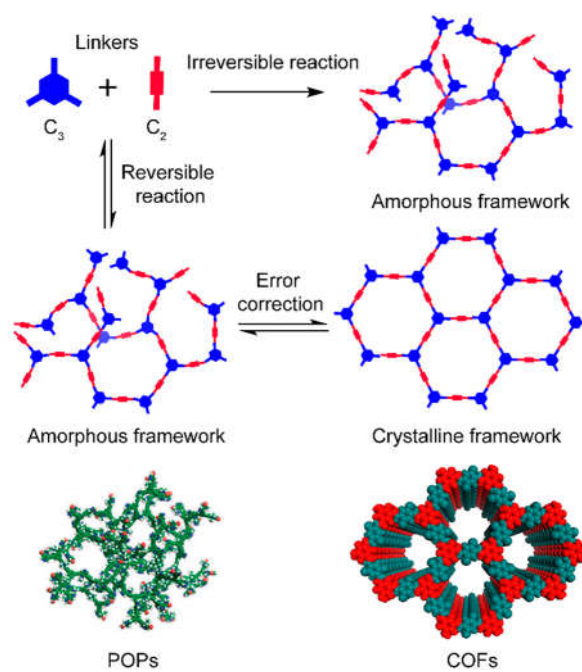


Figure 12. Schematic representation of crystalline and amorphous covalent organic framework formation by reversible and irreversible reactions.<sup>181</sup>

Based on the paradigm of reversible covalent bond formation governing the synthesis of crystalline covalent organic materials, many new reactions have been developed since the discovery of first COFs. Yaghi *et al.* successfully obtained 2D COFs through the co-condensation of boronic acids and catechol to form a boronic ester, and through the self-condensation of boronic esters to form boroxines.<sup>164</sup> Due to the poor stability of boronic esters and boroxines under hydrolysis condition, there was an inherent preference to develop more stable COFs from different coupling linkages. Since then, many alternative reactions and synthetic routes have been developed. Fig. 13 demonstrates the most commonly used organic reactions for COFs synthesis. Depending on the nature of the chemical reactions, the types of COFs can usually be categorized as follow: boroxine,<sup>164</sup> boronate-ester,<sup>139</sup> borosilicate,<sup>218</sup> triazine,<sup>174</sup> imine,<sup>209</sup> hydrazone,<sup>219</sup> borazine,<sup>193</sup> squaraine,<sup>220</sup> azine,<sup>221</sup> phenazine,<sup>222</sup> imide,<sup>212</sup> double-linkage,<sup>223</sup> spiroborate,<sup>224</sup> alkene,<sup>225</sup> amide,<sup>226</sup> viologen,<sup>227</sup> hypercoordinate silicon,<sup>228</sup> urea,<sup>229</sup> and 1,4-dioxin linkages.<sup>230</sup>

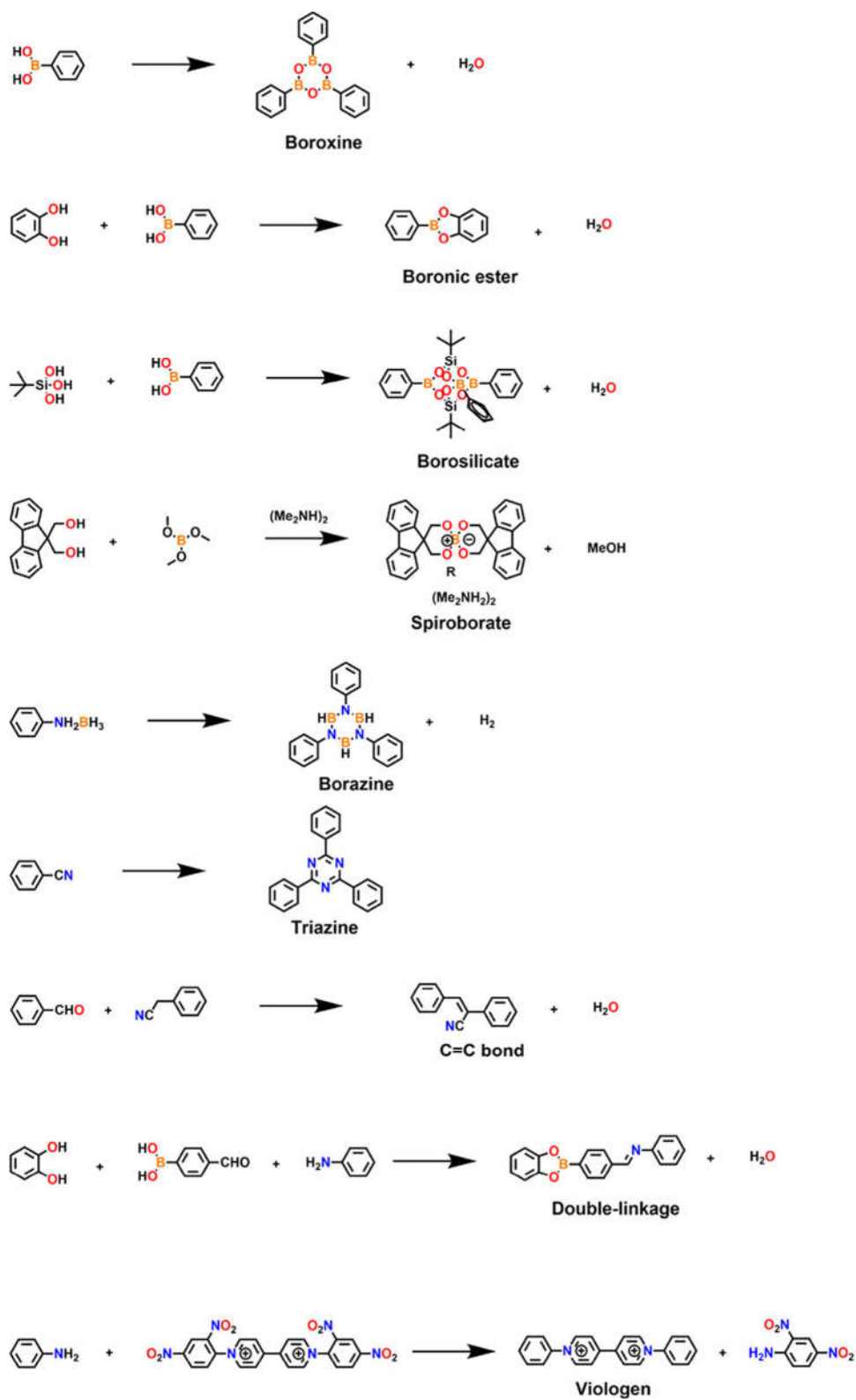


Figure 13. Various linkages explored for the synthesis of COFs (part 1).<sup>190</sup>

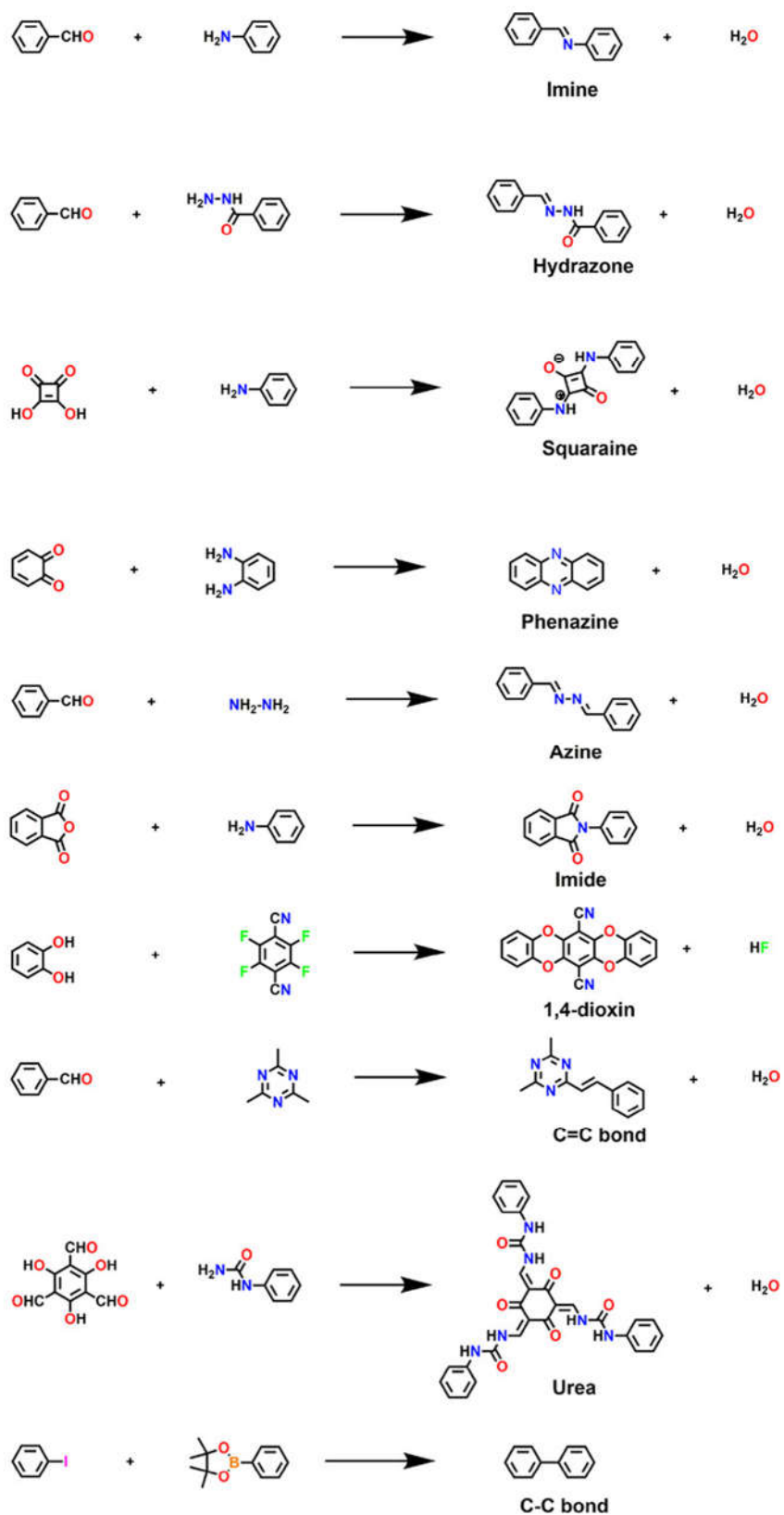


Figure 13. Various linkages explored for the synthesis of COFs (part 2).<sup>190</sup>

## 1) Boron-based COFs

In 2005, Yaghi and co-workers reported the first two members, COF-1 and COF-5, which can be synthesized using a simple “one-pot” procedure under mild reaction conditions in high yields.<sup>164</sup> These two materials showed rigid structures, high thermal stabilities, low densities, high surface areas and permanent porosity, tending to be excellent porous materials. Since then, diverse boron-containing COFs have been constructed with boronic esters or boron anhydrides (boroxine). According to the condensation strategy, the resulted boronic COFs can be categorized into two types: self-condensation of boronic acids to boroxine rings and the co-condensation of boronic acids and catechols to boronic esters. The first COF (COF-1) was prepared through self-condensation of a single building block, yielding boroxine-linked COF (Fig. 14a). The boroxine network COF-1 was formed by self-condensation of 1,4-benzene diboronic acid (BDBA). The COF-1 was expanded with porous 2D graphitic layers, featuring highly crystallinity and high surface area of 711 m<sup>2</sup>g<sup>-1</sup>. During researches of 2D COFs, the eclipsed stacking motive tends to be one of the necessary characterization of structures. Surprisingly, with solvent guest molecules, the COF-1 showed an AB stacking mode. Upon removal of solvent guest molecules, these layers shift toward an AA stacking mode.<sup>164</sup> For the boronate esters COF-5, the network was constructed through co-condensation of boronic acids and catechol derivatives, leading to five-membered ring. By the co-condensation of 2,3,6,7,10,11-hexahydroxytriphenylene (HHTP) and BDBA, the hexagonal framework COF-5 eclipsed an AA stacking with hexagonal 1D channels of 2.7 nm in diameter, featuring highly crystallinity and high surface area of 1590 m<sup>2</sup>g<sup>-1</sup>.

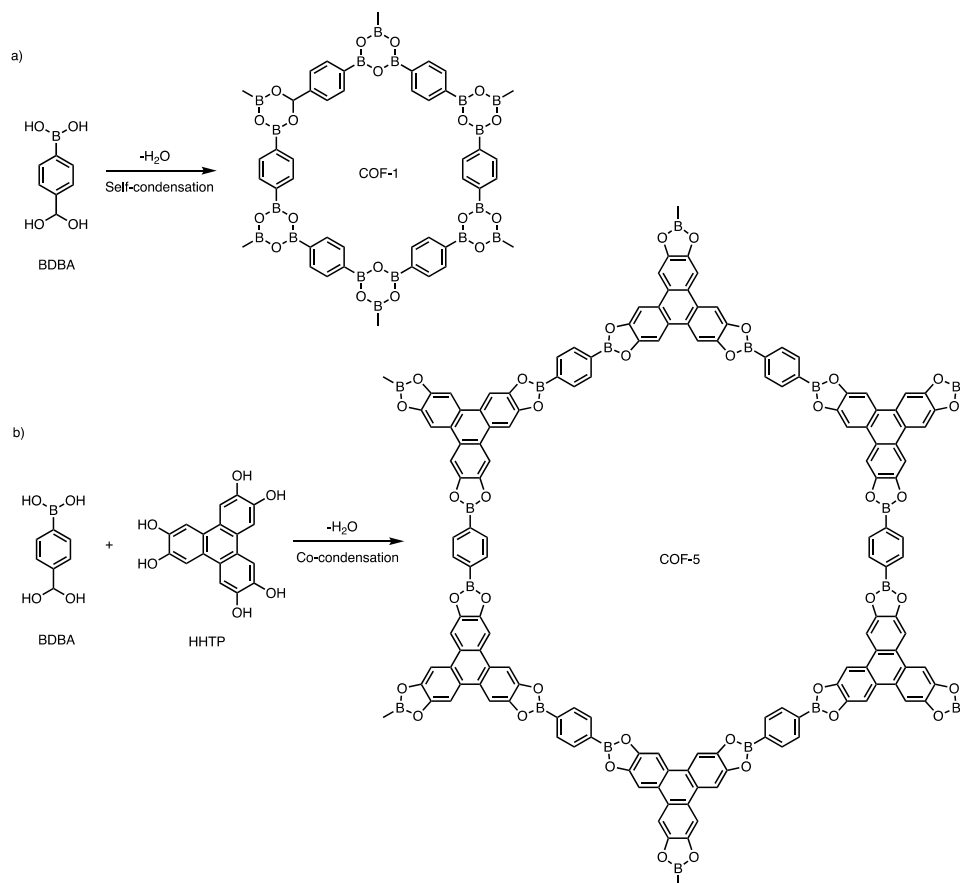


Figure 14. (a) Self-condensation of BDBA to produce COF-1 (b) Co-condensation of BDBA and HHTP to synthesize COF-5.<sup>164</sup>

Recently, two other types of boron-containing COFs have been reported with borosilicate cage and spiroborate linkages. COF-202, with a borosilicate cage linkage, was synthesized *via* co-condensation of *tert*-butylsilane triol(*t*-BuSi(OH)<sub>3</sub>) and tetra(4-dihydroxyborylphenyl)methane (Fig. 15).<sup>218</sup> Unlike the condensation of boronic acid and diol (Fig. 14b), in this case, the two hydroxyl groups of one  $-B(OH)_2$  react individually with different triols. COF-202 has a high thermal stability (up to 450°C) and great resistance to common organic solvents. Moreover, samples of COF-202 maintain both their porosity and their crystallinity after exposure to air for 24 h.<sup>218</sup> Finally, Brunauer-Emmet-Teller (BET) models yielded high surface area values of 2690 m<sup>2</sup>g<sup>-1</sup>.

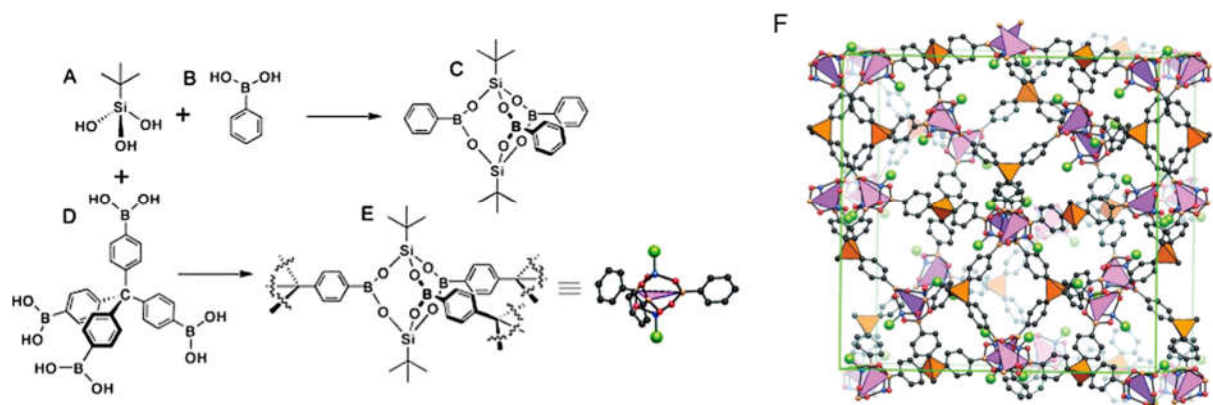


Figure 15. Synthesis of molecular borosilicate cage (C) and COF-202 (F).<sup>218</sup>

Spiroborates, ionic derivatives of boronic acid, have been reported for high resistance toward hydrolysis and high stability in water, methanol, and under basic conditions while boroxine and boronic esters are easy to decompose when encountered with water even in air.<sup>224</sup> With their ionic properties, spiroborates materials tend to function as ion conductive materials for battery application. Up to date, there are rare examples for spiroborates linkage COFs. In 2016, Zhang and his group reported the design and synthesis of porous spiroborate-linked ionic COFs (ICOF-1 and ICOF-2) that exhibit high surface areas, good thermal stability, great resistance to hydrolysis, and high room-temperature ion conductivity.<sup>224</sup> The ICOFs were obtained through the transesterification between borate and polyols by the addition of base catalyst (Fig. 16). The other example of spiroborate COF was reported in 2021.<sup>231</sup> Wang and co-workers designed and synthesized porous cubic 3D COFs (Fig. 17), showing cubic pores, high crystallinity, high surface areas (up to  $1726 \text{ m}^2\text{g}^{-1}$ ) and permanent porosity. They also showed good stability in common organic solvents and aqueous solutions except acidic solution.

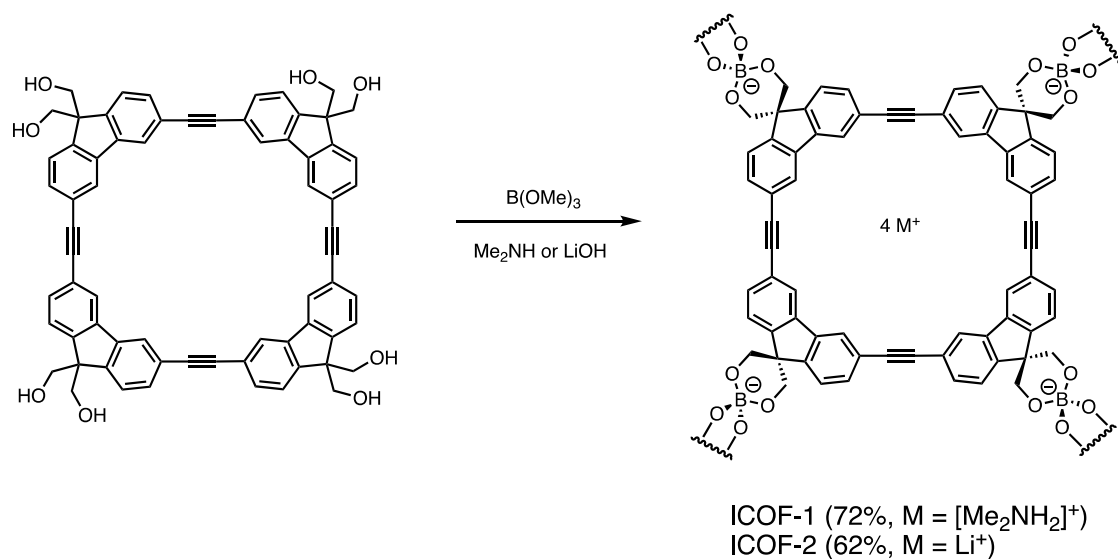


Figure 16. Synthesis of spiroborate linkage COFs.<sup>224</sup>

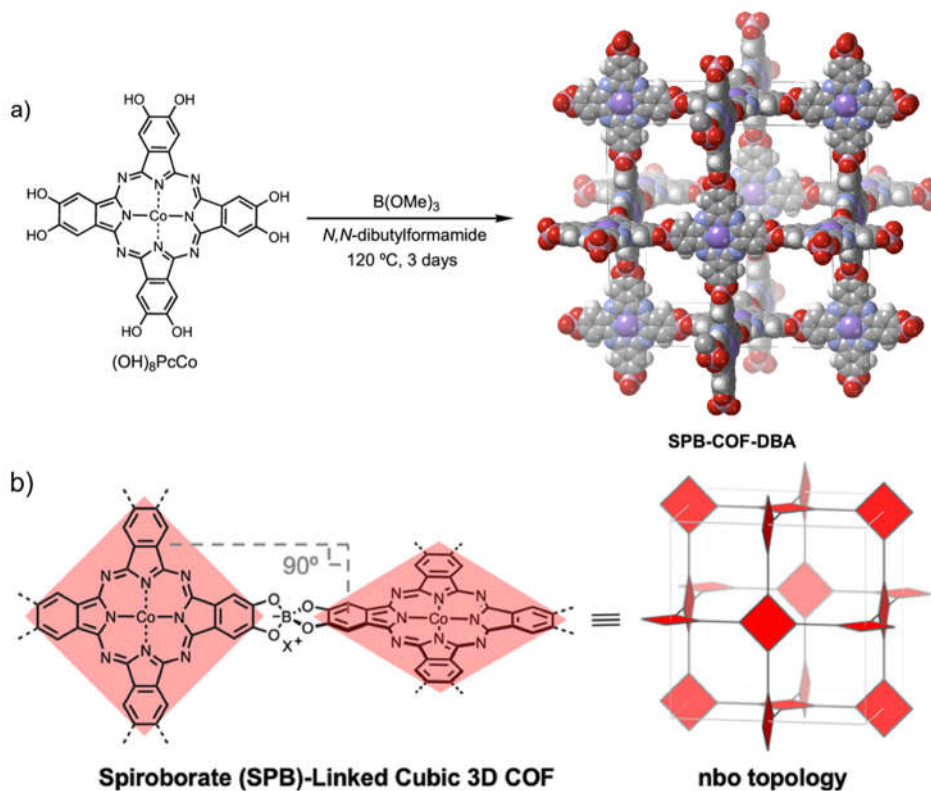


Figure 17. (a) Synthesis of cubic SPB-COF-DBA. All counter cations in the framework are omitted for clarity. White, pink, gray, blue, red and purple atoms represent hydrogen, boron, carbon, nitrogen, oxygen and cobalt, respectively. (b) Topology diagram of cubic SPB-COF-DBA.<sup>231</sup>

## 2) Imine-based COFs

The condensation of aldehydes and amines in the presence of organic acid or Lewis acid catalyst yields imine bonds (in the form of  $-N=CH-$ ). These imine-based COFs exhibit significantly higher stability than boronic esters.<sup>232</sup> Furthermore, a variety of knots and linkers with aldehyde or amines functions can be easily obtained. Due to these advantages, the development of COFs is dominated by imine-based COFs after the first COF with imine linkage was reported. The first imine COF was reported by Yaghi and co-workers in 2009. They designed and synthesized a 3D COF (COF-300) constructed from tetra-(4-anilyl) methane and terephthalaldehyde which is a typical ( $C_2 + T_d$ ) geometry system (yielding **dia** topology).<sup>209</sup> The synthesis is shown in Fig. 18. During the formation of this structure, the diamond topology was expected. However, the big pores are occupied by the long rod-like linkages, thus resulting in 5-fold interpenetrated structures.<sup>209, 233</sup>

The FT-IR spectrum of COF-300 showed the  $C=N$  stretching modes at  $1620\text{ cm}^{-1}$  which is characteristic for imines.<sup>234</sup> Thermal gravimetric analysis shows good thermal stability of COF-300 up to  $490\text{ }^\circ\text{C}$ . Also, the material is insoluble in water and common organic solvents such as hexanes, methanol, acetone, tetrahydrofuran, and *N,N*-dimethylformamide. The application of the Brunauer-Emmett-Teller (BET) model results in a surface area of  $S_{\text{BET}} = 1360\text{ m}^2\text{g}^{-1}$ , showing that the COF-300 is a typically microporous organic material.

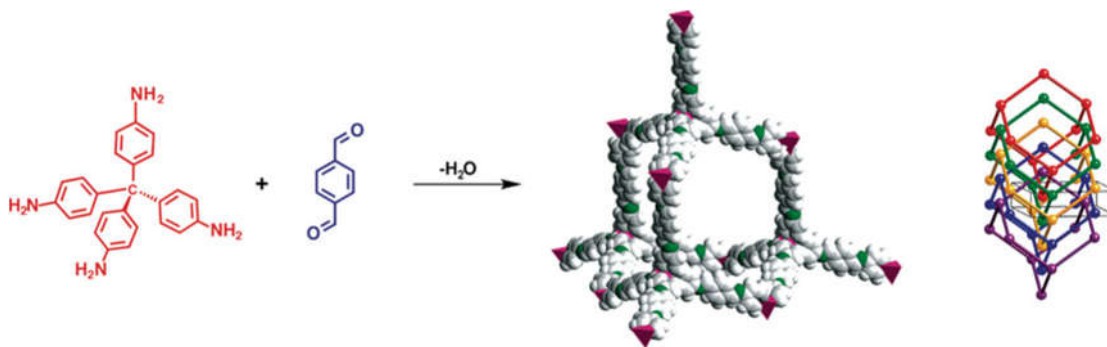


Figure 18. Synthesis of COF-300. The single framework (space filling, C gray and pink, N green, H white) and the dia-c5 topology.<sup>209</sup>

Then, Wang and co-workers reported the first imine-based 2D COF (COF-LZU1), constructed *via* the condensation of 1,3,5-triformylbenzene and 1,4-phenylenediamine, yielding a layered COF with hexagonal channels like the boronic ester COFs.<sup>130</sup> The structure is shown

in Fig. 19a-b. Due to the 2D eclipsed structure, COF-LZU1 possesses a short layer distance of 3.7 Å, making it possible to have incorporation of metal ions between layers. Thus, the Pd/COF-LZU1 was obtained for catalysis application. Generally, the imine-based COFs have comparable crystallinity to boron-containing COFs. But the better stability than boron-containing COFs towards hydrolysis makes imine-based COFs more popular. To date, the large library of available aldehyde and amine linkers and the possibility to construct conjugated  $\pi$ -systems throughout the whole COF sheets makes imine bonds very popular linkage motifs in COFs. Imine-formation is clearly the most common synthesis strategy employed to build COFs.

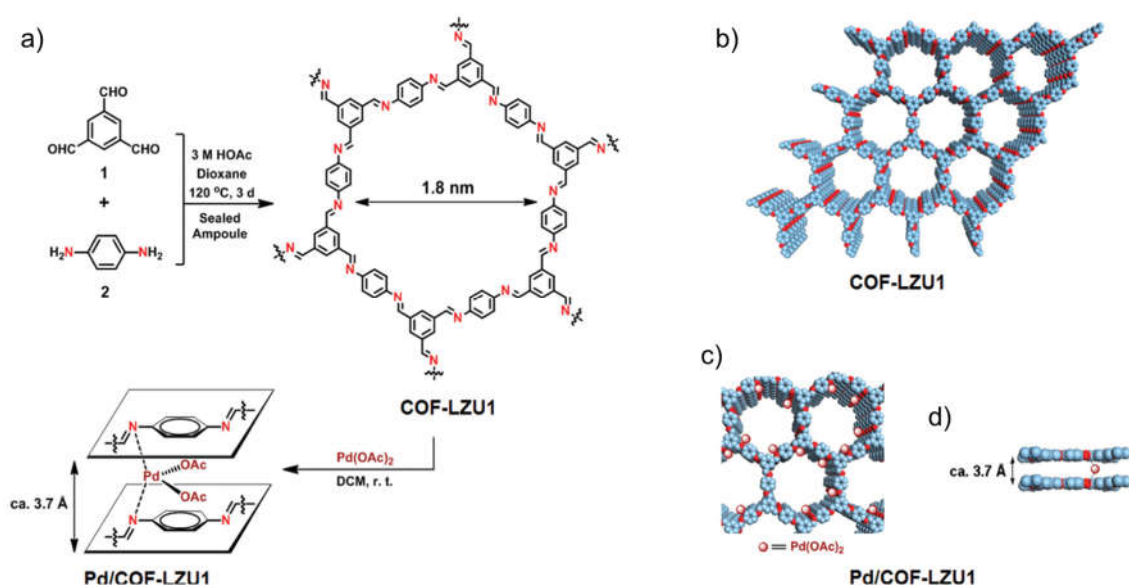


Figure 19. (a) Construction of COF-LZU1 and Pd/COF-LZU1. (b) Proposed structure of COF-LZU1. (c, d) Proposed structure of Pd/COF-LZU1. All structures were simulated with a 2D eclipsed layered-sheet arrangement. C: blue, N: red, and brown spheres represent the incorporated Pd(OAc)<sub>2</sub>. H atoms are omitted for clarity.<sup>130</sup>

### 3) Azine-based COFs

Azine linkage ( $-\text{C}=\text{N}-\text{N}=\text{C}-$ ) was reported by Jiang *et al.* in 2013 to explore a robust linkage for the synthesis of a highly crystalline, porous and stable COF. The azine linkage COFs were based on the condensation between hydrazine and aldehyde derivatives. This condensation is controlled by a thermodynamic reaction resulting in the formation of azine linkages and water as side products. Up to date, the synthesis of several COFs based on azine linkage have been explored by condensation between hydrazine and suitable co-monomers containing multiple aldehyde functionalities. A variety of knots have been applied to azine linkage COFs, leading

to diverse topologies including hexagonal, trigonal, and rhombic COFs (Fig. 20).<sup>125, 235-239</sup> For instance, the first structure labeled Py-Azine COF, was prepared by Dalapati *et al.* with 1,3,6,8-tetrakis(4-formylphenyl)pyrene (TFPPy) as a building block, a planar C<sub>2</sub> tetraaldehyde known for the rhombic geometry induces a crystalline structure.<sup>221</sup> This Py-Azine COF proved to possess high crystallinity, porosity and stability. Especially the chemical stability of azine-linked COF is remarkable showing that the COFs remain crystalline structure either in polar and nonpolar organic solvents or in inorganic acid and base. Among several other applications, the potential of azine bond fluorescence has been reported as a chemical sensor for detection of specific compounds in aqueous solution.

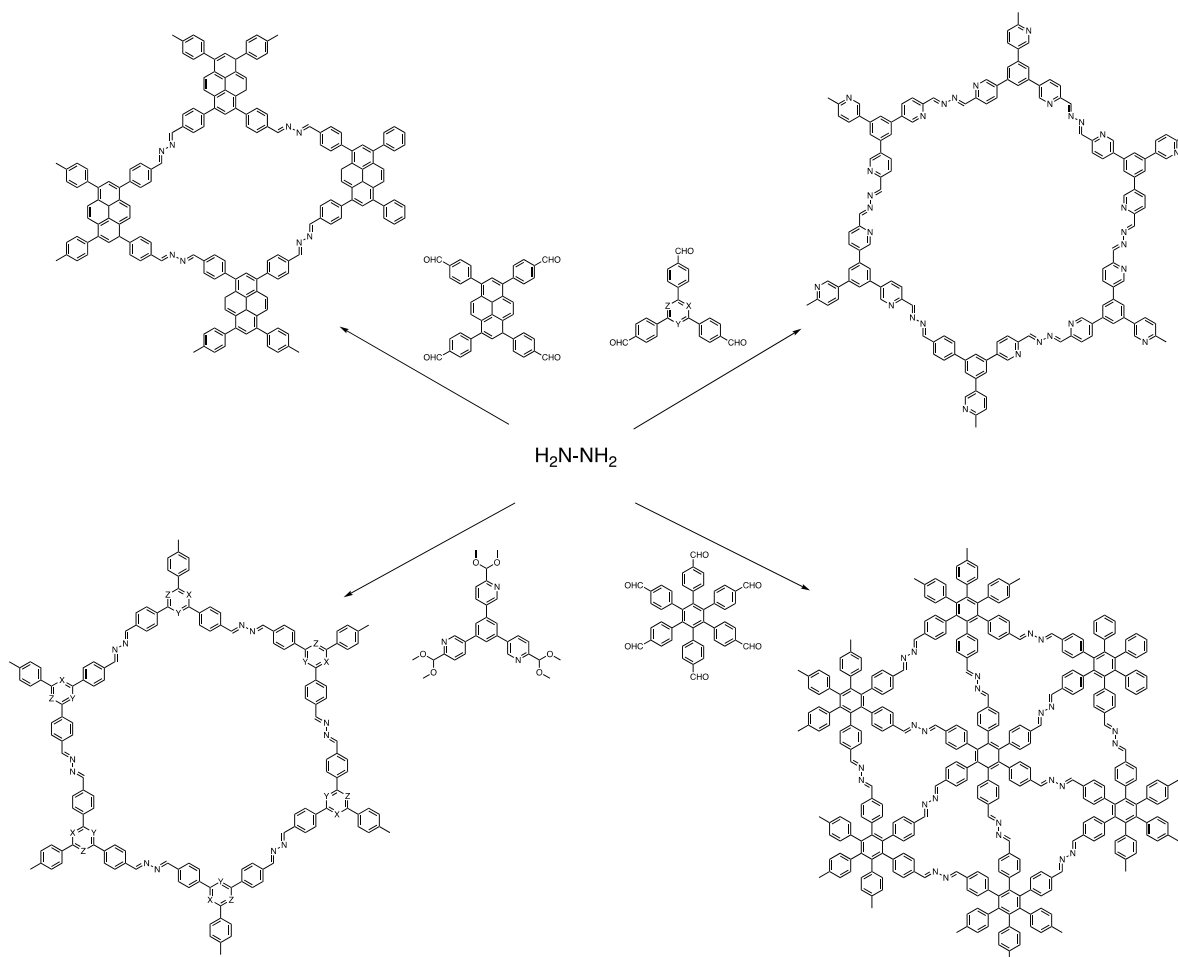


Figure 20. Synthesis of (a) Py-Azine COF, (b) LZU-22, (c) N<sub>x</sub>-COF (x = 0, 1, 2, and 3), and (d) HEX-COF 1.<sup>190</sup>

#### 4) Ketoenamine-based COFs

The first ketoenamine-based COF was introduced by Banerjee *et al.* in 2012. The new protocol to synthesize ketoenamine COF is based on the combination of reversible and irreversible organic reactions.<sup>240</sup> As displayed in Fig. 21, the  $C_3$  symmetric triformylphloroglucinol with different  $C_2$  symmetric diamines are involved in the design of ketoenamine COFs. The whole process of ketoenamine linkage formation can be divided into two steps. As shown in Fig. 21, firstly, a crystalline framework was formed through a usual reversible Schiff base reaction. However, the second step is totally irreversible and consists of the enol-to-keto tautomerization, which enhances the chemical stability.<sup>240</sup> In this case, the irreversible tautomerization was considered to have no effect on the crystallinity, since the transformation involves only shifting of bonds while keeping the atomic positions almost the same.<sup>240</sup> However, in many cases, compared to their imine counterparts, ketoenamine COFs were found to be somewhat less crystalline, which could be assigned to the irreversible tautomerization inhibiting the error correction in the COF lattice.<sup>241</sup>

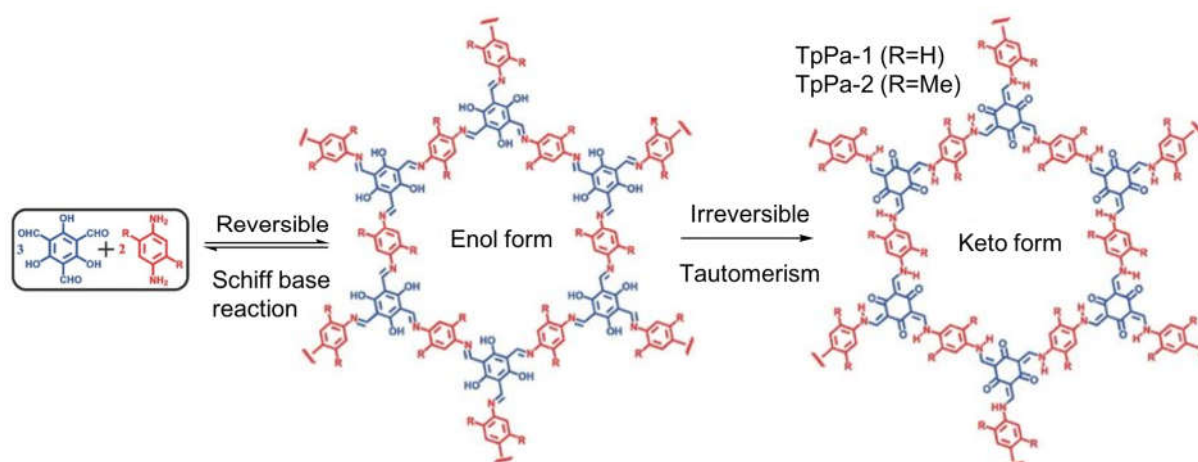


Figure 21. Schematic representation of the  $\beta$ -ketoenamine COF formation via enol-keto tautomerization.

Adapted with permission.<sup>240</sup>

## 5) Imide-based COFs

Imide-based COFs are obtained through the condensation of an amine with acetic anhydride at high temperature (up to 250°C). The imide formation reaction is typically used to produce one-dimensional polyimide polymers which are high-performance polymers known for their good chemical resistance, high thermal stability, and extraordinary mechanical properties.<sup>242</sup> Featuring many of these properties, imide-based COFs are used widely in many aspects such as chemical sensors,<sup>155</sup> energy storage devices<sup>243</sup> and gas separation.<sup>244</sup> Reported by Fang *et al.*, a series of imide-linked COFs were synthesized in the *n*-methyl-2-pyrrolidone/mesitylene mixtures with isoquinoline as catalyst (Fig. 22).<sup>212</sup> All of these COFs tend to be highly crystalline. During the three imide COFs, PI-COF-3 possessing the theoretic biggest pore size has the highest BET surface area of 2346 m<sup>2</sup>g<sup>-1</sup> and the section area of the inside channel was as large as 22 nm<sup>2</sup> where rhodamine B could easily be absorbed into the COF. In 2015, Fang reported a 3D porous crystalline imide-linked COFs with fourfold-interpenetrated diamond networks.<sup>145</sup> For the first time, COFs are employed in controlled drug delivery, for which they show high loadings and good release control. Additionally, imide COFs were developed for multiple applications, such as fluorescent probes, chromatographic packing, and soluble waste remover.<sup>245-247</sup>

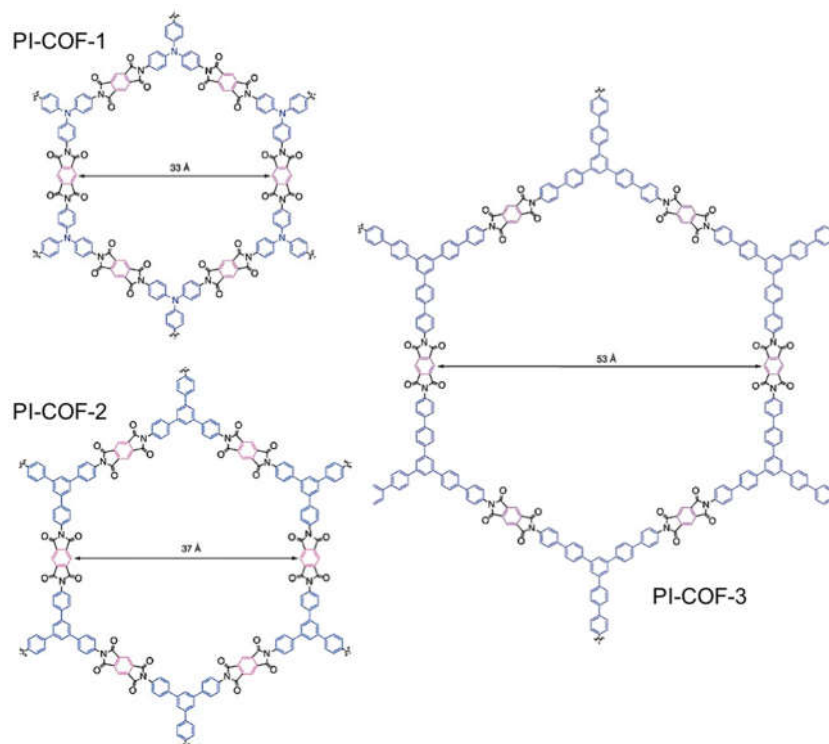


Figure 22. Structures of PI-COF-1, PI-COF-2 and PI-COF-3.<sup>212</sup>

### 1.4.1.3 Application of COFs

COFs combine a number of physical and chemical properties, they are unique among various porous organic materials.<sup>248</sup> For these reasons, COFs tend to be promising subjects for the development of various fields. After the first reported COF, there are already a large number of new COF structures available in the literature, concerning the most varied applications, such as gas storage and separation,<sup>249, 250</sup> heterogeneous catalysis,<sup>251, 252</sup> chemical sensing,<sup>253, 254</sup> controlled drug release,<sup>255, 256</sup> ionic-exchange processes,<sup>257, 258</sup> photoconductivity,<sup>259, 260</sup> energy storage.<sup>261, 262</sup> In the following section, some of those applications will be highlighted.

#### 1) Gas adsorption

Due to the high porosity and low density for these COFs materials, gas adsorption tends to be one of the most potential application of these materials.<sup>248</sup> In the past decade, many researches have been carried out to implement COFs as gas storage materials for relevant compounds such as hydrogen (H<sub>2</sub>),<sup>263</sup> carbon dioxide (CO<sub>2</sub>),<sup>264</sup> methane (CH<sub>4</sub>),<sup>265</sup> and ammonia (NH<sub>3</sub>).<sup>266</sup> Many research works are interesting in the storage of hydrogen because it is a clean source of energy. However, due to the very low density, the storage of hydrogen requires a very high pressure (350 - 700 bar) as gas state or very low temperature to keep it as a liquid. Furthermore, the high instability and reactivity make it more difficult to have large scale distribution of hydrogen. Recent years, among all the porous materials for hydrogen storage, COFs rise as one of the most promising class of materials for H<sub>2</sub> storage.<sup>267</sup> For example, the COF-102 (Fig. 23), a 3D framework synthesized by the self-condensation of tetra(4-dihydroxyborylphenyl)methane, exhibits a maximum adsorption capacity for H<sub>2</sub> of 77 mg g<sup>-1</sup> at 35 bar and 77 K. This result shows a competition against the best MOFs and other porous materials for H<sub>2</sub> capacity at similar high pressure and almost meeting the current benchmarks established for implementing and construction of fuel cells of H<sub>2</sub> viable.<sup>263, 268</sup>

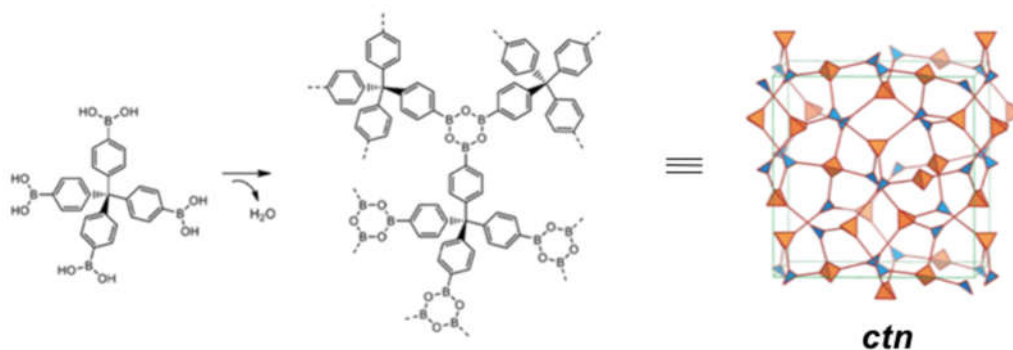


Figure 23. Synthesis of COF-102 and the corresponding expanded **ctn** networks. <sup>166</sup>

## 2) Heterogeneous catalysis

Over several decades, heterogeneous catalysis has been considered as the use of functional porous materials with large surface areas. Among these porous materials, amorphous porous organic polymers and crystalline MOFs have been suggested as candidates for efficient heterogeneous catalysts in fine chemical synthesis.<sup>269-272</sup> As one of the most important members of porous materials, functional COF materials are expected to possess high and efficient potentials as new catalysts. As the cases of other porous solids, COF materials for catalytic application must possess high stability to thermal treatments, water, and most of the organic solvents.<sup>273</sup> Furthermore, for the ideal catalytic performance, it is necessary to have easy accessibility to the catalytic sites and the efficient mass transport inside the porous catalyst. In 2011, the first application of COF for highly efficient catalysis was performed by Wang *et al.*<sup>130</sup> In order to obtain the palladium loaded COF, the imine-linked COF(COF-LZU1) was firstly synthesized from simple building blocks *p*-phenylenediamine and 1,3,5-benzenetricarboxaldehyde (Fig. 19). The 2D eclipsed layered-sheet structure of COF-LZU1 makes the distance of nitrogen atoms to 3.7 Å in the adjacent layers, which is suitable for the strong coordination of metal ions. Then, the COF was treated with Pd(OAc)<sub>2</sub> to form Pd(II)-coordinated COF-LZU1 (Fig. 19). The Pd/COF-LZU1 was applied to catalyze the Suzuki-Miyaura coupling reaction. The catalytic performance was demonstrated with the wide range of reactants showing the excellent yields (96%-98%) of products, along with high stability and recyclability as catalyst.

It should be noted that compared to Pd(II)-containing MOF,<sup>274</sup> Pd/COF-LZU1 requires lower palladium loaded rate and thus shows faster reaction speed and higher reaction yield.

These advantages should be assigned to the suitable distance between the 2D layered-sheet. Nitrogen atoms in adjacent layers can easily incorporate palladium, forming a robust scaffold. Moreover, the regular channels with a diameter of 1.8 nm ensure efficient access to these active sites as well as rapid diffusion of the bulky products. Up to date, a great breakthrough has been made to explore functional COFs materials as catalysts with broad catalytic sites, various structures even from milligram to gram-scaled synthesis.<sup>275-278</sup>

### 3) Photoelectric application

Pyrene-functionalized COFs were developed by Jiang and co-workers for photoelectric applications.<sup>139, 140</sup> PPy-COF and TP-COF possessing 2D structures with high BET surface areas were obtained by the self-condensation and co-condensation of pyrene-2,7-diboronic acid and 2,3,6,7,10,11-hexahydroxytriphenylene (Fig. 24). Both of them show the capacity of harvesting photons from ultraviolet to visible regions and electrical conductivity. The unique properties of these optoelectronic COFs represent an important step toward the applications of functional COFs in optoelectronics and photovoltaics.

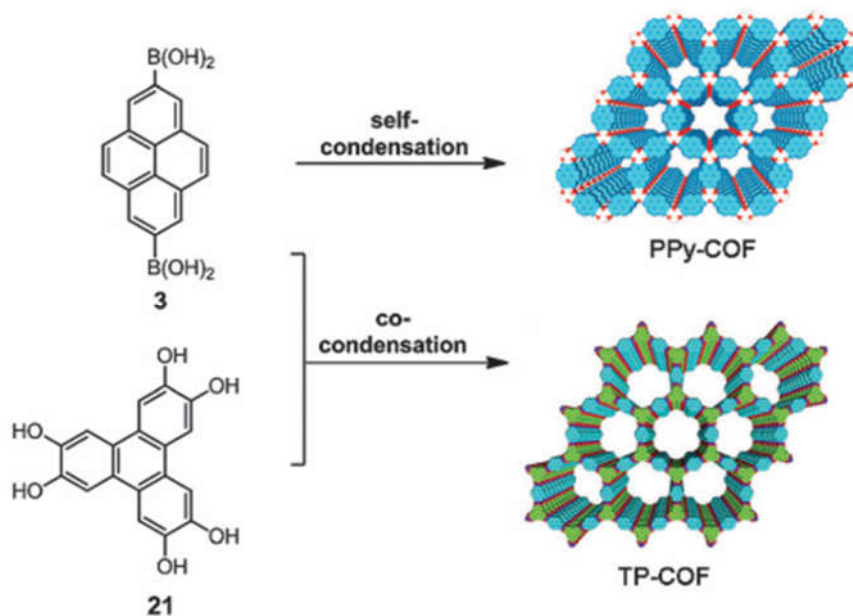


Figure 24. Building units and extended structures of PPy-COF and TP-COF.<sup>139, 140</sup>

#### 4) Energy storage

The current energy storage device market is undoubtedly occupied by lithium ion batteries (LIBs) for their high energy density, large cycle stability and promising efficiency. Nowadays, a great effort has been made for development of lithium ion batteries. However, it is very difficult to obtain organic electrode materials with high capacity and long-term cyclability due to the weak structural and chemical stability and low conductivity of organic materials. During the development, covalent organic frameworks has been seen as promising materials to counter these problems because of their good stability and high porosity and capacity. Among all the materials, COFs with conjugated structures facilitate the improvement of conductivity, tending to be remarkable candidates for energy storage device. In 2019, the synthesis and characterization of two  $\pi$ -conjugated COFs (Fig. 25) were reported by Zhang *et al.*<sup>279</sup> The formation of these two COFs are based on Schiff-base reaction from 2,4,6-triaminopyrimidine (Tm) respectively with 1,4-phthalaldehyde (Pa) and 1,3,5-triformylbenzene (Tb) according to a mechanochemical process. When applied to LIBs, the COFs exhibit favorable electrochemical performance with high reversible discharge capacities at a high current density and excellent long-term cyclability. Notably, after 2000 cycles, capacity retention remains above 70% referring to the initial discharge capacities. Benefiting from the  $\pi$ -conjugated covalent frameworks, the COFs keep good structural and chemical stability as organic electrolyte during the lithium-storage process. Thus, COFs appear as promising electrode materials, providing a feasible way to generate favorable organic electrode materials applied in LIBs for energy storage.

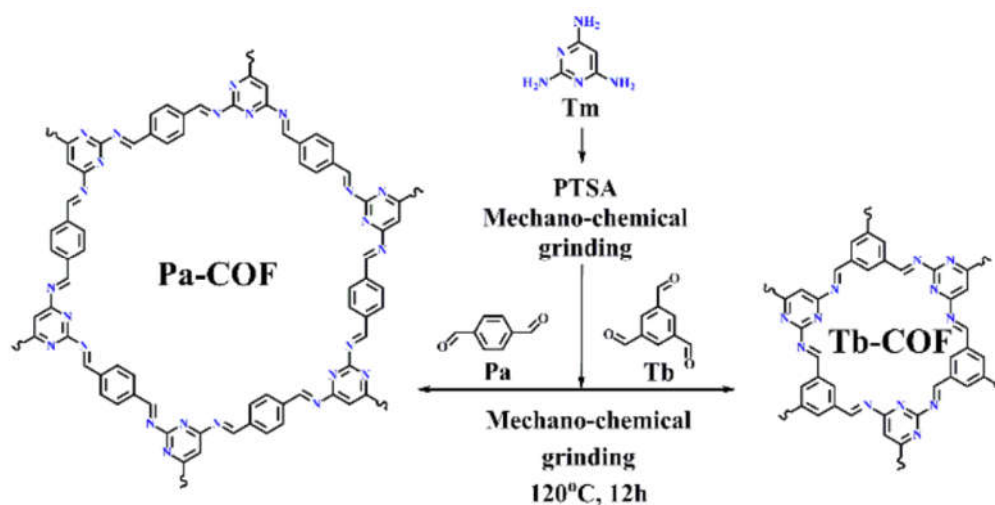


Figure 25. Synthesis and structures of Pa-COF and Tb-COF.<sup>279</sup>

#### 1.4.1.4 COFs based on corroles

The rapid development and numerous applications of COFs have prompted our laboratory to take an interest in COFs chemistry. Our team is specialized in the synthesis and coordination chemistry of porphyrins and corroles. We have seen previously that there are many COFs based on porphyrin moieties but so far, there are only few examples on COFs based on corrole macrocycles. In 2020, two publications were reported by Ma's and Zhang's group respectively. They constructed 2D COFs both based on T-shaped 5,10,15-tris(p-aminophenyl)corrole through Schiff base reaction (Fig. 26). They were built for different applications: (a) photosensitizer, (b) fluorescence sensor. Interestingly, both of them bear the same dissymmetric **hcb** layer. However, by simulation according to PXRD analysis, TPAPC-COF staggered an AB stacking arrangement while CorMeO-COF displayed an AA stacking arrangement probably because of the different linkers. They are both highly crystalline with excellent chemical stability and permanent porosity. The stabilities were checked by treatment with different solvents and aqueous solutions with pH values of 3 and 12. The PXRD patterns presented excellent chemical stability. These results will inspire us to explore new COFs based on different corroles and linkers.

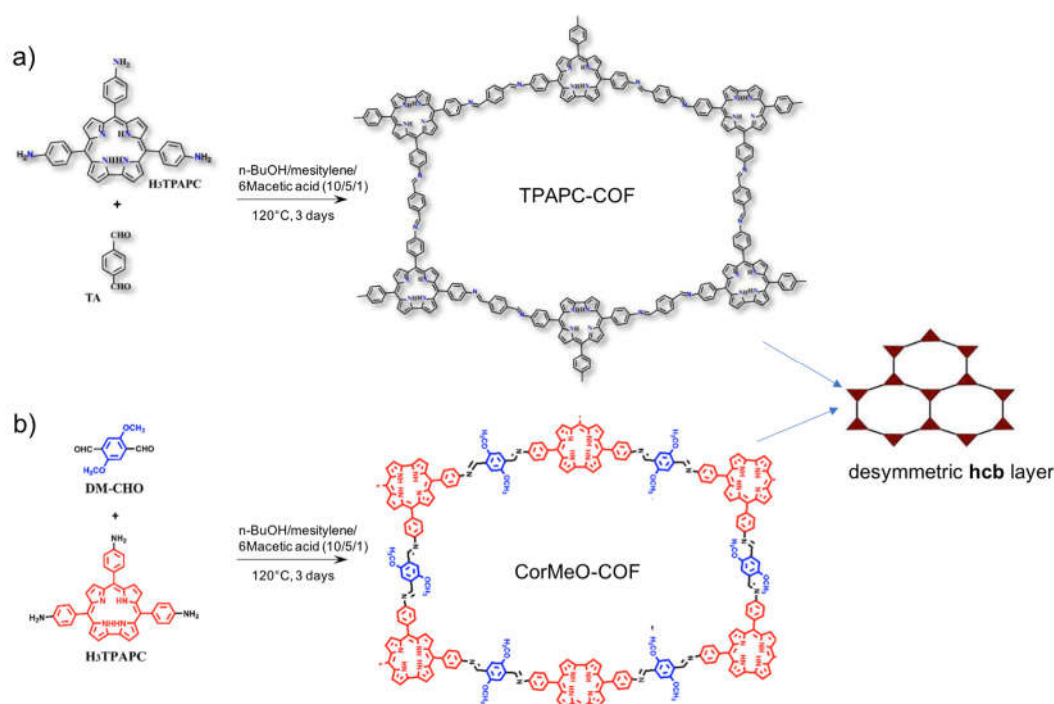


Figure 26. Synthesis and structures of TPAPC-COF (a) and CorMeO-COF (b).<sup>280, 281</sup>

#### 1.4.1.5 Conclusion and Perspectives

In this part, we have reported a comprehensive overview of the structural diversity of covalent organic frameworks developed so far, the accessible variety of COF morphologies, as well as a discussion on demonstrated and potential applications. In recent years, the structural diversity of COFs has greatly expanded, along with an expansion of the scope of COFs. Novel building block structures and geometries have resulted in the development of many COFs with dual or triple pore geometries and new pore shapes. Important knowledge on the factors controlling packing behavior and the crystallinity of COFs as well as insights into the mechanisms of COF formation have been acquired, but many questions remain open. One key challenge in future COF developments is the control of COF crystallization and the development of general rules for the synthesis of highly crystalline COFs. It is anticipated that novel strategies to lock in the spatial positions of building blocks in COFs and thus to achieve improved stacking order will give rise to a pronounced enhancement of their performance in optoelectronics and related applications. The development of new linkage moieties as well as new building blocks in recent years offers numerous possibilities for the design of new COF structures and we expect to see a rapid increase of new structures. Importantly, chemically stable COF linkages open up whole new fields of applications under harsh conditions, including heterogeneous catalysis and electrochemical applications.

#### 1.4.2 Porous organic polymers

Porous organic polymers (POPs) are a class of porous network polymers formed through covalent linkages between organic components. According to the crystallinity, POPs can be generally divided into crystalline materials and amorphous ones (Fig. 27). Amorphous porous organic polymers have been explored into polymers of intrinsic micropores (PIMs),<sup>282, 283</sup> conjugated microporous polymers (CMPs),<sup>284, 285</sup> porous aromatic frameworks (PAFs),<sup>286, 287</sup> *et al.* It is very easy to characterize the order of COFs structures thanks to the dynamic covalent bonding. In contrast, amorphous POPs do not form regular structures and pores. They are obtained according to an irreversible reaction. Covalent bonds are robust and MOFs generally have high stability. This advantage makes them popular on catalyst application because of the high recyclability and stability.<sup>145</sup> Up to date, a great number of amorphous POPs have been

developed mainly by cross-coupling reactions such as Sonogashira,<sup>288, 289</sup> Suzuki,<sup>290, 291</sup> Heck,<sup>292, 293</sup> Click.<sup>294, 295</sup> Similar to MOFs and COFs, porous organic polymers (POPs) are well known for their unique physiochemical properties such as structural diversity,<sup>162</sup> good hydrothermal stability,<sup>296</sup> large surface area,<sup>297</sup> low density.<sup>298</sup> POPs are promising materials for a wide range of applications including gas storage/separation,<sup>299</sup> optoelectronics,<sup>300</sup> catalysis,<sup>271</sup> sensors,<sup>297</sup> drug delivery<sup>301</sup>...

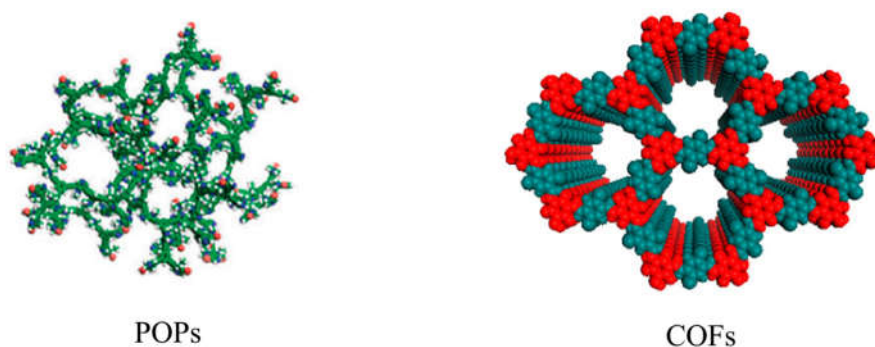


Figure 27. Schematic representation of crystalline COFs and amorphous POPs.<sup>181</sup>

So far to our knowledge, there are only two examples of POPs based on corroles. The first example from our lab was reported in 2019 (Fig. 28).<sup>302</sup> POPs were prepared starting from tetrahedral-shaped building blocks and corrole macrocyclic linkers either as free bases or cobalt complexes. Fig. 28 shows two different synthetic strategies incorporating cobalt corroles into the porous matrix based on Sonogashira cross-coupling reaction between tetra-alkenyl building blocks and diiodo-corrole linkers. The resulted POPs with cobalt corrole showed high permanent porosities and outstanding CO sorption properties with a high selectivity over N<sub>2</sub>, O<sub>2</sub> and CO<sub>2</sub>. Another example of corrole-based POP was published recently by Zhao *et al.* in 2022 (Fig. 29).<sup>303</sup> They have reported porous organic polymers constructed from either Mn or Fe-corrole complexes through Suzuki cross-coupling reaction. The ideal computer-modeled structure is shown in Fig. 29b. The resulted polymers are 2D porous organic polymers, as expected. However, like most amorphous POPs, the PXRD patterns reveal that these CorPOPs are amorphous rather than crystalline. The CorPOP-1(Mn) displays a superior heterogeneous catalytic activity toward solvent-free cycloaddition of carbon dioxide (CO<sub>2</sub>) with high recyclability and stability. These two recent publications on corrole-based porous organic polymers highlight the potential of corrole to construct porous materials for different applications. We were thus inspired by this work to obtain new POPs based on cobalt corrole for CO sorption.

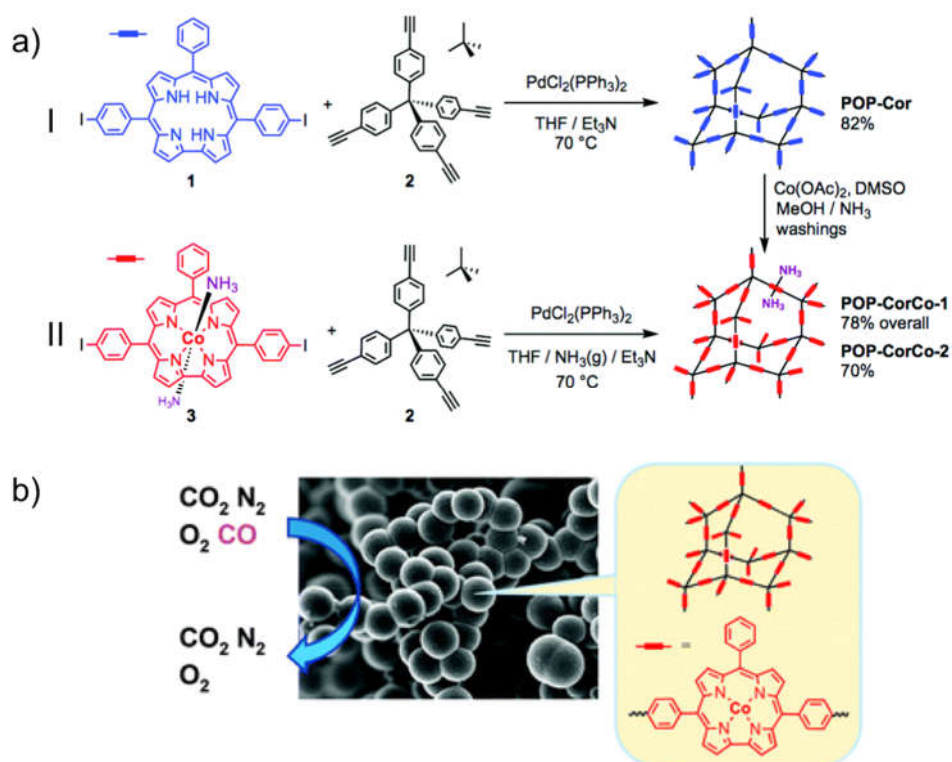


Figure 28. (a) Schematic representation of two synthetic routes for preparing POPs based on cobalt corrole (I) using a post-metalation way and (II) using a direct synthesis from the cobalt corrole complex. (b) selective sorption of cobalt-corrole based POP towards CO vs N<sub>2</sub>, O<sub>2</sub> and CO<sub>2</sub>.<sup>302</sup>

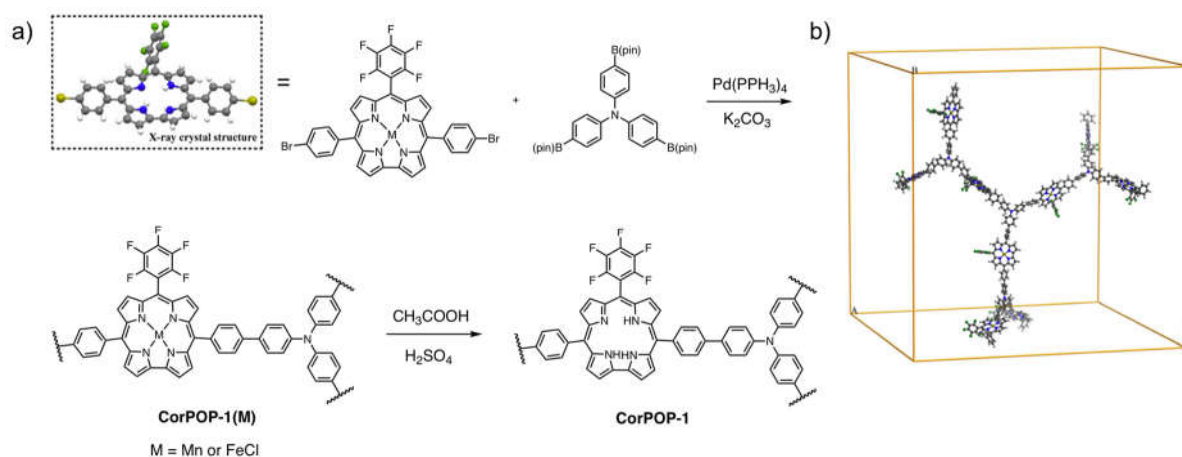


Figure 29. (a) Synthetic route of POPs based on corrole (Mn, FeCl or H<sub>3</sub>) (b) Three-dimensional view of computer-modelled CorPOP-1(Mn).<sup>303</sup>

### 1.4.3 Metal-Organic Frameworks

Metal organic frameworks (MOFs) are a class of polymers made up of organic linkers and metal ions or clusters, also known as porous coordination polymers. MOFs feature many special properties such as high crystallinity, large surface area (ranging from 1000 to 10,000 m<sup>2</sup>/g), high porosity, designable structures compared to traditional porous materials such as zeolites and activated carbons.<sup>304-306</sup> The MOFs family has been explored in the past decades since Yaghi<sup>307</sup> firstly pioneered MOFs in the late 1990s and is still growing rapidly, with thousands of papers published each year.<sup>308</sup> After that, MOFs were distinguished with permanent porosity and high surface areas, due to the strong bonds between metal ions and charged organic ligands.<sup>309</sup> With diversified structures, the pore sizes of MOFs are highly tunable (up to 9.8 nm). With a large variety of metal nodes and theoretically unlimited number of organic linkers, it is easy to tune the compositions and structures of MOFs to achieve targeted functionality in a precise manner. Due to the well-organized structures, huge surface areas, pore volumes, pore size distributions and easily-decorated channels, MOFs have become promising candidates in many applications, including gas storage and separation,<sup>310, 311</sup> luminescence,<sup>312, 313</sup> thin films,<sup>314, 315</sup> proton conduction,<sup>316, 317</sup> catalysis,<sup>318</sup> drug delivery,<sup>319, 320</sup> and energy storage and conversion.<sup>321, 322</sup>

Here we only give a brief introduction to the design of MOFs. Different from COFs or other porous organic materials constructed by organic bonds, MOFs are formed by coordination between metals or metal ions (clusters, multinuclear complexes) and organic multidentate ligands (linkers, see Fig. 30). Basically, the coordination network of MOFs extends through repeating coordination entities in 1, 2, or 3 dimensions. However, during the MOF formation, the fact is that thousands of clusters and linkers can lead to a mixture of molecular 0D complexes, 1D chains, 2D sheets, and 3D frameworks. In order to avoid chaos and obtain the targeted frameworks, mathematical graph theory was applied to design, present and classify the frameworks. Until now, the wide range of these inorganic and organic building blocks offers a great number of MOF topology, enormous flexibility in pore size, shape, and structure, and myriad opportunities for functionalization and grafting which are suitable for a variety of applications.

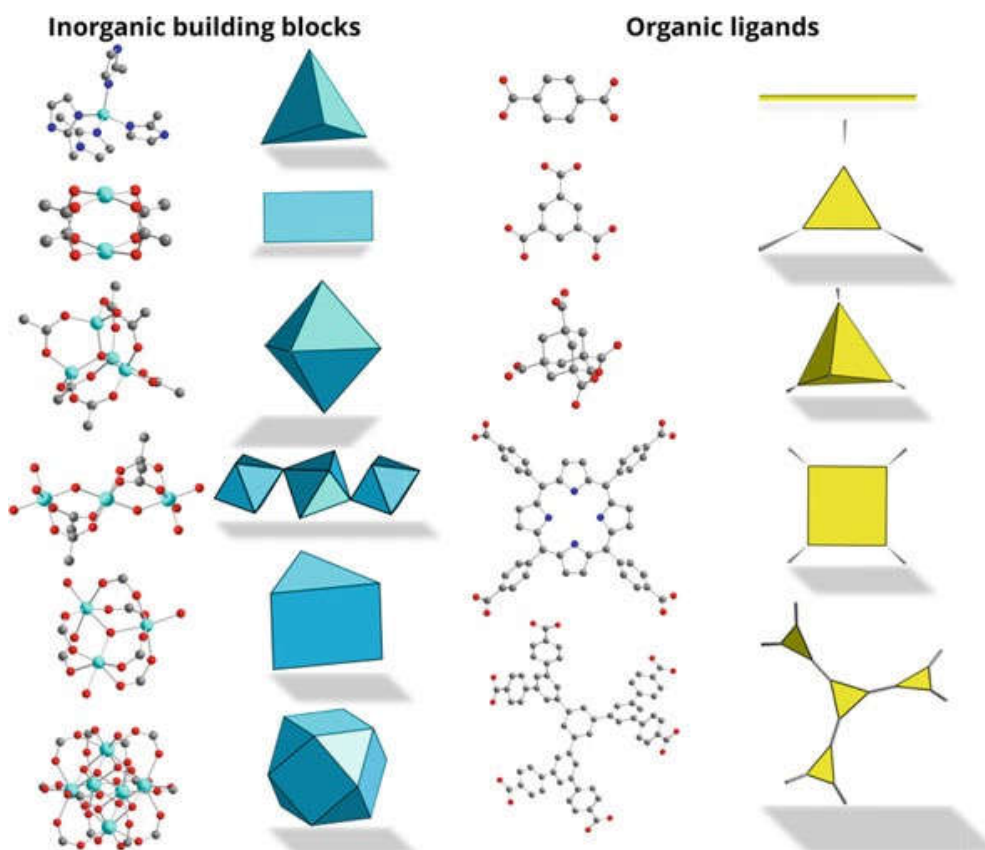


Figure 30. Prototypical examples of the inorganic building blocks and organic ligands, often used for the construction of MOFs.<sup>323</sup>

Up to date, there is a unique example of MOF based on corrole reported (Fig. 31).<sup>324</sup> In 2019, Zhao *et al.* prepared two robust corrole-based metal organic frameworks with zirconium or hafnium clusters. The reported Corrole-MOF-1 and Corrole-MOF-2 were constructed from the 5,10,15-tris(*p*-carboxylphenyl)corrole or iron complex which is considered as ligand and 9-connected  $Zr_6/Hf_6$  clusters. All of them exhibit high stability and porosity, featuring uniform one-dimensional (1D) hexagonal open channels of 23.4 Å. Furthermore, the Corrole-MOF-1(Fe) constructed directly from iron-corrole complex and  $Zr_6$  cluster displayed efficiently catalyze hetero-Diels-Alder (HDA) reactions between unactivated aldehydes and a simple diene. We will thus be able to take inspiration from these results to build a new MOF based on cobalt-corrole complex for CO sorption.

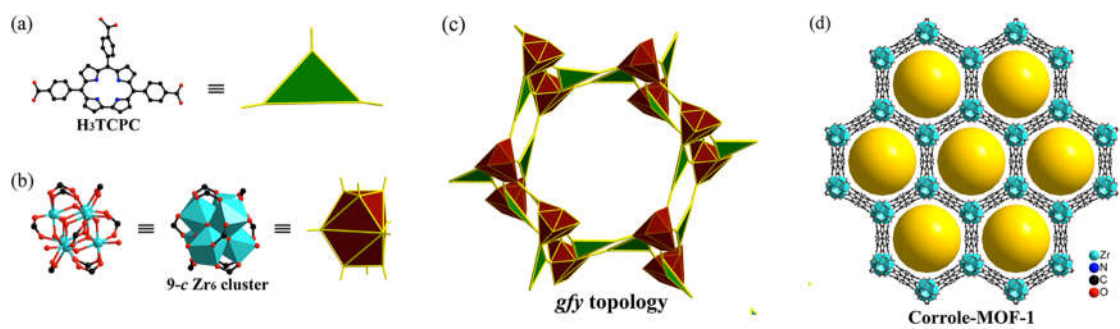


Figure 31. Crystal structure, structural components, and underlying network topology of Corrole-MOF-1 after removal of disorder: (a) tricarboxylic corrolic linker, H<sub>3</sub>TCPC; (b) D<sub>3d</sub>-symmetric 9-connected Zr<sub>6</sub> cluster; (c) schematic representation of the (3,9)-connected net for Corrole-MOF-1 framework; (d) View of Corrole-MOF-1 along the *c* axes, with uniform 1D open channels.<sup>324</sup>

## 1.5 Objectives of the thesis

The early detection of carbon monoxide at low levels is a technological challenge with public and industrial health issues. The electrochemical and semiconductor technologies currently developed make it possible to detect carbon monoxide at concentrations of the order of ten ppm, these thresholds make it possible to avoid fatal intoxication but do not correspond to the criteria of purity of industrial gases or chronic poisoning with low levels of carbon monoxide. In addition, these sensors are not very selective and sensitive to other reducing gases. Infrared detectors allow much lower sensitivity and better selectivity, but their price and size reduce this technology to a niche market. Emerging technologies, especially colorimetric detection, allow low detection thresholds to be reached, but detection reactions are generally irreversible and often not very selective.

During our thesis work, we were therefore interested in SAW sensors. In order to obtain new carbon monoxide detectors, it is necessary to focus first on the development of new sensitive films for these sensors. We therefore decided to focus our work on the development of new porous materials containing cobalt corroles in order to study the efficiency of the metal center on the adsorption of carbon monoxide. We also plan to study the stability and reversibility of these porous materials based on cobalt corroles and to study their gas sorption properties. The ultimate objective of our work is to deposit these new compounds on SAW sensors in order to test them in real conditions (presence of humidity and oxygen) for further detection of CO. The first part of this thesis will deal with the synthesis of various precursors (free-base corroles, porphyrin and platforms) making it possible to obtain new porous materials. Thus, the second part will deal with the synthesis and characterization of COFs. The properties of COFs for the detection of carbon monoxide will also be described in this part.



## References

1. Bonab, M. A. M.; Karimdadashi, R.; Jabbari, G., Design and construction processes of carbon monoxide leak detection system for domestic application. *Mod. Appl. Sci.* **2011**, *5* (2), 161-164.
2. Ryter, S. W.; Sethi, J. M., Exhaled carbon monoxide as a biomarker of inflammatory lung disease. *J. Breath Res.* **2007**, *1* (2), 026004.
3. Han, Y.; Chen, Y.; Ahmad, S.; Feng, Y.; Zhang, F.; Song, W.; Cao, F.; Zhang, Y.; Yang, X.; Li, J.; Zhang, G., High Time- and Size-Resolved Measurements of PM and Chemical Composition from Coal Combustion: Implications for the EC Formation Process. *Environ. Sci. Technol.* **2018**, *52* (11), 6676-6685.
4. Deng, M.; Zhang, S.; Shan, M.; Li, J.; Baumgartner, J.; Carter, E.; Yang, X., The impact of cookstove operation on PM<sub>2.5</sub> and CO emissions: A comparison of laboratory and field measurements. *Environ. Pollut.* **2018**, *243*, 1087-1095.
5. Ng, P. C.; Long, B.; Koyfman, A., Clinical chameleons: an emergency medicine focused review of carbon monoxide poisoning. *Intern. Emerg. Med.* **2018**, *13* (2), 223-229.
6. Dey, S.; Dhal, G. C., Materials progress in the control of CO and CO<sub>2</sub> emission at ambient conditions: An overview. *Mater. Sci. Technol.* **2019**, *2* (3), 607-623.
7. Pham, V. T.; Le, Q. B.; Nguyen, D. A.; Dang, N. D.; Huynh, H. T.; Tran, D. T., Multi-Sensor Data Fusion in A Real-Time Support System for On-Duty Firefighters. *Sensors* **2019**, *19* (21), 4746.
8. Hopper, C. P.; Zambrana, P. N.; Goebel, U.; Wollborn, J., A brief history of carbon monoxide and its therapeutic origins. *Nitric Oxide* **2021**, *111-112*, 45-63.
9. Peers, C.; Steele, D. S., Carbon monoxide: A vital signalling molecule and potent toxin in the myocardium. *J. Mol. Cell. Cardiol.* **2012**, *52* (2), 359-365.
10. Hampson, N. B.; Piantadosi, C. A.; Thom, S. R.; Weaver, L. K., Practice recommendations in the diagnosis, management, and prevention of carbon monoxide poisoning. *Am. J. Respir. Crit. Care Med.* **2012**, *186* (11), 1095-101.
11. Choi, I. S., Carbon monoxide poisoning: systemic manifestations and complications. *J. Korean Med. Sci.* **2001**, *16* (3), 253-261.
12. Akyol, S.; Erdogan, S.; Idiz, N.; Celik, S.; Kaya, M.; Ucar, F.; Dane, S.; Akyol, O., The role of reactive oxygen species and oxidative stress in carbon monoxide toxicity: an in-depth analysis. *Redox Rep.* **2014**, *19* (5), 180-9.

13. Debataraja, A.; Septiani, N. L. W.; Yulianto, B.; Nugraha; Sunendar, B.; Abdullah, H., High performance of a carbon monoxide sensor based on a Pd-doped graphene-tin oxide nanostructure composite. *Ionics*. **2019**, 1-10.
14. Valente-Aguiar, M. S.; Magalhaes, T.; Dinis-Oliveira, R. J.; Valente-Aguiar, M. S.; Magalhaes, T.; Dinis-Oliveira, R. J.; Dinis-Oliveira, R. J., Suicide by Inhalation of Carbon Monoxide of Car Exhausts Fumes. *Curr. Drug Res. Rev.* **2019**, *11* (2), 145-147.
15. Mahajan, S.; Jagtap, S., Metal-oxide semiconductors for carbon monoxide (CO) gas sensing: A review. *Appl. Mater. Today* **2020**, *18*, 100483.
16. Dutta, A.; Kaabbuathong, N.; Grilli, M. L.; Di Bartolomeo, E.; Traversa, E., Study of YSZ-Based Electrochemical Sensors with WO<sub>3</sub> Electrodes in NO<sub>2</sub> and CO Environments. *J. Electrochem. Soc.* **2003**, *150* (2), H33.
17. Brattain, W. H.; Bardeen, J., Surface properties of germanium. *Bell Syst. Tech. J.* **1953**, *32* (1), 1-41.
18. Seiyama, T.; Kato, A.; Fujiishi, K.; Nagatani, M., A New Detector for Gaseous Components Using Semiconductive Thin Films. *Anal. Chem.* **1962**, *34* (11), 1502-1503.
19. Yamazoe, N.; Shimano, K., Receptor Function and Response of Semiconductor Gas Sensor. *J. Sensors* **2009**, *2009*, 875704.
20. Manorama, S. V.; Izu, N.; Shin, W.; Matsubara, I.; Murayama, N., On the platinum sensitization of nanosized cerium dioxide oxygen sensors. *Sens. Actuators B: Chem.* **2003**, *89* (3), 299-304.
21. Fine, G. F.; Cavanagh, L. M.; Afonja, A.; Binions, R., Metal oxide semi-conductor gas sensors in environmental monitoring. *Sensors (Basel)* **2010**, *10* (6), 5469-502.
22. Kanaparthi, S.; Singh, S. G., Chemiresistive Sensor Based on Zinc Oxide Nanoflakes for CO<sub>2</sub> Detection. *ACS Appl. Nano Mater.* **2019**, *2* (2), 700-706.
23. Phanichphant, S., Semiconductor Metal Oxides as Hydrogen Gas Sensors. *Procedia Eng.* **2014**, *87*, 795-802.
24. Jincy, C. S.; Meena, P., Synthesis, characterization, and NH<sub>3</sub> gas sensing application of Zn doped cobalt oxide nanoparticles. *Inorg. Chem. Commun.* **2020**, *120*, 108145.
25. Li, H.-Y.; Huang, L.; Wang, X.-X.; Lee, C.-S.; Yoon, J.-W.; Zhou, J.; Guo, X.; Lee, J.-H., Molybdenum trioxide nanopaper as a dual gas sensor for detecting trimethylamine and hydrogen sulfide. *RSC Adv.* **2017**, *7* (7), 3680-3685.
26. Peterson, P. J. D.; Aujla, A.; Grant, K. H.; Brundle, A. G.; Thompson, M. R.; Vande Hey, J.; Leigh, R. J., Practical Use of Metal Oxide Semiconductor Gas Sensors for Measuring Nitrogen Dioxide and Ozone in Urban Environments. *Sensors* **2017**, *17* (7), 1653.

27. Marín-Hernández, C.; Toscani, A.; Sancenón, F.; Wilton-Ely, J. D. E. T.; Martínez-Máñez, R., Chromo-fluorogenic probes for carbon monoxide detection. *Chem. Commun.* **2016**, 52 (35), 5902-5911.
28. Zhou, Q.; Chen, W.; Xu, L.; Kumar, R.; Gui, Y.; Zhao, Z.; Tang, C.; Zhu, S., Highly sensitive carbon monoxide (CO) gas sensors based on Ni and Zn doped SnO<sub>2</sub> nanomaterials. *Ceram. Int.* **2018**, 44 (4), 4392-4399.
29. Paliwal, A.; Sharma, A.; Tomar, M.; Gupta, V., Carbon monoxide (CO) optical gas sensor based on ZnO thin films. *Sens. Actuators B: Chem.* **2017**, 250, 679-685.
30. Sun, Y.; Zhao, Z.; Suematsu, K.; Li, P.; Yu, Z.; Zhang, W.; Hu, J.; Shimanoe, K., Rapid and Stable Detection of Carbon Monoxide in Changing Humidity Atmospheres Using Clustered In<sub>2</sub>O<sub>3</sub>/CuO Nanospheres. *ACS Sens.* **2020**, 5 (4), 1040-1049.
31. Menetrey, M.; Markovits, A.; Minot, C., Reactivity of a reduced metal oxide surface: hydrogen, water and carbon monoxide adsorption on oxygen defective rutile TiO<sub>2</sub>(110). *Surf. Sci.* **2003**, 524 (1), 49-62.
32. Al-Kuhaili, M. F.; Durrani, S. M. A.; Bakhtiari, I. A., Carbon monoxide gas-sensing properties of CeO<sub>2</sub>-ZnO thin films. *Appl. Surf. Sci.* **2008**, 255 (5, Part 2), 3033-3039.
33. Biabani-Ravandi, A.; Rezaei, M.; Fattah, Z., Catalytic performance of Ag/Fe<sub>2</sub>O<sub>3</sub> for the low temperature oxidation of carbon monoxide. *Chem. Eng. Sci.* **2013**, 219, 124-130.
34. Bittencourt, C.; Felten, A.; Espinosa, E. H.; Ionescu, R.; Llobet, E.; Correig, X.; Pireaux, J. J., WO<sub>3</sub> films modified with functionalised multi-wall carbon nanotubes: Morphological, compositional and gas response studies. *Sens. Actuators B: Chem.* **2006**, 115 (1), 33-41.
35. Sathya Raj, D.; Krishnakumar, T.; Jayaprakash, R.; Prakash, T.; Leonardi, G.; Neri, G., CO sensing characteristics of hexagonal-shaped CdO nanostructures prepared by microwave irradiation. *Sens. Actuators B: Chem.* **2012**, 171-172, 853-859.
36. Nagase, K.; Zheng, Y.; Kodama, Y.; Kakuta, J., Dynamic Study of the Oxidation State of Copper in the Course of Carbon Monoxide Oxidation over Powdered CuO and Cu<sub>2</sub>O. *J. Catal.* **1999**, 187 (1), 123-130.
37. Imamura, S.; Sawada, H.; Uemura, K.; Ishida, S., Oxidation of carbon monoxide catalyzed by manganese-silver composite oxides. *J. Catal.* **1988**, 109 (1), 198-205.
38. Dow, W. P.; Huang, T. J., Effects of Oxygen Vacancy of Yttria-Stabilized Zirconia Support on Carbon Monoxide Oxidation over Copper Catalyst. *J. Catal.* **1994**, 147 (1), 322-332.
39. Bakker, E.; Telting-Diaz, M., Electrochemical Sensors. *Anal. Chem.* **2002**, 74 (12), 2781-2800.

40. Bay, H. W.; Blurton, K. F.; Sedlak, J. M.; Valentine, A. M., Electrochemical technique for the measurement of carbon monoxide. *Anal. Chem.* **1974**, *46* (12), 1837-9.
41. Wojnowski, W.; Majchrzak, T.; Dymerski, T.; Gębicki, J.; Namieśnik, J., Portable Electronic Nose Based on Electrochemical Sensors for Food Quality Assessment. *Sensors (Basel)* **2017**, *17* (12).
42. Mead, M. I.; Popoola, O. A. M.; Stewart, G. B.; Landshoff, P.; Calleja, M.; Hayes, M.; Baldovi, J. J.; McLeod, M. W.; Hodgson, T. F.; Dicks, J.; Lewis, A.; Cohen, J.; Baron, R.; Saffell, J. R.; Jones, R. L., The use of electrochemical sensors for monitoring urban air quality in low-cost, high-density networks. *Atmos. Environ.* **2013**, *70*, 186-203.
43. Majder-Lopatka, M., Effects of interfering gases in electrochemical sensors NH<sub>3</sub> and NO<sub>2</sub>. *MATEC Web Conf.* **2018**, *247*, 00023.
44. Austin, C. C.; Roberge, B.; Goyer, N., Cross-sensitivities of electrochemical detectors used to monitor worker exposures to airborne contaminants: False positive responses in the absence of target analytes. *J. Environ. Monit.* **2006**, *8* (1), 161-166.
45. Cretescu, I.; Lutic, D.; Manea, L. R., Electrochemical Sensors for Monitoring of Indoor and Outdoor Air Pollution. *Electrochem. Sens. Technol.* 2017, IntechOpen, doi:10.5772/intechopen.68512.
46. Djoumi, L.; Vanotti, M.; Blondeau-Patissier, V., Real Time Cascade Impactor Based On Surface Acoustic Wave Delay Lines for PM10 and PM2.5 Mass Concentration Measurement. *Sensors* **2018**, *18* (1), 255.
47. Wohltjen, H.; Dessy, R., Surface acoustic wave probe for chemical analysis. I. Introduction and instrument description. *Anal. Chem.* **1979**, *51* (9), 1458-1464.
48. Devkota, J.; Ohodnicki, P. R.; Greve, D. W., SAW sensors for chemical vapors and gases. *Sensors* **2017**, *17* (4), 801/1-801/28.
49. Waqar, T.; Ersoy, S., Design and Analysis Comparison of Surface Acoustic Wave-Based Sensors for Fabrication Using Additive Manufacturing. *J. Nanomater.* **2021**, *2021*, 5598347.
50. Lucia, F. D.; Jr, P. Z.; Frazatto, F.; Piazzetta, M.; Gobbi, A., Design, Fabrication and Characterization of SAW Pressure Sensors for Extreme Operation Conditions. *Procedia Eng.* **2014**, *87*, 540-543.
51. Khlebarov, Z. P.; Stoyanova, A. I.; Topalova, D. I., Surface acoustic wave gas sensors. *Sens. Actuators B: Chem.* **1992**, *8* (1), 33-40.

52. Bo, L.; Xiao, C.; Cai, H.; Mohammad, M. A.; Tian, X.; Tao, L.; Yi, Y.; Ren, T., Surface acoustic wave devices for sensor applications. *J. Semicond.* **2016**, *37* (2), 021001/1-021001/9.
53. Yunusa, Z.; Hamidon, M. N.; Kaiser, A.; Awang, Z., Gas sensors: a review. *Sens. Transducers J.* **2014**, *168* (4), 61-75, 15 pp.
54. Caliendo, C.; Verardi, P.; Verona, E.; D'Amico, A.; Di Natale, C.; Saggio, G.; Serafini, M.; Paolesse, R.; Huq, S. E., Advances in SAW-based gas sensors. *Smart Mater. Struct.* **1997**, *6* (6), 689-699.
55. Shiokawa, S.; Kondoh, J., Surface acoustic wave sensors. *Jpn. J. Appl. Phys., Part 1* **2004**, *43* (5B), 2799-2802.
56. Drafts, B., Acoustic wave technology sensors. *IEEE Trans. Microwave Theory Tech.* **2001**, *49* (4, Pt. 2), 795-802.
57. Nikolaev, A. L.; Karapetyan, G. Y.; Nesvetaev, D. G.; Lyanguzov, N. V.; Dneprovski, V. G.; Kaidashev, E. M., Preparation and Investigation of ZnO Nanorods Array Based Resistive and SAW CO Gas Sensors. *Springer Proc. Phys.* **2014**, *152* (Advanced Materials), 27-36.
58. Vanotti, M.; Poisson, S.; Soumann, V.; Quesneau, V.; Brandès, S.; Desbois, N.; Yang, J.; André, L.; Gros, C. P.; Blondeau-Patissier, V., Influence of interfering gases on a carbon monoxide differential sensor based on SAW devices functionalized with cobalt and copper corroles. *Sens. Actuators B: Chem.* **2021**, *332*, 129507.
59. Blondeau-Patissier, V.; Vanotti, M.; Prêtre, T.; Rabus, D.; Tortora, L.; Barbe, J. M.; Ballandras, S., Detection and monitoring of carbon monoxide using cobalt corroles film on Love wave devices with delay line configuration. *Procedia Eng.* **2011**, *25*, 1085-1088.
60. Barbe, J.-M.; Canard, G.; Brandes, S.; Guillard, R., Selective chemisorption of carbon monoxide by organic-inorganic hybrid materials incorporating cobalt(III) corroles as sensing components. *Chem. Eur. J.* **2007**, *13* (7), 2118-2129.
61. Quesneau, V.; Shan, W.; Desbois, N.; Brandes, S.; Rousselin, Y.; Vanotti, M.; Blondeau-Patissier, V.; Naitana, M.; Fleurat-Lessard, P.; Van Caemelbecke, E.; Kadish, K. M.; Gros, C. P., Cobalt Corroles with Bis-Ammonia or Mono-DMSO Axial Ligands. Electrochemical, Spectroscopic Characterizations and Ligand Binding Properties. *Eur. J. Inorg. Chem.* **2018**, *2018* (38), 4265-4277.
62. Senge, M. O.; Sergeeva, N. N.; Hale, K. J., Classic highlights in porphyrin and porphyrinoid total synthesis and biosynthesis. *Chem. Soc. Rev.* **2021**, *50* (7), 4730-4789.

63. Dedić, D.; Dorniak, A.; Rinner, U.; Schöfberger, W., Recent Progress in (Photo)-Electrochemical Conversion of CO<sub>2</sub> With Metal Porphyrinoid-Systems. *Front. Chem.* **2021**, *9* (540).
64. Orłowski, R.; Gryko, D.; Gryko, D. T., Synthesis of Corroles and Their Heteroanalogs. *Chem. Rev.* **2017**, *117* (4), 3102-3137.
65. Aviv-Harel, I.; Gross, Z., Coordination chemistry of corroles with focus on main group elements. *Coord. Chem. Rev.* **2011**, *255* (7), 717-736.
66. Johnson, A. W.; Kay, I. T., 306. Corroles. Part I. Synthesis. *J. Chem. Soc. (Resumed)* **1965**, (0), 1620-1629.
67. Paolesse, R.; Mini, S.; Sagone, F.; Boschi, T.; Jaquinod, L.; J. Nurco, D.; M. Smith, K., 5,10,15-Triphenylcorrole: a product from a modified Rothmund reaction. *Chem. Commun.* **1999**, (14), 1307-1308.
68. Gross, Z.; Galili, N.; Saltsman, I., The First Direct Synthesis of Corroles from Pyrrole. *Angew. Chem. Int. Ed. Engl.* **1999**, *38* (10), 1427-1429.
69. Koszarna, B.; Gryko, D. T., Efficient Synthesis of meso-Substituted Corroles in a H<sub>2</sub>O–MeOH Mixture. *J. Org. Chem.* **2006**, *71* (10), 3707-3717.
70. Paolesse, R.; Nardis, S.; Sagone, F.; Khoury, R. G., Synthesis and Functionalization of meso-Aryl-Substituted Corroles. *J. Org. Chem.* **2001**, *66* (2), 550-556.
71. Gross, Z.; Galili, N.; Simkhovich, L.; Saltsman, I.; Botoshansky, M.; Bläser, D.; Boese, R.; Goldberg, I., Solvent-Free Condensation of Pyrrole and Pentafluorobenzaldehyde: A Novel Synthetic Pathway to Corrole and Oligopyrromethenes. *Org. Lett.* **1999**, *1* (4), 599-602.
72. Zipp, C. F.; Michael, J. P.; Fernandes, M. A.; Marques, H. M., The synthesis and characterization of several corroles : research article. *S. Afr. J. Chem.* **2013**, *66* (1), 158-166.
73. Gryko, D. T.; Jadach, K., A Simple and Versatile One-Pot Synthesis of meso-Substituted trans-A<sub>2</sub>B-Corroles. *J. Org. Chem.* **2001**, *66* (12), 4267-4275.
74. Rao, P. D.; Dhanalekshmi, S.; Littler, B. J.; Lindsey, J. S., Rational Syntheses of Porphyrins Bearing up to Four Different Meso Substituents. *J. Org. Chem.* **2000**, *65* (22), 7323-7344.
75. Laha, J. K.; Dhanalekshmi, S.; Taniguchi, M.; Ambroise, A.; Lindsey, J. S., A Scalable Synthesis of Meso-Substituted Dipyrromethanes. *Org. Process Res. Dev.* **2003**, *7* (6), 799-812.

76. Lee, C.-H.; S. Lindsey, J., One-flask synthesis of meso-substituted dipyrromethanes and their application in the synthesis of trans-substituted porphyrin building blocks. *Tetrahedron* **1994**, *50* (39), 11427-11440.
77. Nardis, S.; Mandoj, F.; Stefanelli, M.; Paolesse, R., Metal complexes of corrole. *Coord. Chem. Rev.* **2019**, *388*, 360-405.
78. Mondal, S.; Naik, P. K.; Adha, J. K.; Kar, S., Synthesis, characterization, and reactivities of high valent metal-corrole (M = Cr, Mn, and Fe) complexes. *Coord. Chem. Rev.* **2019**, *400*, 213043.
79. Alemayehu, A. B.; McCormick, L. J.; Vazquez-Lima, H.; Ghosh, A., Relativistic Effects on a Metal-Metal Bond: Osmium Corrole Dimers. *Inorg. Chem.* **2019**, *58* (4), 2798-2806.
80. Kumar, A.; Yadav, P.; Majdoub, M.; Saltsman, I.; Fridman, N.; Kumar, S.; Kumar, A.; Mahammed, A.; Gross, Z., Corroles: The Hitherto Elusive Parent Macrocyclic and its Metal Complexes. *Angew. Chem., Int. Ed.* **2021**, *60* (47), 25097-25103.
81. Di Natale, C.; Gros, C. P.; Paolesse, R., Corroles at work: a small macrocycle for great applications. *Chem. Soc. Rev.* **2022**, *51* (4), 1277-1335.
82. Ueta, K.; Fukuda, M.; Kim, G.; Shimizu, S.; Tanaka, T.; Kim, D.; Osuka, A., The First Silicon(IV) Corrole Complexes: Synthesis, Structures, Properties, and Formation of a  $\mu$ -Oxo Dimer. *Chem. Eur. J.* **2018**, *24* (30), 7637-7646.
83. Pomarico, G.; Monti, D.; Bischetti, M.; Savoldelli, A.; Fronczek, F. R.; Smith, K. M.; Genovese, D.; Prodi, L.; Paolesse, R., Silicon(IV) Corroles. *Chemistry* **2018**, *24* (33), 8438-8446.
84. Einrem, R. F.; Braband, H.; Fox, T.; Vazquez-Lima, H.; Alberto, R.; Ghosh, A., Synthesis and Molecular Structure of  $^{99}\text{Tc}$  Corroles. *Chem. Eur. J.* **2016**, *22* (52), 18747-18751.
85. Ziegler, J. A.; Buckley, H. L.; Arnold, J., Synthesis and reactivity of tantalum corrole complexes. *Dalton trans.* **2017**, *46* (3), 780-785.
86. Armstrong, K. C.; Hohloch, S.; Lohrey, T. D.; Zarkesh, R. A.; Arnold, J.; Anstey, M. R., Control of clustering behavior in anionic cerium(III) corrole complexes: from oligomers to monomers. *Dalton trans.* **2016**, *45* (46), 18653-18660.
87. Aviv, I.; Gross, Z., Corrole-based applications. *Chem. Comm.* **2007**, (20), 1987-1999.
88. Liu, H.-Y.; Mahmood, M. H. R.; Qiu, S.-X.; Chang, C. K., Recent developments in manganese corrole chemistry. *Coord. Chem. Rev.* **2013**, *257* (7), 1306-1333.
89. Zhang, Y.; Wang, Q.; Wen, J.; Wang, X.; Mahmood, M. H.; Ji, L.; Liu, H., DNA Binding and Oxidative Cleavage by a Water-soluble Carboxyl Manganese(III) Corrole. *Chinese J. Chem.* **2013**, *31* (10), 1321-1328.

90. Teo, R. D.; Hwang, J. Y.; Termini, J.; Gross, Z.; Gray, H. B., Fighting Cancer with Corroles. *Chem. Rev.* **2017**, *117* (4), 2711-2729.
91. Lemon, C. M.; Marletta, M. A., Corrole-Substituted Fluorescent Heme Proteins. *Inorg. Chem.* **2021**, *60* (4), 2716-2729.
92. Lopes, S. M. M.; Pineiro, M.; Pinho e Melo, T. M. V. D., Corroles and Hexaphyrins: Synthesis and Application in Cancer Photodynamic Therapy. *Molecules* **2020**, *25* (15), 3450.
93. Sinha, W.; Sommer, M. G.; Deibel, N.; Ehret, F.; Bauer, M.; Sarkar, B.; Kar, S., Experimental and Theoretical Investigations of the Existence of Cu<sup>II</sup>, Cu<sup>III</sup>, and Cu<sup>IV</sup> in Copper Corrolato Complexes. *Angew. Chem. Int. Ed.* **2015**, *54* (46), 13769-13774.
94. Alemayehu, A. B.; McCormick, L. J.; Gagnon, K. J.; Borisov, S. M.; Ghosh, A. Stable Platinum(IV) Corroles: Synthesis, Molecular Structure, and Room-Temperature Near-IR Phosphorescence. *ACS Omega* **2018**, *3* (8), 9360-9368.
95. Yadav, O.; Varshney, A.; Kumar, A., Manganese(III) mediated synthesis of A<sub>2</sub>B Mn(III) corroles: A new general and green synthetic approach and characterization. *Inorg. Chem. Comm.* **2017**, *86*, 168-171.
96. Paolesse, R.; Nardis, S.; Monti, D.; Stefanelli, M.; Di Natale, C., Porphyrinoids for Chemical Sensor Applications. *Chem. Rev.* **2017**, *117* (4), 2517-2583.
97. Brennan, B. J.; Lam, Y. C.; Kim, P. M.; Zhang, X.; Brudvig, G. W., Photoelectrochemical Cells Utilizing Tunable Corroles. *ACS Appl. Mater. Interfaces* **2015**, *7* (29), 16124-16130.
98. Chen, T.-H.; Kwong, K. W.; Lee, N. F.; Ranburger, D.; Zhang, R., Highly efficient and chemoselective oxidation of sulfides catalyzed by iron(III) corroles with iodobenzene diacetate. *Inorganica Chim. Acta* **2016**, *451*, 65-72.
99. Barbe, J.-M.; Canard, G.; Brandès, S.; Guillard, R., Selective Chemisorption of Carbon Monoxide by Organic–Inorganic Hybrid Materials Incorporating Cobalt(III) Corroles as Sensing Components. *Chem. Eur. J.* **2007**, *13* (7), 2118-2129.
100. Barbe, J.-M.; Canard, G.; Brandès, S.; Guillard, R., Organic–Inorganic Hybrid Sol–Gel Materials Incorporating Functionalized Cobalt(III) Corroles for the Selective Detection of CO. *Angew. Chem. Int. Ed.* **2005**, *44* (20), 3103-3106.
101. Barbe, J.-M.; Canard, G.; Brandès, S.; Jérôme, F.; Dubois, G.; Guillard, R., Metallocorroles as sensing components for gas sensors: remarkable affinity and selectivity of cobalt(III) corroles for CO vs. O<sub>2</sub> and N<sub>2</sub>. *Dalton Trans.* **2004**, (8), 1208-1214.

102. Fang, Y.; Ou, Z.; Kadish, K. M., Electrochemistry of Corroles in Nonaqueous Media. *Chem. Rev.* **2017**, *117* (4), 3377-3419.
103. Zhou, Y.; Xing, Y.-F.; Wen, J.; Ma, H.-B.; Wang, F.-B.; Xia, X.-H., Axial Ligands Tailoring the ORR Activity of Cobalt Porphyrin. *Sci. Bull.* **2019**, *64* (16), 1158-1166.
104. Kadish, K. M.; Shen, J.; Frémond, L.; Chen, P.; El Ojaimi, M.; Chkounda, M.; Gros, C. P.; Barbe, J.-M.; Ohkubo, K.; Fukuzumi, S.; Guillard, R., Clarification of the Oxidation State of Cobalt Corroles in Heterogeneous and Homogeneous Catalytic Reduction of Dioxygen. *Inorg. Chem.* **2008**, *47* (15), 6726-6737.
105. Kadish, K. M.; Smith, K. M.; Guiland, R.; Editors, *The Porphyrin Handbook: Volume 16 / Phthalocyanines: Spectroscopic and Electrochemical Characterization*. Academic Press: 2003; 288.
106. Ganguly, S.; Conradie, J.; Bendix, J.; Gagnon, K. J.; McCormick, L. J.; Ghosh, A., Electronic Structure of Cobalt–Corrole–Pyridine Complexes: Noninnocent Five-Coordinate Co(II) Corrole–Radical States. *J. Phys. Chem. A* **2017**, *121* (50), 9589-9598.
107. Simkhovich, L.; Galili, N.; Saltsman, I.; Goldberg, I.; Gross, Z., Coordination Chemistry of the Novel 5,10,15-Tris(pentafluorophenyl)corrole: Synthesis, Spectroscopy, and Structural Characterization of Its Cobalt(III), Rhodium(III), and Iron(IV) Complexes. *Inorg. Chem.* **2000**, *39* (13), 2704-2705.
108. Dong, S. S.; Nielsen, R. J.; Palmer, J. H.; Gray, H. B.; Gross, Z.; Dasgupta, S.; Goddard, W. A., Electronic Structures of Group 9 Metallocorroles with Axial Amines. *Inorg. Chem.* **2011**, *50* (3), 764-770.
109. Maiti, N.; Lee, J.; Kwon, S. J.; Kwak, J.; Do, Y.; Churchill, D. G., Synthetic, crystallographic and electrochemical studies of thienyl-substituted corrole complexes of copper and cobalt. *Polyhedron* **2006**, *25* (7), 1519-1530.
110. Will, S.; Lex, J.; Vogel, E.; Adamian, V. A.; Van Caemelbecke, E.; Kadish, K. M., Synthesis, Characterization, and Electrochemistry of  $\sigma$ -Bonded Cobalt Corroles in High Oxidation States. *Inorg. Chem.* **1996**, *35* (19), 5577-5583.
111. Shah, M. N.; Pathipati, S. R.; Mehmood, S.; Kahn, F. U.; Sohail, M.; Ullah, B.; Yang, Y.; Pan, X., Stable Cobalt Porphyrin Ometed Type Small Molecule Sensor for the Sensitive and Selective Detection of Ammonia Gas at Room Temperature. *Adv. Mater. Technol.* **2021**, *6* (9), 2100147.
112. Ganguly, S.; Renz, D.; Giles, L. J.; Gagnon, K. J.; McCormick, L. J.; Conradie, J.; Sarangi, R.; Ghosh, A., Cobalt- and Rhodium-Corrole-Triphenylphosphine Complexes

- Revisited: The Question of a Noninnocent Corrole. *Inorg. Chem.* **2017**, *56* (24), 14788-14800.
113. Osterloh, W. R.; Quesneau, V.; Desbois, N.; Brandès, S.; Shan, W.; Blondeau-Patissier, V.; Paollesse, R.; Gros, C. P.; Kadish, K. M., Synthesis and the Effect of Anions on the Spectroscopy and Electrochemistry of Mono(dimethyl sulfoxide)-Ligated Cobalt Corroles. *Inorg. Chem.* **2020**, *59* (1), 595-611.
  114. Hitchcock, P. B.; McLaughlin, G. M., Five-co-ordinate cobalt(III): crystal and molecular structure of corrole(triphenylphosphine)cobalt(III). *J. Chem. Soc., Dalton Trans.* **1976**, (19), 1927-1930.
  115. Jiang, X.; Naitana, M. L.; Desbois, N.; Quesneau, V.; Brandès, S.; Rousselin, Y.; Shan, W.; Osterloh, W. R.; Blondeau-Patissier, V.; Gros, C. P.; Kadish, K. M., Electrochemistry of Bis(pyridine)cobalt (Nitrophenyl)corroles in Nonaqueous Media. *Inorg. Chem.* **2018**, *57* (3), 1226-1241.
  116. Simkhovich, L.; Goldberg, I.; Gross, Z., Easy Preparation of Cobalt Corrole and Hexaphyrin and Isolation of New Oligopyrroles in the Solvent-Free Condensation of Pyrrole with Pentafluorobenzaldehyde. *Org. Lett.* **2003**, *5* (8), 1241-1244.
  117. Huang, S.; Fang, Y.; Lü, A.; Lu, G.; Ou, Z.; Kadish, K. M., Synthesis, characterization and solvent/structural effects on spectral and redox properties of cobalt triphenylcorroles in nonaqueous media. *J. Porphyr. Phthalocyanines* **2012**, *16* (07n08), 958-967.
  118. Barbe, J.-M.; Canard, G.; Brandes, S.; Guillard, R., Organic-inorganic hybrid sol-gel materials incorporating functionalized cobalt(III) corroles for the selective detection of CO. *Angew. Chem., Int. Ed.* **2005**, *44* (20), 3103-3106.
  119. Vanotti, M.; Blondeau-Patissier, V.; Rabus, D.; Rauch, J.-Y.; Barbe, J.-M.; Ballandras, S., Development of acoustic devices functionalized with cobalt corroles or metalloporphyrines for the detection of carbon monoxide at low concentration. *Sens. Transducers J.* **2012**, *14-1* (Spec. Issue), 197-211.
  120. Taylor, R. G. D.; Bezzu, C. G.; Carta, M.; Msayib, K. J.; Walker, J.; Short, R.; Kariuki, B. M.; McKeown, N. B., The Synthesis of Organic Molecules of Intrinsic Microporosity Designed to Frustrate Efficient Molecular Packing. *Chem. Eur. J.* **2016**, *22* (7), 2466-2472.
  121. Jiao, Y.; Stillinger, F. H.; Torquato, S., Optimal Packings of Superdisks and the Role of Symmetry. *Phys. Rev. Lett.* **2008**, *100* (24), 245504.
  122. Jiao, Y.; Stillinger, F. H.; Torquato, S., Optimal packings of superballs. *Phys. Rev. E* **2009**, *79* (4), 041309.

123. Li, Z.; Feng, X.; Zou, Y.; Zhang, Y.; Xia, H.; Liu, X.; Mu, Y., A 2D azine-linked covalent organic framework for gas storage applications. *Chem. Comm.* **2014**, *50* (89), 13825-13828.
124. Li, Z.; Zhi, Y.; Feng, X.; Ding, X.; Zou, Y.; Liu, X.; Mu, Y., An Azine-Linked Covalent Organic Framework: Synthesis, Characterization and Efficient Gas Storage. *Chem. Eur. J.* **2015**, *21* (34), 12079-12084.
125. Stegbauer, L.; Hahn, M. W.; Jentys, A.; Savasci, G.; Ochsenfeld, C.; Lercher, J. A.; Lotsch, B. V., Tunable Water and CO<sub>2</sub> Sorption Properties in Isostructural Azine-Based Covalent Organic Frameworks through Polarity Engineering. *Chem. Mater.* **2015**, *27* (23), 7874-7881.
126. Huang, N.; Chen, X.; Krishna, R.; Jiang, D., Two-Dimensional Covalent Organic Frameworks for Carbon Dioxide Capture through Channel-Wall Functionalization. *Angew. Chem. Int. Ed.* **2015**, *54* (10), 2986-2990.
127. Yuan, K.; Liu, C.; Han, J.; Yu, G.; Wang, J.; Duan, H.; Wang, Z.; Jian, X., Phthalazinone structure-based covalent triazine frameworks and their gas adsorption and separation properties. *RSC Adv.* **2016**, *6* (15), 12009-12020.
128. Wang, K.; Huang, H.; Liu, D.; Wang, C.; Li, J.; Zhong, C., Covalent Triazine-Based Frameworks with Ultramicropores and High Nitrogen Contents for Highly Selective CO<sub>2</sub> Capture. *Environ. Sci. Technol.* **2016**, *50* (9), 4869-4876.
129. Ben, T.; Pei, C.; Zhang, D.; Xu, J.; Deng, F.; Jing, X.; Qiu, S., Gas storage in porous aromatic frameworks (PAFs). *Energy Environ. Sci.* **2011**, *4* (10), 3991-3999.
130. Ding, S.-Y.; Gao, J.; Wang, Q.; Zhang, Y.; Song, W.-G.; Su, C.-Y.; Wang, W., Construction of Covalent Organic Framework for Catalysis: Pd/COF-LZU1 in Suzuki–Miyaura Coupling Reaction. *J. Am. Chem. Soc.* **2011**, *133* (49), 19816-19822.
131. Fang, Q.; Gu, S.; Zheng, J.; Zhuang, Z.; Qiu, S.; Yan, Y., 3D Microporous Base-Functionalized Covalent Organic Frameworks for Size-Selective Catalysis. *Angew. Chem. Int. Ed.* **2014**, *53* (11), 2878-2882.
132. Xu, H.; Tao, S.; Jiang, D., Proton conduction in crystalline and porous covalent organic frameworks. *Nat. Mater.* **2016**, *15* (7), 722-726.
133. Ma, H.; Liu, B.; Li, B.; Zhang, L.; Li, Y.-G.; Tan, H.-Q.; Zang, H.-Y.; Zhu, G., Cationic Covalent Organic Frameworks: A Simple Platform of Anionic Exchange for Porosity Tuning and Proton Conduction. *J. Am. Chem. Soc.* **2016**, *138* (18), 5897-5903.

134. Zhao, Y.; Yao, K. X.; Teng, B.; Zhang, T.; Han, Y., A perfluorinated covalent triazine-based framework for highly selective and water-tolerant CO<sub>2</sub> capture. *Energy Environ. Sci.* **2013**, *6* (12), 3684-3692.
135. Li, B.; Zhang, Y.; Krishna, R.; Yao, K.; Han, Y.; Wu, Z.; Ma, D.; Shi, Z.; Pham, T.; Space, B.; Liu, J.; Thallapally, P. K.; Liu, J.; Chrzanowski, M.; Ma, S., Introduction of  $\pi$ -Complexation into Porous Aromatic Framework for Highly Selective Adsorption of Ethylene over Ethane. *J. Am. Chem. Soc.* **2014**, *136* (24), 8654-8660.
136. Xu, F.; Chen, X.; Tang, Z.; Wu, D.; Fu, R.; Jiang, D., Redox-active conjugated microporous polymers: a new organic platform for highly efficient energy storage. *Chem. Comm.* **2014**, *50* (37), 4788-4790.
137. Kou, Y.; Xu, Y.; Guo, Z.; Jiang, D., Supercapacitive Energy Storage and Electric Power Supply Using an Aza-Fused  $\pi$ -Conjugated Microporous Framework. *Angew. Chem. Int. Ed.* **2011**, *50* (37), 8753-8757.
138. Gu, C.; Huang, N.; Chen, Y.; Qin, L.; Xu, H.; Zhang, S.; Li, F.; Ma, Y.; Jiang, D.,  $\pi$ -Conjugated Microporous Polymer Films: Designed Synthesis, Conducting Properties, and Photoenergy Conversions. *Angew. Chem. Int. Ed.* **2015**, *54* (46), 13594-13598.
139. Wan, S.; Guo, J.; Kim, J.; Ihee, H.; Jiang, D., A Belt-Shaped, Blue Luminescent, and Semiconducting Covalent Organic Framework. *Angew. Chem. Int. Ed.* **2008**, *47* (46), 8826-8830.
140. Wan, S.; Guo, J.; Kim, J.; Ihee, H.; Jiang, D., A Photoconductive Covalent Organic Framework: Self-Condensed Arene Cubes Composed of Eclipsed 2D Polypyrene Sheets for Photocurrent Generation. *Angew. Chem. Int. Ed.* **2009**, *48* (30), 5439-5442.
141. Sprick, R. S.; Jiang, J.-X.; Bonillo, B.; Ren, S.; Ratvijitvech, T.; Guiglion, P.; Zwiijnenburg, M. A.; Adams, D. J.; Cooper, A. I., Tunable Organic Photocatalysts for Visible-Light-Driven Hydrogen Evolution. *J. Am. Chem. Soc.* **2015**, *137* (9), 3265-3270.
142. Vyas, V. S.; Haase, F.; Stegbauer, L.; Savasci, G.; Podjaski, F.; Ochsenfeld, C.; Lotsch, B. V., A tunable azine covalent organic framework platform for visible light-induced hydrogen generation. *Nat. Comm.* **2015**, *6* (1), 8508.
143. Zhang, J.-H.; Xie, S.-M.; Chen, L.; Wang, B.-J.; He, P.-G.; Yuan, L.-M., Homochiral Porous Organic Cage with High Selectivity for the Separation of Racemates in Gas Chromatography. *Anal. Chem.* **2015**, *87* (15), 7817-7824.
144. Xie, S.-M.; Zhang, J.-H.; Fu, N.; Wang, B.-J.; Chen, L.; Yuan, L.-M., A chiral porous organic cage for molecular recognition using gas chromatography. *Anal. Chim. Acta* **2016**, *903*, 156-163.

145. Fang, Q.; Wang, J.; Gu, S.; Kaspar, R. B.; Zhuang, Z.; Zheng, J.; Guo, H.; Qiu, S.; Yan, Y., 3D Porous Crystalline Polyimide Covalent Organic Frameworks for Drug Delivery. *J. Am. Chem. Soc.* **2015**, *137* (26), 8352-8355.
146. Pei, C.; Ben, T.; Xu, S.; Qiu, S., Ultrahigh iodine adsorption in porous organic frameworks. *J. Mater. Chem.* **2014**, *2* (20), 7179-7187.
147. Li, H.; Meng, B.; Chai, S.-H.; Liu, H.; Dai, S., Hyper-crosslinked  $\beta$ -cyclodextrin porous polymer: an adsorption-facilitated molecular catalyst support for transformation of water-soluble aromatic molecules. *Chem. Sci.* **2016**, *7* (2), 905-909.
148. Yu, S.-B.; Lyu, H.; Tian, J.; Wang, H.; Zhang, D.-W.; Liu, Y.; Li, Z.-T., A polycationic covalent organic framework: a robust adsorbent for anionic dye pollutants. *Polym. Chem.* **2016**, *7* (20), 3392-3397.
149. Rouquerol, J.; Avnir, D.; Fairbridge, C. W.; Everett, D. H.; Haynes, J. M.; Pernicone, N.; Ramsay, J. D. F.; Sing, K. S. W.; Unger, K. K., Recommendations for the characterization of porous solids (Technical Report). *Pure Appl. Chem.* **1994**, *66* (8), 1739-1758.
150. Sing, K. S. W., Reporting physisorption data for gas/solid systems with special reference to the determination of surface area and porosity (Recommendations 1984). *Pure Appl. Chem.* **1985**, *57* (4), 603-619.
151. Ke, Z.; Cheng, Y.; Yang, S.; Li, F.; Ding, L., Modification of COF-108 via impregnation/functionalization and Li-doping for hydrogen storage at ambient temperature. *Int. J. Hydrog. Energy* **2017**, *42* (16), 11461-11468.
152. Ding, X.; Guo, J.; Feng, X.; Honsho, Y.; Guo, J.; Seki, S.; Maitrad, P.; Saeki, A.; Nagase, S.; Jiang, D., Synthesis of Metallophthalocyanine Covalent Organic Frameworks That Exhibit High Carrier Mobility and Photoconductivity. *Angew. Chem. Int. Ed.* **2011**, *50* (6), 1289-1293.
153. Gao, Q.; Bai, L.; Zhang, X.; Wang, P.; Li, P.; Zeng, Y.; Zou, R.; Zhao, Y., Synthesis of Microporous Nitrogen-Rich Covalent-Organic Framework and Its Application in CO<sub>2</sub> Capture. *Chinese J. Chem.* **2015**, *33* (1), 90-94.
154. Xiong, Y.; Qin, Y.; Su, L.; Ye, F., Bioinspired Synthesis of Cu<sup>2+</sup>-Modified Covalent Triazine Framework: A New Highly Efficient and Promising Peroxidase Mimic. *Chemistry* **2017**, *23* 46, 11037-11045.
155. Das, G.; Biswal, B. P.; Kandambeth, S.; Venkatesh, V.; Kaur, G.; Addicoat, M.; Heine, T.; Verma, S.; Banerjee, R., Chemical sensing in two dimensional porous covalent organic nanosheets. *Chem. Sci.* **2015**, *6* (7), 3931-3939.

156. Feng, D.; Xia, Y., Covalent organic framework as efficient desorption/ionization matrix for direct detection of small molecules by laser desorption/ionization mass spectrometry. *Anal. Chim. Acta* **2018**, *1014*, 58-63.
157. Qian, H.-L.; Yang, C.-X.; Wang, W.-L.; Yang, C.; Yan, X.-P., Advances in covalent organic frameworks in separation science. *J. Chromatogr. A* **2018**, *1542*, 1-18.
158. Sun, Q.; Fu, C.-W.; Aguila, B.; Perman, J.; Wang, S.; Huang, H.-Y.; Xiao, F.-S.; Ma, S., Pore Environment Control and Enhanced Performance of Enzymes Infiltrated in Covalent Organic Frameworks. *J. Am. Chem. Soc.* **2018**, *140* (3), 984-992.
159. Gao, C.; Lin, G.; Lei, Z.; Zheng, Q.; Lin, J.; Lin, Z., Facile synthesis of core-shell structured magnetic covalent organic framework composite nanospheres for selective enrichment of peptides with simultaneous exclusion of proteins. *J. Mater. Chem. B* **2017**, *5* (36), 7496-7503.
160. Bai, L.; Phua, S. Z. F.; Lim, W. Q.; Jana, A.; Luo, Z.; Tham, H. P.; Zhao, L.; Gao, Q.; Zhao, Y., Nanoscale covalent organic frameworks as smart carriers for drug delivery. *Chem. Comm.* **2016**, *52* (22), 4128-4131.
161. Tan, J.; Namuangruk, S.; Kong, W.; Kungwan, N.; Guo, J.; Wang, C., Manipulation of Amorphous-to-Crystalline Transformation: Towards the Construction of Covalent Organic Framework Hybrid Microspheres with NIR Photothermal Conversion Ability. *Angew. Chem. Int. Ed.* **2016**, *55* (45), 13979-13984.
162. Das, S.; Heasman, P.; Ben, T.; Qiu, S., Porous Organic Materials: Strategic Design and Structure-Function Correlation. *Chem. Rev.* **2017**, *117* (3), 1515-1563.
163. Kang, Z.; Peng, Y.; Qian, Y.; Yuan, D.; Addicoat, M. A.; Heine, T.; Hu, Z.; Tee, L.; Guo, Z.; Zhao, D., Mixed Matrix Membranes (MMMs) Comprising Exfoliated 2D Covalent Organic Frameworks (COFs) for Efficient CO<sub>2</sub> Separation. *Chem. Mater.* **2016**, *28* (5), 1277-1285.
164. Côté, A. P.; Benin, A. I.; Ockwig, N. W.; O'Keeffe, M.; Matzger, A. J.; Yaghi, O. M., Porous, Crystalline, Covalent Organic Frameworks. *Science* **2005**, *310* (5751), 1166-1170.
165. Slater, A. G.; Cooper, A. I., Function-led design of new porous materials. *Science* **2015**, *348* (6238), aaa8075.
166. El-Kaderi, H. M.; Hunt, J. R.; Mendoza-Cortés, J. L.; Côté, A. P.; Taylor, R. E.; O'Keeffe, M.; Yaghi, O. M., Designed Synthesis of 3D Covalent Organic Frameworks. *Science* **2007**, *316* (5822), 268-272.

167. Mulzer, C. R.; Shen, L.; Bisbey, R. P.; McKone, J. R.; Zhang, N.; Abruña, H. D.; Dichtel, W. R., Superior Charge Storage and Power Density of a Conducting Polymer-Modified Covalent Organic Framework. *ACS Cent. Sci.* **2016**, *2* (9), 667-673.
168. Waller, P. J.; Gándara, F.; Yaghi, O. M., Chemistry of Covalent Organic Frameworks. *Acc. Chem. Res.* **2015**, *48* (12), 3053-3063.
169. Rogge, S. M. J.; Bavykina, A.; Hajek, J.; Garcia, H.; Olivos-Suarez, A. I.; Sepúlveda-Escribano, A.; Vimont, A.; Clet, G.; Bazin, P.; Kapteijn, F.; Daturi, M.; Ramos-Fernandez, E. V.; Llabrés i Xamena, F. X.; Van Speybroeck, V.; Gascon, J., Metal-organic and covalent organic frameworks as single-site catalysts. *Chem. Soc. Rev.* **2017**, *46* (11), 3134-3184.
170. Wang, X.; Ye, N., Recent advances in metal-organic frameworks and covalent organic frameworks for sample preparation and chromatographic analysis. *Electrophoresis* **2017**, *38* (24), 3059-3078.
171. Yu, J.-T.; Chen, Z.; Sun, J.; Huang, Z.-T.; Zheng, Q.-Y., Cyclotricatechylene based porous crystalline material: Synthesis and applications in gas storage. *J. Mater. Chem.* **2012**, *22* (12), 5369-5373.
172. Bunck, D. N.; Dichtel, W. R., Internal Functionalization of Three-Dimensional Covalent Organic Frameworks. *Angew. Chem. Int. Ed.* **2012**, *51* (8), 1885-1889.
173. Spitler, E. L.; Giovino, M. R.; White, S. L.; Dichtel, W. R., A mechanistic study of Lewis acid-catalyzed covalent organic framework formation. *Chem. Sci.* **2011**, *2* (8), 1588-1593.
174. Kuhn, P.; Antonietti, M.; Thomas, A., Porous, Covalent Triazine-Based Frameworks Prepared by Ionothermal Synthesis. *Angew. Chem. Int. Ed.* **2008**, *47* (18), 3450-3453.
175. Bojdys, M. J.; Jeromenok, J.; Thomas, A.; Antonietti, M., Rational Extension of the Family of Layered, Covalent, Triazine-Based Frameworks with Regular Porosity. *Adv. Mater.* **2010**, *22* (19), 2202-2205.
176. Biswal, B. P.; Chandra, S.; Kandambeth, S.; Lukose, B.; Heine, T.; Banerjee, R., Mechanochemical Synthesis of Chemically Stable Isoreticular Covalent Organic Frameworks. *J. Am. Chem. Soc.* **2013**, *135* (14), 5328-5331.
177. Ritchie, L. K.; Trewin, A.; Reguera-Galan, A.; Hasell, T.; Cooper, A. I., Synthesis of COF-5 using microwave irradiation and conventional solvothermal routes. *Microporous Mesoporous Mater.* **2010**, *132* (1), 132-136.
178. Campbell, N. L.; Clowes, R.; Ritchie, L. K.; Cooper, A. I., Rapid Microwave Synthesis and Purification of Porous Covalent Organic Frameworks. *Chem. Mater.* **2009**, *21* (2), 204-206.

179. Nagai, A.; Guo, Z.; Feng, X.; Jin, S.; Chen, X.; Ding, X.; Jiang, D., Pore surface engineering in covalent organic frameworks. *Nat. Comm.* **2011**, *2* (1), 536.
180. Chan-Thaw, C. E.; Villa, A.; Prati, L.; Thomas, A., Triazine-Based Polymers as Nanostructured Supports for the Liquid-Phase Oxidation of Alcohols. *Chem. Eur. J.* **2011**, *17* (3), 1052-1057.
181. Kandambeth, S.; Dey, K.; Banerjee, R., Covalent Organic Frameworks: Chemistry beyond the Structure. *J. Am. Chem. Soc.* **2019**, *141* (5), 1807-1822.
182. Zhang, Y.-B.; Su, J.; Furukawa, H.; Yun, Y.; Gándara, F.; Duong, A.; Zou, X.; Yaghi, O. M., Single-Crystal Structure of a Covalent Organic Framework. *J. Am. Chem. Soc.* **2013**, *135* (44), 16336-16339.
183. Beaudoin, D.; Maris, T.; Wuest, J. D., Constructing monocrystalline covalent organic networks by polymerization. *Nat. Chem.* **2013**, *5* (10), 830-834.
184. Liu, Y.; Ma, Y.; Zhao, Y.; Sun, X.; Gándara, F.; Furukawa, H.; Liu, Z.; Zhu, H.; Zhu, C.; Suenaga, K.; Oleynikov, P.; Alshammari, A. S.; Zhang, X.; Terasaki, O.; Yaghi, O. M., Weaving of organic threads into a crystalline covalent organic framework. *Science* **2016**, *351* (6271), 365-369.
185. Ma, T.; Kapustin, E. A.; Yin, S. X.; Liang, L.; Zhou, Z.; Niu, J.; Li, L.-H.; Wang, Y.; Su, J.; Li, J.; Wang, X.; Wang, W. D.; Wang, W.; Sun, J.; Yaghi, O. M., Single-crystal x-ray diffraction structures of covalent organic frameworks. *Science* **2018**, *361* (6397), 48-52.
186. Huang, N.; Wang, P.; Jiang, D., Covalent organic frameworks: a materials platform for structural and functional designs. *Nat. Rev. Mater.* **2016**, *1* (10), 16068.
187. Chen, X.; Huang, N.; Gao, J.; Xu, H.; Xu, F.; Jiang, D., Towards covalent organic frameworks with predesignable and aligned open docking sites. *Chem. Comm.* **2014**, *50* (46), 6161-6163.
188. El-Mahdy, A. F. M.; Hung, Y.-H.; Mansoure, T. H.; Yu, H.-H.; Chen, T.; Kuo, S.-W., A Hollow Microtubular Triazine- and Benzobisoxazole-Based Covalent Organic Framework Presenting Sponge-Like Shells That Functions as a High-Performance Supercapacitor. *Chem. Asian J.* **2019**, *14* (9), 1429-1435.
189. Guan, X.; Chen, F.; Fang, Q.; Qiu, S., Design and applications of three dimensional covalent organic frameworks. *Chem. Soc. Rev.* **2020**, *49* (5), 1357-1384.
190. Geng, K.; He, T.; Liu, R.; Dalapati, S.; Tan, K. T.; Li, Z.; Tao, S.; Gong, Y.; Jiang, Q.; Jiang, D., Covalent Organic Frameworks: Design, Synthesis, and Functions. *Chem. Rev.* **2020**, *120* (16), 8814-8933.

191. Abuzeid, H. R.; El-Mahdy, A. F. M.; Kuo, S.-W., Covalent organic frameworks: Design principles, synthetic strategies, and diverse applications. *Giant* **2021**, *6*, 100054.
192. Diercks, C. S.; Yaghi, O. M., The atom, the molecule, and the covalent organic framework. *Science* **2017**, *355* (6328), eaal1585.
193. Jackson, K. T.; Reich, T. E.; El-Kaderi, H. M., Targeted synthesis of a porous borazine-linked covalent organic framework. *Chem. Comm.* **2012**, *48* (70), 8823-8825.
194. Côté, A. P.; El-Kaderi, H. M.; Furukawa, H.; Hunt, J. R.; Yaghi, O. M., Reticular Synthesis of Microporous and Mesoporous 2D Covalent Organic Frameworks. *J. Am. Chem. Soc.* **2007**, *129* (43), 12914-12915.
195. Xie, Y.-F.; Ding, S.-Y.; Liu, J.-M.; Wang, W.; Zheng, Q.-Y., Triazatruxene based covalent organic framework and its quick-response fluorescence-on nature towards electron rich arenes. *J. Mater. Chem. C* **2015**, *3* (39), 10066-10069.
196. Xu, L.; Ding, S.-Y.; Liu, J.; Sun, J.; Wang, W.; Zheng, Q.-Y., Highly crystalline covalent organic frameworks from flexible building blocks. *Chem. Comm.* **2016**, *52* (25), 4706-4709.
197. El-Mahdy, A. F. M.; Kuo, C.-H.; Alshehri, A.; Young, C.; Yamauchi, Y.; Kim, J.; Kuo, S.-W., Strategic design of triphenylamine- and triphenyltriazine-based two-dimensional covalent organic frameworks for CO<sub>2</sub> uptake and energy storage. *J. Mater. Chem. A* **2018**, *6* (40), 19532-19541.
198. El-Mahdy, A. F. M.; Young, C.; Kim, J.; You, J.; Yamauchi, Y.; Kuo, S.-W., Hollow Microspherical and Microtubular [3 + 3] Carbazole-Based Covalent Organic Frameworks and Their Gas and Energy Storage Applications. *ACS Appl. Mater. Interfaces* **2019**, *11* (9), 9343-9354.
199. Feng, X.; Chen, L.; Dong, Y.; Jiang, D., Porphyrin-based two-dimensional covalent organic frameworks: synchronized synthetic control of macroscopic structures and pore parameters. *Chem. Comm.* **2011**, *47* (7), 1979-1981.
200. Feng, X.; Ding, X.; Chen, L.; Wu, Y.; Liu, L.; Addicoat, M.; Irle, S.; Dong, Y.; Jiang, D., Two-dimensional artificial light-harvesting antennae with predesigned high-order structure and robust photosensitising activity. *Sci. Rep.* **2016**, *6* (1), 32944.
201. Wang, P.; Xu, Q.; Li, Z.; Jiang, W.; Jiang, Q.; Jiang, D., Exceptional Iodine Capture in 2D Covalent Organic Frameworks. *Adv. Mater.* **2018**, *30* (29), 1801991.
202. Wang, S.; Sun, Q.; Chen, W.; Tang, Y.; Aguila, B.; Pan, Y.; Zheng, A.; Yang, Z.; Wojtas, L.; Ma, S.; Xiao, F.-S., Programming Covalent Organic Frameworks for Photocatalysis: Investigation of Chemical and Structural Variations. *Matter* **2020**, *2* (2), 416-427.

203. Lu, C.; Li, Y.; Wang, L.-M.; Yan, H.-J.; Chen, L.; Wang, D., Rational design of two-dimensional covalent tilings using a C<sub>6</sub>-symmetric building block via on-surface Schiff base reaction. *Chem. Comm.* **2019**, *55* (9), 1326-1329.
204. Jin, Y.; Hu, Y.; Zhang, W., Tessellated multiporous two-dimensional covalent organic frameworks. *Nat. Rev. Chem.* **2017**, *1* (7), 0056.
205. Chen, X.; Gao, J.; Jiang, D., Designed Synthesis of Porphyrin-based Two-dimensional Covalent Organic Frameworks with Highly Ordered Structures. *Chem. Lett.* **2015**, *44* (9), 1257-1259.
206. Spitler, E. L.; Dichtel, W. R., Lewis acid-catalysed formation of two-dimensional phthalocyanine covalent organic frameworks. *Nat. Chem.* **2010**, *2* (8), 672-677.
207. Trewin, A.; Cooper, A. I., Predicting microporous crystalline polyimides. *CrystEngComm* **2009**, *11* (9), 1819-1822.
208. Lan, Y.; Han, X.; Tong, M.; Huang, H.; Yang, Q.; Liu, D.; Zhao, X.; Zhong, C., Materials genomics methods for high-throughput construction of COFs and targeted synthesis. *Nat. Comm.* **2018**, *9* (1), 5274.
209. Uribe-Romo, F. J.; Hunt, J. R.; Furukawa, H.; Klöck, C.; O’Keeffe, M.; Yaghi, O. M., A Crystalline Imine-Linked 3-D Porous Covalent Organic Framework. *J. Am. Chem. Soc.* **2009**, *131* (13), 4570-4571.
210. Yan, S.; Guan, X.; Li, H.; Li, D.; Xue, M.; Yan, Y.; Valtchev, V.; Qiu, S.; Fang, Q., Three-dimensional Salphen-based Covalent–Organic Frameworks as Catalytic Antioxidants. *J. Am. Chem. Soc.* **2019**, *141* (7), 2920-2924.
211. Baldwin, L. A.; Crowe, J. W.; Pyles, D. A.; McGrier, P. L., Metalation of a Mesoporous Three-Dimensional Covalent Organic Framework. *J. Am. Chem. Soc.* **2016**, *138* (46), 15134-15137.
212. Fang, Q.; Zhuang, Z.; Gu, S.; Kaspar, R. B.; Zheng, J.; Wang, J.; Qiu, S.; Yan, Y., Designed synthesis of large-pore crystalline polyimide covalent organic frameworks. *Nat. Comm.* **2014**, *5* (1), 4503.
213. Lin, G.; Ding, H.; Yuan, D.; Wang, B.; Wang, C., A Pyrene-Based, Fluorescent Three-Dimensional Covalent Organic Framework. *J. Am. Chem. Soc.* **2016**, *138* (10), 3302-3305.
214. Ding, H.; Li, J.; Xie, G.; Lin, G.; Chen, R.; Peng, Z.; Yang, C.; Wang, B.; Sun, J.; Wang, C., An AIEgen-based 3D covalent organic framework for white light-emitting diodes. *Nat. Comm.* **2018**, *9* (1), 5234.

215. Kang, X.; Wu, X.; Han, X.; Yuan, C.; Liu, Y.; Cui, Y., Rational synthesis of interpenetrated 3D covalent organic frameworks for asymmetric photocatalysis. *Chem. Sci.* **2020**, *11* (6), 1494-1502.
216. Feng, X.; Ding, X.; Jiang, D., Covalent organic frameworks. *Chem. Soc. Rev.* **2012**, *41* (18), 6010-6022.
217. Rowan, S. J.; Cantrill, S. J.; Cousins, G. R. L.; Sanders, J. K. M.; Stoddart, J. F., Dynamic Covalent Chemistry. *Angew. Chem. Int. Ed.* **2002**, *41* (6), 898-952.
218. Hunt, J. R.; Doonan, C. J.; LeVangie, J. D.; Côté, A. P.; Yaghi, O. M., Reticular Synthesis of Covalent Organic Borosilicate Frameworks. *J. Am. Chem. Soc.* **2008**, *130* (36), 11872-11873.
219. Uribe-Romo, F. J.; Doonan, C. J.; Furukawa, H.; Oisaki, K.; Yaghi, O. M., Crystalline Covalent Organic Frameworks with Hydrazone Linkages. *J. Am. Chem. Soc.* **2011**, *133* (30), 11478-11481.
220. Nagai, A.; Chen, X.; Feng, X.; Ding, X.; Guo, Z.; Jiang, D., A Squaraine-Linked Mesoporous Covalent Organic Framework. *Angew. Chem. Int. Ed.* **2013**, *52* (13), 3770-3774.
221. Dalapati, S.; Jin, S.; Gao, J.; Xu, Y.; Nagai, A.; Jiang, D., An Azine-Linked Covalent Organic Framework. *J. Am. Chem. Soc.* **2013**, *135* (46), 17310-17313.
222. Guo, J.; Xu, Y.; Jin, S.; Chen, L.; Kaji, T.; Honsho, Y.; Addicoat, M. A.; Kim, J.; Saeki, A.; Ihee, H.; Seki, S.; Irle, S.; Hiramoto, M.; Gao, J.; Jiang, D., Conjugated organic framework with three-dimensionally ordered stable structure and delocalized  $\pi$  clouds. *Nat Comm.* **2013**, *4* (1), 2736.
223. Chen, X.; Addicoat, M.; Jin, E.; Xu, H.; Hayashi, T.; Xu, F.; Huang, N.; Irle, S.; Jiang, D., Designed synthesis of double-stage two-dimensional covalent organic frameworks. *Sci. Rep.* **2015**, *5* (1), 14650.
224. Du, Y.; Yang, H.; Whiteley, J. M.; Wan, S.; Jin, Y.; Lee, S.-H.; Zhang, W., Ionic Covalent Organic Frameworks with Spiroborate Linkage. *Angew. Chem. Int. Ed.* **2016**, *55* (5), 1737-1741.
225. Bi, S.; Yang, C.; Zhang, W.; Xu, J.; Liu, L.; Wu, D.; Wang, X.; Han, Y.; Liang, Q.; Zhang, F., Two-dimensional semiconducting covalent organic frameworks via condensation at arylmethyl carbon atoms. *Nat. Comm.* **2019**, *10* (1), 2467.
226. Waller, P. J.; Lyle, S. J.; Osborn Popp, T. M.; Diercks, C. S.; Reimer, J. A.; Yaghi, O. M., Chemical Conversion of Linkages in Covalent Organic Frameworks. *J. Am. Chem. Soc.* **2016**, *138* (48), 15519-15522.

227. Das, G.; Skorjanc, T.; Sharma, S. K.; Gándara, F.; Lusi, M.; Shankar Rao, D. S.; Vimala, S.; Krishna Prasad, S.; Raya, J.; Han, D. S.; Jagannathan, R.; Olsen, J.-C.; Trabolsi, A., Viologen-Based Conjugated Covalent Organic Networks via Zincke Reaction. *J. Am. Chem. Soc.* **2017**, *139* (28), 9558-9565.
228. Yahiaoui, O.; Fitch, A. N.; Hoffmann, F.; Fröba, M.; Thomas, A.; Roeser, J., 3D Anionic Silicate Covalent Organic Framework with srs Topology. *J. Am. Chem. Soc.* **2018**, *140* (16), 5330-5333.
229. Zhao, C.; Diercks, C. S.; Zhu, C.; Hanikel, N.; Pei, X.; Yaghi, O. M., Urea-Linked Covalent Organic Frameworks. *J. Am. Chem. Soc.* **2018**, *140* (48), 16438-16441.
230. Zhang, B.; Wei, M.; Mao, H.; Pei, X.; Alshimri, S. A.; Reimer, J. A.; Yaghi, O. M., Crystalline Dioxin-Linked Covalent Organic Frameworks from Irreversible Reactions. *J. Am. Chem. Soc.* **2018**, *140* (40), 12715-12719.
231. Wang, X.; Bahri, M.; Fu, Z.; Little, M. A.; Liu, L.; Niu, H.; Browning, N. D.; Chong, S. Y.; Chen, L.; Ward, J. W.; Cooper, A. I., A Cubic 3D Covalent Organic Framework with nbo Topology. *J. Am. Chem. Soc.* **2021**, *143* (37), 15011-15016.
232. Vitaku, E.; Dichtel, W. R., Synthesis of 2D Imine-Linked Covalent Organic Frameworks through Formal Transimination Reactions. *J. Am. Chem. Soc.* **2017**, *139* (37), 12911-12914.
233. Blatov, V. A.; Carlucci, L.; Ciani, G.; Proserpio, D. M., Interpenetrating metal–organic and inorganic 3D networks: a computer-aided systematic investigation. Part I. Analysis of the Cambridge structural database. *CrystEngComm* **2004**, *6* (65), 377-395.
234. Kaya, İ.; Kolcu, F.; Demiral, G.; Ergül, H.; Kiliç, E., Synthesis and characterization of imine polymers of aromatic aldehydes with 4-amino-2-methylquinoline via oxidative polycondensation. *Des. Monomers Polym.* **2015**, *18* (1), 89-104.
235. Alahakoon, S. B.; McCandless, G. T.; Karunathilake, A. A. K.; Thompson, C. M.; Smaldone, R. A., Enhanced Structural Organization in Covalent Organic Frameworks Through Fluorination. *Chem. Eur. J.* **2017**, *23* (18), 4255-4259.
236. Alahakoon, S. B.; Thompson, C. M.; Nguyen, A. X.; Occhialini, G.; McCandless, G. T.; Smaldone, R. A., An azine-linked hexaphenylbenzene based covalent organic framework. *Chem. Comm.* **2016**, *52* (13), 2843-2845.
237. Lu, J.; Lin, F.; Wen, Q.; Qi, Q.-Y.; Xu, J.-Q.; Zhao, X., Large-scale synthesis of azine-linked covalent organic frameworks in water and promoted by water. *New J. Chem.* **2019**, *43* (16), 6116-6120.

238. Li, X.; Qi, Y.; Yue, G.; Wu, Q.; Li, Y.; Zhang, M.; Guo, X.; Li, X.; Ma, L.; Li, S., Solvent- and catalyst-free synthesis of an azine-linked covalent organic framework and the induced tautomerization in the adsorption of U(vi) and Hg(ii). *Green Chem.* **2019**, *21* (3), 649-657.
239. Guan, P.; Qiu, J.; Zhao, Y.; Wang, H.; Li, Z.; Shi, Y.; Wang, J., A novel crystalline azine-linked three-dimensional covalent organic framework for CO<sub>2</sub> capture and conversion. *Chem. Comm.* **2019**, *55* (83), 12459-12462.
240. Kandambeth, S.; Mallick, A.; Lukose, B.; Mane, M. V.; Heine, T.; Banerjee, R., Construction of Crystalline 2D Covalent Organic Frameworks with Remarkable Chemical (Acid/Base) Stability via a Combined Reversible and Irreversible Route. *J. Am. Chem. Soc.* **2012**, *134* (48), 19524-19527.
241. Cusin, L.; Peng, H.; Ciesielski, A.; Samori, P., Chemical Conversion and Locking of the Imine Linkage: Enhancing the Functionality of Covalent Organic Frameworks. *Angew. Chem. Int. Ed.* **2021**, *60* (26), 14236-14250.
242. Baumgartner, B.; Puchberger, M.; Unterlass, M. M., Towards a general understanding of hydrothermal polymerization of polyimides. *Polym. Chem.* **2015**, *6* (31), 5773-5781.
243. Yu, M.; Chandrasekhar, N.; Raghupathy, R. K. M.; Ly, K. H.; Zhang, H.; Dmitrieva, E.; Liang, C.; Lu, X.; Kühne, T. D.; Mirhosseini, H.; Weidinger, I. M.; Feng, X., A High-Rate Two-Dimensional Polyarylimide Covalent Organic Framework Anode for Aqueous Zn-Ion Energy Storage Devices. *J. Am. Chem. Soc.* **2020**, *142* (46), 19570-19578.
244. Yuan, X.; Wang, Y.; Deng, G.; Zong, X.; Zhang, C.; Xue, S., Mixed matrix membrane comprising polyimide with crystalline porous imide-linked covalent organic framework for N<sub>2</sub>/O<sub>2</sub> separation. *Polym. Adv. Technol.* **2019**, *30* (2), 417-424.
245. Zhang, C.; Zhang, S.; Yan, Y.; Xia, F.; Huang, A.; Xian, Y., Highly Fluorescent Polyimide Covalent Organic Nanosheets as Sensing Probes for the Detection of 2,4,6-Trinitrophenol. *ACS Appl. Mater. Interfaces* **2017**, *9* (15), 13415-13421.
246. Wang, T.; Xue, R.; Chen, H.; Shi, P.; Lei, X.; Wei, Y.; Guo, H.; Yang, W., Preparation of two new polyimide bond linked porous covalent organic frameworks and their fluorescence sensing application for sensitive and selective determination of Fe<sup>3+</sup>. *New J. Chem.* **2017**, *41* (23), 14272-14278.
247. Xiao, J.-D.; Qiu, L.-G.; Yuan, Y.-P.; Jiang, X.; Xie, A.-J.; Shen, Y.-H., Ultrafast microwave-enhanced ionothermal synthesis of luminescent crystalline polyimide nanosheets for highly selective sensing of chromium ions. *Inorg. Chem. Comm.* **2013**, *29*, 128-130.

248. Song, Y.; Sun, Q.; Aguila, B.; Ma, S., Opportunities of Covalent Organic Frameworks for Advanced Applications. *Adv. Sci.* **2019**, *6* (2), 1801410.
249. Nemiwal, M.; Sharma, V.; Kumar, D., Improved Designs of Multifunctional Covalent-Organic Frameworks: Hydrogen Storage, Methane Storage, and Water Harvesting. *Mini-Rev. Org. Chem.* **2021**, *18* (8), 1026-1036.
250. Ying, Y.; Peh, S. B.; Yang, H.; Yang, Z.; Zhao, D., Ultrathin Covalent Organic Framework Membranes via a Multi-Interfacial Engineering Strategy for Gas Separation. *Adv. Mater.* **2021**, *n/a* (n/a), 2104946.
251. Guo, J.; Jiang, D., Covalent Organic Frameworks for Heterogeneous Catalysis: Principle, Current Status, and Challenges. *ACS Cent. Sci.* **2020**, *6* (6), 869-879.
252. Zhi, Y.; Wang, Z.; Zhang, H.-L.; Zhang, Q., Recent Progress in Metal-Free Covalent Organic Frameworks as Heterogeneous Catalysts. *Small* **2020**, *16* (24), 2001070.
253. Albacete, P.; López-Moreno, A.; Mena-Hernando, S.; Platero-Prats, A. E.; Pérez, E. M.; Zamora, F., Chemical sensing of water contaminants by a colloid of a fluorescent imine-linked covalent organic framework. *Chem. Comm.* **2019**, *55* (10), 1382-1385.
254. Yuan, H.; Li, N.; Linghu, J.; Dong, J.; Wang, Y.; Karmakar, A.; Yuan, J.; Li, M.; Buenconsejo, P. J. S.; Liu, G.; Cai, H.; Pennycook, S. J.; Singh, N.; Zhao, D., Chip-Level Integration of Covalent Organic Frameworks for Trace Benzene Sensing. *ACS Sensors* **2020**, *5* (5), 1474-1481.
255. Scicluna, M. C.; Vella-Zarb, L., Evolution of Nanocarrier Drug-Delivery Systems and Recent Advancements in Covalent Organic Framework–Drug Systems. *ACS Appl. Nano Mater.* **2020**, *3* (4), 3097-3115.
256. Gao, P.; Shen, X.; Liu, X.; Chen, Y.; Pan, W.; Li, N.; Tang, B., Nucleic Acid-Gated Covalent Organic Frameworks for Cancer-Specific Imaging and Drug Release. *Anal. Chem.* **2021**, *93* (34), 11751-11757.
257. Montoro, C.; Rodríguez-San-Miguel, D.; Polo, E.; Escudero-Cid, R.; Ruiz-González, M. L.; Navarro, J. A. R.; Ocón, P.; Zamora, F., Ionic Conductivity and Potential Application for Fuel Cell of a Modified Imine-Based Covalent Organic Framework. *J. Am. Chem. Soc.* **2017**, *139* (29), 10079-10086.
258. Chen, J.; Li, P.; Zhang, N.; Tang, S., Highly hydroxide-conducting hybrid anion exchange membrane with functional COF-enhanced ion nanochannels. *Electrochim. Acta* **2021**, *391*, 138962.

259. Xu, X.; Wang, S.; Yue, Y.; Huang, N., Semiconductive Porphyrin-Based Covalent Organic Frameworks for Sensitive Near-Infrared Detection. *ACS Appl. Mater. Interfaces* **2020**, *12* (33), 37427-37434.
260. Jin, E.; Geng, K.; Fu, S.; Yang, S.; Kanlayakan, N.; Addicoat, M. A.; Kungwan, N.; Geurs, J.; Xu, H.; Bonn, M.; Wang, H. I.; Smet, J.; Kowalczyk, T.; Jiang, D., Exceptional electron conduction in two-dimensional covalent organic frameworks. *Chem.* **2021**, *7* (12), 3309-3324.
261. Li, J.; Jing, X.; Li, Q.; Li, S.; Gao, X.; Feng, X.; Wang, B., Bulk COFs and COF nanosheets for electrochemical energy storage and conversion. *Chem. Soc. Rev.* **2020**, *49* (11), 3565-3604.
262. Yang, Z.; Liu, J.; Li, Y.; Zhang, G.; Xing, G.; Chen, L., Arylamine-Linked 2D Covalent Organic Frameworks for Efficient Pseudocapacitive Energy Storage. *Angew. Chem. Int. Ed.* **2021**, *60* (38), 20754-20759.
263. Furukawa, H.; Yaghi, O. M., Storage of Hydrogen, Methane, and Carbon Dioxide in Highly Porous Covalent Organic Frameworks for Clean Energy Applications. *J. Am. Chem. Soc.* **2009**, *131* (25), 8875-8883.
264. Gao, Q.; Li, X.; Ning, G.-H.; Xu, H.-S.; Liu, C.; Tian, B.; Tang, W.; Loh, K. P., Covalent Organic Framework with Frustrated Bonding Network for Enhanced Carbon Dioxide Storage. *Chem. Mater.* **2018**, *30* (5), 1762-1768.
265. Mendoza-Cortés, J. L.; Han, S. S.; Furukawa, H.; Yaghi, O. M.; Goddard, W. A., Adsorption Mechanism and Uptake of Methane in Covalent Organic Frameworks: Theory and Experiment. *J. Phys. Chem. A* **2010**, *114* (40), 10824-10833.
266. Doonan, C. J.; Tranchemontagne, D. J.; Glover, T. G.; Hunt, J. R.; Yaghi, O. M., Exceptional ammonia uptake by a covalent organic framework. *Nat. Chem.* **2010**, *2* (3), 235-238.
267. Alahakoon, S. B.; Thompson, C. M.; Occhialini, G.; Smaldone, R. A., Design Principles for Covalent Organic Frameworks in Energy Storage Applications. *ChemSusChem* **2017**, *10* (10), 2116-2129.
268. Li, Y.; Yang, R. T., Hydrogen storage in metal-organic and covalent-organic frameworks by spillover. *AIChE Journal* **2008**, *54* (1), 269-279.
269. Cai, X.; Nie, J.; Lu, C.; Wang, F.; Ma, C.; Yang, G.; Chen, Z.; Zhang, Y., Copper-incorporated porous organic polymer as efficient and recyclable catalyst for azide-alkyne cycloaddition. *Microporous Mesoporous Mater.* **2021**, *310*, 110671.

270. Guo, D.; Li, C.; Zhang, J.; Liu, G.; Luo, X.; Wu, F., Metalloporphyrin-based porous organic polymer as an efficient catalyst for cycloaddition of epoxides and CO<sub>2</sub>. *J. Solid State Chem.* **2021**, *293*, 121770.
271. Guo, T.; Mo, K.; Zhang, N.; Xiao, L.; Liu, W.; Wen, L., Embedded homogeneous ultra-fine Pd nanoparticles within MOF ultra-thin nanosheets for heterogeneous catalysis. *Dalton Trans.* **2021**, *50* (5), 1774-1779.
272. Habib, N. R.; Asedegbega-Nieto, E.; Taddesse, A. M.; Diaz, I., Non-noble MNP@MOF materials: synthesis and applications in heterogeneous catalysis. *Dalton Trans.* **2021**, *50* (30), 10340-10353.
273. Maia, R. A.; Berg, F.; Ritleng, V.; Louis, B.; Esteves, P. M., Design, Synthesis and Characterization of Nickel-Functionalized Covalent Organic Framework NiCl@RIO-12 for Heterogeneous Suzuki–Miyaura Catalysis. *Chem. Eur. J.* **2020**, *26* (9), 2051-2059.
274. Llabrés i Xamena, F. X.; Abad, A.; Corma, A.; Garcia, H., MOFs as catalysts: Activity, reusability and shape-selectivity of a Pd-containing MOF. *J. Catal.* **2007**, *250* (2), 294-298.
275. Hasija, V.; Patial, S.; Raizada, P.; Aslam Parwaz Khan, A.; Asiri, A. M.; Van Le, Q.; Nguyen, V.-H.; Singh, P., Covalent organic frameworks promoted single metal atom catalysis: Strategies and applications. *Coord. Chem. Rev.* **2022**, *452*, 214298.
276. Kan, X.; Wang, J.-C.; Kan, J.-L.; Shang, J.-Y.; Qiao, H.; Dong, Y.-B., Gram-Scale Synthesis of Cu(II)@COF via Solid-State Coordination Approach for Catalysis of Alkyne-Dihalomethane-Amine Coupling. *Inorg. Chem.* **2021**, *60* (5), 3393-3400.
277. López-Magano, A.; Ortín-Rubio, B.; Imaz, I.; MasPOCH, D.; Alemán, J.; Mas-Ballesté, R., Photoredox Heterobimetallic Dual Catalysis Using Engineered Covalent Organic Frameworks. *ACS Catal.* **2021**, *11* (19), 12344-12354.
278. Zhu, D.; Zhang, Z.; Alemany, L. B.; Li, Y.; Nnorom, N.; Barnes, M.; Khalil, S.; Rahman, M. M.; Ajayan, P. M.; Verduzco, R., Rapid, Ambient Temperature Synthesis of Imine Covalent Organic Frameworks Catalyzed by Transition-Metal Nitrates. *Chem. Mater.* **2021**, *33* (9), 3394-3400.
279. Chen, H.; Zhang, Y.; Xu, C.; Cao, M.; Dou, H.; Zhang, X., Two  $\pi$ -Conjugated Covalent Organic Frameworks with Long-Term Cyclability at High Current Density for Lithium Ion Battery. *Chem. Eur. J.* **2019**, *25* (68), 15472-15476.
280. Li, Y.; Chen, M.; Han, Y.; Feng, Y.; Zhang, Z.; Zhang, B., Fabrication of a New Corrole-Based Covalent Organic Framework as a Highly Efficient and Selective Chemosensor for Heavy Metal Ions. *Chem. Mater.* **2020**, *32* (6), 2532-2540.

281. Zhao, Y.; Dai, W.; Peng, Y.; Niu, Z.; Sun, Q.; Shan, C.; Yang, H.; Verma, G.; Wojtas, L.; Yuan, D.; Zhang, Z.; Dong, H.; Zhang, X.; Zhang, B.; Feng, Y.; Ma, S., A Corrole-Based Covalent Organic Framework Featuring Desymmetrized Topology. *Angew. Chem. Int. Ed.* **2020**, *59* (11), 4354-4359.
282. McKeown, N. B.; Budd, P. M.; Msayib, K. J.; Ghanem, B. S.; Kingston, H. J.; Tattershall, C. E.; Makhseed, S.; Reynolds, K. J.; Fritsch, D., Polymers of Intrinsic Microporosity (PIMs): Bridging the Void between Microporous and Polymeric Materials. *Chem. Eur. J.* **2005**, *11* (9), 2610-2620.
283. McKeown, N. B., The synthesis of polymers of intrinsic microporosity (PIMs). *Sci. China Chem.* **2017**, *60* (8), 1023-1032.
284. Zhou, Y.-B.; Zhan, Z.-P., Conjugated Microporous Polymers for Heterogeneous Catalysis. *Chem. Eur. J.* **2018**, *13* (1), 9-19.
285. Lee, J.-S. M.; Cooper, A. I., Advances in Conjugated Microporous Polymers. *Chem. Rev.* **2020**, *120* (4), 2171-2214.
286. Yuan, Y.; Zhu, G., Porous Aromatic Frameworks as a Platform for Multifunctional Applications. *ACS Cent. Sci.* **2019**, *5* (3), 409-418.
287. Ben, T.; Qiu, S., Porous aromatic frameworks: Synthesis, structure and functions. *CrystEngComm* **2013**, *15* (1), 17-26.
288. Yang, G.; Gao, H.; Li, Q.; Ren, S., Preparation and dye adsorption properties of an oxygen-rich porous organic polymer. *RSC Adv.* **2021**, *11* (26), 15921-15926.
289. He, W.; Wen, M.; Shi, L.; Wang, R.; Li, F., Porous polymeric metalloporphyrin obtained through Sonogashira coupling: Catalytic performance at CO<sub>2</sub> cycloaddition to epoxides. *J. Solid State Chem.* **2022**, *309*, 122965.
290. Kundu, S.; Behera, B.; Giri, A.; Saha, N.; Patra, A., N,N'-bicarbazole-benzothiadiazole-based conjugated porous organic polymer for reactive oxygen species generation in live cells. *Chem. Comm.* **2021**, *57* (56), 6875-6878.
291. Yan, Z.; Liu, J.; Miao, C.; Su, P.; Zheng, G.; Cui, B.; Geng, T.; Fan, J.; Yu, Z.; Bu, N.; Yuan, Y.; Xia, L., Pyrene-Based Fluorescent Porous Organic Polymers for Recognition and Detection of Pesticides. *Molecules* **2022**, *27* (1), 126.
292. Mohamed, M. G.; Mansoure, T. H.; Takashi, Y.; Mohamed Samy, M.; Chen, T.; Kuo, S.-W., Ultrastable porous organic/inorganic polymers based on polyhedral oligomeric silsesquioxane (POSS) hybrids exhibiting high performance for thermal property and energy storage. *Microporous Mesoporous Mater.* **2021**, *328*, 111505.

293. Zhao, X.; Qi, Y.; Li, J.; Ma, Q., Porous Organic Polymers Derived from Ferrocene and Tetrahedral Silicon-Centered Monomers for Carbon Dioxide Sorption. *Polymers* **2022**, *14* (3), 370.
294. Cho, K.; Yang, H.-S.; Lee, I.-H.; Lee, S. M.; Kim, H. J.; Son, S. U., Valorization of Click-Based Microporous Organic Polymer: Generation of Mesoionic Carbene–Rh Species for the Stereoselective Synthesis of Poly(arylacetylene)s. *J. Am. Chem. Soc.* **2021**, *143* (11), 4100-4105.
295. Bhaumick, P.; Choudhury, L. H., Multicomponent click polymerization for the synthesis of coumarin containing 1,4-polytriazoles and their application as dye adsorbent. *Polymer* **2022**, *243*, 124580.
296. Zhou, Z.; Yu, F.; Ma, J., Nanoconfinement engineering for enhanced adsorption of carbon materials, metal–organic frameworks, mesoporous silica, MXenes and porous organic polymers: a review. *Environ. Chem. Lett.* **2022**, *20* (1), 563-595.
297. Yuan, R.; Yan, Z.; Shaga, A.; He, H., Design and fabrication of an electrochemical sensing platform based on a porous organic polymer for ultrasensitive ampicillin detection. *Sens. Actuators B: Chem.* **2021**, *327*, 128949.
298. Sajjad, M.; Tao, R.; Kang, K.; Luo, S.; Qiu, L., Phosphine-Based Porous Organic Polymer/rGO Aerogel Composites for High-Performance Asymmetric Supercapacitor. *ACS Appl. Energy Mater.* **2021**, *4* (1), 828-838.
299. Jiang, L.; Wang, P.; Wang, Y.; Wang, Y.; Li, X.; Xia, Q.; Ren, H., Facile synthesis of anionic porous organic polymer for ethylene purification. *J. Colloid Interface Sci.* **2021**, *582*, 631-637.
300. Liu, H.; Wang, Y.; Qin, Z.; Liu, D.; Xu, H.; Dong, H.; Hu, W., Electrically Conductive Coordination Polymers for Electronic and Optoelectronic Device Applications. *J. Phys. Chem. Lett.* **2021**, *12* (6), 1612-1630.
301. Singh, N.; Son, S.; An, J.; Kim, I.; Choi, M.; Kong, N.; Tao, W.; Kim, J. S., Nanoscale porous organic polymers for drug delivery and advanced cancer theranostics. *Chem. Soc. Rev.* **2021**, *50* (23), 12883-12896.
302. Brandès, S.; Quesneau, V.; Fonquernie, O.; Desbois, N.; Blondeau-Patissier, V.; Gros, C. P., Porous organic polymers based on cobalt corroles for carbon monoxide binding. *Dalton Trans.* **2019**, *48* (31), 11651-11662.
303. Zhao, Y.; Peng, Y.; Shan, C.; Lu, Z.; Wojtas, L.; Zhang, Z.; Zhang, B.; Feng, Y.; Ma, S., Metallocorrole-based porous organic polymers as a heterogeneous catalytic nanoplatform for efficient carbon dioxide conversion. *Nano Res.* **2022**, *15* (2), 1145-1152.

304. Li, B.; Wen, H. M.; Cui, Y.; Zhou, W.; Qian, G.; Chen, B., Emerging Multifunctional Metal-Organic Framework Materials. *Adv. Mater.* **2016**, *28* (40), 8819-8860.
305. Allendorf, M. D.; Stavila, V., Crystal engineering, structure–function relationships, and the future of metal–organic frameworks. *CrystEngComm* **2015**, *17* (2), 229-246.
306. Furukawa, H.; Cordova, K. E.; O'Keeffe, M.; Yaghi, O. M., The chemistry and applications of metal-organic frameworks. *Science* **2013**, *341* (6149), 1230444.
307. Yaghi, O. M.; Li, H., Hydrothermal Synthesis of a Metal-Organic Framework Containing Large Rectangular Channels. *J. Am. Chem. Soc.* **1995**, *117* (41), 10401-10402.
308. Jiao, L.; Seow, J. Y. R.; Skinner, W. S.; Wang, Z. U.; Jiang, H.-L., Metal–organic frameworks: Structures and functional applications. *Mater. Today* **2019**, *27*, 43-68.
309. Li, H.; Eddaoudi, M.; Groy, T. L.; Yaghi, O. M., Establishing Microporosity in Open Metal-Organic Frameworks: Gas Sorption Isotherms for Zn(BDC) (BDC = 1,4-Benzenedicarboxylate). *J. Am. Chem. Soc.* **1998**, *120* (33), 8571-8572.
310. Hu, T.-L.; Wang, H.; Li, B.; Krishna, R.; Wu, H.; Zhou, W.; Zhao, Y.; Han, Y.; Wang, X.; Zhu, W.; Yao, Z.; Xiang, S.; Chen, B., Microporous metal–organic framework with dual functionalities for highly efficient removal of acetylene from ethylene/acetylene mixtures. *Nat. Comm.* **2015**, *6* (1), 7328.
311. Cui, W.-G.; Hu, T.-L.; Bu, X.-H., Metal–Organic Framework Materials for the Separation and Purification of Light Hydrocarbons. *Adv. Mater.* **2020**, *32* (3), 1806445.
312. Yao, Z.-Q.; Xu, J.; Zou, B.; Hu, Z.; Wang, K.; Yuan, Y.-J.; Chen, Y.-P.; Feng, R.; Xiong, J.-B.; Hao, J.; Bu, X.-H., A Dual-Stimuli-Responsive Coordination Network Featuring Reversible Wide-Range Luminescence-Tuning Behavior. *Angew. Chem. Int. Ed.* **2019**, *58* (17), 5614-5618.
313. Yao, Z.-Q.; Li, G.-Y.; Xu, J.; Hu, T.-L.; Bu, X.-H., A Water-Stable Luminescent Zn<sup>II</sup> Metal-Organic Framework as Chemosensor for High-Efficiency Detection of Cr<sup>VI</sup>-Anions (Cr<sub>2</sub>O<sub>7</sub><sup>2-</sup> and CrO<sub>4</sub><sup>2-</sup>) in Aqueous Solution. *Chem. Eur. J.* **2018**, *24* (13), 3192-3198.
314. Shekhah, O.; Liu, J.; Fischer, R. A.; Wöll, C., MOF thin films: existing and future applications. *Chem. Soc. Rev.* **2011**, *40* (2), 1081-1106.
315. Zacher, D.; Shekhah, O.; Wöll, C.; Fischer, R. A., Thin films of metal–organic frameworks. *Chem. Soc. Rev.* **2009**, *38* (5), 1418-1429.
316. Li, A.-L.; Gao, Q.; Xu, J.; Bu, X.-H., Proton-conductive metal-organic frameworks: Recent advances and perspectives. *Coord. Chem. Rev.* **2017**, *344*, 54-82.

317. Sun, L.; Campbell, M. G.; Dincă, M., Electrically Conductive Porous Metal–Organic Frameworks. *Angew. Chem. Int. Ed.* **2016**, *55* (11), 3566-3579.
318. Cui, W.-G.; Zhang, G.-Y.; Hu, T.-L.; Bu, X.-H., Metal-organic framework-based heterogeneous catalysts for the conversion of C1 chemistry: CO, CO<sub>2</sub> and CH<sub>4</sub>. *Coord. Chem. Rev.* **2019**, *387*, 79-120.
319. Giménez-Marqués, M.; Hidalgo, T.; Serre, C.; Horcajada, P., Nanostructured metal–organic frameworks and their bio-related applications. *Coord. Chem. Rev.* **2016**, *307*, 342-360.
320. Huxford, R. C.; Della Rocca, J.; Lin, W., Metal–organic frameworks as potential drug carriers. *Curr. Opin. Chem. Biol.* **2010**, *14* (2), 262-268.
321. Wu, H. B.; Lou, X. W., Metal-organic frameworks and their derived materials for electrochemical energy storage and conversion: Promises and challenges. *Sci. Adv.* **2017**, *3* (12), eaap9252.
322. Xia, W.; Mahmood, A.; Zou, R.; Xu, Q., Metal–organic frameworks and their derived nanostructures for electrochemical energy storage and conversion. *Energy Environ. Sci.* **2015**, *8* (7), 1837-1866.
323. Bon, V.; Senkovska, I.; Kaskel, S., Metal-Organic Frameworks. In *Nanoporous Materials for Gas Storage*, Kaneko, K.; Rodríguez-Reinoso, F., Eds. Springer Singapore: Singapore, 2019; pp 137-172.
324. Zhao, Y.; Qi, S.; Niu, Z.; Peng, Y.; Shan, C.; Verma, G.; Wojtas, L.; Zhang, Z.; Zhang, B.; Feng, Y.; Chen, Y.-S.; Ma, S., Robust Corrole-Based Metal–Organic Frameworks with Rare 9-Connected Zr/Hf-Oxo Clusters. *J. Am. Chem. Soc.* **2019**, *141* (36), 14443-14450.

## Chapter 2

# Synthesis of precursors for porous materials



## Chapter 2: Synthesis of precursors for porous materials

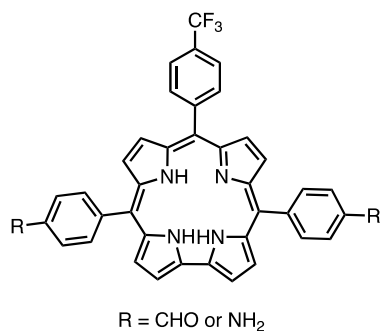
The first objective of this work was to synthesize porous materials based on free-base corroles or cobalt corrole complexes. This part will be devoted to the synthesis and spectroscopic characterization of porous materials as well as their precursors including platforms and linkers. Here, the porous materials refer to Covalent Organic Frameworks (COFs), Metal Organic Frameworks (MOFs) and Porous Organic Polymers (POPs). For each type of porous materials (as well as for the precursors), we have designed different synthetic approaches.

### 2.1 Precursors for COFs

Accordingly, covalent organic frameworks are constructed from organic units which are often named as linker and knot.<sup>1, 2</sup> Through the combination of linkers and knots, it is convenient to obtain various COFs with different topologies. In this part, linkers refer to corroles and knots are called platforms. Furthermore, the choice for linkages is another key point to synthesize COFs. Among diverse reversible reactions, Schiff base reactions tend to be the first pick to synthesize COFs due to their high stability, smooth synthetic condition and wide range of aldehyde- and amino- functions available.<sup>3, 4</sup> All the COFs are based on the Schiff base reaction, thus, the linkers and platforms contain aldehyde- or amino- groups respectively.

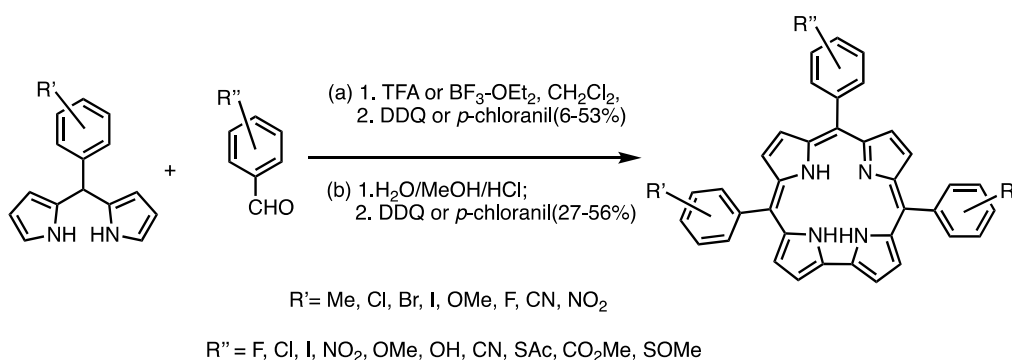
#### 2.1.1 Synthesis of corroles

The corroles used for imine COFs work as linkers which bear the same functions (aldehyde or amine) on the 5,15-*meso*-positions. The general structure of all corroles is *trans*-A<sub>2</sub>B-corrole (Scheme 1). Thus, through the combination of *trans*-A<sub>2</sub>B-corrole with diverse platforms, new original COFs could be obtained. At the 10-*meso*-position of corrole, -CF<sub>3</sub> functions were introduced for the first tests. On one hand, as strong electron withdrawing group, -CF<sub>3</sub> helps to increase the corrole stability. On the other hand, we have found good CO binding ability using cobalt A<sub>3</sub>-corrole complexes bearing CF<sub>3</sub>- functional groups.



Scheme 1. General structure for targeted *trans*-A<sub>2</sub>B-corroles.

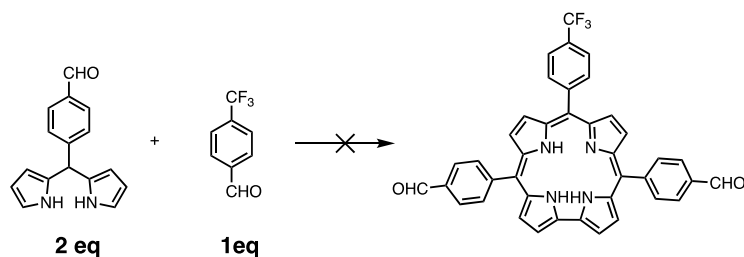
For the synthesis of *trans*-A<sub>2</sub>B-corrole, the classic strategy starting from aromatic aldehydes and dipyrromethanes was mainly applied (Scheme 2). According to the protocol<sup>5, 6</sup> from Gryko *et al.*, slight modifications of the synthetic conditions were made.



Scheme 2. Synthesis of *trans*-A<sub>2</sub>B-corroles from dipyrromethane and aromatic aldehydes using different conditions (a) or (b).<sup>7</sup>

### 2.1.1.1 Synthesis of aldehyde-functionalized corroles (refer to bis-CHO-corrole)

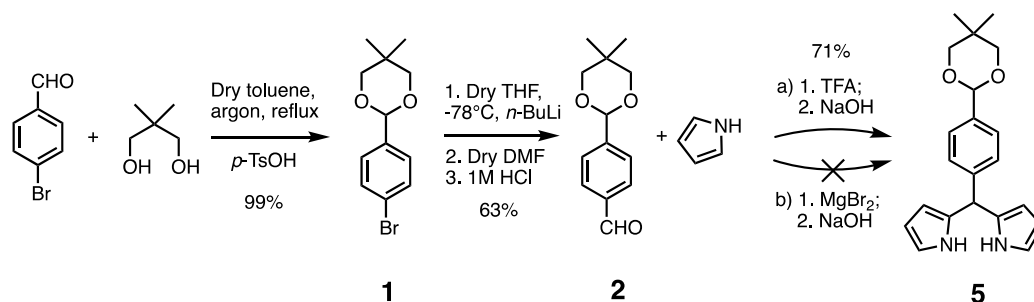
It is very difficult (or impossible) to directly apply 5-(4-formylphenyl)dipyrromethane to synthesize bis-CHO-corroles (Scheme 3). The aldehyde introduced at the meso-position of the dipyrromethane can react also with another dipyrromethane to form polymers. However, there are few examples of *meso*-aldehyde substituted corroles in the literature.<sup>8-10</sup> To temporary protect the aldehyde functions, we have designed and tried several synthetic routes.



Scheme 3. Impossible way to synthesize bis-CHO-corrole from 5-(4-formylphenyl)dipyrromethane.

### 1) Synthesis of acetal dipyrromethane

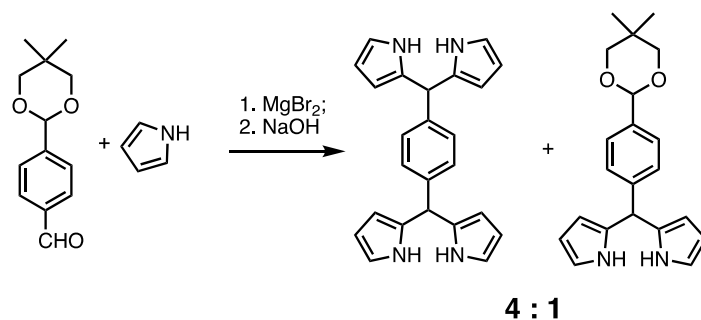
We firstly tried to design and synthesize a dipyrromethane with a protected aldehyde function (Scheme 4). Using *p*-TsOH as a catalyst, the aldehyde was protected by the acetal reaction<sup>11</sup> which is reversible and can lead the aldehyde back under acid condition. A formylation reaction<sup>12</sup> follows to give aldehyde **2** which can further react with pyrrole to afford dipyrromethane **5**. According to the literature<sup>13</sup>, the synthesis of targeted dipyrromethane **5** was carried with trifluoroacetic acid as catalyst. With a slight change of the amount of pyrrole (75 times of aldehyde), we got a 71% yield higher than the reported 48% one.



Scheme 4 Synthetic routes of 5-[4-(5,5-Dimethyl-1,3-dioxan-2-yl)phenyl]dipyrromethane.

We also tried  $\text{MgBr}_2$  to obtain targeted dipyrromethane according to literature.<sup>14</sup> Usually, with  $\text{MgBr}_2$  as catalyst for *meso*-substituted dipyrromethane synthesis, the yield and purity of products tend to be very high. However, in our case, it was quite surprising that almost no targeted dipyrromethane was observed under  $\text{MgBr}_2$  catalysis. Instead, by  $^1\text{H}$  NMR (Fig. 1), we have seen on the NMR spectrum that the main resulted compound was 1,4-bis(dipyrromethane-5-yl)benzene<sup>15</sup> (Scheme 5). In the  $^1\text{H}$  NMR spectrum with  $\text{DMSO-}d_6$ , it was found two single peaks at 1.17 and 0.74 ppm which represent two  $\text{CH}_3$  moieties from the acetal group. The single peak at 10.50 ppm can be assigned to H from pyrroles. The characteristic peak at 5.29 ppm is

attributed to the two methine structure (CH). The single peak at 7.07 ppm represented the H from phenyl. And the peaks at 6.57 ppm, 5.89 ppm, 5.67 ppm should be assigned to the  $\alpha$ -H and  $\beta$ -H of pyrroles. By integration, the ratio for the bis-dipyrromethane and dipyrromethane **5** was 4:1. This could be assigned to  $MgBr_2$  which is a strong Lewis acid that could facilitate the hydrolysis of the acetal function.



Scheme 5. Dipyrromethane synthesis catalyzed by  $MgBr_2$ .

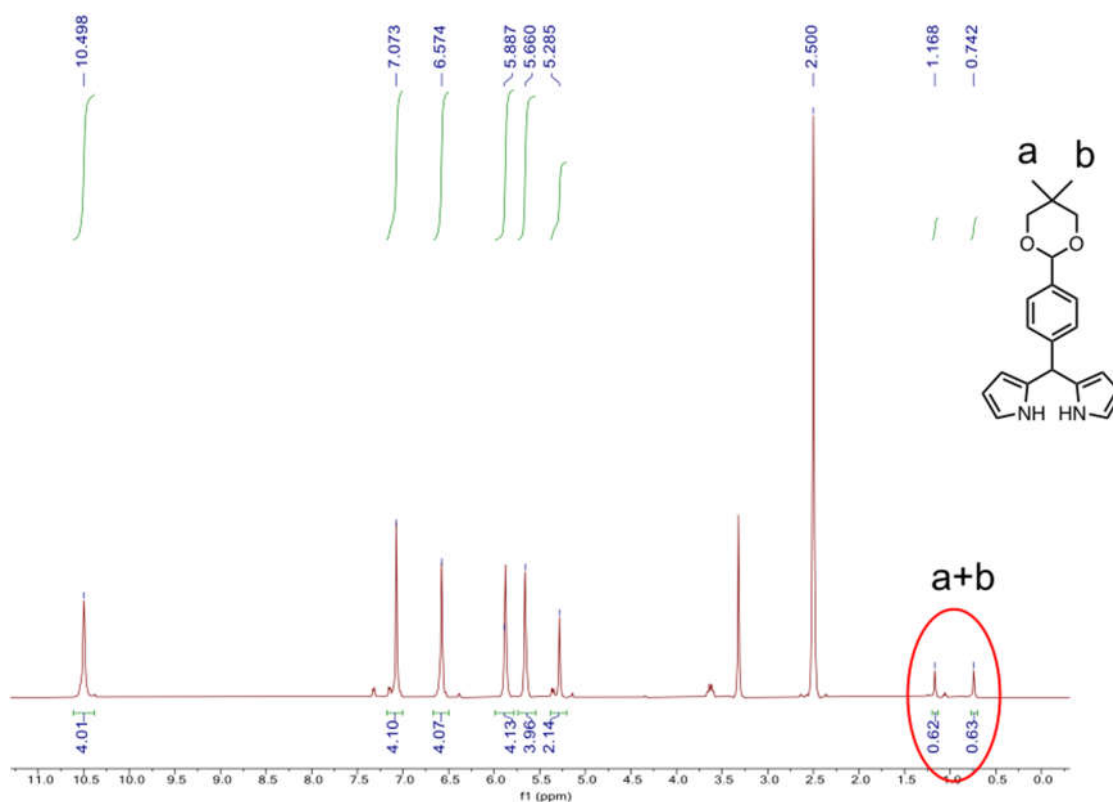
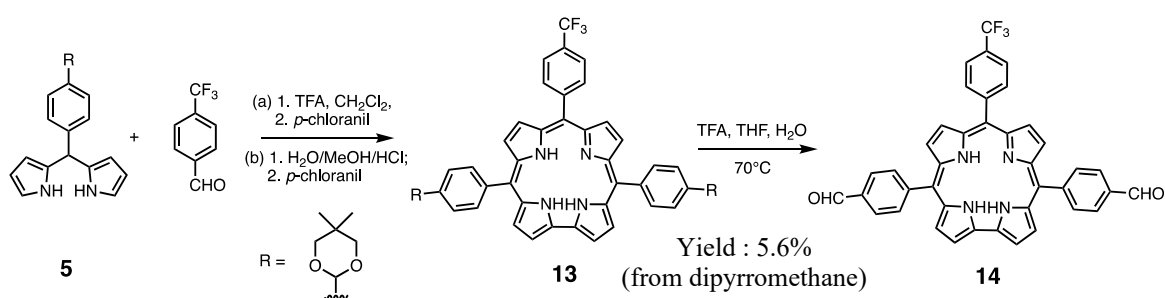


Figure 1.  $^1H$  NMR (500MHz) of mixture compounds from Scheme 1 in  $DMSO-d_6$ .

## 2) Synthesis of bis-CHO-corrole

Generally, synthesis of corroles starting from dipyrromethane and aldehyde are mainly based on two experimental conditions: (1) TFA/ DCM; or (2) H<sub>2</sub>O/MeOH/HCl. Here, we tried both of them to synthesize bis-acetalcorroles (Scheme 6). When using TFA/DCM conditions, the reaction resulted in almost no product. We assumed that during hours of reaction, the acetal was deprotected to aldehyde and further polymerization occurred. When carrying out the reaction in H<sub>2</sub>O/MeOH/HCl, the targeted bis-acetalcorrole can be observed. Through the analysis of the mass spectrum after purification, we found the presence of some side products containing either one or two aldehyde functions which were deprotected from the acetal during the corrole synthesis. In the mass spectrum, the targeted corrole was found at  $m/z = 823.342$  while peaks at  $m/z = 737.264$  and  $651.170$  were observed corresponding to one aldehyde and two aldehyde side products (Fig. 2), respectively.



Scheme 6. Synthetic routes of bis-CHO-corrole.

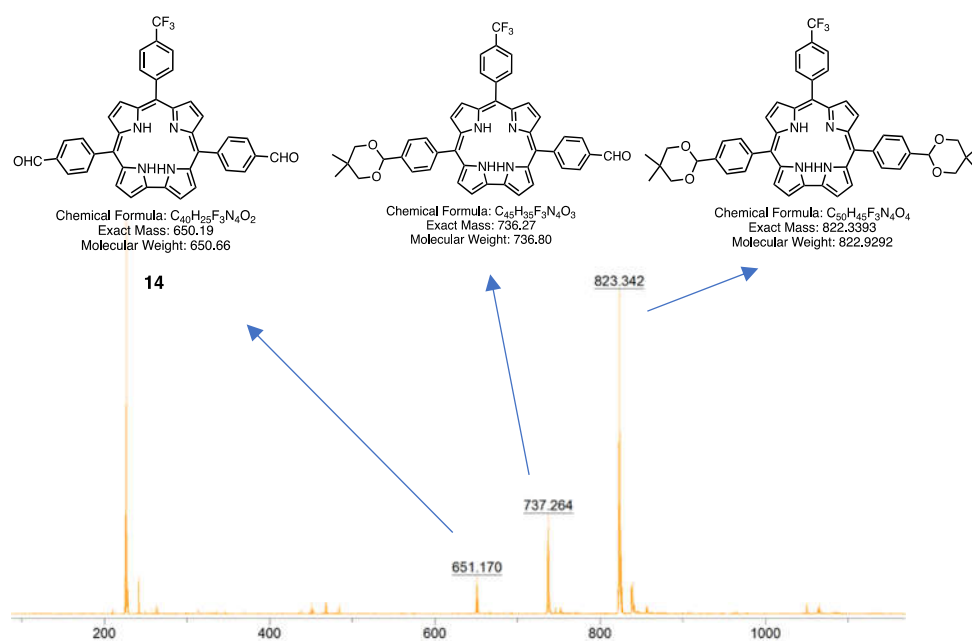


Figure 2. Mass spectrum of corroles 13.

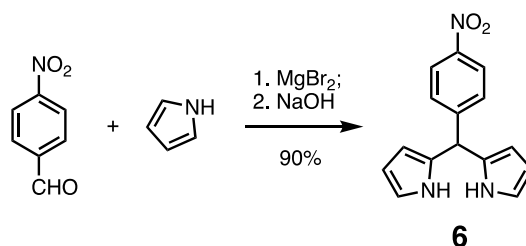
Furthermore, the polarities of the compounds are very close and it's difficult to separate them from the mixture. Thus, we directly used mixture corroles **13** for the next step to produce bis-CHO-corrole **14**. In addition, the yields for these two corroles were around 8-10%. Thus, we have used the mixture directly for the next step. The hydrolysis of the acetal (partially deprotected corrole) was carried out in a mixture of TFA, THF and H<sub>2</sub>O at 70°C. The general yield from dipyrromethane (2 steps) was 5.6%. The low yield of the bis-aldehyde corrole was an inconvenient and also uneconomic to further consider a larger scale of corroles for COF synthesis. The synthesis of COFs from bis-CHO-corrole **14** will be detailed in Chapter 3.

### 2.1.1.2 Synthesis of amino-functionalized corrole (refer to bis-NH<sub>2</sub>-corrole)

We have also designed and synthesized corroles bearing amino functions on the 5,15-*meso*-positions. To the best of our knowledge, it's impossible to directly synthesize corrole from precursors with amino functions, as the latter are easily oxidized. The synthesis of amino containing corroles has been reported in the literatures during the past decades.<sup>16-18</sup> Generally, the amino derivatives are hydrogenated from nitro corroles mainly with two different methods: (1) Pd/C/ H<sub>2</sub>; (2) SnCl<sub>2</sub>/HCl. Inspired by the literature, we choose to conduct hydrogenation of corrole under hydrogen atmosphere with palladium on carbon as catalyst well known to lead to high yields and to process through clean reaction. The reaction condition was modified slightly according to the synthesis of 5,10,15-tris(4-aminophenyl)-corrole reported by Gros et al.<sup>17</sup>

#### 1) Synthesis of nitrodipyrromethane

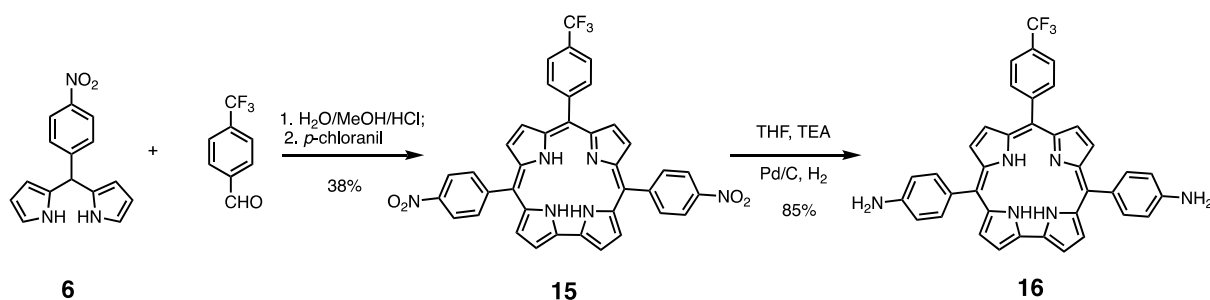
Similarly, the first step is the synthesis of dipyrromethane bearing a nitro functional group at the *meso*-position (Scheme 7). To obtain a high yield and pure dipyrromethane, MgBr<sub>2</sub> was chosen as the catalyst.<sup>14</sup> In an one pot reaction, the quantity of isolated product can reach to 12 g, which make sure that we can easily have enough dipyrromethane for the corrole synthesis.



Scheme 7. Synthesis of 5-(4-nitrophenyl)dipyrromethane.

## 2) Synthesis of bis-amino-corrole

Based on the targeted *trans*-A<sub>2</sub>B-corrole structure, the bis-nitro corrole was synthesized from 5-(4-nitrophenyl)dipyrromethane and 4-(trifluoromethyl)benzaldehyde using H<sub>2</sub>O/MeOH/HCl conditions (Scheme 8). In order to compare the COF synthesis from aldehyde and amino corrole, we kept the same -CF<sub>3</sub> moiety at the 10-*meso*-position of the corrole. As expected, this step gave a good yield of 38%. In addition, the purification of the bis-nitro corrole is easy *via* a fast column chromatography followed by recrystallization in DCM and heptane. For the hydrogenation of the nitro functions, the Pd/C catalyst was activated by heating under vacuum to avoid side products. After loading all the solvent and reagents, the reactor was purged with hydrogen. The process of the reaction was monitored by mass spectrometry until the two nitro functions were reduced to amino groups. The resulted compound was purified by flash chromatography (1g per batch with solid deposit) with DCM/TEA (v:v =100:1) as eluent. The targeted bis-amino corrole was obtained with 85% yield and was very pure. During the whole synthetic route, we have used 4-(trifluoromethyl)benzaldehyde to functionalize the *meso*-positions of the corrole macrocycle. With the same moiety at the *meso*-position, it is convenient to compare the properties of synthesized COFs. The <sup>1</sup>H NMR of corrole **15** and **16** were presented in Fig. 3. The comparison of NMR of -NO<sub>2</sub> and -NH<sub>2</sub> corroles showed an obvious effect of electron attracting or donating moieties on corrole macrocycle. It is worthy to note that the peak around -3.0 ppm representing NH from pyrrole disappeared due to hydrazine.



Scheme 8. Synthetic routes of bis-NH<sub>2</sub>-corrole.

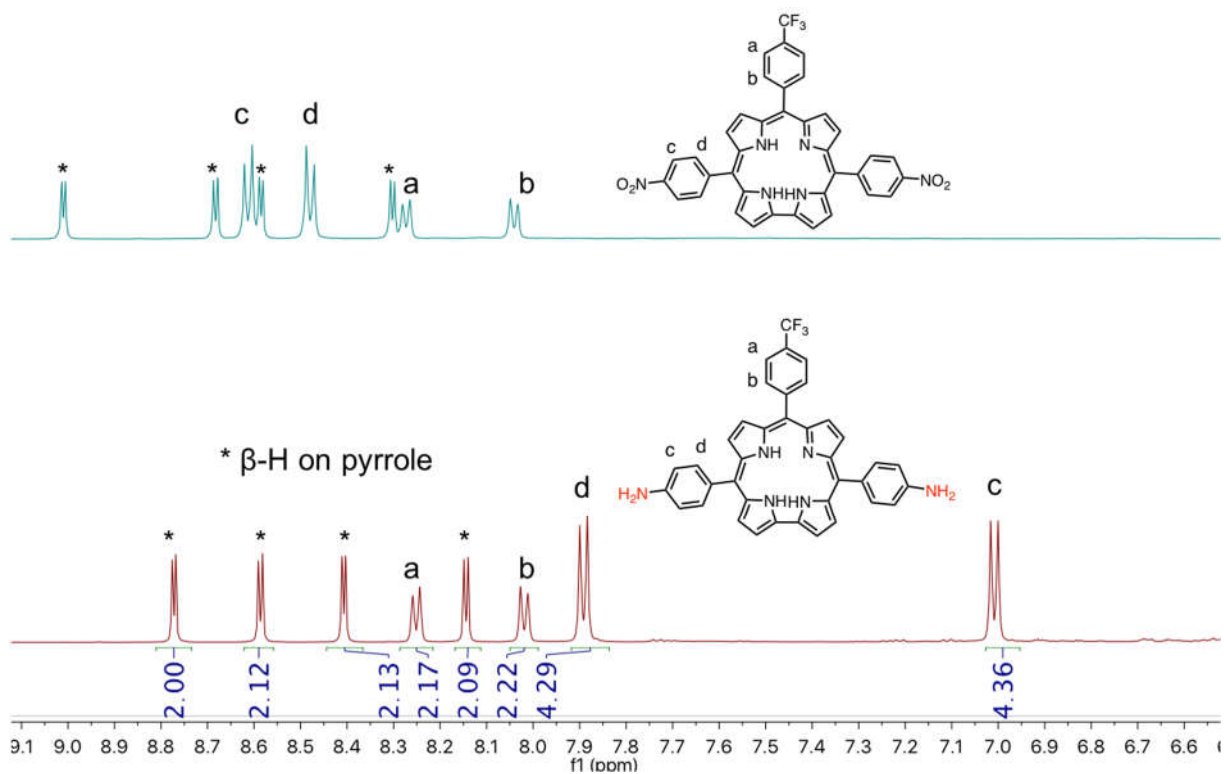


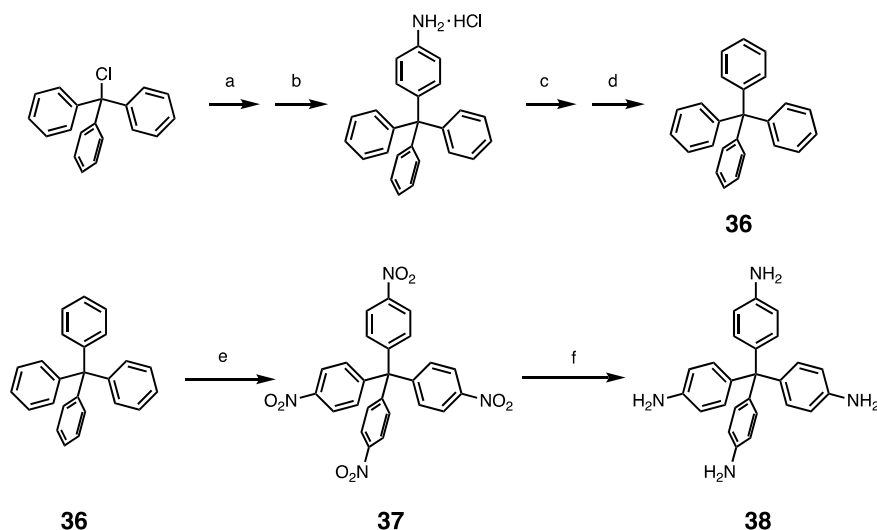
Figure 3.  $^1\text{H}$  NMR (500 MHz) spectrum of corrole **15** and **16** in  $\text{DMSO-}d_6$  after addition of 50  $\mu\text{L}$  of hydrazine.

## 2.1.2 Synthesis of platforms

For the development of imine-based covalent organic frameworks, diverse platforms (also known as knots) applied to COFs construction have been used. To obtain novel COFs based on corrole, we picked some platforms. These platforms are assigned as 2D and 3D types based on the topology classification of COFs. Here, according to the functional moiety, they are divided into aldehyde- and amino-platforms.

### 2.1.2.1 Synthesis of amino-platform

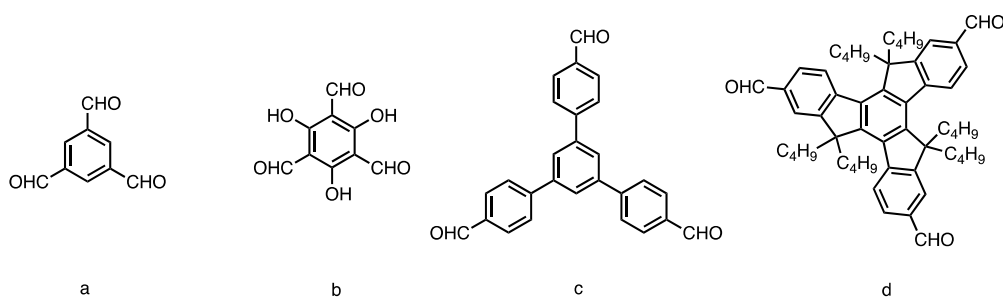
In order to match the aldehyde-corrole, tetra(4-aminophenyl)methane (TAPM) was considered to further build a novel 3D COF. Several COFs based on aldehyde porphyrin and TAPM were reported in the literature during the recent years.<sup>19-21</sup> It is very interesting to try the design of a 3D COF from a corrole instead of a porphyrin. The synthesis of TAPM was modified according to the work published by Ganesan et al.<sup>22</sup> The tetra(4-aminophenyl)methane was synthesized according to the literature except for the hydrogenation step that was done using  $\text{Pd/C-H}_2(\text{gas})$ .



Scheme 9. a) Treated with aniline at 190 °C, b) heat to 80°C with 2N HCl/MeOH, c) -15 °C, H<sub>2</sub>SO<sub>4</sub>/EtOH, isoamyl nitrite, d) heat to 50°C with hypophosphorous acid, e) fuming HNO<sub>3</sub>, acetic acid/acetic anhydride, f) Pd/C, THF, H<sub>2</sub>.

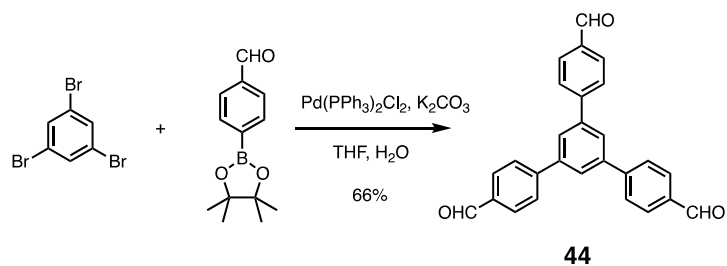
### 2.1.2.2 Synthesis of aldehyde- platforms

Concerning aldehyde- platforms, we had to make a choice among a wide range of aldehyde knots available for further 2D and 3D materials. As 2D platforms, we picked up four different aldehyde platforms, all of them showing C<sub>3</sub> symmetry.

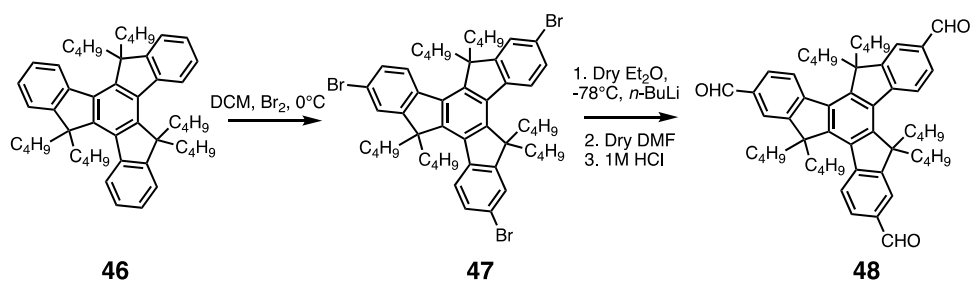


Scheme 10. 2D platforms: a) 1,3,5-Triformylbenzene, b) 1,3,5-Triformyl-2,4,6-trihydroxybenzene, c) 1,3,5-Tris(4-formylphenyl)benzene, d) 5,5,10,10,15,15-Hexabutyl-truxene-2,7,12-tricarboxaldehyde.

Among these four platforms, the 1,3,5-triformylbenzene and 1,3,5-triformyl-2,4,6-trihydroxybenzene were purchased from chemical companies. The two others were synthesized according to the literature (Scheme 11 and Scheme 12).<sup>23-25</sup>

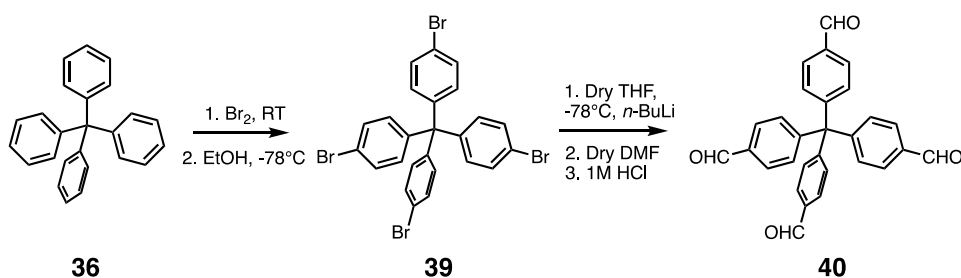


Scheme 11. Synthesis of 1,3,5-Triformyl-2,4,6-trihydroxybenzene.

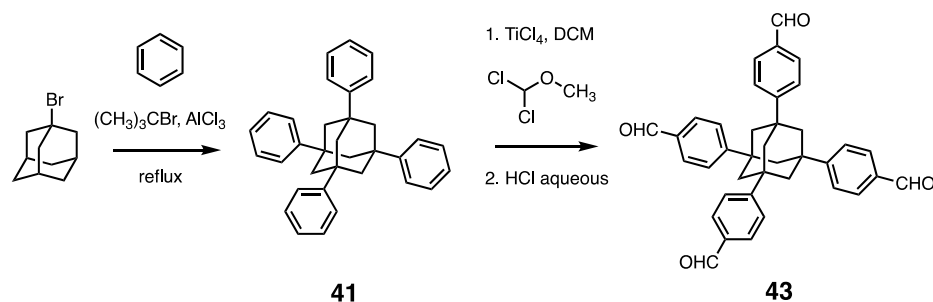


Scheme 12. Synthesis of 5,5,10,10,15,15-Hexabutyltrisformyltruxene.

For the 3D platforms, as described in Chapter 1, the knot used for 3D COF pre-design is a  $T_d$  symmetric moiety or an orthogonal unit. In the literature, tetra(phenyl)methane and adamantane tend to be often used to construct 3D COFs. Thus, we have synthesized two 3D platforms containing aldehyde functions based on tetra(phenyl)methane (Scheme 13) and adamantane (Scheme 14) respectively. For the tetra(4-formylphenyl)methane, we directly synthesized it from tetra(phenyl)methane.



Scheme 13. Synthetic route to tetra(4-formylphenyl)methane from tetra(phenyl)methane.<sup>26</sup>



Scheme 14. Synthesis of 1,3,5,7-Tetra(4-formylphenyl)adamantane.<sup>27</sup>

All the synthesis of COFs will be detailed in Chapter 3.

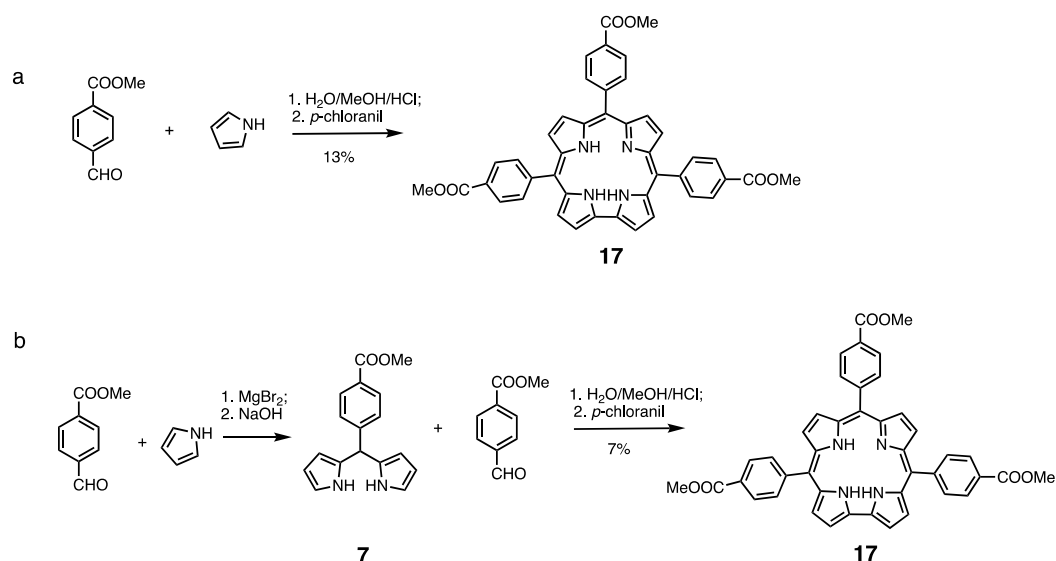
## 2.2 Precursors for MOFs

Different from COFs or POPs, MOFs are constructed via the coordination between metals and ligands. The coordination chemistry gives MOFs a modular nature, which allows for great synthetic tunability, affording both fine chemical and structural control. With creative synthetic design properties such as porosity, stability, particle morphology, and conductivity can be tailored for specific applications. Tuning MOF precursor composition and manipulating conversion processes are two main strategies for chemical and structural control. Thus, we have used two methods to construct MOFs based on corrole: (1) synthesis of MOFs directly from corroles; (2) functionalization of MOFs with corroles.

### 2.2.1 Corroles precursors for MOFs

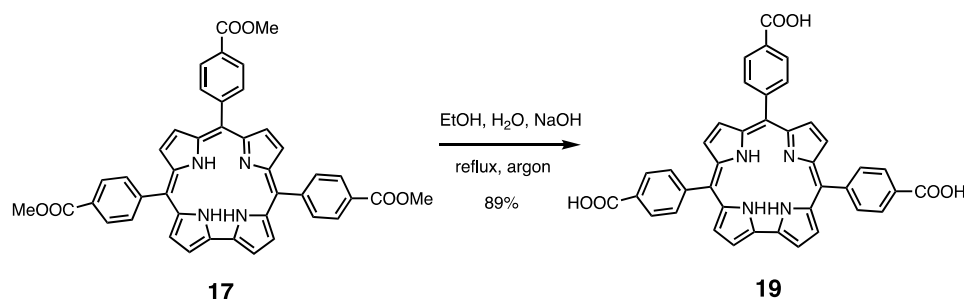
Inspired by the first example of corrole-based MOFs reported by Ma *et al.*,<sup>28</sup> we first plan to repeat this MOF synthesis, then to insert cobalt and apply it for CO sorption. In the literature, they reported MOFs constructed from 5,10,15-tris(p-carboxyphenyl)corrole ( $H_3TCPC$ ) ligand and unprecedented  $D_{3d}$ -symmetric 9-connected  $Zr_6/Hf_6$  clusters. In order to obtain this MOF, 5,10,15-tris(p-carboxyphenyl)corrole was synthesized *via* several methods. We have used two different ways to synthesize 5,10,15-tris(p-carboxymethylphenyl)corrole which is the precursor for 5,10,15-tris(p-carboxyphenyl)corrole (Scheme 15). It was worthy to note that the yield for one pot synthesis is a slightly higher than the yield obtained when starting from dipyrromethane

and aldehyde. Thus, we applied the one pot synthesis to large scale synthesis of 5,10,15-tris(*p*-carboxymethylphenyl)corrole.



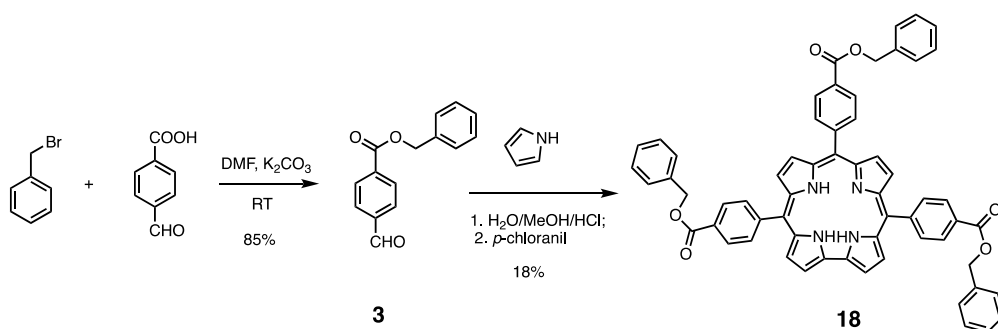
Scheme 15. Synthesis of 5,10,15-Tris(*p*-carboxymethylphenyl)corrole according two methods: a) one pot synthesis from aldehyde and pyrrole; b) synthesis from dipyrromethane and aldehyde.

For the next step, saponification of 5,10,15-tris(*p*-carboxymethylphenyl)corrole was carried in EtOH/H<sub>2</sub>O mixture with NaOH as base reagent (Scheme 16). The whole reaction was protected by argon atmosphere and monitored by mass spectrometry. The sodium salts of 5,10,15-tris(*p*-carboxyphenyl)corrole was acidified by 1M HCl slowly until no more precipitate. The resulted compound was extracted with the mixture of THF and DCM due to the bad solubility in pure DCM. Finally, the crude compound was recrystallized from a THF, DCM and heptane mixture.

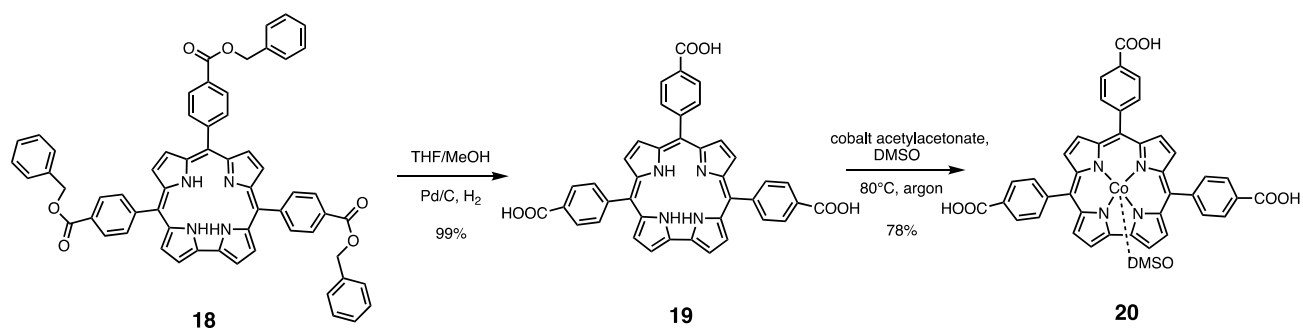


Scheme 16. Synthesis of 5,10,15-tris(*p*-carboxyphenyl)corrole.

The targeted tris-COOH corrole was obtained in 90% yield. However, this last step was not totally reproducible. Thus, we have designed another strategy to synthesize tris-COOH corrole (Schemes 17 and 18). As shown in Scheme 16, 4-(benzyloxycarbonyl)benzaldehyde was obtained after benzylation of 4-formylbenzoic acid with benzyl bromide.<sup>29</sup> Then, we can prepare 5,10,15-tris(4-(benzyloxycarbonyl)phenyl)corrole by one pot synthesis procedure. Under hydrogenation using Pd/C as catalyst, the tris-COOH-corrole was obtained in quantitative yield without traces of any impurity and in addition, the synthesis was shown to be very reproducible (Scheme 17). This reaction is the first example of the synthesis of a tris-COOH corrole by hydrogenation. After that, metalation of the 5,10,15-tris(*p*-carboxyphenyl)corrole with cobalt was followed. The cobalt 5,10,15-tris(*p*-carboxyphenyl)corrole was characterized by <sup>1</sup>H NMR (Fig. 4), hydrogen atoms from the aromatic positions were clearly shown around 9.30 - 8.20 ppm. Peaks around 9.26, 9.03, 8.84, 8.81 ppm represented the hydrogens on pyrrole while the shifts of hydrogens on phenyl centered around 8.40 - 8.27 ppm. Hydrazine was added to raise the resolution of spectrum, however, due to an over excess, hydrazine was also found as an axial ligand coordinated to cobalt metal center of the corrole. The hydrazine replaced dimethyl sulfoxide and the 4 hydrogens shift appeared at -3.40 ppm. The free dimethyl sulfoxide showed normal chemical shift at 2.68 ppm in CD<sub>3</sub>OD. The integration for hydrogen of DMSO should be 6 and the 7 H in Fig. 4 represents trace of DMSO as solvent from the metalation step. And on the <sup>13</sup>C NMR spectrum (Fig. 5), the peak at 40.4 ppm represented normal shift of free dimethyl sulfoxide.



Scheme 17. Synthesis of 5,10,15-tris(4-(benzyloxycarbonyl)phenyl)corrole.



Scheme 18. Synthesis of 5,10,15-tris(p-carboxylphenyl)corrole with saponification with hydrogenation.

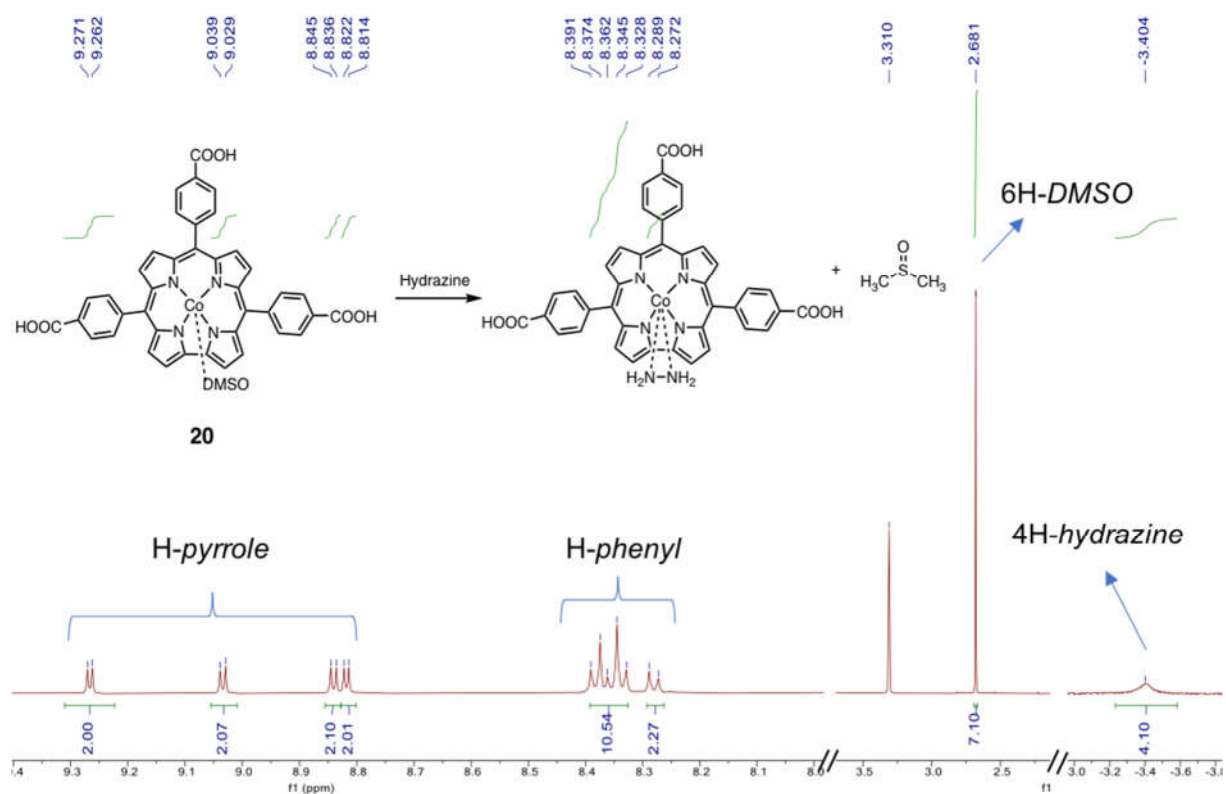


Figure 4.  $^1\text{H}$  NMR (500 MHz) spectrum of corrole **20** in  $\text{CD}_3\text{OD}$  after addition of  $50\ \mu\text{L}$  of hydrazine.

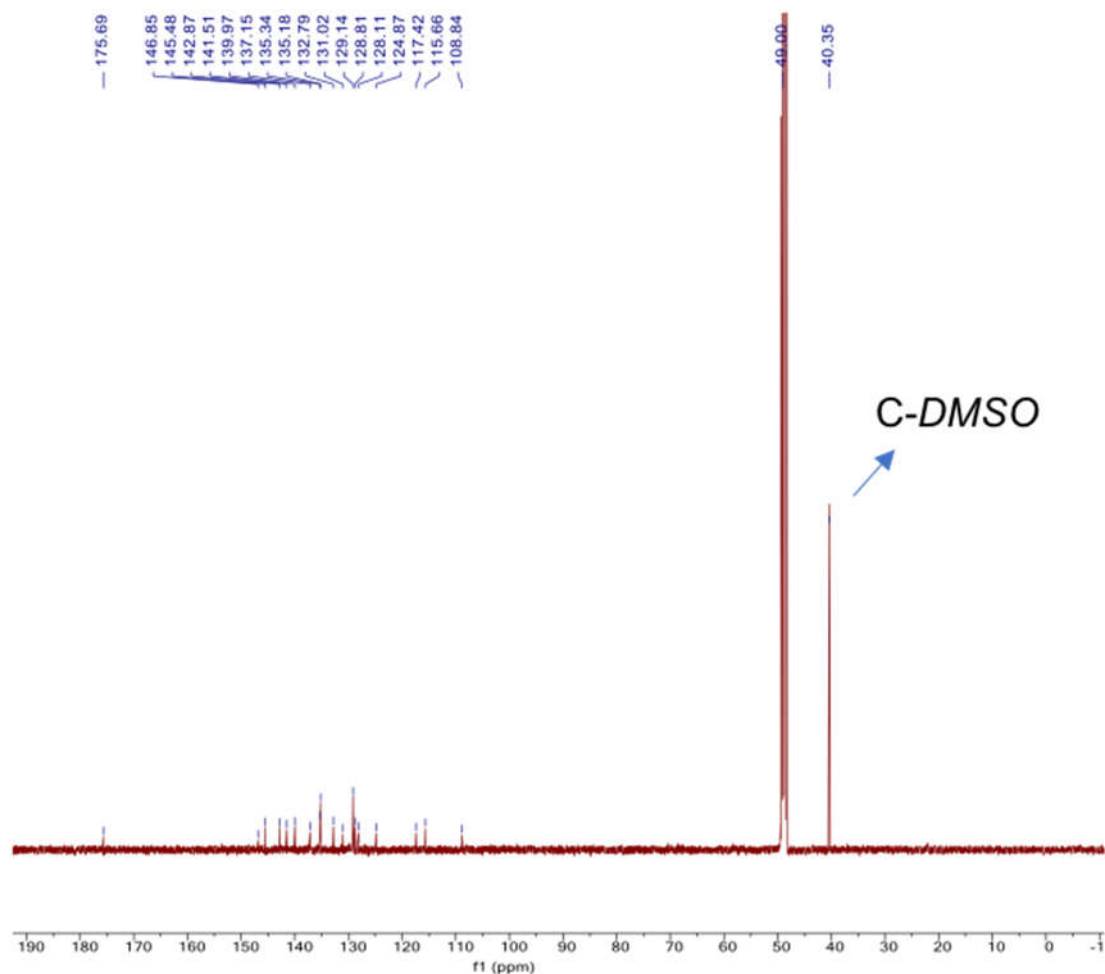


Figure 5.  $^{13}\text{C}$  NMR (125 MHz) spectrum of corrole **20** in  $\text{CD}_3\text{OD}$  after addition of 50  $\mu\text{L}$  of hydrazine.

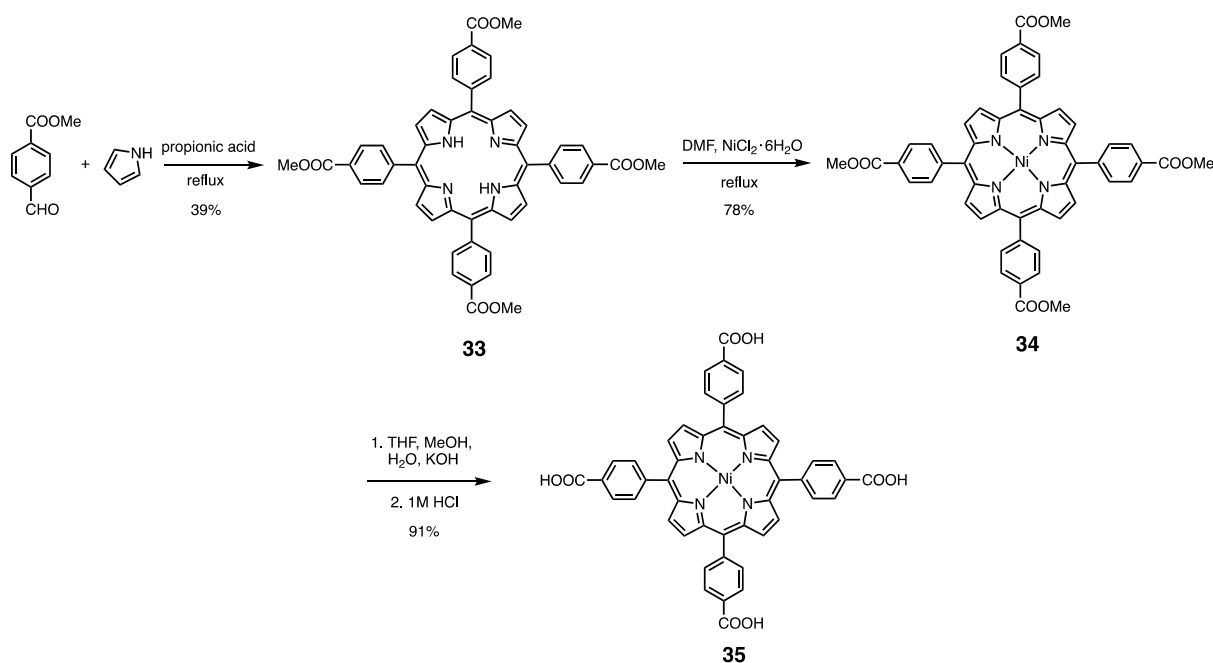
## 2.2.2 Precursors for MOFs functionalization

In this part, we will present the synthesis of precursors which can be used to functionalize well known MOFs from the literature (reported without doping of corroles). For this extended work, preparations of precursors can be divided into two parts: (a) porphyrin for MOF construction; (b) corroles for further functionalization of MOF.

### 2.2.2.1 Porphyrin precursor for MOF construction

Here, we choose PCN-222 as the target to be potentially functionalized with corrole due to the high porosity, high stability and enough pore size for containing corroles. The Ni-porphyrin was synthesized exactly the same way as described in the literature.<sup>30</sup> In order to synthesize PCN-222, the Ni-tetracarboxyporphyrin was obtained according to Scheme 19. With an one pot

synthesis from 4-carboxymethylbenzaldehyde, porphyrin **33** obtained for following steps. Then, metalation of porphyrin was carried to have porphyrin **34** followed by saponification to obtain porphyrin **35**. Here, the metalation was conducted before saponification because it is more difficult to purify porphyrin **35** bearing 4 carboxylic acid groups.

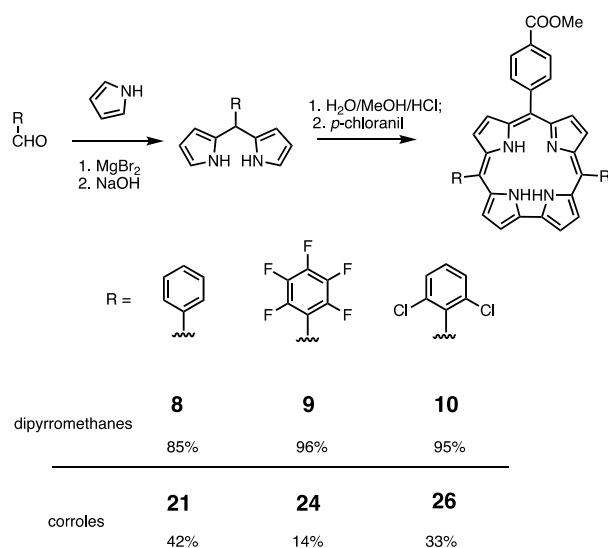


Scheme 19. Synthetic route to [5,10,15,20-Tetrakis(4-carboxyphenyl)porphyrinato]-Ni(II).<sup>30-32</sup>

#### 2.2.2.2 Corroles precursors for further MOF functionalization

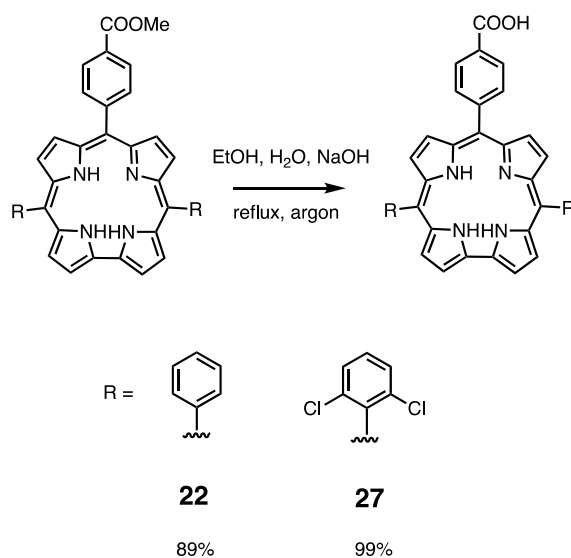
In order to incorporate corroles into PCN-222, several corroles containing carboxylic acid functions were designed and synthesized. All of ester corrole were synthesized starting from dipyrromethanes and 4-carboxymethylbenzaldehyde with MeOH/ $\text{H}_2\text{O}$ /HCl conditions. The -COOH corrole were obtained by saponification or hydrolysis. Here, all corroles were functionalized with carboxylic acid group on the 10-*meso*-position of corrole ( $A_2B$ -*trans*-corrole). We have chosen three different moieties to functionalize the 5,15-*meso*-positions of the corrole macrocycle. The three moieties possess different electron withdrawing groups which may modulate the CO binding affinities. It is interesting to further compare the electronic effect of different moieties. For the corroles shown below (Scheme 20), the whole process started from the synthesis of dipyrromethane in high yields (85%, 96%, 95% respectively for compounds **8**, **9**, **10**). All the reactions were catalyzed by  $\text{MgBr}_2$ . Then, dipyrromethanes were

further reacted with 4-carboxymethylbenzaldehyde in MeOH/H<sub>2</sub>O/HCl to give corroles **21**, **24**, **26** (in 41%, 14%, 33% yields, respectively).

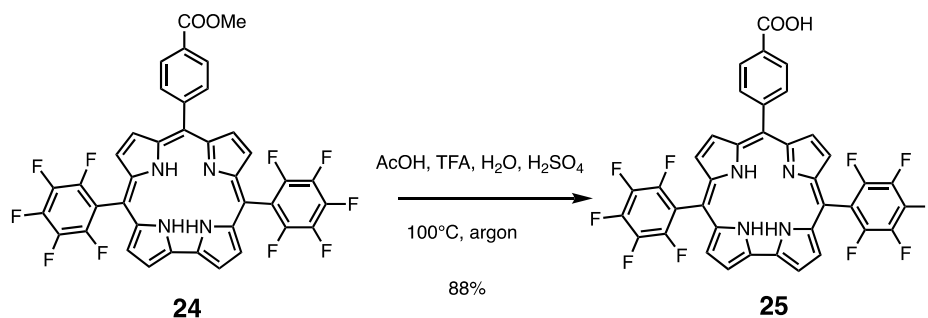


Scheme 20. Synthesis of dipyrromethanes **8**, **9**, **10** and corresponding corroles **21**, **24**, **26**.

Saponification of the ester corroles **21** and **26** proceed under alkaline condition using sodium hydroxide in a mixture of water and ethanol (Scheme 21). Both reactions showed high yield and the final products were obtained without further purification. Hydrolysis of corrole **24** was previously reported by Honig *et al.*, thus the same process was repeated (Scheme 22) under acid condition.

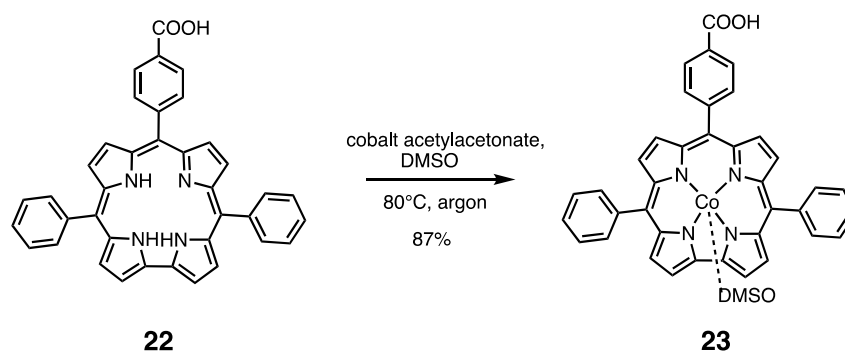


Scheme 21. Synthesis of corroles **22** and **27**.



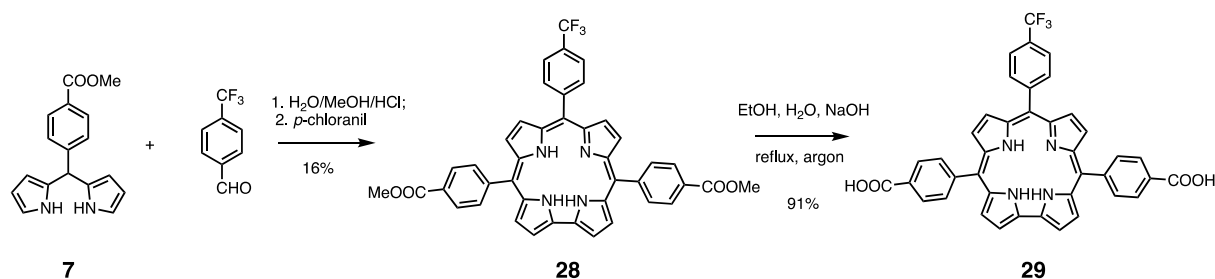
Scheme 22. Synthesis of corrole **25**.

Two methods can be used to functionalize PCN-222 with cobalt corrole: post-metallation or pre-metallation with cobalt. We have synthesized three different free base corroles and have used them firstly in the post-functionalization of PCN-222 followed by cobalt metalation. To be different from previous methods, we have also selected and synthesized the cobalt complex of 5,15-diphenyl-10(4-carboxyphenyl)corrole (Scheme 23) to directly applied for functionalization of PCN-222. The two different methods may lead to different CO binding. It is thus very interesting to further compare them.



Scheme 23. Synthesis of 5,15-diphenyl-10-(4-carboxyphenyl)corrole cobalt complex.

Furthermore, we have also synthesized an A<sub>2</sub>B-corrole bearing two carboxylic acid moieties on at the 5,15-*meso*-positions (Scheme 24). The two carboxylic acid moieties may make it easier to functionalize PCN-222. We keep -CF<sub>3</sub> at the 10-position of the corrole to be similar to the corroles previously used for the COFs.



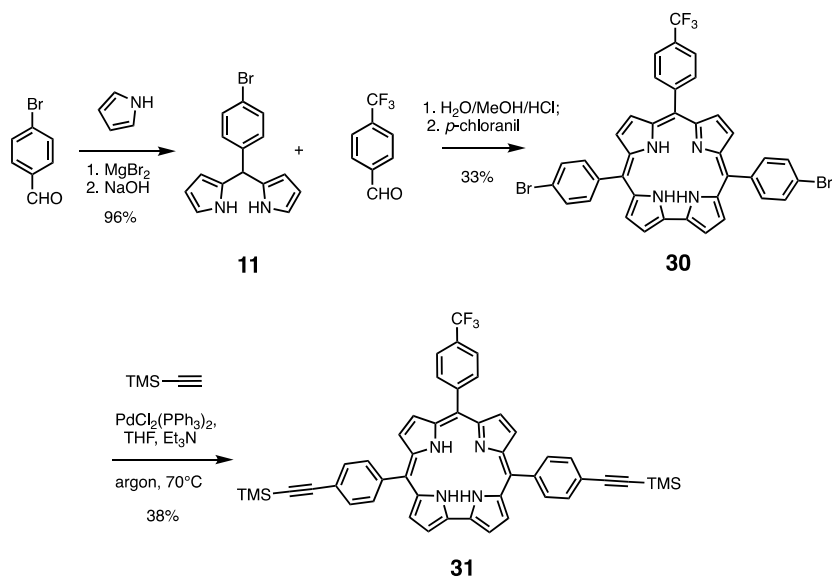
Scheme 24. Synthesis of 5,15-di(4-carboxyphenyl)-10-(4-trifluoromethyl)corrole.

## 2.3 Precursors for POPs

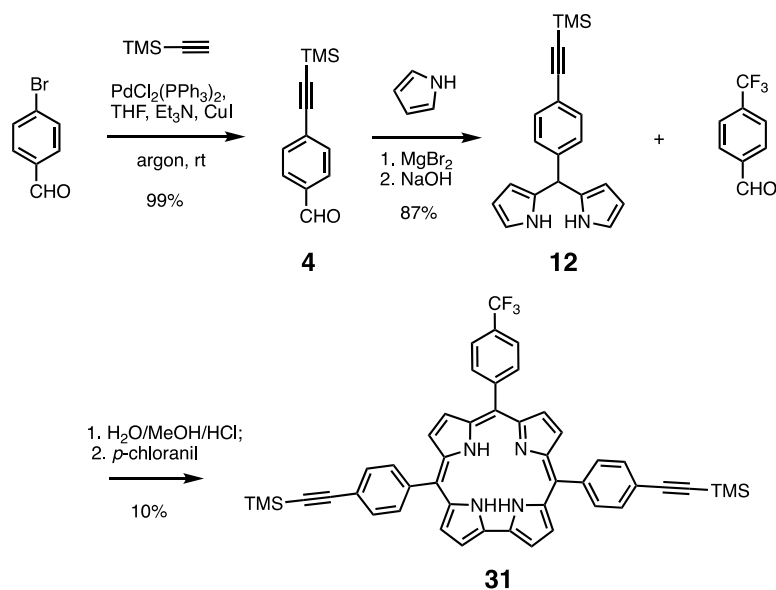
As another part of my PhD work, we were also interested in the synthesis of POPs based on corroles. As presented in Chapter 1, there are two examples of amorphous POPs based corroles. Among them, the POP constructed from diiodocorrole and tetra-alkyne platform through Sonogashira cross-coupling reaction is more attractive.<sup>33</sup> In order to have a more rigid 3D structure, we plan to use 1,3,5,7-tetrakis(4-iodophenyl)adamantane as a rigid platform and the di-alkyne corrole will be the linker. The synthesis of this corrole and platform was described below.

### 2.3.1 Synthesis of the corrole precursor

Different from the previous reported POP based on diiodocorrole and tetra-alkyne platform,<sup>33</sup> we have designed and synthesized di-alkyne corrole and tetra-iodo platform. It is easier to obtain di-alkyne corrole and tetra-iodo platform in few steps. The synthesis of di-alkyne corrole was described in detail. Here, we tried two different strategies to obtain this corrole (Schemes 25 and 26). The main difference between these two processes is the order of the insertion of the alkyne groups either at the beginning or at the end of the synthesis. By comparing protocol and overall yield, the second method (Scheme 26) tended to be a better choice due to the simple and easy purification of the targeted corrole and high and almost quantitative yield when starting from 4-bromobenzaldehyde.

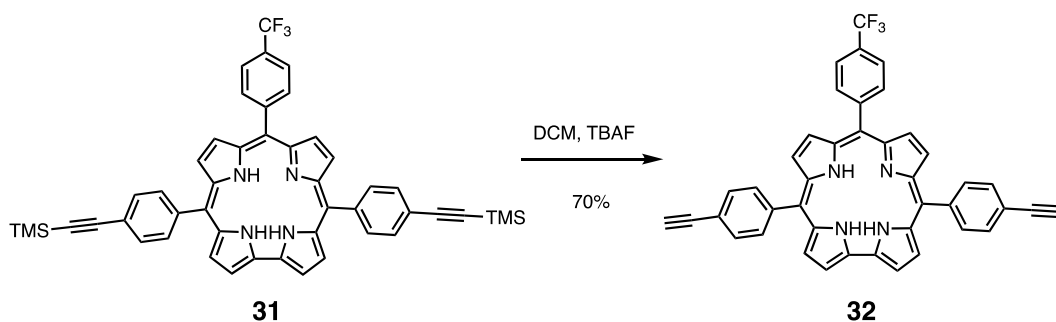


Scheme 25. Synthetic route of 5,15-di(4-(trimethylsilylethynyl)phenyl)-10-(4-trifluoromethyl)corrole with post-synthesis using trimethylsilylacetylene.



Scheme 26. Synthetic route of 5,15-di(4-(trimethylsilylethynyl)phenyl)-10-(4-trifluoromethyl)corrole with pre-synthesis using trimethylsilylacetylene.

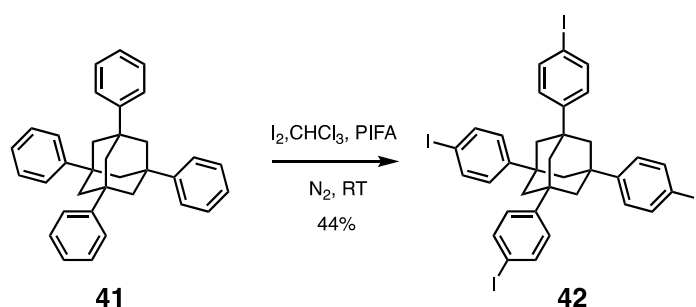
For the next step, the trimethylsilylacetylene functions were deprotected with TBAF (Scheme 27). The resulted di-alkyne corrole was purified by flash chromatography, giving a high yield of 95%.



Scheme 27. Synthesis of 5,15-di(4-ethynylphenyl)-10-(4-trifluoromethyl)corrole.

### 2.3.2 Synthesis of the adamantane precursor

Finally in order to design a POP with a more rigid platform, we were interested in the synthesis of 1,3,5,7-tetra(4-iodophenyl)adamantane. Firstly, 1,3,5,7-tetraphenyladamantane was obtained from 1-bromoadamantane and benzene (also used as solvent). The electrophilic substitution reaction between adamantane and benzene was carried under the catalyzis of *t*-butylbromide and aluminum chloride. Halogenation with iodine of adamantane **41** gave targeted 1,3,5,7-tetra(4-iodophenyl)adamantane **42** (Scheme 28).<sup>34</sup>



Scheme 28. Synthesis of 1,3,5,7-tetra(4-iodophenyl)adamantane.

## 2.4 Conclusion

This chapter mainly presented the synthesis of the precursors involved in the construction of different porous materials: COFs, MOFs and POPs. The characterizations of these precursors are presented in the experimental part. In this chapter, we mainly synthesized different corroles. The corroles can be used for COFs construction, MOFs functionalization and POPs construction. In the next chapter we are more particularly interested in the synthesis and characterization of new COFs.



## References

1. Guan, X.; Chen, F.; Fang, Q.; Qiu, S., Design and applications of three dimensional covalent organic frameworks. *Chem. Soc. Rev.* **2020**, *49* (5), 1357-1384.
2. Geng, K.; He, T.; Liu, R.; Dalapati, S.; Tan, K. T.; Li, Z.; Tao, S.; Gong, Y.; Jiang, Q.; Jiang, D., Covalent Organic Frameworks: Design, Synthesis, and Functions. *Chem. Rev.* **2020**, *120* (16), 8814-8933.
3. Haase, F.; Lotsch, B. V., Solving the COF trilemma: towards crystalline, stable and functional covalent organic frameworks. *Chem. Soc. Rev.* **2020**, *49* (23), 8469-8500.
4. Li, X.; Cai, S.; Sun, B.; Yang, C.; Zhang, J.; Liu, Y., Chemically Robust Covalent Organic Frameworks: Progress and Perspective. *Matter* **2020**, *3* (5), 1507-1540.
5. Gryko, D. T.; Koszarna, B., Refined methods for the synthesis of meso-substituted A<sub>3</sub>- and trans-A<sub>2</sub>B-corroles. *Org. Biomol. Chem.* **2003**, *1* (2), 350-357.
6. Koszarna, B.; Gryko, D. T., Efficient Synthesis of meso-Substituted Corroles in a H<sub>2</sub>O-MeOH Mixture. *J. Org. Chem.* **2006**, *71* (10), 3707-3717.
7. Orłowski, R.; Gryko, D.; Gryko, D. T., Synthesis of Corroles and Their Heteroanalogs. *Chem. Rev.* **2017**, *117* (4), 3102-3137.
8. Gryko, D. T.; Piechota, K. E., Straightforward route to trans-A<sub>2</sub>B-corroles bearing substituents with basic nitrogen atoms. *J. Porphyr. Phthalocyanines* **2002**, *06* (02), 81-97.
9. Fang, J.-J.; Lan, J.; Yang, G.; Yuan, G.-Q.; Liu, H.-Y.; Si, L.-P., Synthesis of cobalt A<sub>2</sub>B triaryl corroles bearing aldehyde and amide pyridyl groups and their performance in electrocatalytic hydrogen evolution. *New J. Chem.* **2021**, *45* (11), 5127-5136.
10. Liu, B.; Fang, H.; Li, X.; Cai, W.; Bao, L.; Rudolf, M.; Plass, F.; Fan, L.; Lu, X.; Guldi, D. M., Synthesis and Photophysical Properties of a Sc<sub>3</sub>N@C<sub>80</sub>-Corrole Electron Donor-Acceptor Conjugate. *Chem. Eur. J.* **2015**, *21* (2), 746-752.
11. Eberhard, J.; Peuntinger, K.; Fröhlich, R.; Guldi, D. M.; Mattay, J., Synthesis and Properties of Acridine and Acridinium Dye Functionalized Bis(terpyridine) Ruthenium(II) Complexes. *Eur. J. Org. Chem.* **2018**, *2018* (20), 2682-2700.
12. Hong, S.; Rohman, M. R.; Jia, J.; Kim, Y.; Moon, D.; Kim, Y.; Ko, Y. H.; Lee, E.; Kim, K., Porphyrin Boxes: Rationally Designed Porous Organic Cages. *Angew. Chem. Int. Ed.* **2015**, *54* (45), 13241-13244.
13. Thamyongkit, P.; Yu, L.; Padmaja, K.; Jiao, J.; Bocian, D. F.; Lindsey, J. S., Porphyrin Dyads Bearing Carbon Tethers for Studies of High-Density Molecular Charge Storage on Silicon Surfaces. *J. Org. Chem.* **2006**, *71* (3), 1156-1171.

14. Laha, J. K.; Dhanalekshmi, S.; Taniguchi, M.; Ambroise, A.; Lindsey, J. S., A Scalable Synthesis of Meso-Substituted Dipyrrromethanes. *Org. Process Res. Dev.* **2003**, *7* (6), 799-812.
15. Mangham, B.; Hanson-Heine, M. W. D.; Davies, E. S.; Wriglesworth, A.; George, M. W.; Lewis, W.; Kays, D. L.; McMaster, J.; Besley, N. A.; Champness, N. R., Influence of molecular design on radical spin multiplicity: characterisation of BODIPY dyad and triad radical anions. *Phys. Chem. Chem. Phys.* **2020**, *22* (8), 4429-4438.
16. Li, C.-Y.; Zhang, X.-B.; Han, Z.-X.; Åkermark, B.; Sun, L.; Shen, G.-L.; Yu, R.-Q., A wide pH range optical sensing system based on a sol-gel encapsulated amino-functionalised corrole. *Analyst* **2006**, *131* (3), 388-393.
17. Gros, C. P.; Desbois, N.; Michelin, C.; Demilly, E.; Tilkin-Mariamé, A.-F.; Mariamé, B.; Gallardo, F., Synthesis and Antiviral Activity Evaluation of Nitroporphyrins and Nitrocorroles as Potential Agents against Human Cytomegalovirus Infection. *ACS Infect. Dis.* **2015**, *1* (8), 350-356.
18. Zhao, Y.; Dai, W.; Peng, Y.; Niu, Z.; Sun, Q.; Shan, C.; Yang, H.; Verma, G.; Wojtas, L.; Yuan, D.; Zhang, Z.; Dong, H.; Zhang, X.; Zhang, B.; Feng, Y.; Ma, S., A Corrole-Based Covalent Organic Framework Featuring Desymmetrized Topology. *Angew. Chem. Int. Ed* **2020**, *59* (11), 4354-4359.
19. Meng, Y.; Luo, Y.; Shi, J.-L.; Ding, H.; Lang, X.; Chen, W.; Zheng, A.; Sun, J.; Wang, C., 2D and 3D Porphyrinic Covalent Organic Frameworks: The Influence of Dimensionality on Functionality. *Angew. Chem. Int. Ed.* **2020**, *59* (9), 3624-3629.
20. Lin, G.; Ding, H.; Chen, R.; Peng, Z.; Wang, B.; Wang, C., 3D Porphyrin-Based Covalent Organic Frameworks. *J. Am. Chem. Soc* **2017**, *139* (25), 8705-8709.
21. Hynek, J.; Zelenka, J.; Rathouský, J.; Kubát, P.; Ruml, T.; Demel, J.; Lang, K., Designing Porphyrinic Covalent Organic Frameworks for the Photodynamic Inactivation of Bacteria. *ACS Appl. Mater. Interfaces* **2018**, *10* (10), 8527-8535.
22. Ganesan, P.; Yang, X.; Loos, J.; Savenije, T. J.; Abellon, R. D.; Zuilhof, H.; Sudhölter, E. J. R., Tetrahedral n-Type Materials: Efficient Quenching of the Excitation of p-Type Polymers in Amorphous Films. *J. Am. Chem. Soc* **2005**, *127* (42), 14530-14531.
23. Janeta, M.; Bury, W.; Szafert, S., Porous Silsesquioxane–Imine Frameworks as Highly Efficient Adsorbents for Cooperative Iodine Capture. *ACS Appl. Mater. Interfaces* **2018**, *10* (23), 19964-19973.
24. Dehmlow, E. V.; Kelle, T., Synthesis of New Truxene Derivatives: Possible Precursors of Fullerene Partial Structures? *Synth. Commun.* **1997**, *27* (11), 2021-2031.

25. Zhou, H.; Zhao, X.; Huang, T.; Lu, R.; Zhang, H.; Qi, X.; Xue, P.; Liu, X.; Zhang, X., Synthesis of star-shaped monodisperse oligo(9,9-di-n-octylfluorene-2,7-vinylene)s functionalized truxenes with two-photon absorption properties. *Org. Biomol. Chem.* **2011**, *9* (5), 1600-1607.
26. Klumpen, C.; Winterstein, S.; Papastavrou, G.; Senker, J., Anhydrous proton conduction in porous organic networks. *J. Mater. Chem. A* **2018**, *6* (43), 21542-21549.
27. Zhu, D. Y.; Landis, R. F.; Li, C.-H.; Gupta, A.; Wang, L.-S.; Geng, Y.; Gopalakrishnan, S.; Guo, J. W.; Rotello, V. M., Dynamically crosslinked polymer nanocomposites to treat multidrug-resistant bacterial biofilms. *Nanoscale* **2018**, *10* (39), 18651-18656.
28. Zhao, Y.; Qi, S.; Niu, Z.; Peng, Y.; Shan, C.; Verma, G.; Wojtas, L.; Zhang, Z.; Zhang, B.; Feng, Y.; Chen, Y.-S.; Ma, S., Robust Corrole-Based Metal–Organic Frameworks with Rare 9-Connected Zr/Hf-Oxo Clusters. *J. Am. Chem. Soc.* **2019**, *141* (36), 14443-14450.
29. Ma, T.; Huang, M.; Li, A.; Zhao, F.; Li, D.; Liu, D.; Zhao, L., Design, synthesis and biological evaluation of benzimidazole derivatives as novel human Pin1 inhibitors. *Bioorg. Med. Chem. Lett.* **2019**, *29* (14), 1859-1863.
30. Keum, Y.; Park, S.; Chen, Y.-P.; Park, J., Titanium-Carboxylate Metal-Organic Framework Based on an Unprecedented Ti-Oxo Chain Cluster. *Angew. Chem. Int. Ed.* **2018**, *57* (45), 14852-14856.
31. Cichocka, M. O.; Liang, Z.; Feng, D.; Back, S.; Siahrostami, S.; Wang, X.; Samperisi, L.; Sun, Y.; Xu, H.; Hedin, N.; Zheng, H.; Zou, X.; Zhou, H.-C.; Huang, Z., A Porphyrinic Zirconium Metal–Organic Framework for Oxygen Reduction Reaction: Tailoring the Spacing between Active-Sites through Chain-Based Inorganic Building Units. *J. Am. Chem. Soc.* **2020**, *142* (36), 15386-15395.
32. Feng, L.; Wang, Y.; Yuan, S.; Wang, K.-Y.; Li, J.-L.; Day, G. S.; Qiu, D.; Cheng, L.; Chen, W.-M.; Madrahimov, S. T.; Zhou, H.-C., Porphyrinic Metal–Organic Frameworks Installed with Bronsted Acid Sites for Efficient Tandem Semisynthesis of Artemisinin. *ACS Catal.* **2019**, *9* (6), 5111-5118.
33. Brandès, S.; Quesneau, V.; Fonquernie, O.; Desbois, N.; Blondeau-Patissier, V.; Gros, C. P., Porous organic polymers based on cobalt corroles for carbon monoxide binding. *Dalton Trans.* **2019**, *48* (31), 11651-11662.
34. Xie, L.-H.; Suh, M. P., High CO<sub>2</sub>-Capture Ability of a Porous Organic Polymer Bifunctionalized with Carboxy and Triazole Groups. *Chem. Eur. J.* **2013**, *19* (35), 11590-11597.



## Chapter 3

# Synthesis of COFs based on cobalt corroles



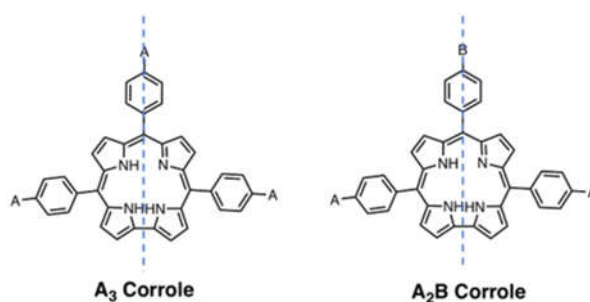
## Chapter 3: Synthesis of COFs based on cobalt corroles

We have shown in Chapter 1 that cobalt corroles were capable of selectively adsorbing carbon monoxide. Our group has already published results concerning this property.<sup>1-3</sup> However, when we use monomer corroles complexes, the number of active sites of many cobalt corroles complex are much lower than expected. Generally, for these corroles,  $\pi$ -stacking is likely to occur, being the predominant effect for non-porous solid state of corroles, thus making parts of cobalt sites unavailable for carbon monoxide binding. Moreover, after several cycles of CO sorption *vs* N<sub>2</sub>, O<sub>2</sub> and CO<sub>2</sub>, a decrease of CO chemisorption was observed due to partial degradation of the corroles metal complexes. In order to get more efficient active species, we have been interested in the development of new porous materials based on cobalt corroles, and more particularly the covalent organic frameworks (COFs) which are the main subject of our research subject. The COFs are generally very stable and should allow the increase of the CO sorption volume compared to non-porous corrole solid. Up to date, there are only two examples of COFs based on corroles which are presented in chapter 1.<sup>4,5</sup> In this chapter, the study of new COFs based on cobalt corroles will be presented with their CO sorption properties.

### 3.1 Design of COFs for this project

In order to construct novel COFs, it is necessary to pre-design the structure and topology of COFs. As described in chapter 1, the topologies of COFs are decided by linkers and knots, which are also called systems ( $C_x + C_y$ ). Through combination of diverse linkers and knots, different topologies can be achieved. According to different requirements of stabilities and applications, appropriate linkages can be used for many COFs. As presented before, two corrole-based COFs have been reported and both are based on an imine linkage (the most commonly encountered type of bonding among all COF linkages). Furthermore, in recent years, many examples of porphyrin-based COFs with imine linkage have been reported.<sup>6-9</sup> Corrole, as a member of the porphyrin family, is a very interesting macrocycle to further construct novel COFs *via* imine linkage.

Corrole, often  $A_3$  or *trans*- $A_2B$  substituted, is an  $C_2$  symmetric molecule bearing most of the time aryl groups at the 5,10,15-*meso* positions (Scheme 1). Reported by Ma and Zhang et al,<sup>4,5</sup> the T-shaped 5,10,15-tris(*p*-aminophenyl)corrole was applied to construct 2D COFs. We tried to reproduce these COFs but very quickly we realized that these COFs were not stable under the air. Thus, we planned to focus on the use of a more stable *trans*- $A_2B$  corrole with an attracting EWG  $-CF_3$  group for the construction of new COFs. With the  $C_2$  symmetric structure and reactive functions at the 5,15-*meso* positions, we wish to use corrole as linker for further COF construction. It is worthy to note that the corrole linker is in an unusual approximately T-shape (when  $A_3$ ) or linear shape (when  $A_2B$ ) due to the absence of a carbon at the 20-*meso* position compared to porphyrin.



Scheme 1. Structures of  $A_3$  corrole and *trans*  $A_2B$  corrole.

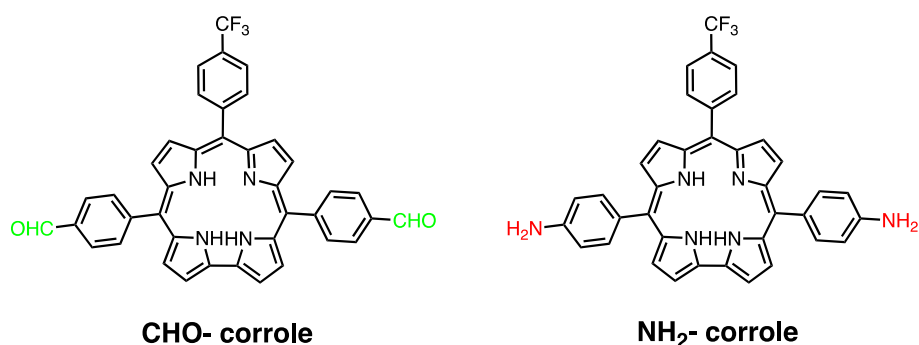
Thus, the topology of the targeted COFs will be in the system ( $C_2 + C_y$ ). According to the topology diagrams presented in Chapter 1, we can have ( $C_2 + C_3$ ) and ( $C_2 + T_d$ ) systems which represent 2D and 3D topologies, respectively. Furthermore, there are two reactive functions on corrole linker, thus, the knots used to react with the corrole should contain 3 or 4 reactive functions to construct either 2D layer or 3D network. In the literature, there are many examples of 2D COFs based on 1,3,5-triformylbenzene through imine linkage. For 3D COFs, tetraphenylmethane is generally considered as a great  $T_d$  knot to construct 3D networks and it was usually functionalized into tetra(4-aminophenyl)methane or tetra(4-formylphenyl)methane. For the rest of our work, we will use these last two precursors. As a reminder, all the precursors for COF constructions were described in Chapter 2.

### 3.1.1 Synthetic methods for the preparation of COFs

During the development of COFs synthesis, many synthetic methods have been reported by different groups: solvothermal synthesis,<sup>10, 11</sup> microwave synthesis,<sup>12, 13</sup> ionothermal synthesis,<sup>14, 15</sup> mechanochemical synthesis,<sup>16, 17</sup> interfacial synthesis<sup>18, 19</sup> and synthesis under ambient conditions.<sup>20, 21</sup> Among all these synthetic methods, the solvothermal approach has been widely used for the construction of high quality COFs. For the solvothermal synthesis, the reaction time, temperature, solvent condition and catalyst concentration are the most important factors to be considered in the preparation of highly crystalline COFs.<sup>22</sup> In this manuscript, among the different experiments available for COFs synthesis, solvothermal approach was mainly used.

## 3.2 Synthesis of COFs from aldehyde-corrole

The imine bond can be formed by the reaction of an aromatic amine and an aldehyde in the presence of organic acid or Lewis acid catalyst at high temperature (usually 120°C). Considering the stability problems of certain corroles, we have proposed to build a COF from aldehyde-corrole which is comparatively more stable compared to an amino-corrole (Scheme 2). With amino functions, amino-corrole can be easier oxidized by O<sub>2</sub>. Checked by H NMR spectra and TLC monitoring, after a long time, amino-corrole have degradation: H NMR not clean anymore and many impurities showed on TLC.



Scheme 2. Structures of aldehyde- and amino- corroles.

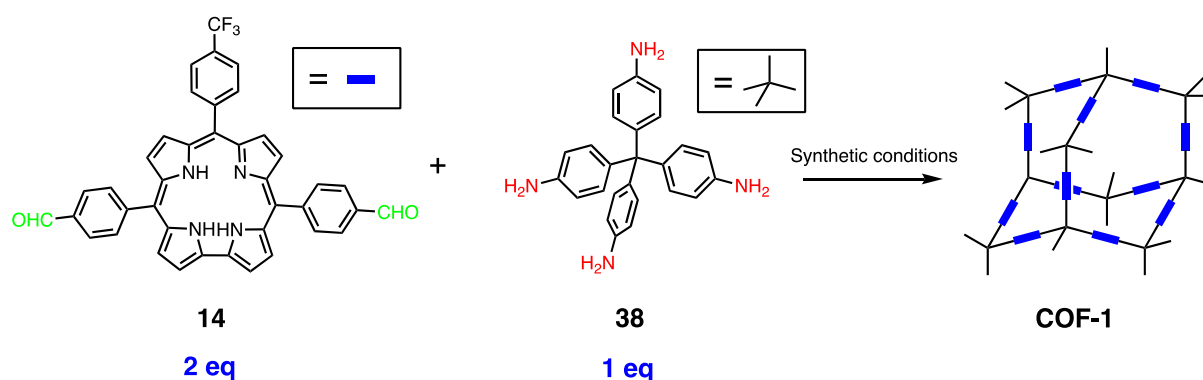
At the beginning of this PhD work, there were no examples of COFs based on corroles but COFs based on imine linked porphyrins have been widely reported.<sup>23-27</sup> Among these porphyrin COFs, aldehyde- and amino- porphyrins have been used as building blocks. Due to the similarity in structures and properties between corroles and porphyrins, it should be easier to optimize the synthetic conditions for corrole-based COFs. Thus, we were directly inspired by synthetic conditions of porphyrin COFs to further develop and obtain COFs based on corrole macrocycles (Table 1).

Table 1. Synthetic conditions for COFs based on porphyrins.

COFs	Porphyrin linker	Type	Synthetic condition	ref
3D-TPP	5,15-bis(4-formylphenyl)-10,20-diphenylporphyrin	3D	1,4-Dioxane / 3 M AcOH (35 :2 v/v), 120°C, 72 h	33
3D-Por-COF	5,10,15,20-tetrakis(4-benzaldehyde)porphyrin	3D	<i>o</i> -DCB / <i>n</i> -BuOH / 6 M AcOH (9:1:1 v/v/v), 120°C, 7d	9
2D-PdPor-COF	[5,10,15,20-tetrakis(4-benzaldehyde)-porphyrin]palladium	2D	<i>o</i> -DCB / <i>n</i> -BuOH / 3 M AcOH (5:5:1 v/v/v), 120°C, 72 h	32
Por-C=N-COF	5,10,15,20-tetrakis(4-benzaldehyde)porphyrin	2D	<i>o</i> -DCB / <i>n</i> -BuOH / 3 M AcOH (5:5:1 v/v/v), 120°C, 72 h	31
PPOP-1	5,15-di(4-aminophenyl)-10,20-diphenylporphyrin	3D	<i>o</i> -DCB / <i>n</i> -BuOH / 6 M AcOH (7:3:1 v/v/v), 120°C, 72 h	30
CPF-1	5,15-di(4-aminophenyl)-10,20-diphenylporphyrin	2D	1,4-dioxane / mesitylene/ 6 M AcOH (15:15:1 v/v/v), 120°C, 72 h	29
PCOF-1	5, 10, 15, 20-tetra(4-aminophenyl)porphyrin	3D	<i>o</i> -DCB / mesitylene / 6 M AcOH (17:3:2 v/v/v), 120°C, 7 d	24
TT-Por-COF	5, 10, 15, 20-tetra(4-aminophenyl)porphyrin	2D	<i>o</i> -DCB / benzyl alcohol / 6 M AcOH (5:15:2 v/v/v), 120°C, 72 h	28

From Table 1, we can see that COFs based on porphyrin (with aldehyde or amino functions) are synthesized under catalysis of aqueous acetic acid (3 M or 6 M) at 120°C for a long reaction time. Also, the solvents used for the synthesis are high boiling point solvents e.g. like 1,4-Dioxane, *o*-DCB, *n*-BuOH, mesitylene. It should be noted that due to the use of aqueous acetic acid, the solvents are required to possess some hydrophilicity to further allow water and acetic acid to take part in the imine formation well. Moreover, the mixture of water and acetic acid is very important to produce crystalline COFs.<sup>34</sup>

In Scheme 3 below we present a first try to synthesize COF from the aldehyde-corrole linker **14** and the tetra(4-aminophenyl)methane platform **38** (Scheme 3). In order to obtain a complete and well organized structure, we used a 2 : 1 ratio (corrole **14** : platform **38**) ratio of the starting precursors.-All the reactions were carried in one solvent or mixtures of solvents using aqueous acetic acid as a catalyst. We have tried several different synthetic conditions, all synthetic condition optimizations for COF-1 are presented in Table 2.



Scheme 3. Synthesis of COF-1 from corrole **14** and platform **38**.

Table 2. Synthetic conditions for COF-1 synthesis

	Solvent				Catalyst		Crystallinity	S <sub>BET</sub> (m <sup>2</sup> /g)
	1,4-Dioxane	THF	<i>n</i> -BuOH	<i>o</i> -DCB	6M AcOH			
<b>1</b>	1 mL	-	-	-	0.1 mL	Amorphous	-	
<b>2</b>	-	-	0.1 mL	0.9 mL	0.1 mL	Amorphous	-	
<b>3</b>	-	1 mL	-	-	0.1 mL	-	-	

Firstly, we tried small scale tests for the synthesis. Experiments 1 and 2 were carried out with 6 M aqueous acetic acid at 80°C and the solvents were 1,4-dioxane and a mixture of *n*-BuOH / *o*-DCB. The reported COF based porphyrin were synthesized at 120°C, but we first tried 80°C here considering that corrole is generally less stable than porphyrin. A mixture of corrole **14** (10.0 mg, 0.016 mmol, 2 eq) and platform **38** (3.00 mg, 0.008 mmol, 1 eq), 6 M aqueous acetic acid, and solvents were placed in a Schlenk tube of suitable volume. The mixture was sonicated for a short period, degassed via freeze-pump-thaw cycles, sealed with a glass stopper and kept at 80°C for 24 h. The tube was then cooled at room temperature, and the

precipitate was collected by centrifugation or filtration and washed with an appropriate solvent at room temperature. The residue was dried under vacuum and kept under nitrogen or argon in the dark. The COFs n°1 and n°2 were first characterized by Powder X-ray Diffraction but, to our surprise, they do not show any crystallinity. Both COFs have been obtained in quite low yield (less than 30%) so we did not get enough quantity for BET measurement. Regarding experiment n°3, we used THF as solvent to increase solubility as much as possible. However, we did not observe the formation of a COF. During these first tests, we preferred to heat only to 80°C (usually 120°C when preparing porphyrin-COFs) as high temperature, acidic environment and long reaction time have shown to be sometimes harmful to the corrole macrocycle. The low yield of COFs n°1 and n°2 could be influenced by the low reaction temperature. Therefore, we tried to raise the reaction temperature to 120°C in the following experiments (Table 3).

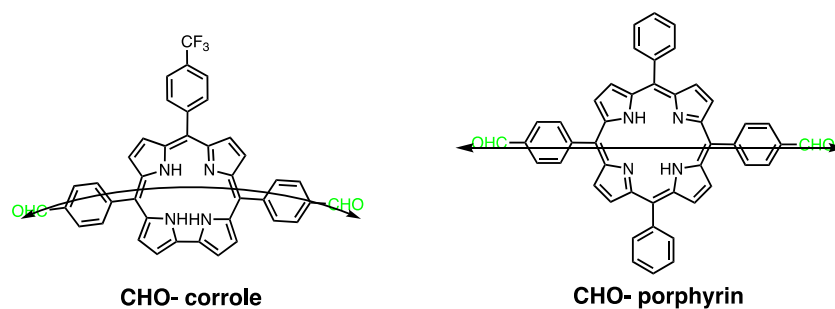
Table 3. Optimization of synthetic conditions for COF-1.

	Solvent					Catalyst		Crystallinity	S <sub>BET</sub> (m <sup>2</sup> /g)
	1,4-Dioxane	mesitylene	<i>n</i> -BuOH	<i>o</i> -DCB	DMSO	6M AcOH			
<b>1</b>	2 mL	-	-	-	-	0.2 mL	Amorphous	400	
<b>2</b>	1.8 mL	0.2 mL	-	-	-	0.2 mL	Amorphous	329	
<b>3</b>	-	-	-	2 mL	-	0.2 mL	Amorphous	298	
<b>4</b>	-	-	0.2 mL	1.8 mL	-	0.2 mL	Amorphous	395	
<b>5</b>	-	-	-	-	2 mL	0.2 mL	Amorphous	170	

For the reactions in Table 3, corrole **14** (26.0 mg, 0.04 mmol, 2 eq) and platform **38** (7.60 mg, 0.02 mmol, 1 eq) were used again. During the reactions, experiments n°3 and 4 yielded powder like precipitates while n° 1, 2 and 5 yielded sponge like solid. Out of our expectations, none of them showed crystallinity while porphyrin-COFs analogs show good crystallinity. This could be assigned to the specific molecular structure of the corrole which is twisted line shape linker whereas the porphyrin precursor is more linear (Scheme 4). At least, the n°1 synthesized in 1,4-dioxane showed the highest BET surface area around 400 m<sup>2</sup>g<sup>-1</sup>.

In order to check the reproducibility and obtain higher amount of samples for further CO binding test, synthetic condition n°1 of COF-1 was repeated on a larger scale (corrole **14** (72.8 mg, 0.11 mmol, 2 eq) and platform **38** (21.3 mg, 0.055 mmol, 1 eq)). The product was collected, washed and dried, yielding 20 mg of powder (21%) which is still quite low compared to most porphyrin-COFs. The <sup>1</sup>H NMR of COF-1 was recorded with decomposing by DCl in DMSO-

$d_6$  and adding hydrazine to increase resolution (experimental sections: part 6). The NMR spectrum exactly presented bis-CHO corrole and tetra-NH<sub>2</sub> platform as linkers of COF-1. It was still amorphous and showed 430 m<sup>2</sup>g<sup>-1</sup> of BET surface area which is close to the test n°1. Considering the low yield of corrole **14** described in Chapter 2 and the low yield of COF synthesis, we concluded that it was not efficient to use bis- aldehyde corrole **14** as a linker to build COF.

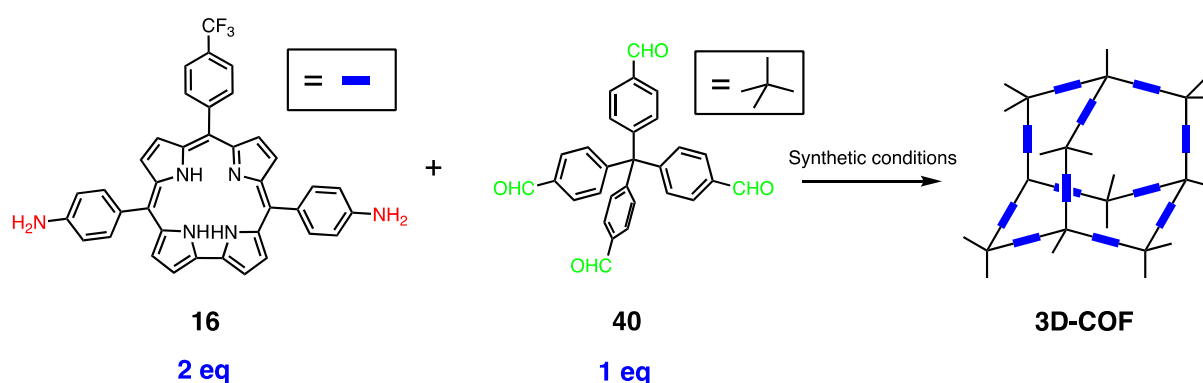


Scheme 4. Structures of CHO-corrole and CHO-porphyrin.

### 3.3 Synthesis of COFs from amino- corrole

According to Table 1, imine COFs can be obtained from aldehyde-porphyrin, or amino-porphyrin monomer. The synthesis conditions for both are similar, thus we considered to apply 5,10-amino corrole as linker to synthesize COFs. In chapter 2, we described the synthesis of 5-(4-nitrophenyl)dipyrromethane and its A<sub>2</sub>B-corrole (bis-nitro corrole **15**) with good yield (38%). After that, the bis-amino corrole was obtained by reduction in H<sub>2</sub> with palladium catalyst with a very good yield of 85%. Compared to the synthesis of aldehyde corrole, amino corrole can be synthesized in easier way and much higher yield, which make it a promising monomer for imine COFs. The following part focused on the application of amino corrole **16** as COFs linkers.

#### 3.3.1 Synthesis of 3D-COF-Cor based on amino corrole



Scheme 5. Synthesis of 3D-COF from corrole **16** and platform **40**.

In order to raise the crystallinity and BET surface area, optimization of synthetic conditions for the 3D-COFs-Cor was required. To obtain the best synthetic condition, we have tried several experiments carried in different solvents (Table 4). These experiments were launched with the same quantity of starting materials: corrole **16** (28.9 mg, 0.046 mmol, 2 eq) and platform **40** (10.0 mg, 0.023 mmol, 1 eq). All the reactions were catalyzed with 6M acetic acid at 120°C during 24h and resulted materials were characterized with PXRD and BET measurements.

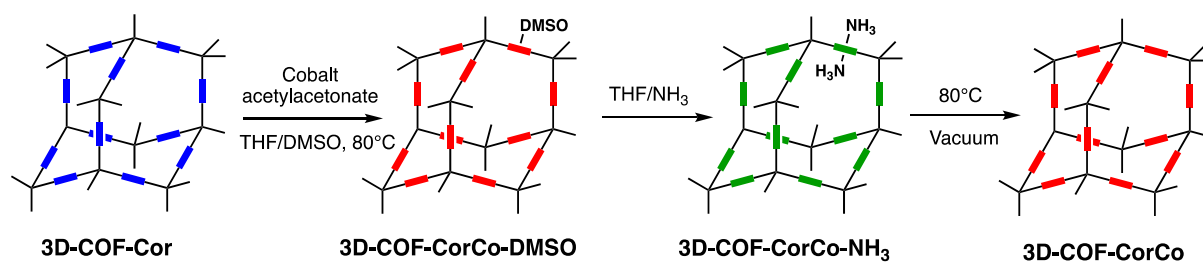
Table 4. Optimization of synthetic conditions for 3D-COF-Cor.

	Solvent					Crystallinity	S <sub>BET</sub> (m <sup>2</sup> /g)	Yield
	<i>o</i> -DCB	<i>n</i> -BuOH	Mesitylene	Dioxane	DMF			
<b>1</b>	1 mL	2 mL	-	-	-	Amorphous	500	65%
<b>2</b>	1.5 mL	1.5 mL	-	-	-	Amorphous	461	43%
<b>3</b>	2 mL	1 mL	-	-	-	Amorphous	461	46%
<b>4</b>	-	2mL	1 mL	-	-	Amorphous	262	34%
<b>5</b>	-	1 mL	2 mL	-	-	Amorphous	198	38%
<b>6</b>	1.5 ml	-	-	1.5 ml	-	-	-	-
<b>7</b>	-	-	1.5 ml	1.5 mL	-	-	-	-
<b>8</b>	-	-	-	-	3 mL	Amorphous	70	49%

Inside tubes n°1 to 3, powder like precipitates were observed after heated for 5 h which means the imine condensation worked fastest in the mixture of *o*-DCB/ *n*-BuOH. Tubes n°4 and 5 also showed powder like precipitates but they form more slowly than tubes n°1 to 3. For tubes n°6 and 7, there were no precipitate and this could be due to the use of 1,4-Dioxane. For n°8, a gel like solid was observed. All COFs showed no crystallinity and the highest BET

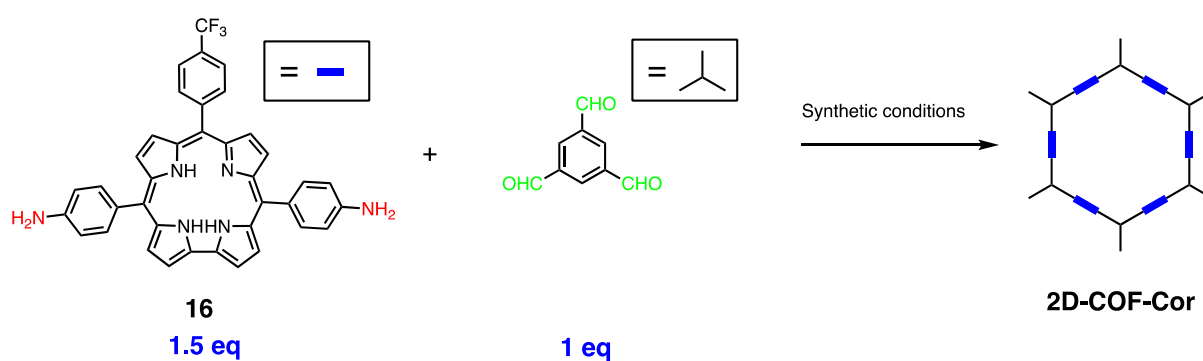
surface area is  $500 \text{ m}^2\text{g}^{-1}$  (tube 1, yield 65%, mixture of *n*-BuOH/*o*-DCB/acetic acid (10:5:1, V/V/V)) (Table 4). The gel like solid in tube n°8 had the lowest BET surface area. After the optimization of the synthetic conditions for the 3D-COF-Cor, we selected the conditions of tubes n°1 for a synthesis on a larger scale. Corrole **16** (144 mg, 0.231 mmol, 2 eq) and platform **40** (50.0 mg, 0.115 mmol, 1 eq) were placed in a 50 mL Schlenk tube, charged with the mixture of *n*-BuOH/*o*-DCB/acetic acid (10:5:1, V/V/V in mL). The mixture was sonicated for 10 min and degassed *via* freeze-pump-thaw cycles. Then, the tube was sealed by a glass stopper. The mixture was heated for 3 days at  $120^\circ\text{C}$ . After collected, the large scale gives a good reproducible yield (64% *versus* 65% before). In order to check the reproducibility in larger scale, the reaction was repeated with 404 mg of corrole **16** and 104 mg of platform **40**. After collected, the 3D-COF-Cor was given with a quite reproducible yield of 56% which means a possibility for practical application.

Until this step, the 3D-COF-Cor was successfully obtained and all the corroles inside this material are in their free base form. Desired COFs must have cobalt complexed corroles in order to be able to bind CO. These cobalt complexes were obtained *via* the metalation of the free base corroles in the synthesized 3D-COF-Cor (Scheme 6). In a flask was added 3D COF, followed by a solution of cobalt acetylacetonate in the mixture of DMSO and THF. The mixture was heated at  $80^\circ\text{C}$  for 5 h under argon without stirring. After cooling down the solution, the suspension was centrifugated. After removing the supernatant, the solid was washed with THF several times to afford COF with cobalt corroles and DMSO ligand (3D-COF-CorCo-DMSO). Then the 3D-COF-CorCo-DMSO was further washed with a solution of THF saturated with  $\text{NH}_3(\text{g})$  to afford 3D-COF-CorCo-NH<sub>3</sub>. The solid was then dried under vacuum. The 3D-COF-CorCo-NH<sub>3</sub> was degassed under vacuum at  $80^\circ\text{C}$  to afford 3D-COF-Cor-Co (without ligands) which was used for further CO sorption tests.



Scheme 6. Synthetic route to obtain 3D-COF-CorCo.

### 3.3.2 Synthesis of 2D-COF-Cor based on amino corrole



Scheme 7. Synthesis of 2D-COF from corrole **16** and 1,3,5-triformylbenzene.

The synthesis of 2D-COF-Cor is shown in Scheme 7, corrole **16** and 1,3,5-triformylbenzene were used as monomers to construct the framework. During the reaction, all COFs precipitated in the tubes within 6 h. After collection, all of them tend to be powder like materials. The analyzes by PXRD and BET showed that the COFs synthesized in a mixture of mesitylene/*n*-BuOH present the highest crystallinity and BET surface area.

Table 5. Optimization of synthetic conditions for 2D-COF-Cor.

	Solvent				Crystallinity	S <sub>BET</sub> (m <sup>2</sup> /g)	Yield
	EtOH	Mesitylene	<i>n</i> -BuOH	<i>o</i> -DCB			
<b>1</b>	1 mL	2 mL	-	-	High	926	89%
<b>2</b>	1.5 mL	1.5 mL	-	-	High	1126	91%
<b>3</b>	2 mL	1 mL	-	-	High	1081	80%
<b>4</b>	-	1 mL	2 mL	-	High	1141	79%
<b>5</b>	-	1.5 mL	1.5 mL	-	Moderate	551	92%
<b>6</b>	-	2 mL	1 mL	-	Moderate	929	82%
<b>7</b>	-	-	1 mL	2 mL	Low	964	85%
<b>8</b>	-	-	1.5 mL	1.5 mL	Low	1008	95%
<b>9</b>	-	-	2 mL	1 mL	Low	914	80%

After the optimization step, we selected protocol n°4 because the COF obtained presented the best BET. A large scale synthesis of 2D-COF-Cor was performed in the mixture of *n*-BuOH/mesitylene/acetic acid (10:5:1, V/V/V in mL) with corrole **16** (231 mg, 0.37 mmol, 1.5 eq) and 1,3,5-triformylbenzene (40.0 mg, 0.25 mmol, 1 eq). We obtained the COF with a yield of 81% which is close to the optimized one (79%). To check reproducibility, we used twice as much of corrole **16** (462 mg). Once again, we obtained a highly reproducible yield of 81%.

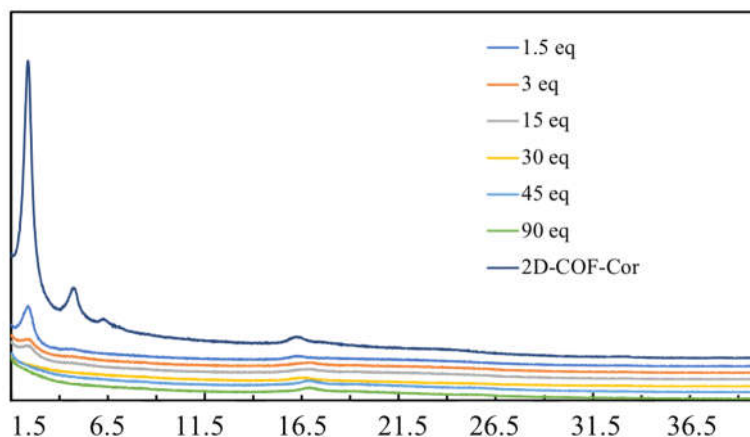
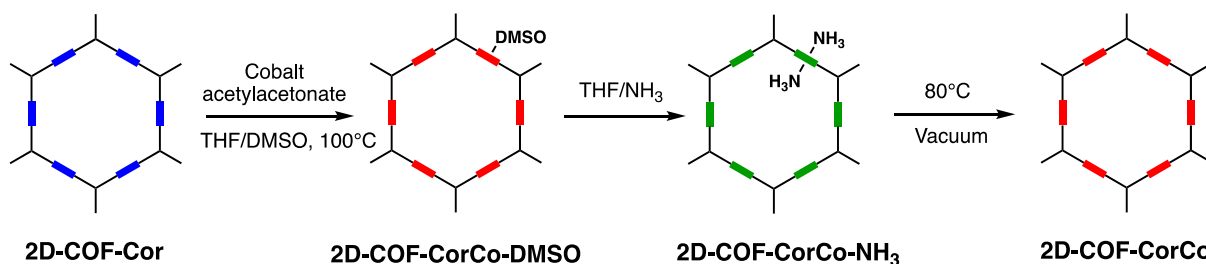


Figure 1. PXRD of aniline modulation for 2D-COF-Cor.

It was reported by Wang *et al.* that aniline can be used as the monofunctional competitor to modulate synthesis of COFs.<sup>35</sup> The introduction of aniline resulted in the enhanced crystallinity, surface area and pore volume, which is beneficial for the enrichment capability of the resulting COFs. Thus, we have also introduced aniline as modulator to improve crystallinity of 2D-COF-Cor. The quantity of aniline was introduced as 1.5, 3, 15, 30, 45, 90 equivalents of the platform. With the addition of aniline, the crystallinity of 2D-COF-Cor reduced obviously (Fig. 1). When it came to 45 and 90 eq, isolated materials have shown to present no crystallinity.

After that, we were interested in the metalation of COF by Cobalt. For this, we used a similar procedure developed during the preparation of 3D-COF-Cor (Scheme 8). The only difference is the temperature control. When 2D-COF-Cor was metalated at 80°C, we observed a low metalation rate of 25% (checked by ICP). By increasing the temperature to 100°C, the cobalt metalation *ratio* can reach 84%. Like 3D-COF-CorCo, 2D-COF-CorCo was obtained by metalating the 2D-COF-Cor, exchanging DMSO ligand with NH<sub>3</sub>, then removing the NH<sub>3</sub> units by heating at 80°C under vacuum.



### 3.3.3 Characterization of 2D/3D-COF-Cor and its cobalt complexes

#### 3.3.3.1 <sup>1</sup>H NMR Spectroscopy

The integrity and the ratio of the building blocks in COFs were further confirmed by <sup>1</sup>H NMR analysis. Few milligrams of a suspension of polymers (10 mg) in 500 μL deuterated dimethyl sulfoxide (DMSO-*d*<sub>6</sub>) was decomposed after adding 10 μL deuterium chloride (DCl, 7 M) which hydrolyzes the imine functions and releases the starting amino and aldehyde derivatives. When all solids disappeared, 50 μL of hydrazine (64% in H<sub>2</sub>O, 1.03 g/mL) was added in order to reduce any traces of corrole radical cations that usually impeded the good resolution of the <sup>1</sup>H NMR spectrum. For 2D-COF-Cor shown in Fig. 2, all peaks are assigned to the amino-corrole and 1,3,5-triformylbenzene by comparing to the spectra of the starting compounds. The signals at 8.77, 8.58, 8.39 and 8.12 ppm correspond to the β-pyrrolic protons of the corrole, and the aryl protons of the C<sub>6</sub>H<sub>4</sub>-CF<sub>3</sub> fragment are located at 8.23 and 8.01 ppm. The two more shielded doublets at 7.87 and 6.99 ppm correspond to the protons on the 5-*meso*- and 15-*meso*-phenyl rings. The signals of the aryl platform appear at 7.42 and 7.68 ppm and no aldehyde function was observed. It turns out that the hydrazide form of 1,3,5-trisformylbenzene was obtained after the reaction with hydrazine, and only the CH=NNH<sub>2</sub> function can be seen at 7.68 ppm. An average ratio of 1 corrole for 1 platform was determined by integration of the signals for 2D-COF-Cor, which is not close to the theoretical stoichiometric ratio of 1.5 corrole for 1 platform. Since the imine formation is a reversible reaction, it is acceptable that one part of the corroles is lacking, which means that the material presents some corrole defects. Concerning the 3D COF, the same <sup>1</sup>H NMR analysis was carried out (Fig. 3) and a similar ratio (1.1 corrole: 1 platform) was found, compared to a 2 : 1 ratio that is theoretically expected for a stoichiometric defect-free material. Furthermore, the <sup>1</sup>H NMR spectra clearly show that there are no side products formed during the COF synthesis, which means that there is no occurring degradation of corrole-NH<sub>2</sub>. The results proved that the COFs structure helps to stabilize the corrole macrocycle.

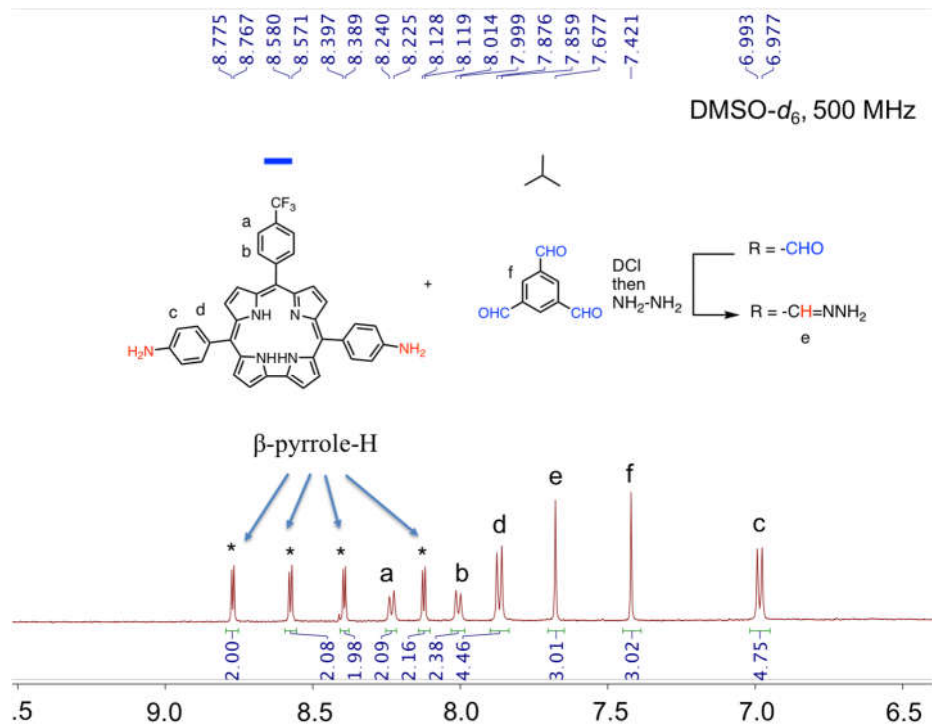


Figure 2.  $^1\text{H}$  NMR spectrum of 2D-COF-Cor decomposed by DCl.

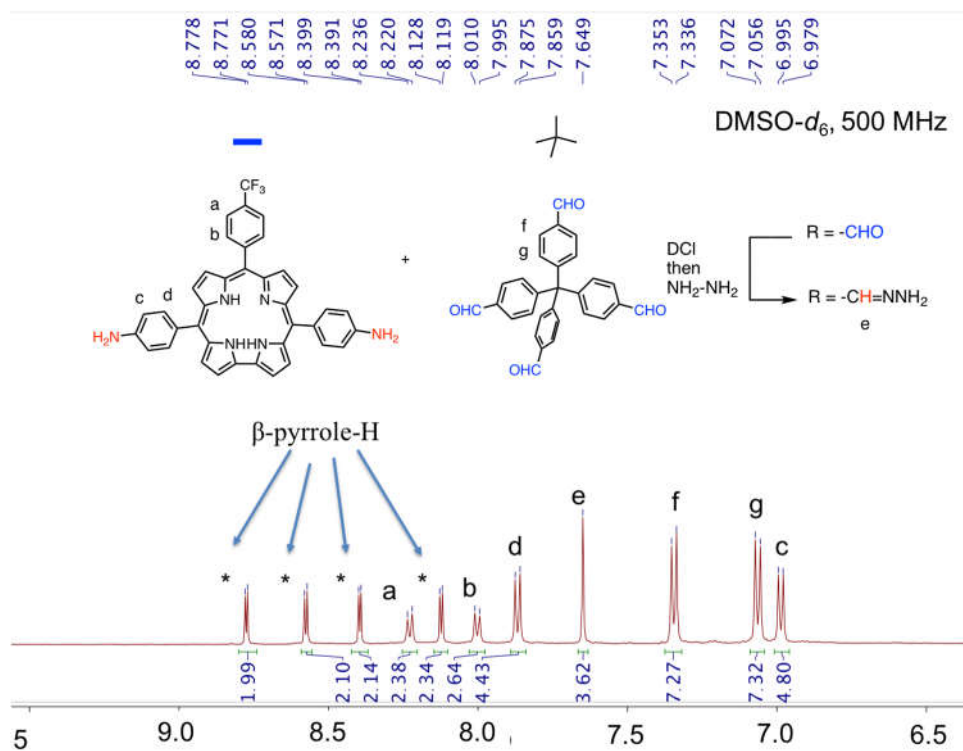


Figure 3.  $^1\text{H}$  NMR spectrum of 3D-COF-Cor decomposed by DCl.

### 3.3.3.2 Infrared Spectroscopy

The 2D-COF-Cor and 3D-COF-Cor clearly exhibit the formation of networks linked by C=N bonds that give a typical C=N stretching vibration at about  $1610\text{ cm}^{-1}$ .<sup>36, 37</sup> Indeed, the comparison of the IR spectra for the starting compounds e.g. 1,3,5-triformylbenzene and corrole-NH<sub>2</sub> clearly shows the formation of the imine bond by the vibration at  $1614\text{ cm}^{-1}$  for 2D-COF-Cor (Fig. 4). However, a peak at  $1699\text{ cm}^{-1}$  attests to the presence of the terminal aldehyde groups in the resulting material, while the consumption of the amino groups, evidenced by the absence of the NH vibration around  $3460\text{ cm}^{-1}$  is nearly complete. The sharp peak at  $1323\text{ cm}^{-1}$  was tentatively assigned to the C–N stretching of the aromatic amine (Ph-N) groups which become bigger by the formation of conjugated imine linkages. The peaks at  $1167$  and  $1128\text{ cm}^{-1}$  can be assigned to the C–N stretching of azomethine (C–C=N–C) groups.<sup>38</sup> All of these results further support the formation of the imine networks.

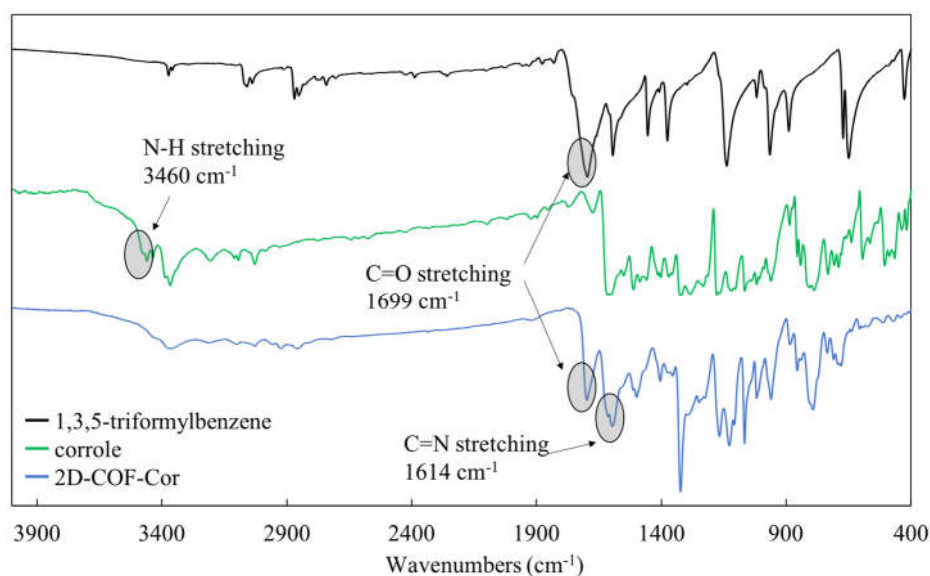


Figure 4. FTIR spectra of 1,3,5-triformylbenzene, corrole-NH<sub>2</sub> **16** and 2D-COF-Cor.

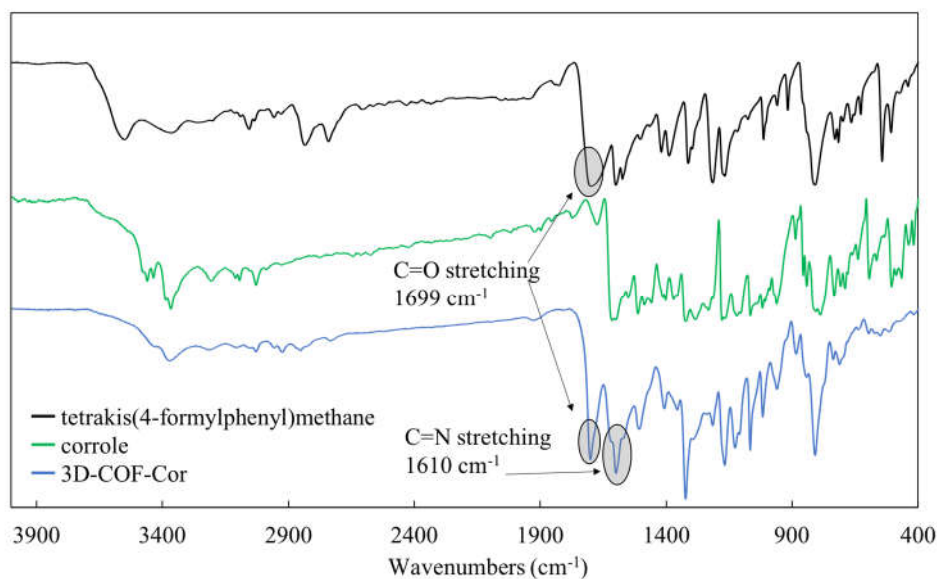


Figure 5. FT-IR spectra of tetrakis(4-formylphenyl)methane, corrole-NH<sub>2</sub> **16** and 3D-COF-Cor.

The IR spectrum of 3D-COF-Cor also clearly shows the vibration of imine bond at 1610 cm<sup>-1</sup>. The mirror difference from 2D-COF-Cor comes from the conjugation by the 2D platform (Fig. 5). We also compared the FTIR spectra of COFs-Cor and their corresponding cobalt complex counterparts (Fig. 6 and 7). After the cobalt metalation of the corroles within 2D-COF-Cor, the characteristic peaks of 2D-COF-CorCo-DMSO and 2D-COF-CorCo-NH<sub>3</sub> still match with that of the 2D-COF-Cor. After the metalation of 2D-COFs, the imine bond around 1614 cm<sup>-1</sup> and the peaks in the range of 3500-2800 cm<sup>-1</sup> remain visible. Interestingly, for COF-CorCo-DMSO (Fig. 6 and 7), a weak peak around 1014 cm<sup>-1</sup> was more prominent and can be assigned to the S=O stretching from the DMSO ligands.<sup>39</sup> When NH<sub>3</sub> is coordinated to cobalt as the ligand, the peak at 3349 cm<sup>-1</sup> in Fig. 4 clearly shows the N-H vibration for 2D-COF-CorCo-NH<sub>3</sub>. For 3D-COF-CorCo-NH<sub>3</sub>, the similar N-H vibration appears at 3352 cm<sup>-1</sup> (Fig. 7).

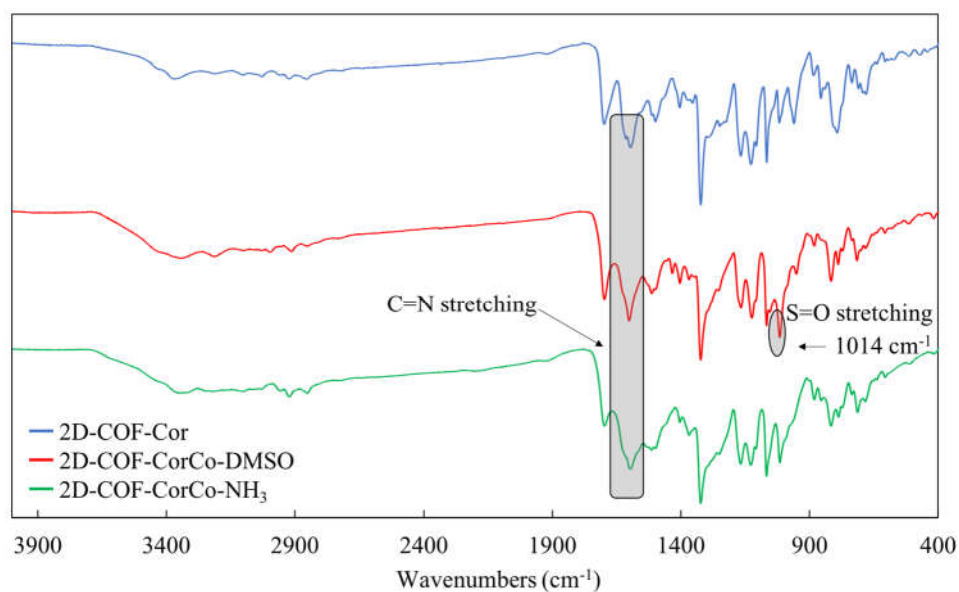


Figure 6. FTIR spectra of 2D-COF-Cor, 2D-COF-CorCo-DMSO and 2D-COF-CorCo-NH<sub>3</sub>.

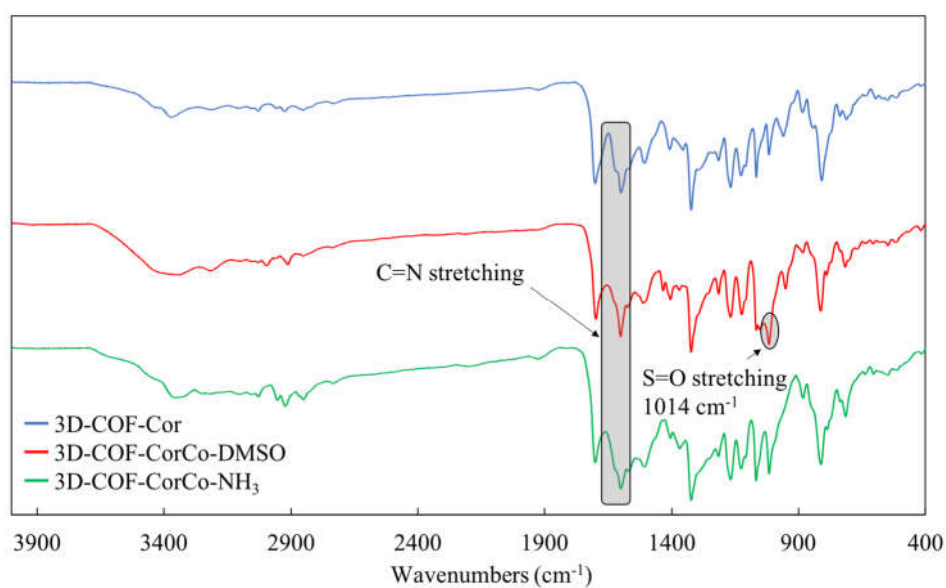


Figure 7. FT-IR spectra of 3D-COF-Cor, 3D-COF-CorCo-DMSO and 3D-COF-CorCo-NH<sub>3</sub>.

During the FTIR analysis of 2D-COF-CorCo-NH<sub>3</sub> and 3D-COF-CorCo-NH<sub>3</sub>, a release of NH<sub>3</sub> ligand were observed due to the high vacuum in the IR apparatus (Fig. 8). From Fig. 8, the N-H vibration from NH<sub>3</sub> ligand was located at 3349 and 3352  $\text{cm}^{-1}$ .

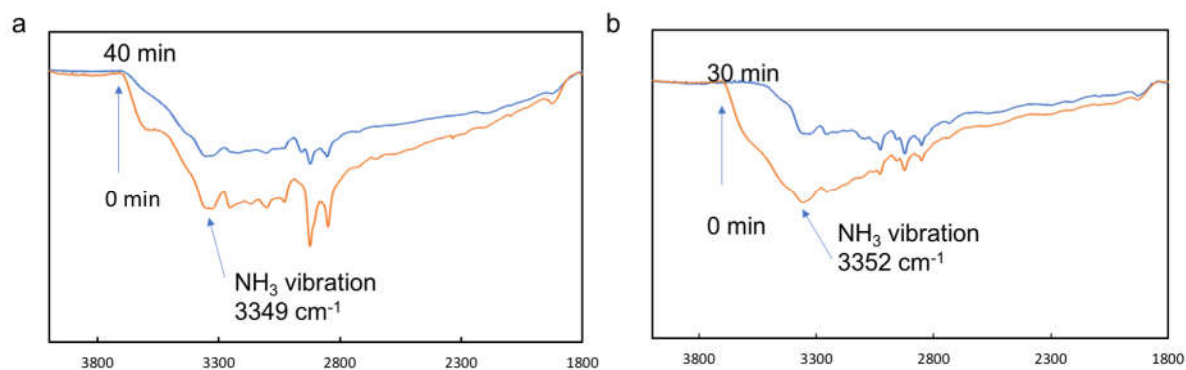


Figure 8. FT-IR spectra of NH<sub>3</sub> release under vacuum from 2D-COF-CorCo-NH<sub>3</sub> (a) and 3D-COF-CorCo-NH<sub>3</sub> (b).

### 3.3.3.3 Powder X-ray diffraction

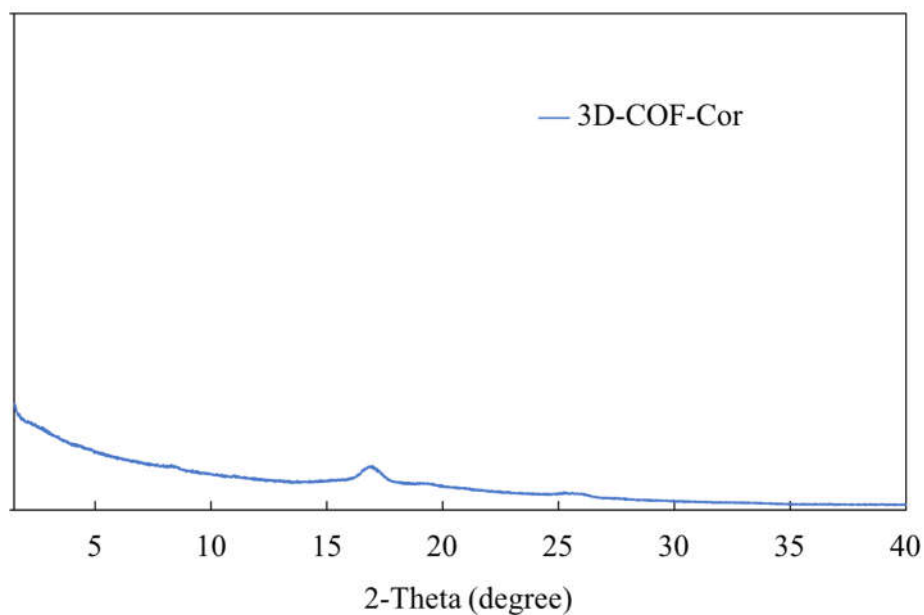


Figure 9. Experimental PXRD patterns of 3D-COF-Cor.

PXRD analysis was also employed to determine the crystallinity of the synthesized COFs. For 3D-COF-Cor, the PXRD indicates the amorphous nature of the material since we can observe no distinct diffraction features (Fig. 9). We assumed that the non-C<sub>2</sub> symmetric structure of corrole makes it very difficult to form well-organized diamond-like 3D structure for 3D-COF-Cor. According to the literature, the 3D COF based on bifunctional C<sub>2</sub> symmetric porphyrin also shows no crystallinity.<sup>40</sup>

2D-COF-Cor shows a good crystallinity while 3D-COF-Cor is amorphous. The experimental PXRD pattern displayed in Fig. 10a shows three intense peaks at  $2\theta = 2.37^\circ$ ,  $4.75^\circ$  and  $6.47^\circ$  and a broad and weak peak at  $24.5^\circ$ , which are assigned to the (100), (200), (210) and (001) lattice planes respectively, indicating long-range order in this framework. By comparison with already described 2D COFs, the morphology of the experimental patterns suggests that the 2DCOF-Cor is formed thanks to the eclipsed AA stacking mode. The Pawley-refined profile is highly consistent with the experimentally observed pattern, resulting in a good agreement factor ( $R_{wp} = 3.23\%$  and  $R_p = 2.27\%$ ) and the reasonable profile difference (Fig. 10a). The eclipsed AA and AB stacking mode were presented in Fig. 10b and 10d. The unit cell parameters were determined as  $a = b = 43.0 \text{ \AA}$ , considering the crystal structure as a hexagonal packing. In addition, the broad signal at  $24.5^\circ$  indicates a layer spacing between two adjacent corroles around  $3.6 \text{ \AA}$ , which should be enough to allow the post-metalation of the COF with cobalt. The structure model of 2D-COF-Cor was generated with the Materials Studio programs (Fig. 11). The initial unit cell dimension was set to the theoretical parameters. The Le Bail refinement was performed to optimize the lattice parameters iteratively until the  $R_{wp}$  value converges and the overlay of the observed with refined profiles shows good agreement. The atomic positions and total energies were then fully optimized using Forcite module of Materials Studio. The final crystal structure was then optimized using the Castep module of Materials Studio. The simulated layer spacing is  $3.65 \text{ \AA}$  which is very close to the experimental pattern. This evidences that the macrocycles are still accessible despite their  $\pi$ - $\pi$  stacking in the network. The crystallinity of the metalated COF 2D-COF-CorCo was also investigated and it shows two main peaks at  $2\theta = 2.46^\circ$  and  $4.81^\circ$  (Fig. 12). This result indicates that after inserting cobalt into the corrole macrocycles, 2D-COF-CorCo retains the same topology but a slight shrinking of the lattice parameters was observed.

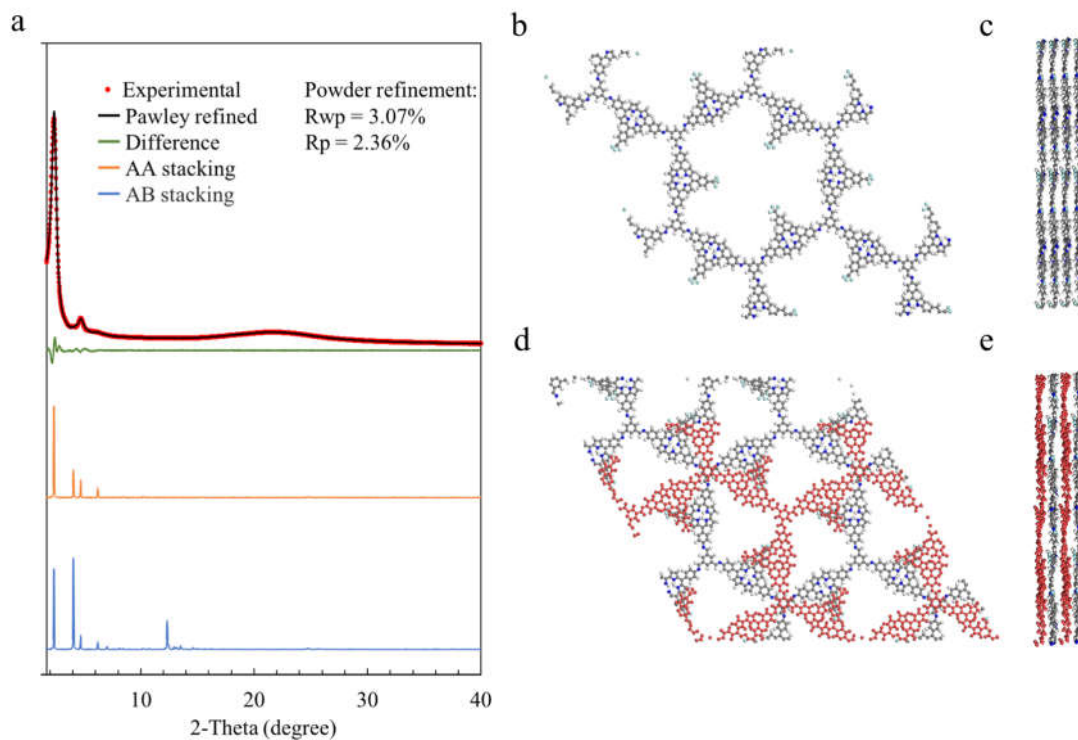


Figure 10. a. PXRD patterns of 2D-COF-Cor with the experimental in red, Pawley refined in black, difference between experimental and refined data in green, and simulated AA and AB stacking respectively in orange and blue. Space-filling models of the 2D-COF-Cor in b and c. AA stacking from top and side views respectively and d and e. AB stacking from top and side views respectively.

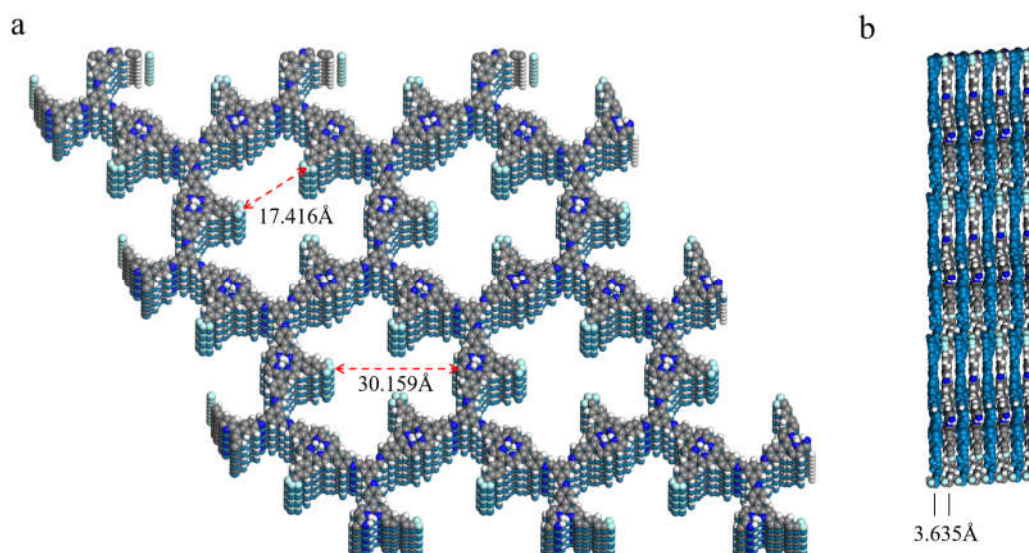


Figure 11. a. Top view and b. side view of the optimized 2D-COF-Cor in the staggered AA stacking mode shown as space-filling model, indicating the pore aperture and stacking distance.

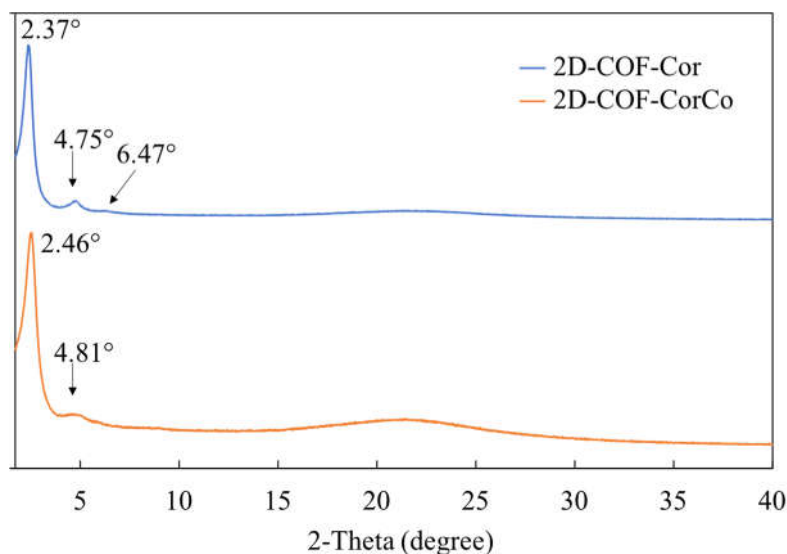


Figure 12. Experimental PXRD patterns of 2D-COF-Cor and 2D-COF-CorCo.

#### 3.3.3.4 Scanning electron microscopy

The macroscopic morphology of the free base COFs (2D-COF-Cor and 3D-COF-Cor) and their corresponding metalated COFs (2D-COF-CorCo-DMSO and 3D-COF-CorCo-DMSO) have been examined by Scanning Electron Microscopy (SEM) coupled with Energy Dispersive X-ray Spectrometry (EDS). Regular plate-shaped nanoparticles with a narrow thickness in the range 400-800 nm and 1.0-1.5  $\mu\text{m}$  length have been obtained for both 2D-COF-Cor (Fig. 13a) and 2D-COF-CorCo-DMSO (Fig. 13b). Aside from those plate-shaped nanoparticles, granular crystallites bearing a sphere-like morphology are also present. Interestingly, the morphology and particle size remain similar after the insertion of cobalt into the corrole core (Fig. 13c). For 3D-COF-Cor and 3D-COF-CorCo-DMSO, a mixture of sphere-like and network-like nanoparticles were observed (Fig. 12b, 13d). We can assume that the smallest particles tend to aggregate to form spherical nanoparticles with size 1.5-2.0  $\mu\text{m}$ , which are favored under the solvothermal conditions. This may be the reason why there are two different shapes of nanoparticles existing in 3D-COF-Cor and 3D-COF-CorCo-DMSO.

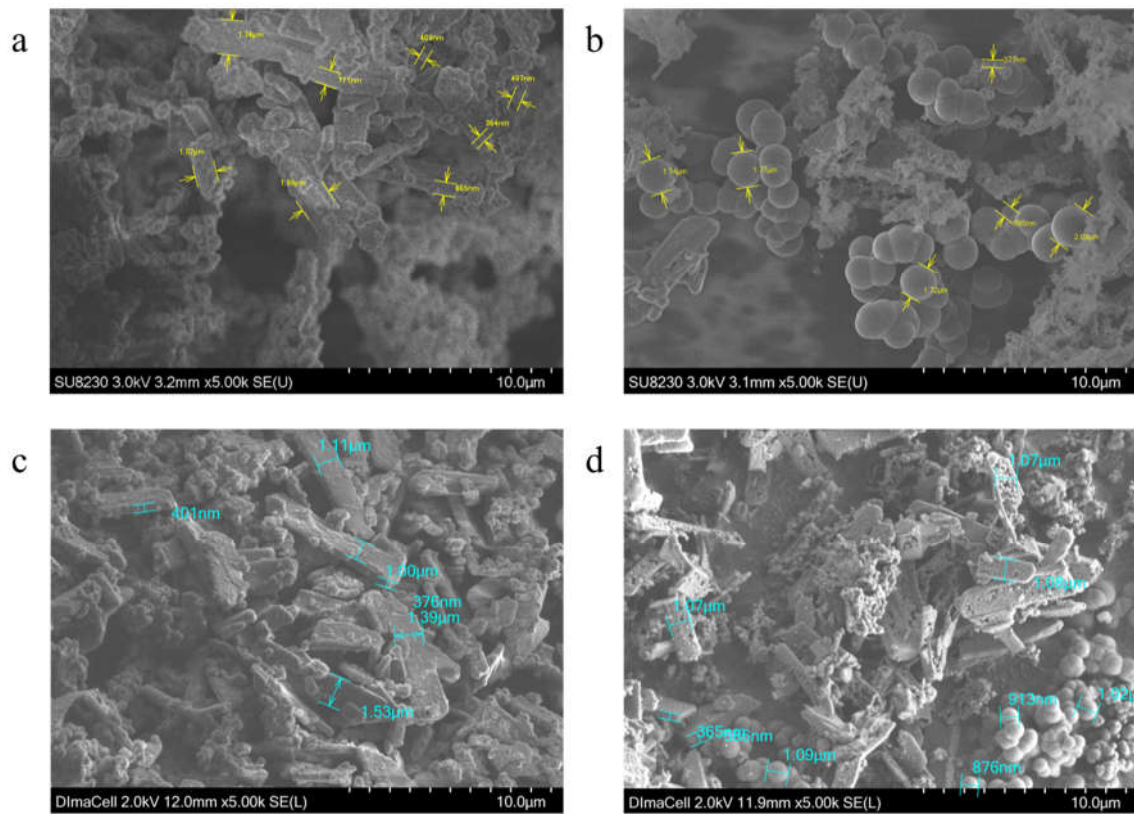


Figure 13. SEM images of COFs: a. 2D-COF-Cor, b. 3D-COF-Cor, c. 2D-COF-CorCo-DMSO, d. 3D-COF-CorCo-DMSO.

### 3.3.3.5 Energy dispersive X-ray spectroscopy

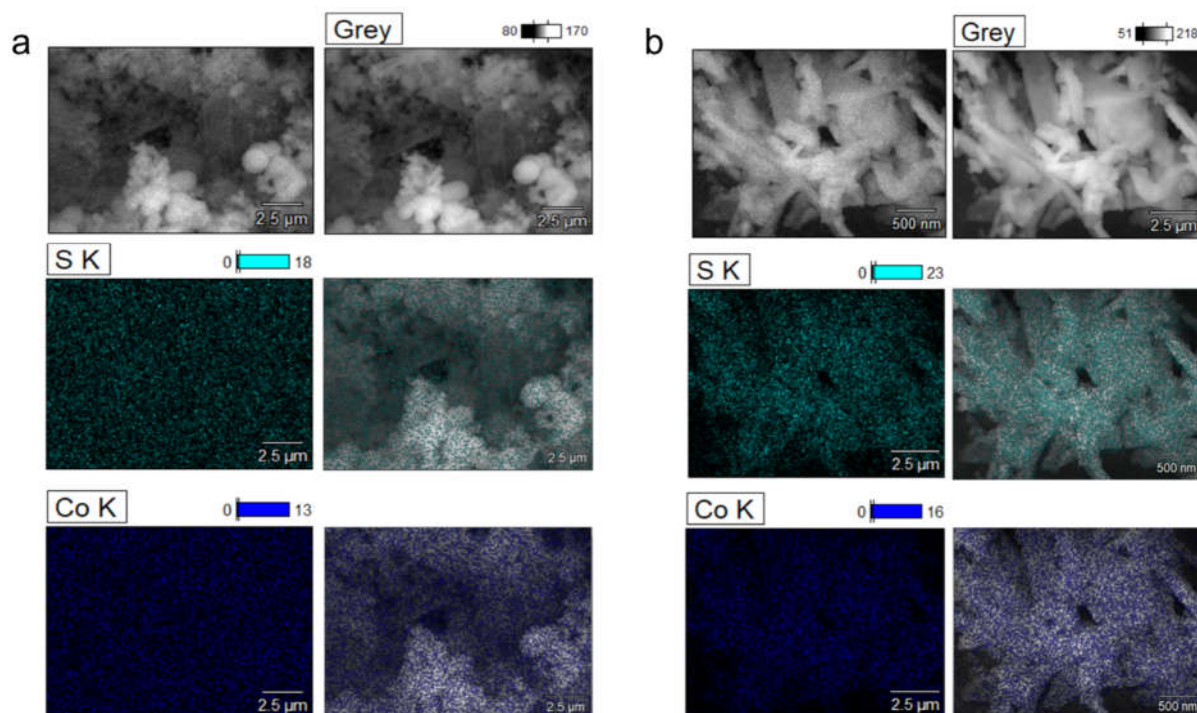


Figure 14. EDS mapping of 3D-COF-CorCo-DMSO (a) and 2D-COF-CorCo-DMSO (b) for sulfur and cobalt distributions.

We are also interested in mapping by EDS, the 2D/3D-COF-CorCo-DMSO taking cobalt and sulfur as the specific elements (Fig. 14). It was observed that sulfur and cobalt distributed evenly which means that the 2D/3D-COF-Cor was well metalated. Furthermore, we can also estimate the metalation ratio of cobalt by EDS. For each corrole unit, there is one  $-CF_3$  moiety. If all corroles are metalated, the theoretical atomic ratio of cobalt to fluorine should be 0.33. There are 7 points (Fig. 15) extracted to show the element analysis of 3D-COF-CorCo-DMSO in atom% (Table 6). The average atomic ratio for Co/F calculated from EDS mapping is 0.19 (Table 7). The cobalt metalation ratio is calculated as 58 %. For 3D-COF-CorCo, we obtain 4.59 % wt for Co ( $0.078 \text{ mmol g}^{-1}$ ), against a theoretical value of 6.25 % wt, giving a 74% metalation ratio.

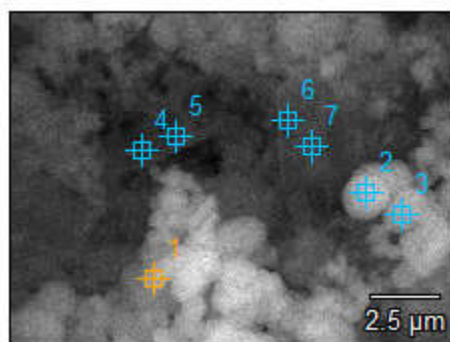


Figure 15. Extracted points for EDS analysis of 3D-COF-CorCo-DMSO.

Table 6. EDS analysis of 3D-COF-CorCo-DMSO in atom %.

	<b>C</b>	<b>O</b>	<b>F</b>	<b>S</b>	<b>Co</b>
<b>point 1</b>	70.14	20.94	4.73	0.45	0.93
<b>point 2</b>	73.33	18.55	4.88	0.41	0.91
<b>point 3</b>	74.81	16.9	4.94	0.41	1.01
<b>point 4</b>	70.07	17.36	6.3	0.72	1.31
<b>point 5</b>	66.94	21.49	9.09	0.85	1.64
<b>point 6</b>	68.93	18.67	6.55	0.68	1.23
<b>point 7</b>	69.08	18.83	6.32	0.63	1.26

Table 7. Metalation ratio calculation from EDS for 3D-COF-CorCo-DMSO.

	<i>Co/F</i> (Atomic ratio)	<i>Metalation</i> (Co/F EDS ÷ theo)
<b><i>Point 1</i></b>	0.20	0.60
<b><i>point 2</i></b>	0.19	0.58
<b><i>point 3</i></b>	0.20	0.60
<b><i>point 4</i></b>	0.21	0.64
<b><i>point 5</i></b>	0.18	0.56
<b><i>point 6</i></b>	0.19	0.58
<b><i>Point 7</i></b>	0.20	0.60
<b><i>average</i></b>	<b>0.19</b>	<b>0.58</b>

Concerning the 2D-COF-CorCo-DMSO, 6 points (Fig. 16) were extracted (Table 8). The average atomic ratio for Co/F calculated from EDS mapping is 0.22 (Table 9). The cobalt metalation ratio is calculated as 67 %. And for 2D-COF-CorCo, we obtain 5.88 %wt for Co (0.099 mmol g<sup>-1</sup>), against a theoretical value of 7.45 %wt, giving a 78% metalation ratio. For

2D and 3D COF, the estimated cobalt metalation ratio from EDS is close to ICP. Due to the experimental error related to each of the analysis techniques, we considered that the metalation ratio calculated from EDS and ICP are concordant.

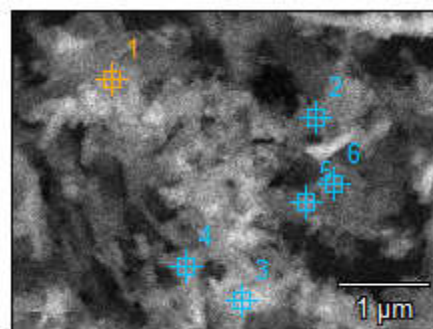


Figure 16. Extracted points for EDS analysis of 2D-COF-CorCo-DMSO.

Table 8. EDS analysis of 2D-COF-CorCo-DMSO in atom %.

	<b>C</b>	<b>O</b>	<b>F</b>	<b>S</b>	<b>Co</b>
<b>point 1</b>	80.78	6.75	6.72	2.32	3.44
<b>point 2</b>	77.39	10.63	9.35	1.15	1.5
<b>point 3</b>	79.62	8.69	8.57	1.35	1.78
<b>point 4</b>	79.4	8.68	8.5	1.48	1.94
<b>point 5</b>	78.96	9.22	8.4	1.47	1.94
<b>point 6</b>	79.18	9.21	8.34	1.37	1.89

Table 9. Metalation ratio calculation from EDS for 2D-COF-CorCo-DMSO.

	<i>Co/F</i> (Atomic ratio)	<i>Metalation</i> ( <i>Co/F EDS</i> ÷ <i>theo</i> )
<i>point 1</i>	0.51	1.54*
<i>point 2</i>	0.16	0.48*
<i>point 3</i>	0.21	0.64
<i>point 4</i>	0.23	0.70
<i>point 5</i>	0.23	0.70
<i>point 6</i>	0.23	0.70
<b>average</b>	<b>0.22</b>	<b>0.67</b>

\* Point 1 and point 2 were not taken into account.

### 3.3.3.6 Thermogravimetric analysis

Thermal stability of the COFs materials was investigated by thermogravimetric analyses (TGA) conducted in the range of 20 °C to 900 °C with a heating rate of 10 °C min<sup>-1</sup> under a synthetic air gas flow (Fig. 17). The TGA curves for these COFs materials exhibited almost no weight loss between 200 °C and 300 °C and only 3D-COF-CorCo and 2D-COF-Cor showed a ~3 % weight loss due to water adsorption by the porosity of the materials. A second step was clearly observed due to the calcination of the organic part of the materials that occurs in a higher temperature range. The calcination temperature was similar for both COFs, as it was observed in the range of 300 – 650 °C for 2D-COF-Cor and 3D-COF-Cor, and a shorter range of 300 – 460 °C was recorded for their metalated analogues. This result is clearly assigned to the destabilization of the corrole complexes compared to their respective free base. A plateau for 2D-COF-CorCo and 3D-COF-CorCo was reached at 9.0 % and 7.3 % respectively, and these values are in good agreement with the expected amount of cobalt (II) oxide (calcd for CoO: 9.5 % and 7.9 % according to ICP results). It is worthy of note that, when considering the corroles as fully metalated, the expected theoretical amount of cobalt(II) oxide were calculated as 10.5% and 8.8 %. From the TGA analyses, we then calculate the metalation ratios to be about 95 % and 92 % for 2D and 3D COF respectively, which is close to the EDS and ICP results. Interestingly, the similarity of the thermograms between the free base COF in one hand and the metalated materials in the other hand clearly attests that despite their different topology, the 2D-COF and 3D-COF present the same stability. This result demonstrates that the thermal stability is dominated by both the nature of the linkages that connect corroles and platforms, and by the nature of the corrole itself, and that neither the crystallinity nor the topology of the framework are preponderant for the control of the thermal stability.

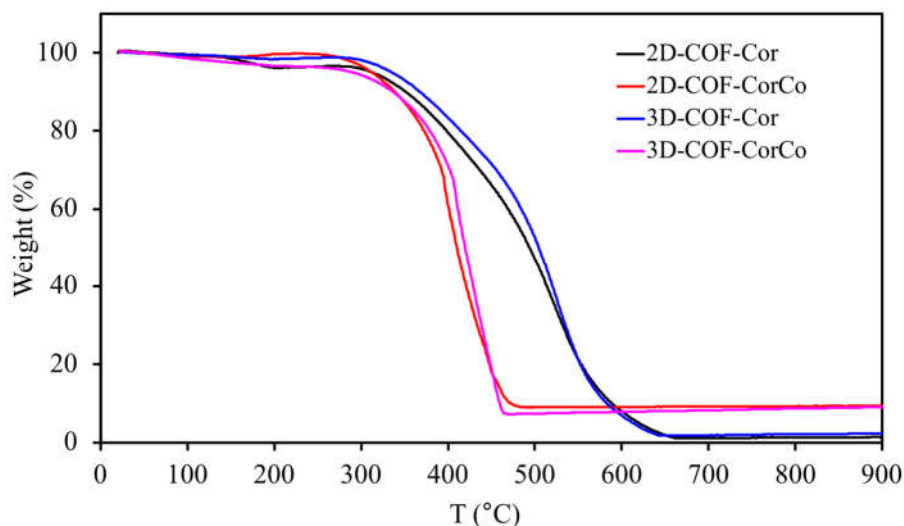


Figure 17. Thermogravimetric analysis recorded for 2D-COF-Co, 2D-COF-CorCo, 3D-COF-Cor, and 3D-COF-CorCo under N<sub>2</sub>/O<sub>2</sub> gas flow.

Table 7. Thermogravimetric data for the 3D-COF-CorCo.

Material	$\Delta m_{\text{exp}}(\%)$	$\% \text{CoO}_{\text{exp}}(\text{calcd})^{\text{a}}$	Co metalation ratio
3D-COF-CorCo	7.3	7.9	92%
2D-COF-CorCo	9.0	9.5	95%

### 3.3.3.7 Gas sorption analysis

In order to analyze the permanent porosity of COFs, nitrogen adsorption-desorption measurements were carried out at 77 K for the four materials. Before gas adsorption measurements, all the COFs were heated under vacuum at 80 °C for at least 3 h until the pressure reached  $5 \times 10^{-5}$  atm, making sure no solvent remained in the porous structure. 2D and 3D-COF-Cor both displayed nearly reversible type-I sorption behaviors (Fig. 18a and Fig. 19a). For the 2D COF, the sorption curves showed high nitrogen uptake at low relative pressure ( $P/P_0 < 0.2$ ), which is a significant feature of microporous materials presenting also small mesopores of ~2 nm. The isotherm of 3D-COF-Cor exhibits a typical type-I morphology with reversible desorption step. In addition, the high uptake in the higher-pressure range ( $P/P_0 > 0.95$ ) is characteristic of intergranular sorption due to the presence of voids between the particles. After optimization of the COF synthesis with different reaction solvent systems and ratios, the highest BET surface area of 2D-COF-Cor and 3D-COF-Cor were obtained using the mixture *n*-

BuOH/mesitylene/acetic acid (10:5:1, V/V/V) and mixture *n*-BuOH/*o*-DCB/acetic acid (10:5:1, V/V/V) respectively. The BET model was applied to the isotherm of 2D-COF-Cor and 3D-COF-Cor following the Rouquerol recommendations<sup>41</sup> to afford a BET surface area of 1141 m<sup>2</sup> g<sup>-1</sup> and 489 m<sup>2</sup> g<sup>-1</sup>, respectively. Further studies were conducted on 2D and 3D-COF-Cor produced from large scale synthesis, and each sample exhibited a BET surface area of 1266 m<sup>2</sup> g<sup>-1</sup> and 484 m<sup>2</sup> g<sup>-1</sup> respectively, which corresponds to the best optimization results and show the good reproducibility of the material synthesis. In the literature, the two reported COFs based on another free base corrole present a lower porosity<sup>36,37</sup> around 745 and 634 m<sup>2</sup> g<sup>-1</sup> compared to 1266 m<sup>2</sup> g<sup>-1</sup> for the 2D-COF-Cor, first described in the present study. Our team<sup>42</sup> and others<sup>43</sup> also recently described a 3D POP based on corrole which gave a values of 645 and 416 m<sup>2</sup> g<sup>-1</sup> compared to 484 m<sup>2</sup> g<sup>-1</sup> for our 3D COF. The study of the metalated 2D and 3D-COF-CorCo also revealed a typical type-I isotherm with a sharp uptake at relative low pressure ( $P/P_0 < 0.1$ ), confirming their permanent porosity and the presence of microporosity with almost no mesoporosity, in contrary to the non-metalated materials. The BET surface areas were calculated to 638 and 489 m<sup>2</sup> g<sup>-1</sup>, respectively. After metalation, the BET surface area of 2D-COF-CorCo displayed a sharp decrease due to the stacking of 2D layers and some shrinking of the framework, as previously revealed by PXRD analyses. These structural and porosity changes were triggered by the insertion of cobalt into the corrole. Nonlocal density functional theory (NLDFT) fitting of the adsorption branch for 2D-COF-Cor and 3D-COF-Cor displays pore size distributions with average pore widths of 6.1 Å, 10.4 Å, 23.5 Å and 5.7 Å, 11.6 Å, 25 Å, respectively (Fig. 18b and 19b). This reveals the presence of micropores and small mesopores, as well as irregularities, in their structures. But the mesoporous contribution is low for the 3D COFs, and it tends to vanish for the 2D COFs after the metalation. Furthermore, the BET surface area of 2D and 3D-COF-CorCo after CO adsorption cycles showed a slight decrease compared to those before the CO adsorption cycles.

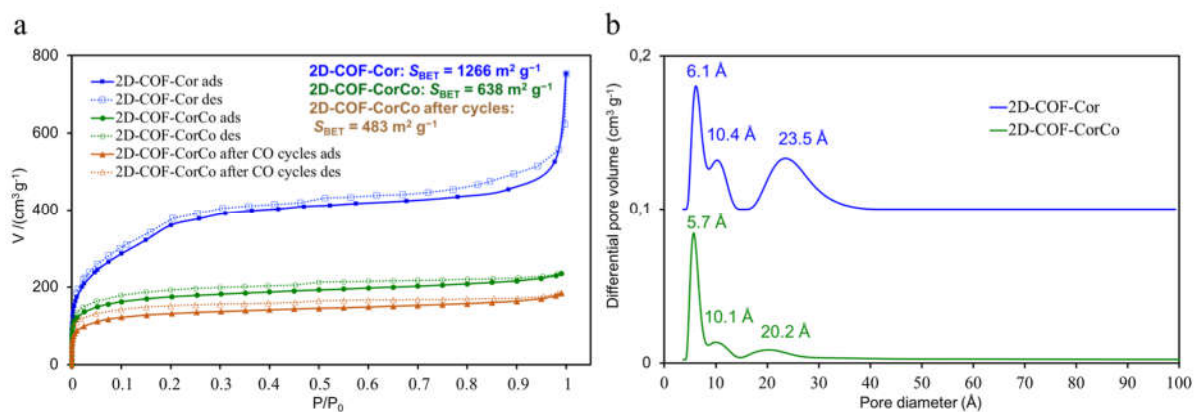


Figure 18. a. N<sub>2</sub> adsorption (closed symbols) and desorption (open symbols) isotherms recorded at 77 K for 2D-COF-Cor (blue square), 2D-COF-CorCo (green square), 2D-COF-CorCo after CO cycles (brown square). b. The respective pore size distribution curves of 2D-COF-Cor and 2D-COF-CorCo calculated using the NLDFT method.

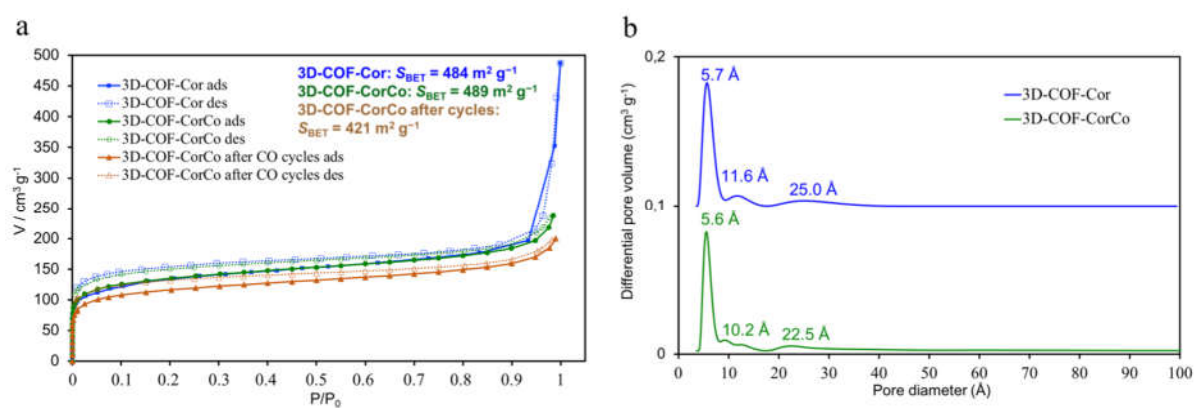


Figure 19. a. N<sub>2</sub> adsorption (closed symbols) and desorption (open symbols) isotherms recorded at 77 K for 3D-COF-Cor (blue square), 3D-COF-CorCo (green square), 3D-COF-CorCo after CO cycles (brown square). b. The respective pore size distribution curves of 3D-COF-Cor and 3D-COF-CorCo calculated using the NLDFT method.

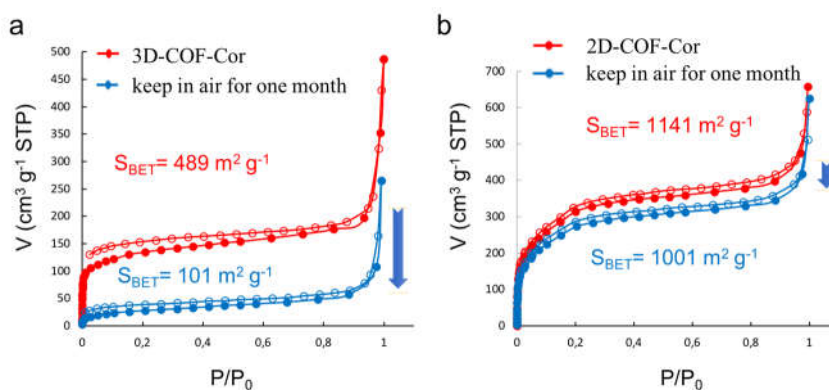


Figure 20. N<sub>2</sub> adsorption (closed symbols) and desorption (open symbols) isotherms recorded at 77 K for 3D-COF-Cor (a) and 2D-COF-Cor (b), before (red curve) and after one month (blue curve).

Apart from the basic analysis for BET surface area, we also made a comparison for the COF-Cor before and after kept in air for one month. In Fig. 20a, BET surface area of 3D-COF-Cor decreased from  $489 \text{ m}^2\text{g}^{-1}$  to  $101 \text{ m}^2\text{g}^{-1}$  after one month contact with air. But for 2D-COF-Cor, a slight decrease from  $1141 \text{ m}^2\text{g}^{-1}$  to  $1001 \text{ m}^2\text{g}^{-1}$  presented in Fig. 20b. The BET surface area is simply associated with the surface to volume ratio. The decrease may represent a collapse of internal structure which means 3D-COF-Cor is less stable than 2D-COF-Cor for micro-structure. 2D-COF-Cor presented a rigid structure against collapse. That is also associated with the high crystallinity of 2D-COF-Cor.

### 3.3.3.8 CO adsorption analysis

The CO adsorption properties of 2D-COF-CorCo and 3D-COF-CorCo were also evaluated along with the selectivity for CO vs.  $\text{N}_2$ ,  $\text{O}_2$  and  $\text{CO}_2$ , which are the main components of the air, and the main potential interferents. As displayed in Fig. 21a and Fig. 21b, the adsorption isotherms for the gases were recorded at 298 K showing different adsorption volumes at 1 atm. At first glance, the results indicate a good capacity and selectivity for CO adsorption 2D-COF-CorCo and 3D-COF-CorCo. At 1 atm, the two materials display a CO uptake of  $32.2 \text{ cm}^3 \text{ g}^{-1}$  and  $20.5 \text{ cm}^3 \text{ g}^{-1}$  at 298 K, respectively. Most importantly, for CO adsorption, both materials displayed a sharp uptake at a very low pressure ( $< 0.01 \text{ atm}$ ) which is dominated by the binding of CO molecules on the cobalt in the corrole through a chemisorption process. After saturation of all the accessible cobalt sites by CO molecules, the rest of the adsorption process was then led by physisorption due to the porosity of the materials. 2D and 3D-COF-CorCo also exhibit adsorption for  $\text{N}_2$ ,  $\text{O}_2$  and  $\text{CO}_2$  but only through physisorption, and no chemisorption was observed since no interaction occurred between these gases and cobalt corrole.<sup>42, 44</sup> Among these gases, a high uptake of  $\text{CO}_2$  at 1 atm occurred through a physisorption process due to the stronger interactions between the surface of the materials and  $\text{CO}_2$ . Up to now, only our team has reported porous materials based on cobalt corrole with a high affinity for CO at very low partial pressure,<sup>42</sup> which is a prerequisite to provide a good selectivity in gas mixture containing a low concentration of CO. In order to describe the CO adsorption process, the isotherm data were fitted with a triple-site Langmuir model while a single-site Langmuir model enabled the fitting of the  $\text{CO}_2$ ,  $\text{N}_2$  and  $\text{O}_2$  adsorption isotherms. The half saturation pressure for the selective sorption process was estimated to  $0.65 \times 10^{-4} \text{ atm}$  and  $0.46 \times 10^{-4} \text{ atm}$  for 2D-COF-CorCo and 3D-COF-CorCo, respectively. The two first components of the triple-site Langmuir model were assigned to the chemisorption of CO to the cobalt, which gives an estimation of chemisorbed

CO of  $12.6 \text{ cm}^3 \text{ g}^{-1}$  and  $6.7 \text{ cm}^3 \text{ g}^{-1}$ , respectively. These data gave further evidence of the high affinity of the materials for CO sorption and selectivity against  $\text{N}_2$ ,  $\text{O}_2$  and  $\text{CO}_2$ . Compared to the reported cobalt complexed POPs,<sup>42</sup> the 2D-COF-CorCo presented a higher ratio of cobalt active site of 56.2 % against 35.2% of 3D-COF-CorCo, which could be assigned to the higher crystallinity and stability of the porous structure, as well as to the regularity and uniformity of the pores distribution. Furthermore, interpenetration of the framework often happens in 3D COFs<sup>45, 46</sup> which should reduce the porosity in the case of 3D-COF-CorCo, and inhibits the accessibility of the cobalt sites and therefore the further binding with CO molecules.

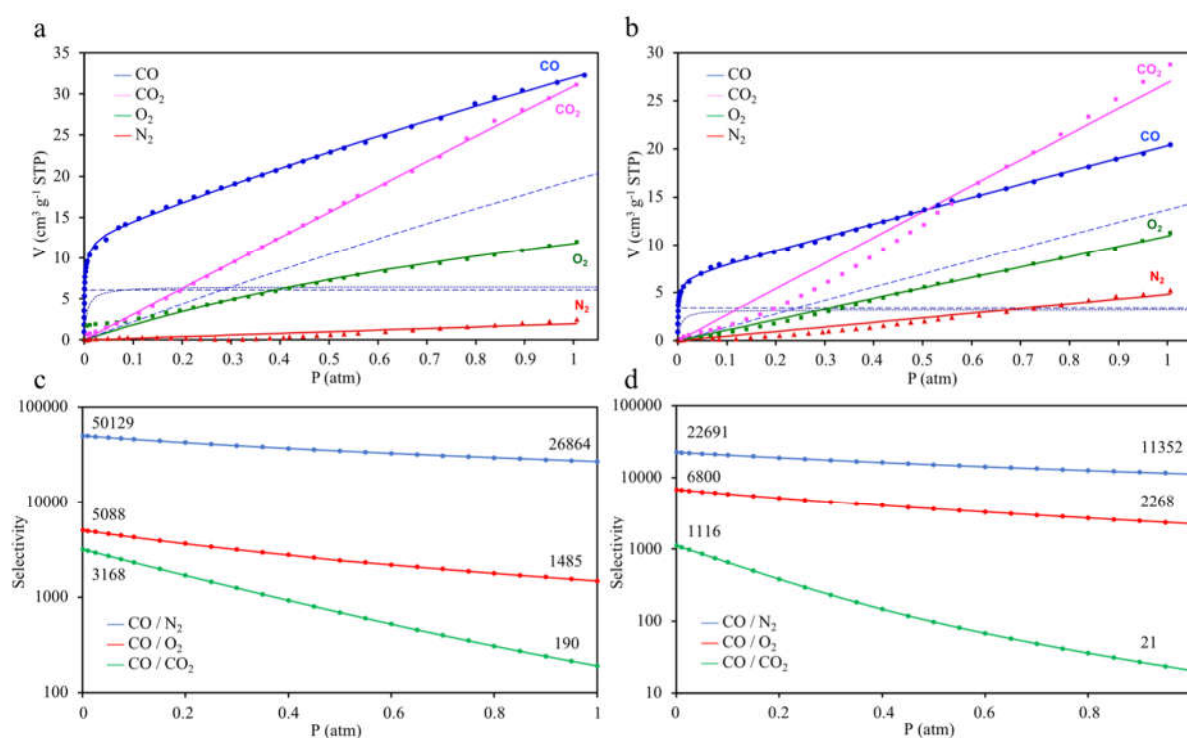


Figure 21. a-b. Adsorption isotherms of CO (blue), CO<sub>2</sub> (pink), N<sub>2</sub> (red) and O<sub>2</sub> (green) recorded at 298 K for 2D-COF-CorCo (a) and 3D-COF-CorCo (b). c-d) Solid lines represent fitting curves using a single-site Langmuir model for N<sub>2</sub>, O<sub>2</sub> and CO<sub>2</sub>, and a triple-site Langmuir model for CO. IAST selectivity calculations at 298 K for CO over CO<sub>2</sub>, N<sub>2</sub> and O<sub>2</sub> for 2D-COF-CorCo (c) and 3D-COF-CorCo (d) assuming a 0.01: 99.99 mixture (100 ppm CO in N<sub>2</sub>, O<sub>2</sub> or CO<sub>2</sub>).

The selectivity for CO over O<sub>2</sub>, N<sub>2</sub> and CO<sub>2</sub> was determined by IAST calculations according to the fitting parameters deduced from the multisite and single site Langmuir models, considering a gas mixture containing 100 ppm of CO in the other gases (Fig. 21c, d). These conditions were chosen to estimate the suitability of the materials for CO sensing in a real

atmosphere, which is mainly composed by  $N_2$ ,  $O_2$  and  $CO_2$ . At zero pressure, the calculations gave very high selectivity values for CO over  $N_2$  (50129 and 22691) and  $O_2$  (5088 and 6800) for 2D and 3D-COF-CorCo, respectively. These values correspond to the ratio of their corresponding Henry constants at zero pressure. In all cases, the selectivities decrease gradually with increasing pressure, but still remain higher than 11000 over  $N_2$  and 1400 over  $O_2$  at 1 atm. Aside from the selectivity, 2D-COF-CorCo showed the highest capacity for CO at low pressure ( $P < 0.1$  atm) compared to either 3D-COF-CorCo or the recently reported POPs based on cobalt corrole.<sup>42</sup> This result should be assigned to the better accessibility of the cobalt site in 2D-COF-CorCo for CO binding owing to the better structuration and organization of the pore channels. Accordingly, it is considered that the selectivity of 2D/3D-COF-CorCo for CO over  $N_2$ ,  $O_2$  and  $CO_2$  is far higher than those reported for other porous materials like MOFs and POPs.<sup>42, 47, 48</sup> Despite the lower selectivity for CO over  $CO_2$  compared to other gases, the CO/ $CO_2$  selectivity is still high ( $> 20$ ) at 1 atm even with a CO/ $CO_2$  ratio of 0.01/99.99. However, in a real atmosphere containing 400 ppm of  $CO_2$ , only the selectivities at low partial pressures of  $CO_2$  must be considered for the targeted application as CO sensors. Furthermore, the reversibility of the materials for CO was studied by recording successive CO adsorption cycles after degassing at 80 °C between each sorption cycle (Fig. 22 and 23). The results showed that after 4 cycles, both COFs gave satisfactory reversibility results. The slight decrease of CO adsorption between the first and fourth cycle could be assigned to a partial collapse of the structures and porosities, as shown by the decrease of their BET surfaces after 4 cycles (Fig. 18a and 19a).

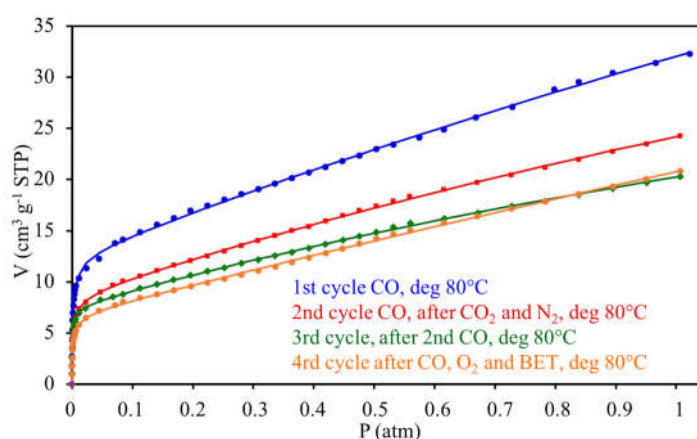


Figure 22. CO adsorption isotherms for 2D-COF-CorCo recorded at 298 K for four successive cycles (1<sup>st</sup> cycle: blue symbols; 2<sup>nd</sup> cycle: red symbols; 3<sup>rd</sup> cycle: green symbols; 4<sup>th</sup> cycle: orange symbols). The sample was degassed at 80 °C during 3 h between each adsorption measurement.

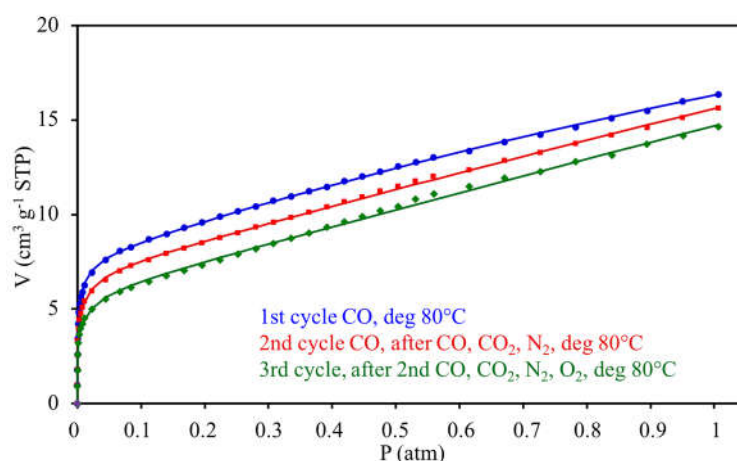


Figure 23. CO adsorption isotherms for 3D-COF-CorCo recorded at 298 K for four successive cycles (1<sup>st</sup> cycle: blue symbols; 2<sup>nd</sup> cycle: red symbols; 3<sup>rd</sup> cycle: green symbols). The sample was degassed at 80 °C during 3 h between each adsorption measurement.

The reversibility study of the CO adsorption for 2D and 3D-COF-CorCo were also carried out by FTIR spectroscopy in transmission mode using KBr pellets of COFs under either a CO atmosphere or under vacuum (Fig. 24 and 25). Before exposure to CO, the activation of these materials was achieved under vacuum at 20 °C in order to remove the coordinated ammine on the cobalt corrole. After 24 h, the ammine ligands were removed since the characteristic stretching vibration of NH<sub>3</sub> totally vanished. Then, the KBr pellet was placed in a CO atmosphere (1 bar) for 1 h and the chamber was purged for 5 min with nitrogen to remove extra CO (Fig. 24a). For 2D-COF-CorCo, an intense vibration band at 2044 cm<sup>-1</sup> appeared and this frequency value is characteristic to CO bounded to a metal ion *via* the carbon atom.<sup>42</sup> The lower value compared to free CO (2143 cm<sup>-1</sup>) is assigned to the sigma donation of CO from the carbon orbital into the empty *d*<sub>z2</sub> orbital of cobalt. The electron density can also be  $\pi$ -backdonated from *d* orbitals of the cobalt to  $\pi$ -antibonding orbitals of CO.<sup>49-51</sup> This  $\pi$ -backdonation tends to weaken the CO bond vibration leading to a red-shift of the CO stretching frequency with respect to free CO (2143 cm<sup>-1</sup>), as already observed in a Co(III) corrole series.<sup>42, 44</sup>

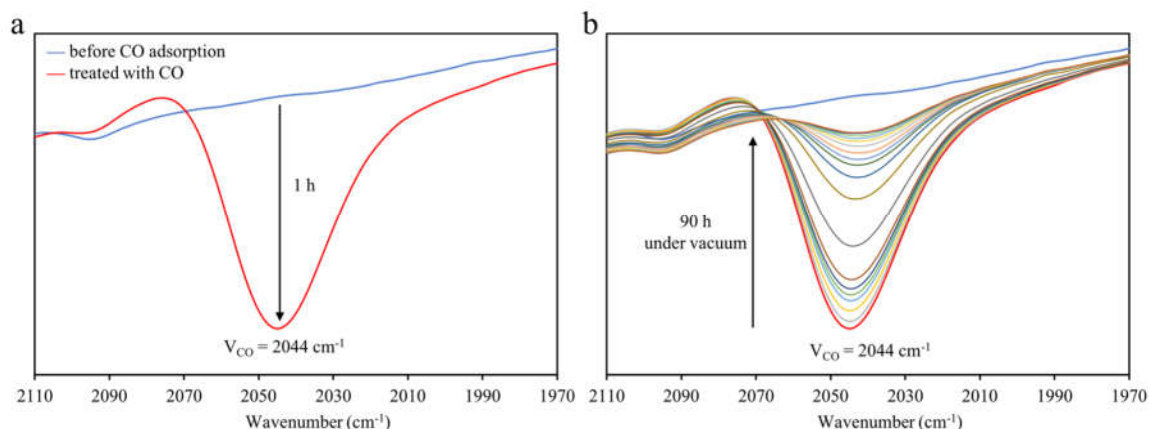


Figure 24. FTIR monitoring of the adsorption/desorption process recorded for 2D-COF-CorCo: a. activated 2D-COF-CorCo and treated with CO for 1 h, b. during desorption under vacuum (1 min to 90 h).

Successive spectra were then recorded after exposure the chamber to vacuum (2 mbar). As displayed in Fig. 24b, a constant decrease of the bonded CO vibration intensity was observed over time under vacuum. After 90 h, the CO vibration almost disappeared and the intensity didn't change any more, which means that there was no more CO coordinated on cobalt corroles. However, the half-desorption time was rather short since it was estimated to 30 min (Fig. 26). These data clearly reveal that CO adsorption in the COFs involved the coordination of the gaseous molecules on the cobalt atom according to a reversible process.

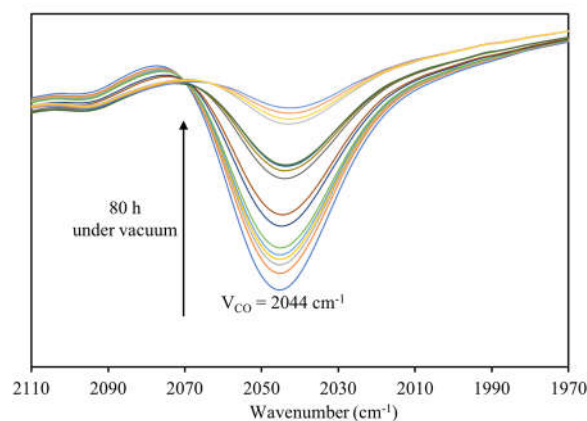


Figure 25. FTIR monitoring of the second adsorption/desorption process recorded for 2D-COF-CorCo.

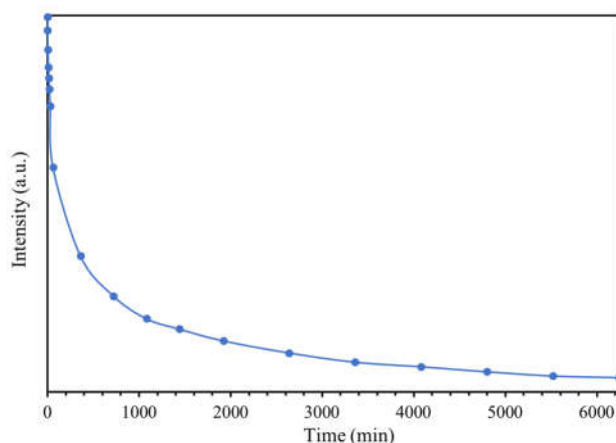


Figure 26. Intensity changes of FT-IR spectrum at  $2044\text{ cm}^{-1}$  of 2D-COF-CorCo during desorption.

For 3D-COF-CorCo, similar results for the reversible process were observed (Fig. 27). The only difference is that it took only 36 h to remove all the bonded CO to the cobalt corroles. However, both of them showed a fast CO desorption in the first hour which indicated a fast and reversible CO desorption. The reversibility for CO binding on 2D and 3D-COF-CorCo was studied by carrying out two cycles of adsorption and desorption of CO, and monitored by FTIR. For 2D-COF-CorCo, after 80 h vacuum, the CO was desorbed until it reached an equilibrium but it did not desorb completely (Fig. 24b). This could be caused by the  $\pi$ -stacking structure of 2D COF, which makes it more difficult to release CO. For 3D-COF-CorCo, the first cycle of sorption and desorption of CO presented the same behavior as for 2D-COF-CorCo. However, for the second cycle the desorption of CO was total (Fig. 28). These results showed good reversibility of CO binding and desorption for 2D and 3D-COF-CorCo. The half-desorption time was rather short since it was estimated to 45min (Fig. 29) means a fast desorption of CO and good reversibility.

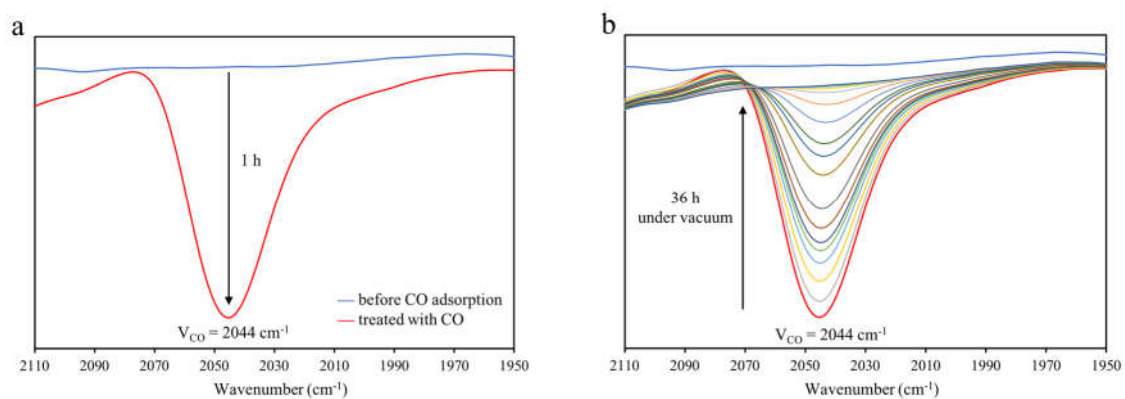


Figure 27. FTIR monitoring of the adsorption/desorption process recorded for 3D-COF-CorCo: a. activated 2D-COF-CorCo and treated with CO for 1 h, b. during desorption under vacuum (1 min to 36 h).

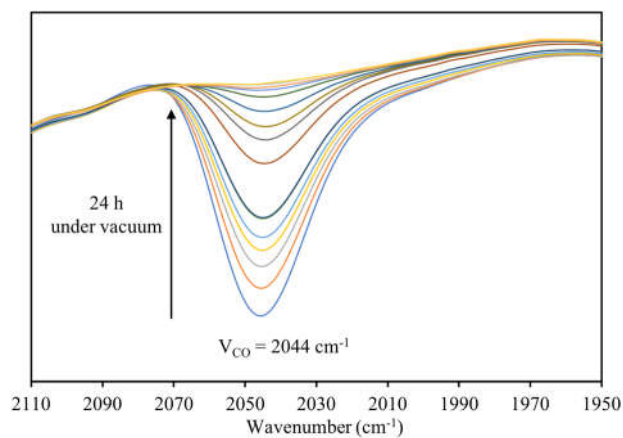


Figure 28. FTIR monitoring of the second adsorption/desorption process recorded for 3D-COF-CorCo.

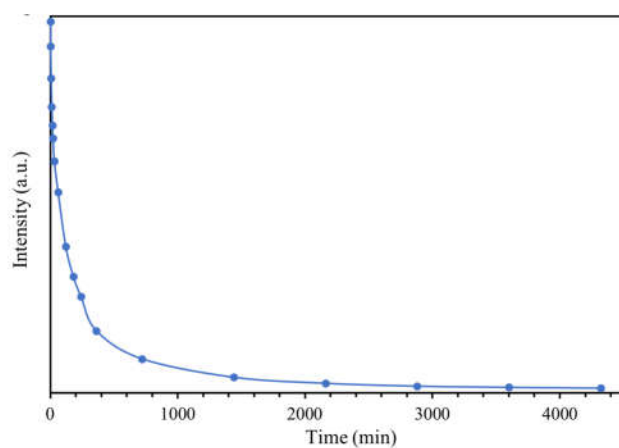
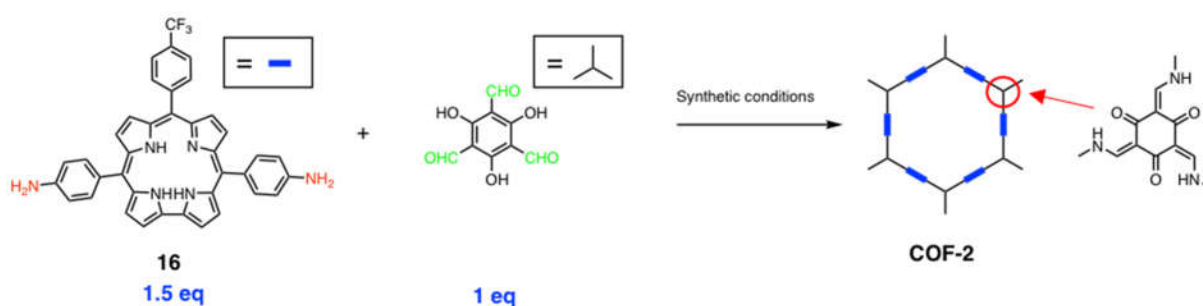


Figure 29. Intensity changes of FT-IR spectrum at  $2044 \text{ cm}^{-1}$  of 3D-COF-CorCo during desorption.

### 3.3.4 Synthesis of COFs based on other platforms

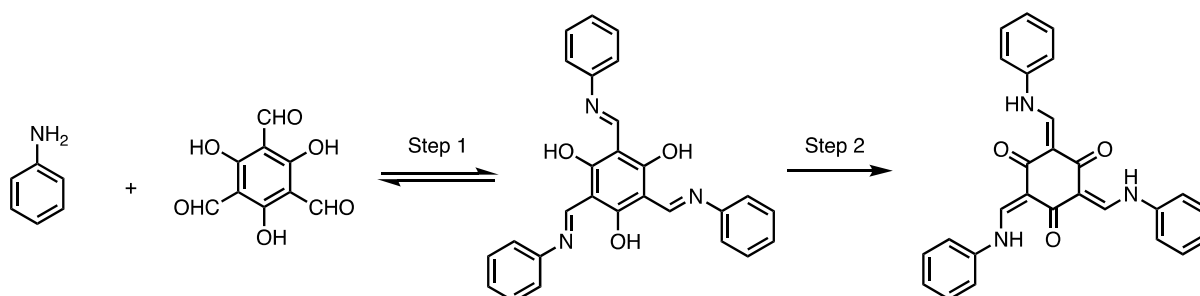
We have just detailed and presented the preparation of new COFs from tetra(4-formylphenyl)methane and 1,3,5-triformylbenzene platforms. In parallel, we have also explored other symmetric aldehyde derivates as platforms: like truxene, adamantane and 2,4,6-trihydroxy-1,3,5-benzenetricarbaldehyde.

#### 3.3.4.1 Synthesis of COFs based on 2,4,6-trihydroxy-1,3,5-benzenetricarbaldehyde



Scheme 9. Synthesis of COF-2.

Several publications report that the use of 2,4,6-trihydroxy-1,3,5-benzenetricarbaldehyde (commercially available) makes it possible to synthesize “locked” COFs.<sup>52, 53</sup> In the first step, a reversible Schiff base reaction leads to the formation of a crystalline framework, and the second step is an irreversible enol-to-keto tautomerization, which enhances the chemical stability (Scheme 10). We thus tried to use the corrole amino **16** to prepare this new COF (Scheme 9). The different optimization tests are presented in Table 8.



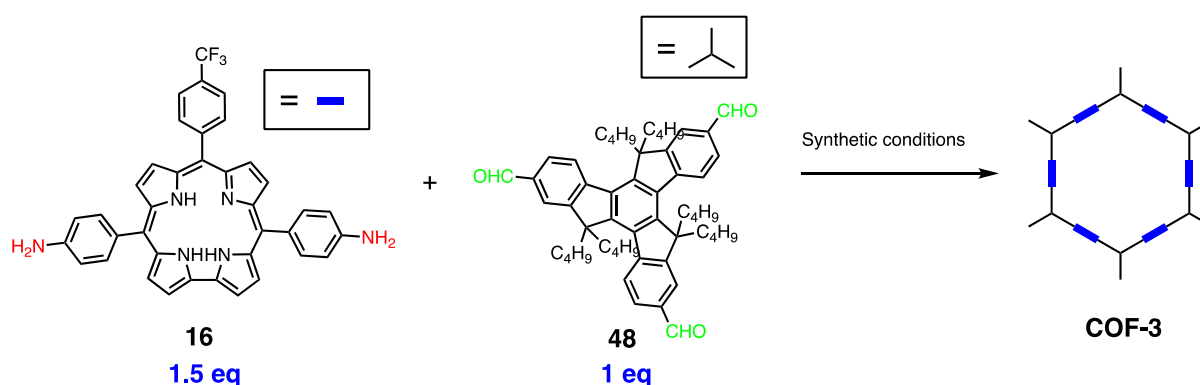
Scheme 10. Formation of  $\beta$ -Ketoenamine linkage.

Table 8. Optimization of synthetic conditions for COF-2.

	Solvent				Crystallinity	S <sub>BET</sub> (m <sup>2</sup> /g)	Yield
	EtOH	Mesitylene	<i>n</i> -BuOH	<i>o</i> -DCB			
<b>1</b>	1 mL	2 mL	-	-	Amorphous	324	91%
<b>2</b>	1.5 mL	1.5 mL	-	-	Amorphous	380	85%
<b>3</b>	2 mL	1 mL	-	-	Amorphous	430	96%
<b>4</b>	-	1 mL	2 mL	-	Amorphous	490	90%
<b>5</b>	-	1.5 mL	1.5 mL	-	Amorphous	392	89%
<b>6</b>	-	2 mL	1 mL	-	Amorphous	306	87%
<b>7</b>	-	-	1 mL	2 mL	Amorphous	412	94%
<b>8</b>	-	-	1.5 mL	1.5 mL	Amorphous	398	93%
<b>9</b>	-	-	2 mL	1 mL	Amorphous	453	88%

We carried out 9 tests by mainly varying the solvents. In all the tubes, the solvent was at the end colorless which means that the corrole dyes were consumed. All of the yields were mostly greater than 90%. It was therefore expected, like 2D-COF-Cor, to have high crystallinity and BET surface area. However, the various tests led to amorphous materials and with a low specific surface area. This could be explained by the fact that the product precipitates too fast. And if the irreversible enol ketone tautomerism occurs too soon, the framework doesn't have a crystal structure because it cannot go back.

### 3.3.4.2 Synthesis of COFs based on truxene



Scheme 11. Synthesis of COF-3.

We have also synthesized a truxene unit functionalized by three aldehyde functions (see chapter 2, part 2.1.2.2) in order to use it as a platform with the amino corrole **16** (Scheme 11). This moiety has the particularity of being flat, we hope to improve the crystallinity of COF.

The optimization synthesis (variation of solvent mixtures) is showed in Table 9. For each of the three trials, we had the same problem. During the washing of materials, a release of the corrole was observed (green color of the solvent characteristic of the corrole). It is deduced from this that this COF tends to degrade, it is therefore not very stable. It could be assigned to the special structure of truxene. With the long chains at vertical direction on two sides, it is very difficult for truxene to have 2D layer accumulation due to the space hinder (Fig. 30). Compared to 2D-COF-Cor which has  $\pi$ - $\pi$  stacking between layers, COF-3 is less stable and presents no crystallinity.

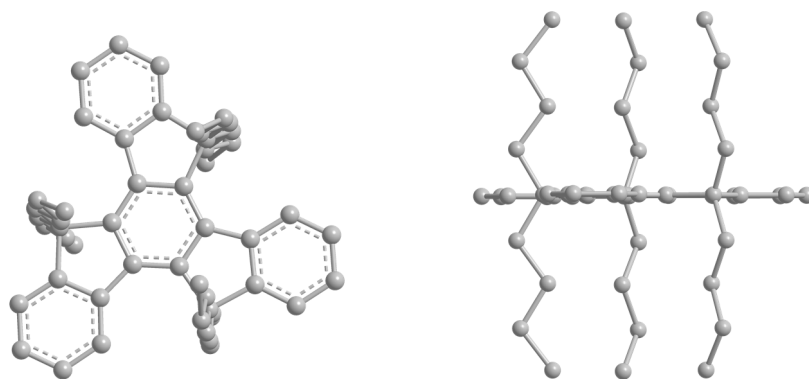
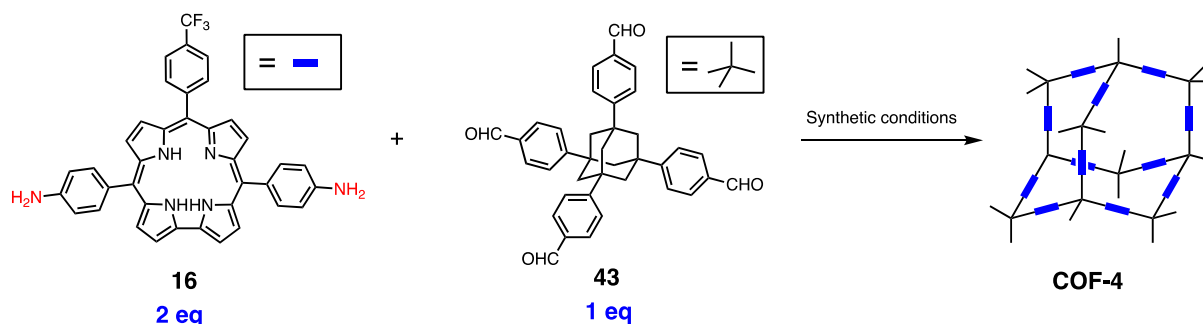


Figure 30. Structure simulation photo of truxene from front (left) and side (right).

Table 9. Optimization of synthetic conditions for COF-3.

	Solvent				Crystallinity	$S_{\text{BET}}$ ( $\text{m}^2/\text{g}$ )
	EtOH	Mesitylene	<i>n</i> -BuOH	<i>o</i> -DCB		
<b>1</b>	1.5 mL	1.5 mL	-	-	Amorphous	-
<b>2</b>	-	1.5 mL	1.5 mL	-	Amorphous	-
<b>3</b>	-	-	1.5 mL	1.5 mL	Amorphous	-

### 3.3.4.3 Synthesis of COFs based on adamantane



Scheme 12. Synthesis of COF-4.

Table 10. Optimization of synthetic conditions for COF-4.

	Solvent				Crystallinity	S <sub>BET</sub> (m <sup>2</sup> /g)	Yield
	EtOH	Mesitylene	<i>n</i> -BuOH	<i>o</i> -DCB			
<b>1</b>	1 mL	2 mL	-	-	Amorphous	418	63%
<b>2</b>	1.5 mL	1.5 mL	-	-	Amorphous	367	52%
<b>3</b>	2 mL	1 mL	-	-	Amorphous	425	58%
<b>4</b>	-	1 mL	2 mL	-	Amorphous	470	68%
<b>5</b>	-	1.5 mL	1.5 mL	-	Amorphous	439	71%
<b>6</b>	-	2 mL	1 mL	-	Amorphous	398	54%
<b>7</b>	-	-	1 mL	2 mL	Amorphous	500	55%
<b>8</b>	-	-	1.5 mL	1.5 mL	Amorphous	430	67%
<b>9</b>	-	-	2 mL	1 mL	Amorphous	410	53%

Finally, we prepared the precursor adamantane **43**. This compound can be considered as a more rigid analogue of compound **40** (used to prepare 3D COF). Considering the similarity between platforms **40** and **43**, we used the same synthetic conditions for optimization (Table 10). However, after verification by PXRD, none of COFs of different tests showed crystallinity. Furthermore, the porosities are very close to 3D-COF-Cor. This may be a proof that the corrole tends to be a nonlinear linker.

### 3.4 Conclusion

In this chapter, we tried different routes to obtain COF: from an aldehyde-corrole or from an amino-corrole. The use of aldehyde-corrole is not a perfect route because COF is obtained with a low yield and the synthesis of the corrole is complicated. With amino-corrole as a linker, we tried five different aldehyde platforms to construct COFs. The 1,3,5-triformylbenzene and the tetra(4-formylphenyl)methane **40** platforms are the most interesting at the moment. Through optimization and large-scale synthesis, we obtained two COFs (2D-COF-Cor and 3D-COF-Cor) and their cobalt complexes. The resulted porous 2D-COF-Cor showed good crystallinity with a hexagonal packing and an AA arrangement. Interestingly, the crystallinity and permanent porosity were preserved after post-metalation with cobalt. In contrast, three dimensional 3D-COF-Cor showed a microporous but amorphous structure. Both corrole-based materials also show a high surface area that reached  $1266 \text{ m}^2 \text{ g}^{-1}$  in the case of the 2D COF. In contrast, 3D COF showed a lower BET surface area of  $484 \text{ m}^2 \text{ g}^{-1}$ . Post-metalation allowed us to insert cobalt into the corrole macrocycle almost quantitatively in order to obtain the targeted COFs-CorCo for further CO adsorption. Both of them exhibited outstanding affinities and selectivities for CO binding over  $\text{N}_2$ ,  $\text{O}_2$  and  $\text{CO}_2$ . It is also worth noting that the adsorption of CO for COFs-Co is reversible through at least 4 cycles, even if a slight decrease of CO uptake was observed. However, the CO adsorption for both COFs tend to be stable after 4 cycles since it did not decrease anymore after 4 cycles. We have also shown that the combination of crystallinity and regular porosity of the framework allow a better accessibility of the cobalt corrole for gas binding. Desorption of CO was studied by FTIR that showed that both COFs exhibit a fast desorption of CO with a half-desorption time estimated to 30 min. This result is a real prerequisite to build sensors with fast response. These results demonstrate that the combination of cobalt corroles and COF materials provides an attractive strategy for the selective CO capture, and our work are currently in progress for developing new gas sensor technologies featuring great potential of applications.

## References

1. Barbe, J.-M.; Canard, G.; Brandes, S.; Guillard, R., Selective chemisorption of carbon monoxide by organic-inorganic hybrid materials incorporating cobalt(III) corroles as sensing components. *Chem. Eur. J.* **2007**, *13* (7), 2118-2129, S2118/1-S2118/3.
2. Barbe, J.-M.; Canard, G.; Brandès, S.; Jérôme, F.; Dubois, G.; Guillard, R., Metalloporroles as sensing components for gas sensors: remarkable affinity and selectivity of cobalt(III) porroles for CO vs. O<sub>2</sub> and N<sub>2</sub>. *Dalton Trans.* **2004**, (8), 1208-1214.
3. Vanotti, M.; Poisson, S.; Soumann, V.; Quesneau, V.; Brandès, S.; Desbois, N.; Yang, J.; André, L.; Gros, C. P.; Blondeau-Patissier, V., Influence of interfering gases on a carbon monoxide differential sensor based on SAW devices functionalized with cobalt and copper porroles. *Sens. Actuators B: Chem.* **2021**, *332*, 129507.
4. Zhao, Y.; Dai, W.; Peng, Y.; Niu, Z.; Sun, Q.; Shan, C.; Yang, H.; Verma, G.; Wojtas, L.; Yuan, D.; Zhang, Z.; Dong, H.; Zhang, X.; Zhang, B.; Feng, Y.; Ma, S., A Porrole-Based Covalent Organic Framework Featuring Desymmetrized Topology. *Angew. Chem. Int. Ed.* **2020**, *59* (11), 4354-4359.
5. Li, Y.; Chen, M.; Han, Y.; Feng, Y.; Zhang, Z.; Zhang, B., Fabrication of a New Porrole-Based Covalent Organic Framework as a Highly Efficient and Selective Chemosensor for Heavy Metal Ions. *Chem. Mater.* **2020**, *32* (6), 2532-2540.
6. Zou, L.; Sa, R.; Zhong, H.; Lv, H.; Wang, X.; Wang, R., Photoelectron Transfer Mediated by the Interfacial Electron Effects for Boosting Visible-Light-Driven CO<sub>2</sub> Reduction. *ACS Catal.* **2022**, *12* (6), 3550-3557.
7. Feng, K.; Hao, H.; Huang, F.; Lang, X.; Wang, C., A 2D porphyrin-based covalent organic framework with TEMPO for cooperative photocatalysis in selective aerobic oxidation of sulfides. *Mater. Chem. Front.* **2021**, *5* (5), 2255-2260.
8. Gole, B.; Stepanenko, V.; Rager, S.; Grüne, M.; Medina, D. D.; Bein, T.; Würthner, F.; Beuerle, F., Microtubular Self-Assembly of Covalent Organic Frameworks. *Angew. Chem. Int. Ed.* **2018**, *57* (3), 846-850.
9. Lin, G.; Ding, H.; Chen, R.; Peng, Z.; Wang, B.; Wang, C., 3D Porphyrin-Based Covalent Organic Frameworks. *J. Am. Chem. Soc.* **2017**, *139* (25), 8705-8709.
10. Huang, L.; Luo, Z.; Zhou, Y. N.; Zhang, Q.; Zhu, H.; Zhu, S., Solvothermal synthesis of covalent triazine framework and its application in photodegradation of organic dyes. *Mater. Today Chem.* **2021**, *20*, 100475.

11. Wei, H.; Chai, S.; Hu, N.; Yang, Z.; Wei, L.; Wang, L., The microwave-assisted solvothermal synthesis of a crystalline two-dimensional covalent organic framework with high CO<sub>2</sub> capacity. *Chem. Comm.* **2015**, *51* (61), 12178-12181.
12. Díaz de Greñu, B.; Torres, J.; García-González, J.; Muñoz-Pina, S.; de los Reyes, R.; Costero, A. M.; Amorós, P.; Ros-Lis, J. V., Microwave-Assisted Synthesis of Covalent Organic Frameworks: A Review. *ChemSusChem* **2021**, *14* (1), 208-233.
13. Chen, L.; Du, J.; Zhou, W.; Shen, H.; Tan, L.; Zhou, C.; Dong, L., Microwave-Assisted Solvothermal Synthesis of Covalent Organic Frameworks (COFs) with Stable Superhydrophobicity for Oil/Water Separation. *Chem.: Asian J.* **2020**, *15* (21), 3421-3427.
14. Maschita, J.; Banerjee, T.; Savasci, G.; Haase, F.; Ochsenfeld, C.; Lotsch, B. V., Ionothermal Synthesis of Imide-Linked Covalent Organic Frameworks. *Angew. Chem. Int. Ed.* **2020**, *59* (36), 15750-15758.
15. Dong, B.; Wang, W.-J.; Pan, W.; Kang, G.-J., Ionic liquid as a green solvent for ionothermal synthesis of 2D keto-enamine-linked covalent organic frameworks. *Mater. Chem. Phys.* **2019**, *226*, 244-249.
16. Wang, X.; Ma, R.; Hao, L.; Wu, Q.; Wang, C.; Wang, Z., Mechanochemical synthesis of covalent organic framework for the efficient extraction of benzoylurea insecticides. *J. Chromatogr. A* **2018**, *1551*, 1-9.
17. Zhang, P.; Dai, S., Mechanochemical synthesis of porous organic materials. *J. Mater. Chem. A* **2017**, *5* (31), 16118-16127.
18. Chen, L.-Y.; Gai, Y.-N.; Gai, X.-T.; Qin, J.; Wang, Z.-G.; Cui, L.-S.; Guo, H.; Jiang, M.-Y.; Zou, Q.; Zhou, T.; Gai, J.-G., Interfacial synthesized covalent organic framework nanofiltration membranes for precisely ultrafast sieving. *Chem. Eng. J.* **2022**, *430*, 133024.
19. Sun, B.; Liu, J.; Cao, A.; Song, W.; Wang, D., Interfacial synthesis of ordered and stable covalent organic frameworks on amino-functionalized carbon nanotubes with enhanced electrochemical performance. *Chem. Comm.* **2017**, *53* (47), 6303-6306.
20. Liu, Y.; Wang, Y.; Li, H.; Guan, X.; Zhu, L.; Xue, M.; Yan, Y.; Valtchev, V.; Qiu, S.; Fang, Q., Ambient aqueous-phase synthesis of covalent organic frameworks for degradation of organic pollutants. *Chem. Sci.* **2019**, *10* (46), 10815-10820.
21. Peng, Y.; Wong, W. K.; Hu, Z.; Cheng, Y.; Yuan, D.; Khan, S. A.; Zhao, D., Room Temperature Batch and Continuous Flow Synthesis of Water-Stable Covalent Organic Frameworks (COFs). *Chem. Mater.* **2016**, *28* (14), 5095-5101.

22. Geng, K.; He, T.; Liu, R.; Dalapati, S.; Tan, K. T.; Li, Z.; Tao, S.; Gong, Y.; Jiang, Q.; Jiang, D., Covalent Organic Frameworks: Design, Synthesis, and Functions. *Chem. Rev.* **2020**, *120* (16), 8814-8933.
23. Chi, S.-Y.; Chen, Q.; Zhao, S.-S.; Si, D.-H.; Wu, Q.-J.; Huang, Y.-B.; Cao, R., Three-dimensional porphyrinic covalent organic frameworks for highly efficient electroreduction of carbon dioxide. *J. Mater. Chem. A* **2022**, *10* (9), 4653-4659.
24. Liu, Y.; Yan, X.; Li, T.; Zhang, W.-D.; Fu, Q.-T.; Lu, H.-S.; Wang, X.; Gu, Z.-G., Three-dimensional porphyrin-based covalent organic frameworks with tetrahedral building blocks for single-site catalysis. *New J. Chem.* **2019**, *43* (43), 16907-16914.
25. Liu, C.; Chen, M.; Li, H.; Shi, Q.; Feng, Y.; Zhang, B., Crystalline Covalent Organic Frameworks Based on Mixed Metallo- and Tetrahydroporphyrin Monomers for Use as Efficient Photocatalysts in Dye Pollutant Removal. *Cryst. Growth Des.* **2022**, *22* (8), 4745-4756.
26. Sun, N.; Jin, Y.; Wang, H.; Yu, B.; Wang, R.; Wu, H.; Zhou, W.; Jiang, J., Photoresponsive Covalent Organic Frameworks with Diarylethene Switch for Tunable Singlet Oxygen Generation. *Chem. Mater.* **2022**, *34* (4), 1956-1964.
27. Liu, S.; Liu, Z.; Meng, Q.; Chen, C.; Pang, M., Facile Synthesis of a Cubic Porphyrin-Based Covalent Organic Framework for Combined Breast Cancer Therapy. *ACS Appl. Mater. Interfaces* **2021**, *13* (48), 56873-56880.
28. Keller, N.; Calik, M.; Sharapa, D.; Soni, H. R.; Zehetmaier, P. M.; Rager, S.; Auras, F.; Jakowetz, A. C.; Görling, A.; Clark, T.; Bein, T., Enforcing Extended Porphyrin J-Aggregate Stacking in Covalent Organic Frameworks. *J. Am. Chem. Soc.* **2018**, *140* (48), 16544-16552.
29. Ding, Z.-D.; Wang, Y.-X.; Xi, S.-F.; Li, Y.; Li, Z.; Ren, X.; Gu, Z.-G., A Hexagonal Covalent Porphyrin Framework as an Efficient Support for Gold Nanoparticles toward Catalytic Reduction of 4-Nitrophenol. *Chem. Eur. J.* **2016**, *22* (47), 17029-17036.
30. Zhu, W.; Ding, Z.-D.; Wang, X.; Li, T.; Shen, R.; Li, Y.; Li, Z.; Ren, X.; Gu, Z.-G., A three-dimensional porphyrin-based porous organic polymer with excellent biomimetic catalytic performance. *Polym. Chem.* **2017**, *8* (30), 4327-4331.
31. Samal, M.; Valligatla, S.; Saad, N. A.; Rao, M. V.; Rao, D. N.; Sahu, R.; Biswal, B. P., A thiazolo[5,4-d]thiazole-bridged porphyrin organic framework as a promising nonlinear optical material. *Chem. Comm.* **2019**, *55* (74), 11025-11028.

32. Meng, Y.; Luo, Y.; Shi, J.-L.; Ding, H.; Lang, X.; Chen, W.; Zheng, A.; Sun, J.; Wang, C., 2D and 3D Porphyrinic Covalent Organic Frameworks: The Influence of Dimensionality on Functionality. *Angew. Chem. Int. Ed.* **2020**, *59* (9), 3624-3629.
33. Hynek, J.; Zelenka, J.; Rathouský, J.; Kubát, P.; Ruml, T.; Demel, J.; Lang, K., Designing Porphyrinic Covalent Organic Frameworks for the Photodynamic Inactivation of Bacteria. *ACS Appl. Mater. Interfaces* **2018**, *10* (10), 8527-8535.
34. Huang, X.; Sun, C.; Feng, X., Crystallinity and stability of covalent organic frameworks. *Sci. China Chem.* **2020**, *63* (10), 1367-1390.
35. Yang, X.; Zhang, S.; Wang, J.; Wang, W.; Li, J.; Chen, J.; Zhao, Y.; Wang, C.; Wang, Z., Modulated construction of imine-based covalent organic frameworks for efficient adsorption of polycyclic aromatic hydrocarbons from honey samples. *Anal. Chim. Acta* **2020**, *1134*, 50-57.
36. Zhao, Y.; Dai, W.; Peng, Y.; Niu, Z.; Sun, Q.; Shan, C.; Yang, H.; Verma, G.; Wojtas, L.; Yuan, D.; Zhang, Z.; Dong, H.; Zhang, X.; Zhang, B.; Feng, Y.; Ma, S., A Corrole-Based Covalent Organic Framework Featuring Desymmetrized Topology. *Angew. Chem. Int. Ed.* **2020**, *59* (11), 4354-4359.
37. Li, Y.; Chen, M.; Han, Y.; Feng, Y.; Zhang, Z.; Zhang, B., Fabrication of a New Corrole-Based Covalent Organic Framework as a Highly Efficient and Selective Chemosensor for Heavy Metal Ions. *Chem. Mater.* **2020**, *32* (6), 2532-2540.
38. Kaleeswaran, D.; Vishnoi, P.; Murugavel, R., [3+3] Imine and  $\beta$ -ketoenamine tethered fluorescent covalent-organic frameworks for CO<sub>2</sub> uptake and nitroaromatic sensing. *J. Mater. Chem. C* **2015**, *3* (27), 7159-7171.
39. Neuman, N. I.; Singha Hazari, A.; Beerhues, J.; Doctorovich, F.; Vaillard, S. E.; Sarkar, B., Synthesis and Characterization of a Cobalt(III) Corrole with an S-Bound DMSO Ligand. *Eur. J. Inorg. Chem.* **2021**, *2021* (35), 3540-3548.
40. Hynek, J.; Zelenka, J.; Rathouský, J.; Kubát, P.; Ruml, T.; Demel, J.; Lang, K., Designing Porphyrinic Covalent Organic Frameworks for the Photodynamic Inactivation of Bacteria. *ACS Appl. Mater. Interfaces* **2018**, *10* (10), 8527-8535.
41. Rouquerol, J.; Llewellyn, P.; Rouquerol, F., Is BET equation applicable to microporous adsorbents? *Stud. Surf. Sci. Catal.* **2007**, *160*, 49-56.
42. Brandès, S.; Quesneau, V.; Fonquernie, O.; Desbois, N.; Blondeau-Patissier, V.; Gros, C. P., Porous organic polymers based on cobalt corroles for carbon monoxide binding. *Dalton Trans.* **2019**, *48* (31), 11651-11662.

43. Zhao, Y.; Peng, Y.; Shan, C.; Lu, Z.; Wojtas, L.; Zhang, Z.; Zhang, B.; Feng, Y.; Ma, S., Metalloporphyrin-based porous organic polymers as a heterogeneous catalytic nanoplatform for efficient carbon dioxide conversion. *Nano Res.* **2021**, *15* (2), 1145-1152.
44. Barbe, J.-M.; Canard, G.; Brandès, S.; Jérôme, F.; Dubois, G.; Guillard, R., Metalloporphyrins as sensing components for gas sensors: remarkable affinity and selectivity of cobalt(III) porphyrins for CO vs. O<sub>2</sub> and N<sub>2</sub>. *Dalton Trans.* **2004**, (8), 1208-1214.
45. Bisbey, R. P.; Dichtel, W. R., Covalent Organic Frameworks as a Platform for Multidimensional Polymerization. *ACS Cent. Sci.* **2017**, *3* (6), 533-543.
46. Meng, Y.; Luo, Y.; Shi, J. L.; Ding, H.; Lang, X.; Chen, W.; Zheng, A.; Sun, J.; Wang, C., 2D and 3D Porphyrinic Covalent Organic Frameworks: The Influence of Dimensionality on Functionality. *Angew. Chem. Int. Ed.* **2020**, *59* (9), 3624-3629.
47. Evans, A.; Luebke, R.; Petit, C., The use of metal-organic frameworks for CO purification. *J. Mater. Chem. A* **2018**, *6* (23), 10570-10594.
48. Bloch, E. D.; Hudson, M. R.; Mason, J. A.; Chavan, S.; Crocellà, V.; Howe, J. D.; Lee, K.; Dzubak, A. L.; Queen, W. L.; Zadrozny, J. M.; Geier, S. J.; Lin, L.-C.; Gagliardi, L.; Smit, B.; Neaton, J. B.; Bordiga, S.; Brown, C. M.; Long, J. R., Reversible CO Binding Enables Tunable CO/H<sub>2</sub> and CO/N<sub>2</sub> Separations in Metal-Organic Frameworks with Exposed Divalent Metal Cations. *J. Am. Chem. Soc.* **2014**, *136* (30), 10752-10761.
49. Frenking, G.; Fröhlich, N., The Nature of the Bonding in Transition-Metal Compounds. *Chem. Rev.* **2000**, *100* (2), 717-774.
50. Zhou, M.; Andrews, L.; Bauschlicher, C. W., Spectroscopic and Theoretical Investigations of Vibrational Frequencies in Binary Unsaturated Transition-Metal Carbonyl Cations, Neutrals, and Anions. *Chem. Rev.* **2001**, *101* (7), 1931-1962.
51. Wu, X.; Zhao, L.; Jiang, D.; Fernández, I.; Berger, R.; Zhou, M.; Frenking, G., Barium as Honorary Transition Metal in Action: Experimental and Theoretical Study of Ba(CO)<sup>+</sup> and Ba(CO)<sup>-</sup>. *Angew. Chem. Int. Ed. Engl.* **2018**, *57* (15), 3974-3980.
52. Kandambeth, S.; Mallick, A.; Lukose, B.; Mane, M. V.; Heine, T.; Banerjee, R., Construction of Crystalline 2D Covalent Organic Frameworks with Remarkable Chemical (Acid/Base) Stability via a Combined Reversible and Irreversible Route. *J. Am. Chem. Soc.* **2012**, *134* (48), 19524-19527.
53. DeBlase, C. R.; Silberstein, K. E.; Truong, T.-T.; Abruña, H. D.; Dichtel, W. R.,  $\beta$ -Ketoenamine-Linked Covalent Organic Frameworks Capable of Pseudocapacitive Energy Storage. *J. Am. Chem. Soc.* **2013**, *135* (45), 16821-16824.



## General conclusion and perspectives

The objective of this thesis was to develop porous materials based on cobalt corroles in order to further deposit them on SAW sensors to achieve highly sensitive and selective carbon monoxide detectors. Among various porous materials, we focused on covalent organic frameworks (COFs), which typically possess high permanent porosities, large surface areas and excellent thermal stabilities. Given these ideal characteristics, we aimed to design and synthesize many COFs with different structures or topologies.

First, we successfully prepared aldehyde and amino functionalized corrole linkers and a variety of platforms which were used to form the desired COFs via imine condensation. For the first tests, we used bis-aldehyde corrole **14** as a linker and tetra(4-aminophenyl)methane **38** as a platform to build COF-1. Given the low yield of bis-aldehyde corrole and COF-1, it was difficult to produce a large quantity of COF-1 for further analysis and application. Thus, we selected bis-amino corrole **16** as a linker to synthesize COFs. Several platforms such as tetra(4-formylphenyl)methane **40**, 1,3,5-triformylbenzene, 2,4,6-trihydroxybenzene-1,3,5-tricarbaldehyde, 5,5,10,10,15,15-Hexabutyl-2,7,12-triformyltruxene **48** and 1,3,5,7-tetrakis-4-formylphenyladamantane **43** were applied with the amino corrole linker for COF synthesis, and, in each case, we optimized the synthetic conditions before producing the materials on a larger scale. With the optimization and characterization by PXRD and BET measurements, we have been able to find the best reaction conditions for synthesis of the desired COFs.

With tetra(4-formylphenyl)methane **40** and 1,3,5-triformylbenzene, we synthesized two materials named 3D-COF-Cor and 2D-COF-Cor, respectively. 3D-COF-Cor showed normal BET surface area as compared to the reported POP-Cor as well as an amorphous structure. 2D-COF-Cor presented much higher porosity and higher crystallinity. Furthermore, these two materials could be reproduced in good yields on a larger scale. Next, cobalt metalation for corrole units in the COFs was carried out to obtain materials suitable for testing CO binding. The cobalt metalation of 3D-COF-Cor and 2D-COF-Cor were carried out with cobalt acetylacetonate in a mixture of DMSO and THF at 80°C and 100°C, respectively. The difference in temperature required for metalation was attributed to differences in topology between the two COFs, where 2D-COF-Cor presented a 2D layer stacking structure which is more difficult for cobalt insertion into the corrole. In the metalated COFs, a DMSO molecule

is coordinated to the cobalt center and is difficult, yet necessary to remove for further CO binding. Thus, we exchanged the DMSO ligand with two NH<sub>3</sub> molecules and NH<sub>3</sub> can be removed easily by smoothly heating at 80°C under vacuum. This series of reaction steps afforded 3D-COF-CorCo and 2D-COF-CorCo without any ligand on the cobalt center, a material suitable for CO binding studies. During the CO sorption tests, 3D-COF-CorCo and 2D-COF-CorCo presented high selectivity and sensitivity for CO. However, 2D-COF-CorCo showed a higher affinity for CO as compared to 3D-COF-CorCo. Thus, it was concluded that 2D-COF-CorCo could be a promising material for sensor application.

In the following part, we also tried to synthesize COF-2, COF-3 and COF-4 based on 2,4,6-trihydroxybenzene-1,3,5-tricarbaldehyde, 5,5,10,10,15,15-Hexabutyl-2,7,12-triformyltruxene **48** and 1,3,5,7-tetrakis-4-formylphenyladamantane **43**, respectively. Among them, COF-2 was synthesized by imine condensation and keto-enol tautomerism. With these two steps, COF-2 can be stabilized by the irreversible enol form to display higher resistance to acidic or basic environment. However, COF-2 presented lower BET surface area along with poor crystallinity as compared to 2D-COF-Cor, thus, more optimization will have to be done to obtain the best COF-2. COF-3 was found to be unstable with constant degradation, an observation attributed to the long chains on the truxene which disrupt the  $\pi$ - $\pi$  stacking between the 2D layers. Without rigid nanoparticles, COF-3 started to degrade rapidly. COF-4 possessed a similar structure as that of 3D-COF-Cor. Indeed, COF-4 presented a similar BET surface area and an amorphous structure as 3D-COF-Cor, but we expected that the rigid adamantane platform would improve the porosity and crystallinity of COF-4. However, measurements revealed that the characteristics of COF-4 were not improved from 3D-COF-Cor.

Since we already obtained 3D-COF-CorCo and 2D-COF-CorCo, for the next step, we planned to apply them on a SAW sensor. With the surface covered by silicon or silicon dioxide, 3-aminopropyltriethoxysilane (APTES) was considered to be a perfect coupling agent as it allows for further attachment of molecules through its terminal amines and exhibits self-assembled mono-layers. In addition, silanization is a reaction often used to attach APTES onto various surfaces. This reaction involves the initial hydroxylation of silicon dioxide, or glass, with subsequent hydrolysis of the APTES ethoxy groups with ethanol as the leaving group, resulting in an aminopropyl-terminated surface. This amino-functionalized sensor should be easily coated with our imine COFs, and thus it is a promising route to apply COFs on a SAW sensor.

In chapter 2, we also synthesized many other corroles which could potentially be used to synthesize metal-organic frameworks (MOFs) and porous organic polymers (POPs). Inspired by recently reported corrole-based MOF based, we will try to reproduce this MOF-corrole and metalate it with cobalt to test its ability for CO detection. Also reported in chapter 2 was the synthesis of mono-COOH corroles. Since it has already been shown that MOF PCN-222 contains free zirconium sites, it is anticipated that mono-COOH corroles could be used to functionalize PCN-222. Moreover, the high porosity and stability of PCN-222 make it a suitable carrier to hold corroles. For corrole-based POPs based, we synthesized bis-alkyne corrole and 1,3,5,7-Tetrakis(4-iodophenyl)adamantane, and following the early reported POP-Cor by our group, we can try similar reaction conditions to synthesize new POP based on a more rigid adamantane platform.

In parallel to CO detection, we could also apply the COFs for other applications by inserting different metals in the corrole linkers. Since we can easily repeat the synthesis of COFs with free base corrole on a large scale, it gives a rich platform to test the insertion of other metal ions such as Mn, Fe, Cu, Ga... These metal-derivatives could be applied in many areas of research such as catalysis, anticancer drugs, photodynamic therapy and hydrogen evolution... Thus, COFs based on corroles can be seen as promising materials for various applications.



# Experimental Section

## A. Materials and Instrumentation

### Reagent and materials

All the chemicals and solvents were purchased from commercial sources, unless otherwise noted, the reagents and solvents were directly used in the synthesis, requiring no further purification. All the reagent and materials were mainly purchased from Sigma-Aldrich®, Alfa Aesar®, Acros®, Fluorochem®, Carlo ERBA® and VWR chemicals®. DMF was dried over 3 Å molecular sieves. Pyrrole was purified by distillation before using for the synthesis of dipyrromethanes and corroles. The other dry solvents such as THF, DCM and MeOH were obtained from a solvent purification system (PureSolv) of Innovative Technology. Column chromatography purification was carried out on silica gel (Silica 60, 40-63 µm Aldrich®). Analytical thin-layer chromatography (TLC) was carried out using Merck silica gel 60 F-254 plates (precoated sheets, 0.2 mm thick, with fluorescence indicator F254).

### NMR Spectroscopy

NMR solvents were purchased from Eurisotope and were used without further purification. <sup>1</sup>H NMR spectra were recorded on Bruker Avance NEO spectrometers (400 and 500 MHz). All NMR shift values were expressed in ppm. The measurements were made at the PACSMUB-WPCM technological platform, which relies on the “Institut de Chimie Moléculaire de l’Université de Bourgogne” and Welience "TM", a Burgundy University private subsidiary. For free-base corroles, drops of hydrazine were added to remove the presence of any radical corrole and to further enhance the resolution of spectrum. The peak of hydrazine appears at 3.40 ppm in DMSO-*d*<sub>6</sub>. For the <sup>1</sup>H NMR of COFs, COFs (10 mg) and DMSO-*d*<sub>6</sub> (500 µL) were added in NMR tube. DCl in D<sub>2</sub>O (7 M, 10 µL, ~ 2 eq. of C=N linkages) was added in the tube to decompose COFs. When all solids disappeared, 50 µL of hydrazine (64% in H<sub>2</sub>O, 1.03 g/mL, 15 eq.) was added. The spectra of COFs were carried in 500 MHz spectrometers.

### UV-Visible Spectroscopy

All UV-Visible spectra were recorded on a Cary 50 UV-Visible spectrophotometer. All solvents used were of EPR quality. Quartz cells with optical path from 0.1 mm to 10 mm were used. Standard additions method was used to determine molar attenuation coefficients of new

products. The concentrations of all samples were diluted to low level ( $\times 10^{-5}$  mol/L).

### **Mass Spectrometry**

MALDI-TOF mass spectra were run on a BRUKER Ultraflex II and on a Microflex LRF spectrometers using dithranol as a matrix. High-resolution mass spectra (HRMS) were recorded on a LTQ Orbitrap XL (Thermo) or on an Orbitrap Exploris 240 (Thermo) instruments in the ESI mode.

### **Infrared Spectroscopy**

Infrared spectra were recorded on a IRFT BRUKER Vertex 70v. Sample consisted of pellets (3 mg of product dispersed in 200 mg of KBr and pressed at 10 tons) which were set up on a P/N 19900 sample holder purchased from Greasby Specac. Baseline were recorded on a pellet of pure KBr (200 mg).

### **Thermogravimetric analysis**

Thermogravimetric (TGA) analyses were recorded using a Netzsch STA 409 PC thermal analyzer. The samples (approximately 7.0 mg) were heated from 298 to 1273 K with a heating rate of  $5 \text{ K min}^{-1}$  under a flow of nitrogen ( $30 \text{ mL min}^{-1}$ ) and oxygen ( $10 \text{ mL min}^{-1}$ ).

### **Adsorption volumetric analysis**

Nitrogen adsorption/desorption isotherms were measured at 77 K on a Micromeritics ASAP 2020 instrument. The residual solvent molecules trapped inside the pores of the solids was then removed by degassing the samples (50 – 100 mg), transferred in a pre-weighted glass, in a dynamic vacuum at 298 K for at least 5 h before measurements. The specific surface area was determined using the Langmuir and the Brunauer–Emmett–Teller (BET) calculations, and the pore volumes were obtained directly from the  $\text{N}_2$  adsorption/desorption isotherms at  $P/P_0 = 0.99$ . To avoid large discrepancies between the two values of the surface area due to the invalid BET assumption for microporous solids over the usual range  $0.05 < P/P_0 < 0.25$ , a suitable pressure range was applied using a range that gives increasing values of  $V_{\text{N}_2}(P_0 - P)$  with  $P/P_0$  as required by the groups of Snurr and Rouquerol. Based on the consistency of this criteria, the pressure range used for the BET surface area calculations was then  $1.5 \times 10^{-3} < P/P_0 < 0.05$ . The pore size was determined using the Horvath–Kawazoe (HK) equation with the Saito-Foley model.

Low-pressure gas adsorption measurements for CO<sub>2</sub>, N<sub>2</sub>, and CO at 298 K were run on the same apparatus. The sample temperature was maintained using a Lauda cooler circulator and a double circulating jacket connected to a thermostatic bath in which the sample tube was dipped.

### **Scanning electron microscopy**

The scanning electron microscopy images were obtained with two different machines. Part of the images come from Hitachi SU8230 Field Emission Scanning Electron Microscopy equipped with the Quorum PP3010T cryogenic stage (Cryo-SEM). The preparation and analysis of samples were carried out at DimaCell Imaging Center facilities (INRAE, University of Burgundy Franche-Comté) The other images were collected on a Hitachi SU8230 Field Emission Scanning Electron microscopy which belongs to the Technical Analysis – Instrumentation Department of the Carnot Interdisciplinary Laboratory in Burgundy. This machine is backed by the M3 “Mathematics – Matter – Materials” research federation of the University of Burgundy and the ARCEN technical platform.

### **Energy dispersive X-ray spectroscopy (EDS)**

EDS measurements were performed on a Hitachi SU8230 Field Emission Scanning Electron Microscopy apparatus equipped with an Oxford EDS detector and having resolution of 0.8 nm @ 15KV / 1.1 nm @ 1KV. Measurements were conducted at DimaCell Imaging Center facilities (INRAE, University of Burgundy Franche-Comté).

### **Inductively coupled plasma atomic emission spectroscopy (ICP-AES)**

All Metal quantifications (Co, Zn, etc...) were carried out with an ICP-AES iCAP 7400, samples were prepared by microwaving up to 10 mg of POPs into a solution of pure nitric acid.

### **Elementary analysis**

The organic content of all samples was determined from CHNS elemental analysis performed on a FTA/ThermoFinnigan Flash 1112 analyser.

### **Material Studio**

The geometry optimization of lattice structure and refinement of PXRD pattern were performed at forcite module and reflex module in Material Studio, respectively. Thanks for the help from Prof. Bao Zhang from – School of Chemical Engineering and Technology, Tianjin University, Tianjin 300350, China.

### **Powder X-ray diffraction**

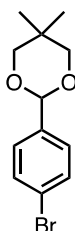
Powder X-ray diffraction (PXRD) experiments were performed on an Empyrean diffractometer from the PANalytical company in the range  $2^\circ < 2\theta < 50^\circ$ . The uncrushed samples were placed between two Mylar sheets and the analyses were performed in transmission mode using a focusing X-ray mirror equipped with fixed divergent and anti-scattering slits (aperture  $0.5^\circ$ ) and 0.02 rad Soller slits. The data collection was run with a copper anticathode X-ray tube ( $\text{CuK}_{\alpha 1} = 1.54060 \text{ \AA}$  /  $\text{CuK}_{\alpha 2} = 1.54443 \text{ \AA}$ ) and with a PIXcel<sup>3D</sup> detector equipped with an anti-scattering slit of 5 mm.

## B. Synthetic procedures

The synthesis protocols of all compounds including dipyrromethanes, corroles, platforms and porous materials are presented in detail in this part.

### 1. Synthesis of aldehyde derivatives as precursors of corroles

#### 1-Bromo-4-(4,4-dimethyl-2,6-dioxan-1-yl)benzene (**1**)



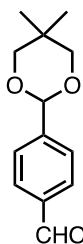
Chemical Formula: C<sub>12</sub>H<sub>15</sub>BrO<sub>2</sub>  
Exact Mass: 270.0255  
Molecular Weight: 271.1540

The procedure from literature was slightly modified. The *p*-bromobenzaldehyde (30.0 g, 0.16 mol, 1 eq), 2,2-dimethylpropane-1,3-diol (25.0 g, 0.24 mol, 1.5 eq) and *p*-TsOH (1.25 g, 7.26 mmol, 0.04 eq) were placed in a round bottom flask equipped with a Dean-Stark trap. Dry toluene (100 mL) was added under nitrogen and the mixture was heated to reflux for 12 h. After cooling, the solution was evaporated to dryness and crude compound was purified by column chromatography (Silica, DCM/heptane = 1:1), giving compound **1** as colorless crystals.

**Yield:** 43.2 g (99%)

**<sup>1</sup>H NMR (500 MHz, CDCl<sub>3</sub>)** δ 7.50 (d, *J* = 8.5 Hz, 2H), 7.39 (d, *J* = 8.5 Hz, 2H), 5.35 (s, 1H), 3.76 (d, *J* = 11.0 Hz, 2H), 3.64 (d, *J* = 11.0 Hz, 2H), 1.28 (s, 3H), 0.80 (s, 3H).

## 4-(4,4-Dimethyl-2,6-dioxan-1-yl)benzaldehyde (2)



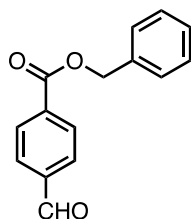
Chemical Formula: C<sub>13</sub>H<sub>16</sub>O<sub>3</sub>  
Exact Mass: 220.1099  
Molecular Weight: 220.2680

The procedure from literature was slightly modified. A 1.6 M solution of *n*-BuLi in hexane (120 mL, 0.19 mol, 1.2 eq) was slowly added to a degassed solution of **1** (43.0 g, 0.16 mol, 1 eq) in dry THF (500 mL) at -78 °C under argon. When the addition was completed, the solution was stirred for 30 min at -78 °C then allowed to warm to 0 °C (over 1 h) and cooled again to -78 °C. Dry DMF (25.0 mL, 0.32 mol, 2 eq) was then added and the resulting mixture allowed to warm to 0 °C (over 1 h). An aqueous 1 M HCl solution (200 mL) was added and the mixture was concentrated. The aqueous layer was extracted twice with DCM. The combined organic layers were washed with water, dried (MgSO<sub>4</sub>), and evaporated to dryness. The crude compound was purified by column chromatography (Silica, DCM/heptane = 1:1), giving compound **2** as colorless crystals.

**Yield:** 22.0 g (63%)

**<sup>1</sup>H NMR (500 MHz, CDCl<sub>3</sub>)** δ 10.03 (s, 1H), 7.89 (d, *J* = 8.5 Hz, 2H), 7.68 (d, *J* = 8.5 Hz, 2H), 5.45 (s, 1H), 3.80 (d, *J* = 11.0 Hz, 2H), 3.67 (d, *J* = 11.0 Hz, 2H), 1.29 (s, 3H), 0.82 (s, 3H)

#### 4-(Benzyloxycarbonyl)benzaldehyde (3) <sup>4</sup>



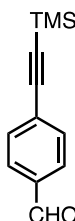
Chemical Formula: C<sub>15</sub>H<sub>12</sub>O<sub>3</sub>  
Exact Mass: 240.0786  
Molecular Weight: 240.2580

The procedure from literature was slightly modified. A solution of 4-formylbenzoic acid (9.00 g, 60.0 mmol, 1 eq) and K<sub>2</sub>CO<sub>3</sub> (16.6 g, 120.0 mmol, 2 eq) in DMF (120 mL) was added benzyl bromide (12.3 g, 72 mmol, 1.2 eq) slowly. After completion of addition, the reaction was stirred at RT for 12 h. Water was added and extracted with EtOAc for 3 times. The combined organic layers were washed with brine and dried over magnesium sulfate and concentrated under reduced pressure. The crude product was purified by column chromatography (Silica, CHCl<sub>3</sub>/heptane = 3:7), giving compound as colorless oil. To keep it stable, the compound was stored under argon atmosphere.

**Yield:** 12.3 g (85%)

**<sup>1</sup>H NMR (500 MHz, CDCl<sub>3</sub>)** δ 10.10 (s, 1H), 8.23 (d, *J* = 8.5 Hz, 2H), 7.95 (d, *J* = 8.5 Hz, 2H), 7.47-7.37 (m, 5H), 5.40 (s, 2H).

#### 4-(Trimethylsilylethynyl)benzaldehyde (**4**)<sup>5</sup>



Chemical Formula: C<sub>12</sub>H<sub>14</sub>OSi  
Exact Mass: 202.0814  
Molecular Weight: 202.3280

The procedure from literature was slightly modified. In a round bottom flask, 4-bromobenzaldehyde (5.55 g, 30.0 mmol, 1 eq), PdCl<sub>2</sub>(PPh<sub>3</sub>)<sub>2</sub> (421 mg, 0.06 mmol, 2 mol%), and CuI (228 mg, 1.20 mmol, 4 mol%) were dissolved in dry THF (30 mL). Et<sub>3</sub>N (6.24 mL, 45.0 mmol, 1.5 eq) and trimethylsilylacetylene (4.47 mL, 31.5 mmol, 1.05 eq) were added and the reaction mixture was stirred overnight under argon at room temperature. When the reaction is completed, the volatiles were removed under reduced pressure. The obtained crude product was purified by column chromatography (silica, heptane), giving compound **4** as colorless powder. To keep it stable, the compound was stored under argon atmosphere.

**Yield:** 6.01 g (99%)

**<sup>1</sup>H NMR (500 MHz, CDCl<sub>3</sub>)** δ 10.00 (s, 1H), 7.81 (d, *J* = 8.5 Hz, 2H), 7.60 (d, *J* = 8.5 Hz, 2H), 0.27 (s, 9H).

## 2. Synthesis of dipyrromethane derivatives as precursors of corroles

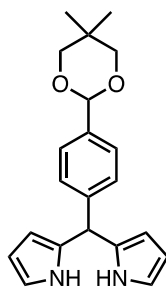
### General procedure for the synthesis of dipyrromethanes<sup>6</sup>

**A:** In an Erlenmeyer were added aldehyde (30.0 mmol) and pyrrole (160 mL, 2.36 mol) and the mixture was degassed by a stream of nitrogen for 10 min. TFA (258  $\mu$ L, 3.0 mmol) was added, and the mixture was stirred for 1 h at room temperature. The mixture was treated with powdered NaOH (4.0 g, 0.10 mol), stirred for 1 h and then filtered on celite. The filtrate was concentrated, and the pyrrole was recovered. Traces of pyrrole were removed by dissolving the oil in DCM and the organic fraction was washed three times with water then evaporated and dried.

**B:** In an Erlenmeyer were added aldehyde (50.0 mmol) and pyrrole (347 mL, 5.00 mol) and the mixture was degassed by a stream of nitrogen for 10 min. MgBr<sub>2</sub> (4.60 g, 25.0 mmol) was added, and the mixture was stirred for 1.5 h at room temperature. The mixture was treated with powdered NaOH (10.0 g, 0.25 mol), stirred for 1 h and then filtered on celite. The filtrate was concentrated, and the pyrrole was recovered. Traces of pyrrole were removed by dissolving the oil in a mixture of ethyl acetate and heptane (400 mL, 1:1) and the volatiles were removed. The solid was then dissolved in DCM and filtered on short plug of silica.

**C:** In an Erlenmeyer were added aldehyde (35.0 mmol) and pyrrole (347 mL, 5.00 mol) and the mixture was degassed by a stream of nitrogen for 10 min. InCl<sub>3</sub> (1.11 g, 5.00 mmol) was added, and the mixture was stirred for 1.5 h at room temperature under argon. The mixture was treated with powdered NaOH (6.00 g, 0.15 mol), stirred for 1 h and then filtered on celite. The filtrate was concentrated, and the pyrrole was recovered. The traces of pyrrole were removed by dissolving the oil in a mixture of ethyl acetate and heptane (400 mL, 1:1) and the volatiles were removed. The solid was then dissolved in DCM and filtered on short plug of silica.

## 5-[4-(5,5-Dimethyl-1,3-dioxan-2-yl)phenyl]dipyrromethane (5)



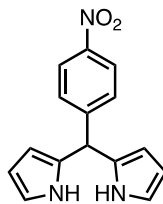
Chemical Formula:  $C_{21}H_{24}N_2O_2$   
Exact Mass: 336.1838  
Molecular Weight: 336.4350

The synthesis of compound **5** was already reported in the literature.<sup>7</sup> However, the procedure used to synthesize compound **5** is based on general procedure for the synthesis of dipyrromethanes (**Method A**). Compound **5** was obtained by using compound **2** (22.0 g, 0.10 mol, 1 eq) and freshly distilled pyrrole (545 mL, 7.86 mol, 78.6 eq). The TFA (985  $\mu$ L, 11.5 mmol, 0.12 eq) was added slowly. After 1 h, powder NaOH (13.0 g, 3.25 mol, 32.5 eq) was added to quench the reaction. The mixture was filtered on celite and the pyrrole was recovered. The crude compound was purified on a silica gel plug with DCM as eluent and further recrystallization from mixture of THF and heptane, giving colorless solid.

**Yield:** 24.0 g (71%)

**<sup>1</sup>H NMR (500 MHz, DMSO-*d*<sub>6</sub>)**  $\delta$  10.54 (s, 2H), 7.33 (d,  $J = 8.5$  Hz, 2H), 7.15 (d,  $J = 8.5$  Hz, 2H), 6.61 (m, 2H), 5.90 (m, 2H), 5.65 (m, 2H), 5.37 (s, 1H), 5.36 (s, 1H), 3.64 (m, 4H), 1.17 (s, 3H), 0.74 (s, 3H).

## 5-(4-Nitrophenyl)dipyrromethane (**6**)<sup>8</sup>



Chemical Formula: C<sub>15</sub>H<sub>13</sub>N<sub>3</sub>O<sub>2</sub>

Exact Mass: 267.1008

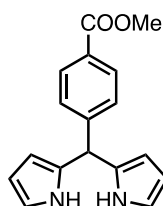
Molecular Weight: 267.2880

The dipyrromethane **6** was obtained according to the procedure described above using general procedure for the synthesis of dipyrromethanes (**Method B**). For the reaction, 4-nitrobenzaldehyde (7.56 g, 50 mmol, 1 eq) and freshly distilled pyrrole (347 mL, 5.00 mol, 100 eq) were used. The further recrystallization gives yellow-brown powder.

**Yield:** 12.0 g (90%)

**<sup>1</sup>H NMR (500 MHz, DMSO-*d*<sub>6</sub>)** δ 10.67 (s, 2H), 8.17 (d, *J* = 8.5 Hz, 2H), 7.41 (d, *J* = 8.5 Hz, 2H), 6.65 (m, 2H), 5.93 (m, 2H), 5.69 (m, 2H), 5.53 (s, 1H).

## 5-(4-Carbomethoxyphenyl)dipyrromethane (7)



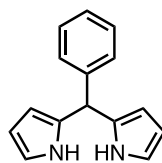
Chemical Formula: C<sub>17</sub>H<sub>16</sub>N<sub>2</sub>O<sub>2</sub>  
Exact Mass: 280.1212  
Molecular Weight: 280.3270

The dipyrromethane **7** was carried out by a modification of the procedure reported by Laha *et al.*<sup>6</sup>, using general procedure for the synthesis of dipyrromethanes (**Method B**). For the reaction, 4-carbomethoxybenzaldehyde (8.21 g, 50 mmol, 1 eq) and freshly distilled pyrrole (347 mL, 5.00 mol, 100 eq) were used. Further recrystallization gives colorless powder.

**Yield:** 22.8 g (81%)

**<sup>1</sup>H NMR (500 MHz, DMSO-*d*<sub>6</sub>)** δ 10.62 (s, 2H), 7.89 (d, *J* = 8.5 Hz, 2H), 7.30 (d, *J* = 8.5 Hz, 2H), 6.63 (m, 2H), 5.93-5.91 (m, 2H), 5.69-5.67 (m, 2H), 5.46 (s, 1H), 3.83 (s, 3H)

## 5-Phenyldipyrromethane (**8**)<sup>6</sup>



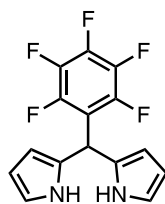
Chemical Formula: C<sub>15</sub>H<sub>14</sub>N<sub>2</sub>  
Exact Mass: 222.1157  
Molecular Weight: 222.2910

The synthesis of dipyrromethane **8** was carried out by a modification of the procedure reported by Laha *et al.*<sup>6</sup>, using general procedure for the synthesis of dipyrromethanes (**Method B**). For the reaction, benzaldehyde (5.31 g, 50 mmol, 1 eq) and freshly distilled pyrrole (347 mL, 5.00 mol, 100 eq) were used. Further recrystallization gives white powder.

**Yield:** 18.8 g (85%)

**<sup>1</sup>H NMR (500 MHz, DMSO-*d*<sub>6</sub>)** δ 10.56 (s, 2H), 7.30-7.17 (m, 5H), 6.61 (m, 2H), 5.91 (m, 2H), 5.67 (m, 2H), 5.35 (s, 1H)

## 5-(Pentafluorophenyl)dipyrromethane (**9**)<sup>6</sup>



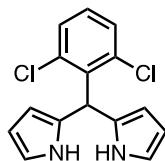
Chemical Formula: C<sub>15</sub>H<sub>9</sub>F<sub>5</sub>N<sub>2</sub>  
Exact Mass: 312.0686  
Molecular Weight: 312.2430

The synthesis of dipyrromethane **9** was carried out by a modification of the procedure reported by Laha *et al.*<sup>6</sup>, using general procedure for the synthesis of dipyrromethanes (**Method B**). For the reaction, pentafluorobenzaldehyde (9.80 g, 50 mmol, 1 eq) and freshly distilled pyrrole (347 mL, 5.00 mol, 100 eq) were used. Further recrystallization gives colorless powder.

**Yield:** 15.0 g (96%)

**<sup>1</sup>H NMR (500 MHz, DMSO-*d*<sub>6</sub>)** δ 10.69 (s, 2H), 6.64 (m, 2H), 5.93 (m, 2H), 5.79 (m, 2H), 5.77 (s, 1H).

## 5-(2,6-Dichlorophenyl)dipyrromethane (**10**)<sup>9</sup>



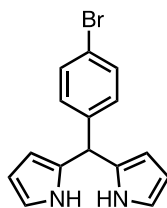
Chemical Formula: C<sub>15</sub>H<sub>12</sub>Cl<sub>2</sub>N<sub>2</sub>  
Exact Mass: 290.0378  
Molecular Weight: 291.1750

Dipyrromethane **10** was obtained according to the procedure described above using general procedure for the synthesis of dipyrromethanes (**Method B**). For the reaction, 2,6-dichlorobenzaldehyde (8.75 g, 50 mmol, 1 eq) and freshly distilled pyrrole (347 mL, 5.00 mol, 100 eq) were used. Further recrystallization gives colorless powder.

**Yield:** 13.8 g (95%)

**<sup>1</sup>H NMR (500 MHz, DMSO-*d*<sub>6</sub>)** δ 10.48 (s, 2H), 7.41 (m, 2H), 7.26 (m, 1H), 6.60 (m, 2H), 6.21 (s, 1H), 5.89 (m, 2H), 5.68 (s, 1H).

## 5-(4-Bromophenyl)dipyrromethane (**11**)<sup>10</sup>



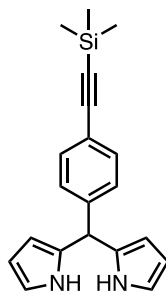
Chemical Formula: C<sub>15</sub>H<sub>13</sub>BrN<sub>2</sub>  
Exact Mass: 300.0262  
Molecular Weight: 301.1870

Dipyrromethane **11** was obtained according to the procedure described above using general procedure for the synthesis of dipyrromethanes (**Method B**). For the reaction, 4-bromobenzaldehyde (9.25 g, 50 mmol, 1 eq) and freshly distilled pyrrole (347 mL, 5.00 mol, 100 eq) were used. Further recrystallization gives colorless powder.

**Yield:** 14.5 g (96%)

**<sup>1</sup>H NMR (500 MHz, DMSO-*d*<sub>6</sub>)**  $\delta$  10.57 (s, 2H), 7.46 (d, *J* = 8.5 Hz, 2H), 7.10 (d, *J* = 8.5 Hz, 2H), 6.61 (m, 2H), 5.89 (m, 2H), 5.64 (m, 2H), 5.34 (s, 1H).

## 5-(4-(Trimethylsilylethynyl)phenyl)dipyrromethane (**12**)<sup>11</sup>



Chemical Formula: C<sub>20</sub>H<sub>22</sub>N<sub>2</sub>Si

Exact Mass: 318.1552

Molecular Weight: 318.4950

Dipyrromethane **12** was obtained according to the procedure described above using general procedure for the synthesis of dipyrromethanes (**Method C**). For the reaction, compound **4** (10.1 g, 50 mmol, 1 eq) and freshly distilled pyrrole (495 mL, 7.14 mol, 143 eq) were used. Further recrystallization gives colorless powder.

**Yield:** 13.9 g (87%)

**<sup>1</sup>H NMR (400 MHz, DMSO-*d*<sub>6</sub>)** δ 10.57 (s, 2H), 7.36 (d, *J* = 8.5 Hz, 2H), 7.13 (d, *J* = 8.5 Hz, 2H), 6.61 (m, 2H), 5.89 (m, 2H), 5.63 (m, 2H), 5.37 (s, 1H), 0.22 (s, 9H).

### 3. Synthesis of corroles

#### General procedure A: synthesis of corroles from dipyrromethane<sup>12</sup>

Dipyrromethane (10.0 mmol, 1 eq) and aldehyde (5.0 mmol, 0.5 eq) were dissolved in 500 mL of methanol. Then, a solution of HCl (36%, 25.0 mL) in H<sub>2</sub>O (500 mL) was added, and the reaction mixture was stirred at room temperature for 2 hours. The mixture was extracted with chloroform and the organic phase was washed three times with water, dried and completed to 1.50 L. *p*-Chloranil (1.5 eq) was added and the reaction mixture was stirred overnight at room temperature protected from light and the solution was evaporated. The resulted compound was purified by column with DCM as eluent. Then the crude compound was recrystallized with THF and heptane to afford crystal power. The solid was filtered and dried by vacuum.

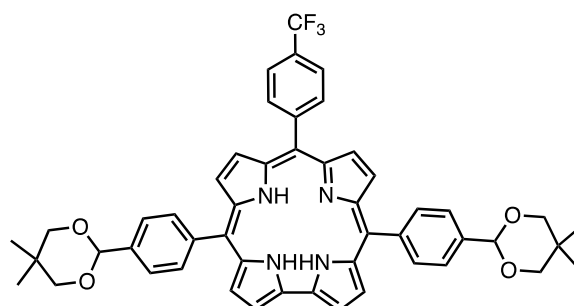
#### General procedure B: one pot synthesis of A<sub>3</sub> free-base corrole<sup>12</sup>

To a solution of aldehyde (1 eq, 20 mmol) in methanol (400 mL) in an erlenmeyer was added pyrrole (2 eq). Then an aqueous solution of hydrochloric acid was added (8.50 mL of concentrated HCl in 400 mL of distilled water). The mixture was protected from light and stirred during 3 hours. The solution was diluted with chloroform (300 mL). The organic phase was washed twice with water, dried over magnesium sulfate and completed to 1200 mL with chloroform. *p*-Chloranil was added (1 eq, 20 mmol) and the reaction mixture was stirred, protected from light, during overnight at room temperature and the solution was evaporated.

#### General procedure C: synthesis of carboxylic acid corroles by saponification<sup>13</sup>

According to the procedure reported by Yadav *et al.*, a modification was conducted for our experiments. For the saponification of corrole with mono-carboxymethyl, corrole (1 mmol, 1 eq) and NaOH (30 mmol, 30 eq) were added into the mixture of EtOH (95 mL) and H<sub>2</sub>O (5 mL) under argon. The mixture was stirred and heated to reflux for 12 h. The reaction was monitored by mass spectrometry. After cooling, the mixture was acidified by 1M HCl solution monitored by pH. Until no precipitate appears, the crude compound was collected by centrifugation, washed with H<sub>2</sub>O and dried under vacuum, giving pure compound. For the other corroles containing two or three carboxymethyl functions, the amount of NaOH were adjusted to 60 eq or 90 eq.

**5,15-Di(4-(5,5-dimethyl-1,3-dioxacyclohex-2-yl)phenyl)-10(4-trifluoromethylphenyl)corrole (13)**

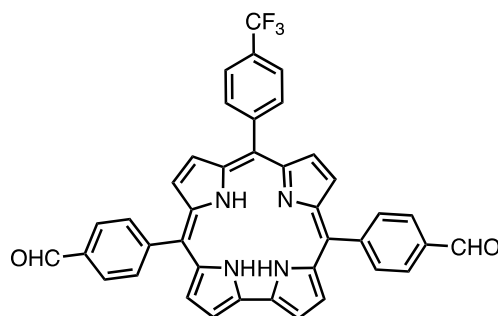


Chemical Formula:  $C_{50}H_{45}F_3N_4O_4$   
Exact Mass: 822.3393  
Molecular Weight: 822.9292

The synthesis of 5,15-di(4-(5,5-dimethyl-1,3-dioxacyclohex-2-yl)phenyl)-10(4-trifluoromethyl)corrole was based on the general procedure **A**. The **13** is not described. For the reaction, dipyrromethane **5** (3.36 g, 10.0 mmol, 1 eq) and 4-trifluoromethylbenzaldehyde (871 mg, 5.0 mmol, 0.5 eq) were used. The collected residue after purification gives a mixture of targeted corrole **13** and sides products (corroles partially and/or totally deprotected). The mixture (212 mg) was directly used for next step.

General procedure **B** was also conducted for corrole **13** but the reaction didn't work.

## 5,15-Di(4-formylphenyl)-10(4-trifluoromethylphenyl)corrole (14)



Chemical Formula:  $C_{40}H_{25}F_3N_4O_2$   
Exact Mass: 650.1930  
Molecular Weight: 650.6612

The corrole **14** is not described. The previously isolated mixture of corrole **13** and partially and/or totally deprotected corroles (212 mg) was dissolved in the mixture of THF (20 mL), H<sub>2</sub>O (20 mL) and TFA (20 mL) under argon. The mixture was heated at 70°C for 2 h. The reaction was monitored by mass spectrometry. After cooling, the mixture was diluted by H<sub>2</sub>O, extracted with DCM. The organic layer was washed by NaHCO<sub>3</sub> solution and dried by Na<sub>2</sub>SO<sub>4</sub>. The crude compound was purified by column chromatography with DCM as eluent, further recrystallized from THF/heptane, giving purple powder.

**Yield:** 183 mg (5.6%) (calculated from 4-trifluoromethylbenzaldehyde)

**<sup>1</sup>H NMR (500 MHz, DMSO-*d*<sub>6</sub>, 10 μL Hydrazine, imine form was observed)** δ 8.92 (d, *J* = 4.0 Hz, 2H), 8.67 (d, *J* = 4.5 Hz, 2H), 8.52 (d, *J* = 4.0 Hz, 2H), 8.31 (d, *J* = 8.0 Hz, 2H), 8.26 (d, *J* = 4.5 Hz, 2H), 8.22 (d, *J* = 8.0 Hz, 4H), 8.06 (d, *J* = 8.5 Hz, 2H), 8.00 (s, 2H), 7.89 (d, *J* = 8.0 Hz, 4H).

**<sup>13</sup>C NMR (125 MHz, DMSO-*d*<sub>6</sub>, 10 μL Hydrazine, imine form was observed)** δ 164.5, 149.3, 141.2, 140.4, 139.9, 138.9, 136.1, 135.1, 134.9, 134.2, 132.1, 126.2, 125.5, 124.7, 123.9, 123.5, 121.5, 114.9, 113.6, 105.1.

**<sup>19</sup>F NMR (470 MHz, DMSO-*d*<sub>6</sub>, 10 μL Hydrazine)** δ -60.15 (s, 3F).

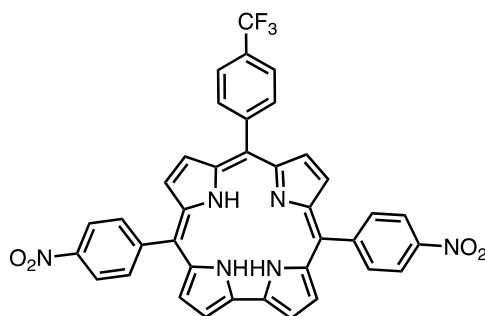
**MS (MALDI-TOF):** *m/z* = 651.062 [M+H]<sup>+</sup>, 651.201 calcd for C<sub>40</sub>H<sub>26</sub>F<sub>3</sub>N<sub>4</sub>O<sub>2</sub>.

**HR-MS (ESI):** *m/z* = 651.2002 [M+H]<sup>+</sup>, 651.2002 calcd for C<sub>40</sub>H<sub>26</sub>F<sub>3</sub>N<sub>4</sub>O<sub>2</sub>.

**UV-vis (DCM):** λ<sub>max</sub> (nm) (ε × 10<sup>-3</sup> L mol<sup>-1</sup> cm<sup>-1</sup>) 433 (88.0), 587 (18.1), 628 (14.6), 661 (10.1), 700 (2.1).

**FTIR (KBr, cm<sup>-1</sup>):** 1699 (C=O aldehyde).

## 5,15-di(4-nitrophenyl)-10(4-trifluoromethylphenyl)corrole (**15**)<sup>14</sup>



Chemical Formula: C<sub>38</sub>H<sub>23</sub>F<sub>3</sub>N<sub>6</sub>O<sub>4</sub>  
Exact Mass: 684.1733  
Molecular Weight: 684.6352

Corrole **15** was synthesized according to general procedure **A**. The corrole **15** is described.<sup>14</sup> For the reaction, dipyrromethane **6** (2.67 g, 10.0 mmol, 1 eq) and 4-trifluoromethylbenzaldehyde (870 mg, 5.0 mmol, 0.5 eq) were used. The residue was purified and recrystallized, giving purple crystals.

Yield: 1.30 g (38%)

<sup>1</sup>H NMR (500 MHz, DMSO-*d*<sub>6</sub>, 10 μL Hydrazine) δ 9.04 (d, *J* = 4.0 Hz, 2H), 8.70 (d, *J* = 4.5 Hz, 2H), 8.63 (d, *J* = 8.5 Hz, 4H), 8.59 (d, *J* = 4.0 Hz, 2H), 8.50 (d, *J* = 8.5 Hz, 4H), 8.32 (d, *J* = 4.5 Hz, 2H), 8.28 (d, *J* = 8.0 Hz, 2H), 8.05 (d, *J* = 8.0 Hz, 2H).

<sup>13</sup>C NMR (125 MHz, DMSO-*d*<sub>6</sub>, 10 μL Hydrazine) δ 149.4, 148.9, 145.8, 140.3, 140.3, 136.2, 135.7, 135.1, 132.7, 127.2, 125.3, 125.2, 124.2, 123.8, 123.1, 122.3, 116.6, 111.4, 107.7.

<sup>19</sup>F NMR (470 MHz, DMSO-*d*<sub>6</sub>, 10 μL Hydrazine) δ -60.25 (s, 3F).

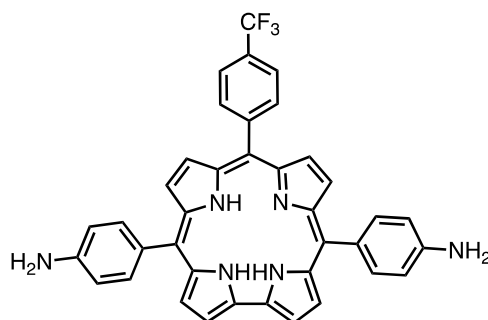
MS (MALDI-TOF): *m/z* = 683.87 [M]<sup>+</sup>, 684.17 calcd for C<sub>38</sub>H<sub>23</sub>F<sub>3</sub>N<sub>6</sub>O<sub>4</sub>.

HR-MS (ESI): *m/z* = 685.1810 [M+H]<sup>+</sup>, 685.1806 calcd for C<sub>38</sub>H<sub>24</sub>F<sub>3</sub>N<sub>6</sub>O<sub>4</sub>.

UV-vis (DCM): λ<sub>max</sub> (nm) (ε × 10<sup>-3</sup> L mol<sup>-1</sup> cm<sup>-1</sup>) 440.5 (97.2); 596.5 (32.4); 640.5 (29.3).

Elementary analysis (%): calculated for C<sub>38</sub>H<sub>23</sub>F<sub>3</sub>N<sub>6</sub>O<sub>4</sub>·0.3H<sub>2</sub>O: C 66.19, H 3.60, N 12.19; found: C 66.05, H 2.92, N 11.98.

## 5,15-Di(4-aminophenyl)-10(4-trifluoromethylphenyl)corrole (16)



Chemical Formula: C<sub>38</sub>H<sub>27</sub>F<sub>3</sub>N<sub>6</sub>  
Exact Mass: 624.2249  
Molecular Weight: 624.6712

Reduction of nitrocorrole **15** was carried out *via* a small modification of the procedure reported by Gros et al.<sup>15</sup> 266 mg of Pd/C (10%) was activated through heating and vacuum. After cooling, a solution of corrole **15** (1.03 g, 1.5 mmol, 1 eq) in dry THF (250 mL) was added to the former flask under argon and dry triethylamine (900  $\mu$ L) was followed. The flask was charged with dihydrogen to remove the argon and fill the flask. The mixture was stirred under dihydrogen for 12 h and reaction was stopped until all nitrocorrole was reduced to aminocorrole **16**. The mixture was filtered on Celite and evaporated to remove solvent. The crude compound was purified on flash chromatography (Silica, DCM/TEA = 100:1), giving purple solid. Corrole **16** was kept under argon atmosphere and stored in the fridge.

**Yield:** 0.80 g (89%)

**<sup>1</sup>H NMR (500 MHz, DMSO-*d*<sub>6</sub>, 10  $\mu$ L Hydrazine)**  $\delta$  8.78 (d, *J* = 4.0 Hz, 2H), 8.59 (d, *J* = 4.5 Hz, 2H), 8.41 (d, *J* = 4.0 Hz, 2H), 8.25 (d, *J* = 8.0 Hz, 2H), 8.14 (d, *J* = 4.5 Hz, 2H), 8.02 (d, *J* = 8.0 Hz, 2H), 7.88 (d, *J* = 8.0 Hz, 4H), 6.99 (d, *J* = 8.0 Hz, 4H).

**<sup>13</sup>C NMR (125 MHz, DMSO-*d*<sub>6</sub>, 10  $\mu$ L Hydrazine)**  $\delta$  149.7, 147.5, 140.8, 140.1, 136.5, 135.4, 135.3, 132.0, 129.9, 126.4, 126.1, 123.6, 123.6, 123.2, 121.3, 115.4, 114.0, 113.9, 103.7.

**<sup>19</sup>F NMR (470 MHz, DMSO-*d*<sub>6</sub>, 10  $\mu$ L Hydrazine)**  $\delta$  -60.12 (s, 3F).

**MS (MALDI-TOF):** *m/z* = 624.21 [M]<sup>+</sup>, 624.22 calcd for C<sub>38</sub>H<sub>27</sub>F<sub>3</sub>N<sub>6</sub>.

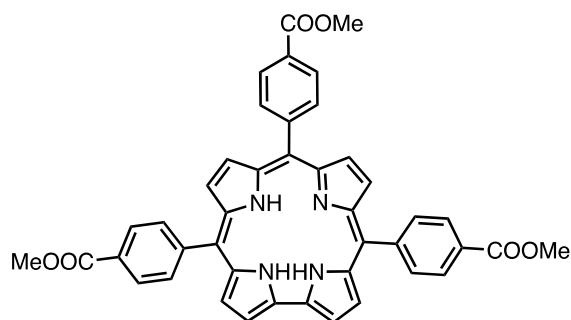
**HR-MS (ESI):** *m/z* = 625.2320 [M+H]<sup>+</sup>, 625.2322 calcd for C<sub>38</sub>H<sub>28</sub>F<sub>3</sub>N<sub>6</sub>.

**UV-vis (DCM):**  $\lambda_{\text{max}}$  (nm) ( $\epsilon \times 10^{-3}$  L mol<sup>-1</sup> cm<sup>-1</sup>) 433 (67.7), 557 (8.0), 629 (11.5), 663 (12.9), 720 (13.4).

**Elementary analysis (%):** calculated for C<sub>38</sub>H<sub>27</sub>F<sub>3</sub>N<sub>6</sub> · 0.5 H<sub>2</sub>O: C 71.31, H 4.43, N 13.10; found: C 71.84, H 4.32, N 12.94.

**FTIR (cm<sup>-1</sup>):** 3368 (N-H).

## 5,10,15-Tris(4-carboxymethylphenyl)corrole (**17**)<sup>16</sup>



Chemical Formula: C<sub>43</sub>H<sub>32</sub>N<sub>4</sub>O<sub>6</sub>  
Exact Mass: 700.2322  
Molecular Weight: 700.7510

Corrole **17** was synthesized according to described procedures above.

**General procedure A:** Dipyrromethane **7** (2.08 g, 10 mmol, 1 eq) and 4-carboxymethyl benzaldehyde (820 mg, 5 mmol, 0.5 eq) were used in the reaction. The residue was purified and recrystallized, giving purple solid.

**Yield:** 230 mg (7%)

**General procedure B:** 4-carboxymethylbenzaldehyde (6.56 g, 40 mmol, 1 eq) and freshly distilled pyrrole (5.60 mL, 80 mmol, 2 eq) were used in the reaction. The crude compound was purified by column chromatography (Silica, DCM:AcOEt = 99:1) and recrystallized from THF/heptane, giving purple solid. The corrole **17** is described.<sup>16</sup>

**Yield:** 1.06 g (13%)

**<sup>1</sup>H NMR (500 MHz, DMSO-*d*<sub>6</sub>, 10  $\mu$ L Hydrazine)**  $\delta$  8.98 (d, *J* = 4.0 Hz, 2H), 8.67 (d, *J* = 4.5 Hz, 2H), 8.55 (d, *J* = 4.0 Hz, 2H), 8.39 (m, 8H), 8.34-8.31 (m, 4H), 8.24 (m, 2H), 4.02 (s, 9H).

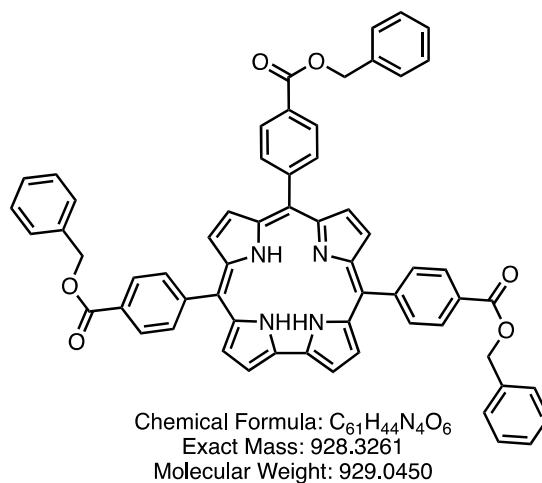
**MS (MALDI-TOF):** *m/z* = 701.486 [M+H]<sup>+</sup>, 701.240 calcd for C<sub>43</sub>H<sub>33</sub>N<sub>4</sub>O<sub>6</sub>.

**HR-MS (ESI):** *m/z* = 701.2396 [M+H]<sup>+</sup>, 701.2395 calcd for C<sub>43</sub>H<sub>33</sub>N<sub>4</sub>O<sub>6</sub>.

**UV-vis (DCM):**  $\lambda_{\max}$  (nm) ( $\epsilon \times 10^{-3}$  L mol<sup>-1</sup> cm<sup>-1</sup>) 426 (52.1), 580 (9.6), 625 (7.5), 659 (5.6), 718 (2.2).

**FTIR (KBr, cm<sup>-1</sup>):** 1718 (C=O ester).

## 5,10,15-Tris(4-(benzyloxycarbonyl)phenyl)corrole (18)



The corrole **18** is not described. Corrole **18** was synthesized according to the described general procedure **B**. For the reaction, aldehyde **3** (9.60 g, 40.0 mmol, 1 eq) and freshly distilled pyrrole (5.36 g, 80.0 mmol, 2 eq) were used. The collected crude compound was purified by short plug (silica, DCM) and recrystallized from THF/MeOH, giving purple crystals.

**Yield:** 2.18 g (18%)

**$^1H$  NMR (500 MHz, DMSO- $d_6$ , 10  $\mu$ L Hydrazine)**  $\delta$  8.90 (d,  $J$  = 4.0 Hz, 2H), 8.65 (d,  $J$  = 4.5 Hz, 2H), 8.53 (d,  $J$  = 4.0 Hz, 2H), 8.39 (m, 8H), 8.34-8.31 (m, 4H), 8.23 (d,  $J$  = 8.0 Hz, 2H), 7.59 (d,  $J$  = 7.5 Hz, 6H), 7.47 (t,  $J$  = 7.5 Hz, 6H), 7.42-7.39 (m, 3H), 5.50 (s, 6H).

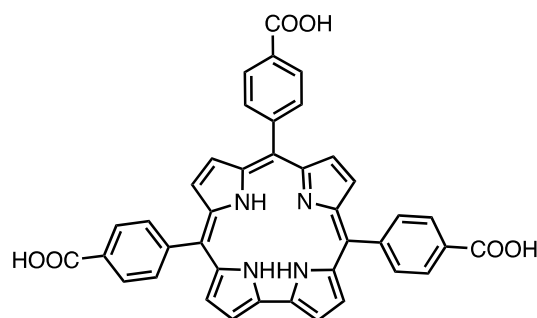
**MS (MALDI-TOF):**  $m/z$  928.15  $[M]^+$ , 928.32 calcd for  $C_{61}H_{44}N_4O_6$ .

**HR-MS (ESI):**  $m/z$  929.3331  $[M+H]^+$ , 929.3334 calcd for  $C_{61}H_{45}N_4O_6$ .

**UV-vis (DCM):**  $\lambda_{max}$  (nm) ( $\epsilon \times 10^{-3}$  L mol $^{-1}$  cm $^{-1}$ ) 428 (106.4), 585 (18.3), 622 (14.7), 660 (10.2).

**FTIR (KBr, cm $^{-1}$ ):** 1718 (C=O ester).

## 5,10,15-tris(4-carboxylphenyl)corrole (**19**)<sup>16</sup>



Chemical Formula: C<sub>40</sub>H<sub>26</sub>N<sub>4</sub>O<sub>6</sub>  
Exact Mass: 658.1852  
Molecular Weight: 658.6700

To obtain reported corrole **19**, two strategies were designed and carried out.

### A. Saponification of carboxymethyl corrole **17**

According to general procedure **C**. Corrole **17** (1.28 g, 1.83 mmol, 1 eq) and NaOH (6.58 g, 164 mmol, 90 eq) were used in the reaction along with EtOH (190 mL) and H<sub>2</sub>O (10 mL).

**Yield:** 1.07 g (89%)

### B. Hydrogenation of benzyloxycarbonyl corrole **18**

500 mg of Pd/C (10%) was activated through heating under vacuum. After cooling, a solution of corrole **18** (1.60 g, 1.72 mmol) in a mixture of dry THF (125 mL) and MeOH (125 mL) was added to the former flask under argon. The flask was charged with dihydrogen to remove the argon and fill the flask. The mixture was stirred under dihydrogen for 2 h and reaction was monitored by mass spectrum. The mixture was filtered on Celite and evaporated to remove solvent. The crude compound was collected and recrystallized from THF/MeOH/heptane, giving purple solid.

**Yield:** 1.13 g (99%)

**<sup>1</sup>H NMR (500 MHz, DMSO-*d*<sub>6</sub>, 10 μL Hydrazine)** δ 8.90 (d, *J* = 4.0 Hz, 2H), 8.63 (d, *J* = 4.5 Hz, 2H), 8.49 (d, *J* = 4.0 Hz, 2H), 8.30-8.27 (m, 6H), 8.21-8.18 (m, 6H), 8.02 (d, *J* = 8.0 Hz, 2H).

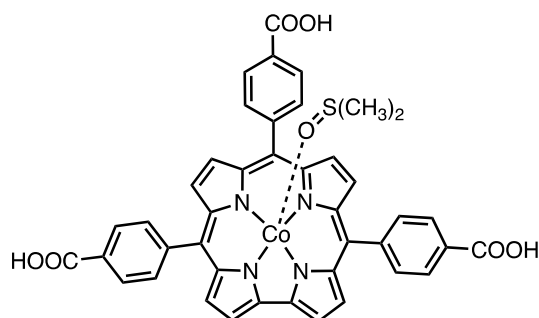
**MS (MALDI-TOF):** *m/z* 659.20 [M+H]<sup>+</sup>, 659.19 calcd for C<sub>40</sub>H<sub>27</sub>N<sub>4</sub>O<sub>6</sub>.

**HR-MS (ESI):** *m/z* 659.1918 [M+H]<sup>+</sup>, 659.1925 calcd for C<sub>40</sub>H<sub>27</sub>N<sub>4</sub>O<sub>6</sub>.

**UV-vis (DCM):** λ<sub>max</sub> (nm) (ε × 10<sup>-3</sup> L mol<sup>-1</sup> cm<sup>-1</sup>) 428 (105.6), 585 (17.3), 623 (14.4), 660 (11.1), 700 (6.9) nm

**FTIR (KBr, cm<sup>-1</sup>):** 2998 (broad peak, OH carboxyl), 1672 (C=O carboxyl).

## Dimethylsulfoxide [5,10,15-tris(4-carboxylphenyl)corrolato]-cobalt(III) (**20**)



Chemical Formula:  $C_{42}H_{29}CoN_4O_7S$   
Exact Mass: 792.1089  
Molecular Weight: 792.7082

The corrole **20** is not described. In a round bottom flask, a solution of corrole **19** (105 mg, 0.16 mmol, 1 eq) and cobalt acetylacetonate (43.7 mg, 0.17 mmol, 1.05 eq) in dimethylsulfoxide was degassed with argon. The mixture was heated at 80°C for 40 min under argon and the reaction was monitored by mass spectrometry. After cooling, the mixture was poured into degassed water and diluted HCl solution (0.1M) was added to precipitate the cobalt complex. The corrole complex was collected by centrifugation and washed with water 2 times, dried under vacuum, giving pure compound.

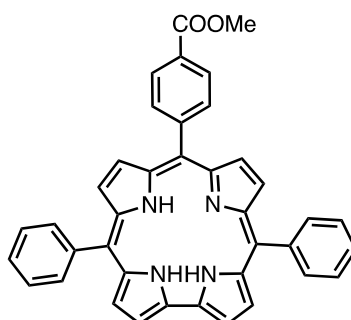
**Yield:** 99 mg (78%)

**$^1H$  NMR (500 MHz, MeOD- $d_4$ , 10  $\mu$ L Hydrazine)**  $\delta$  9.27 (d,  $J$  = 4.5 Hz, 2H), 9.03 (d,  $J$  = 4.0 Hz, 2H), 8.84 (d,  $J$  = 4.5 Hz, 2H), 8.82 (d,  $J$  = 4.0 Hz, 2H), 8.39-8.33 (m, 10H), 8.29-8.27 (m, 2H), 2.68 (s, 6H).

**$^{13}C$  NMR (125 MHz, MeOD- $d_4$ , 10  $\mu$ L Hydrazine)**  $\delta$  175.7, 146.9, 145.5, 142.9, 141.5, 140.0, 137.2, 135.3, 135.2, 132.8, 131.0, 129.1, 128.8, 128.1, 124.9, 117.4, 115.7, 108.8, 40.4.

**FTIR (KBr,  $cm^{-1}$ ):** 3068 (broad peak, OH carboxyl), 1699 (C=O carboxyl), 1014 (S=O DMSO).

## 5,15-Diphenyl-10-(4-carboxymethylphenyl)corrole (**21**)<sup>17</sup>



Chemical Formula: C<sub>39</sub>H<sub>28</sub>N<sub>4</sub>O<sub>2</sub>  
Exact Mass: 584.2212  
Molecular Weight: 584.6790

The corrole **21** is described.<sup>17</sup> Corrole **21** was synthesized according to the described general procedure **A** above. For the reaction, dipyrromethane **8** (2.22 g, 10.0 mmol, 1 eq) and 4-carboxymethylbenzaldehyde (821 mg, 5.0 mmol, 0.5 eq) were used. The crude compound was collected and recrystallized, giving purple powder.

**Yield:** 1.23 g (42%)

**<sup>1</sup>H NMR (500 MHz, CDCl<sub>3</sub>, 10 μL Hydrazine)** δ 8.88 (d, *J* = 4.0 Hz, 2H), 8.84 (d, *J* = 5.0 Hz, 2H), 8.52 (d, *J* = 4.0 Hz, 2H), 8.46 (d, *J* = 5.0 Hz, 2H), 8.40 (d, *J* = 8.0 Hz, 2H), 8.33-8.32 (m, 4H), 8.23 (d, *J* = 8.5 Hz, 2H), 7.78 (t, *J* = 7.5 Hz, 4H), 7.64 (t, *J* = 7.5 Hz, 2H), 4.07 (s, 3H).

**<sup>13</sup>C NMR (125 MHz, CDCl<sub>3</sub>, 10 μL Hydrazine)** δ 167.6, 147.4, 141.1, 139.9, 139.7, 136.1, 135.2, 135.0, 131.6, 128.5, 128.1, 127.6, 127.6, 125.6, 122.6, 116.3, 115.9, 108.6, 52.4.

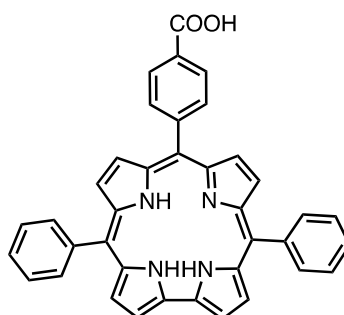
**MS (MALDI-TOF):** *m/z* = 584.834 [M]<sup>+</sup>, 584.22 calcd for C<sub>39</sub>H<sub>28</sub>N<sub>4</sub>O<sub>2</sub>.

**HR-MS (ESI):** *m/z* = 585.2286 [M+H]<sup>+</sup>, 585.2285 calcd for C<sub>39</sub>H<sub>29</sub>N<sub>4</sub>O<sub>2</sub>.

**UV-vis (DCM):** λ<sub>max</sub> (nm) (ε × 10<sup>-3</sup> L mol<sup>-1</sup> cm<sup>-1</sup>) 415 (113.6), 434 (86.3), 576 (17.7), 614 (13.2), 650 (8.6).

**FTIR (KBr, cm<sup>-1</sup>):** 1704 (C=O ester),

## 5,15-Diphenyl-10-(4-carboxylphenyl)corrole (**22**)<sup>17</sup>



Chemical Formula: C<sub>38</sub>H<sub>26</sub>N<sub>4</sub>O<sub>2</sub>  
Exact Mass: 570.2056  
Molecular Weight: 570.6520

The corrole **22** is described.<sup>17</sup> Corrole **22** was obtained according to the described general procedure **C** above. For the reaction, corrole **21** (750 mg, 1.28 mmol, 1 eq) and NaOH (1.54 g, 38.4 mmol, 30 eq) were used. The crude compound was collected and recrystallized, giving purple solid.

**Yield:** 651 mg (89%)

**<sup>1</sup>H NMR (500 MHz, DMSO-*d*<sub>6</sub>, 10 μL Hydrazine)** δ 8.91 (d, *J* = 4.0 Hz, 2H), 8.62 (d, *J* = 4.5 Hz, 2H), 8.48 (d, *J* = 4.0 Hz, 2H), 8.31 (d, *J* = 4.5 Hz, 2H), 8.27 (d, *J* = 8.0 Hz, 4H), 8.25 (d, *J* = 8.0 Hz, 2H), 8.05 (d, *J* = 8.0 Hz, 2H), 7.79 (t, *J* = 7.5 Hz, 4H), 7.64 (t, *J* = 7.5 Hz, 2H).

**<sup>13</sup>C NMR (125 MHz, DMSO-*d*<sub>6</sub>, 10 μL Hydrazine)** δ 171.3, 146.0, 142.1, 140.8, 139.9, 136.2, 135.9, 134.5, 133.7, 131.7, 127.5, 127.3, 125.9, 125.0, 124.3, 121.0, 114.5, 113.2, 106.6.

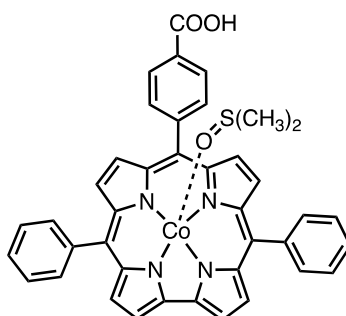
**MS (MALDI-TOF):** *m/z* = 570.86 [M]<sup>+</sup>, 570.21 calcd for C<sub>38</sub>H<sub>26</sub>N<sub>4</sub>O<sub>2</sub>.

**HR-MS (ESI):** *m/z* = 571.2129 [M+H]<sup>+</sup>, 571.2129 calcd for C<sub>38</sub>H<sub>27</sub>N<sub>4</sub>O<sub>2</sub>.

**UV-vis (DCM):** λ<sub>max</sub> (nm) (ε × 10<sup>-3</sup> L mol<sup>-1</sup> cm<sup>-1</sup>) 428 (81.7), 463 (42.0), 557 (7.4), 583 (7.4), 652 (11.5), 691 (16.9).

**FTIR (KBr, cm<sup>-1</sup>):** 3018 (broad peak, OH carboxyl), 1673 (C=O carboxyl).

## Dimethylsulfoxide [5,15-diphenyl-10-(4-carboxylphenyl)corrolato]-cobalt(III)(23)



Chemical Formula:  $C_{40}H_{29}CoN_4O_3S$   
Exact Mass: 704.1292  
Molecular Weight: 704.6902

In a round bottom flask, a solution of corrole **22** (200 mg, 0.35 mmol, 1 eq) and cobalt acetylacetonate (95.1 mg, 0.37 mmol, 1.05 eq) in dimethylsulfoxide (100 mL) was degassed with argon. The mixture was heated at 80°C for 40 min under argon and the reaction was monitored by mass spectrometry. After cooling, the mixture was poured into ice water and HCl solution (1M) was added to let the product precipitate, followed by addition of saturated NaCl solution. The corrole complex was collected by centrifugation and washed with water 2 times, then dried under vacuum, to give pure compound.

**Yield:** 215 mg (87%)

**$^1H$  NMR (500 MHz, MeOD- $d_4$ , 10  $\mu$ L Hydrazine)**  $\delta$  9.11 (d,  $J$  = 4.0 Hz, 2H), 8.94 (d,  $J$  = 4.5 Hz, 2H), 8.78 (d,  $J$  = 4.5 Hz, 2H), 8.70 (d,  $J$  = 4.0 Hz, 2H), 8.35 (d,  $J$  = 8.0 Hz, 2H), 8.26 (d,  $J$  = 8.0 Hz, 4H), 8.23 (d,  $J$  = 8.0 Hz, 2H), 7.79 (t,  $J$  = 8.0 Hz, 4H), 7.72 (t,  $J$  = 8.0 Hz, 2H), 2.67 (s, 6H), -3.49 (s, 4H).

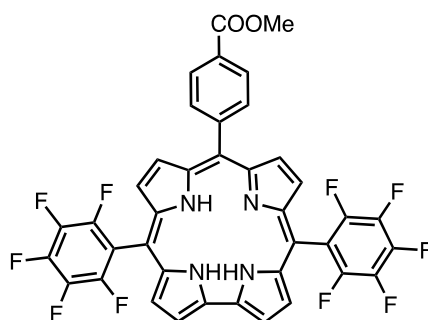
**MS (MALDI-TOF):**  $m/z$  = 626.19 [M-DMSO] $^+$ , 626.11 calcd for  $C_{38}H_{23}CoN_4O_2$ .

**HR-MS (ESI):**  $m/z$  = 626.1146 [M-DMSO] $^+$ , 626.1148 calcd for  $C_{38}H_{23}CoN_4O_2$ .

**UV-vis (DCM):**  $\lambda_{max}$  (nm) ( $\epsilon \times 10^{-3}$  L mol $^{-1}$  cm $^{-1}$ ) 389 (45.8), 568 (8.7).

**FTIR (KBr, cm $^{-1}$ ):** 2996 (broad peak, OH carboxyl), 1700 (C=O carboxyl), 1010 (S=O DMSO).

## 5,15-Dipentafluorophenyl-10-(4-carboxymethylphenyl)corrole (**24**)<sup>18</sup>



Chemical Formula: C<sub>39</sub>H<sub>18</sub>F<sub>10</sub>N<sub>4</sub>O<sub>2</sub>  
Exact Mass: 764.1270  
Molecular Weight: 764.5830

Corrole **24** was obtained according to general procedure **A** described above. For the reaction, dipyrromethane **9** (3.12 g, 10 mmol, 1 eq) and 4-carboxymethylbenzaldehyde (821 mg, 5 mmol, 0.5 eq) were used. The crude compound was collected and recrystallized, giving purple solid.

**Yield:** 550 mg (14%)

**<sup>1</sup>H NMR (500 MHz, CDCl<sub>3</sub>)** δ 9.10 (d, *J* = 4.0 Hz, 2H), 8.74 (d, *J* = 4.5 Hz, 2H), 8.66 (d, *J* = 4.5 Hz, 2H), 8.58 (d, *J* = 4.0 Hz, 2H), 8.37 (d, *J* = 8.0 Hz, 2H), 8.25 (d, *J* = 8.0 Hz, 2H), 4.02 (s, 3H).

**<sup>13</sup>C NMR (125 MHz, DMSO-*d*<sub>6</sub>)** δ 167.3, 147.2, 146.3, 145.2, 143.0, 140.9, 139.0, 138.9, 137.1, 137.0, 134.8, 129.6, 128.6, 127.6, 126.0, 117.7, 114.1, 112.4, 77.2, 52.5.

**<sup>19</sup>F NMR (470 MHz, DMSO-*d*<sub>6</sub>)** δ -137.83 (m, 4F), -152.63 (m, 2F), -161.66 (m, 4F).

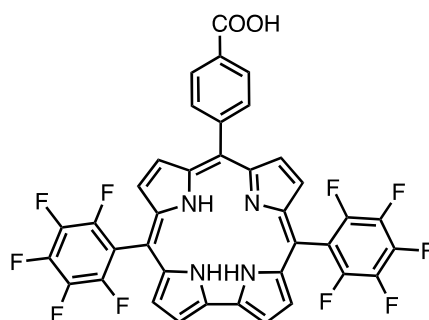
**MS (MALDI-TOF):** *m/z* = 765.24 [M+H]<sup>+</sup>, 765.13 calcd for C<sub>39</sub>H<sub>19</sub>F<sub>10</sub>N<sub>4</sub>O<sub>2</sub>.

**HR-MS (ESI):** *m/z* = 765.1342 [M+H]<sup>+</sup>, 765.1343 calcd for C<sub>39</sub>H<sub>19</sub>F<sub>10</sub>N<sub>4</sub>O<sub>2</sub>.

**UV-vis (DCM):** λ<sub>max</sub> (nm) (ε × 10<sup>-3</sup> L mol<sup>-1</sup> cm<sup>-1</sup>) 411 (148.0), 424 (132.4), 566 (24.3), 612 (14.5), 642 (5.9).

**FTIR (KBr, cm<sup>-1</sup>):** 1706 (C=O ester).

## 5,15-Dipentafluorophenyl-10-(4-carboxyphenyl)corrole (**25**)<sup>18</sup>



Chemical Formula: C<sub>38</sub>H<sub>16</sub>F<sub>10</sub>N<sub>4</sub>O<sub>2</sub>  
Exact Mass: 750.1114  
Molecular Weight: 750.5560

Corrole **25** was obtained according to a method previously described in the literature.<sup>18</sup> Corrole **24** (400 mg, 0.52 mmol) was dissolved in a mixture of AcOH (10 mL), TFA (5 mL) and 5% aqueous H<sub>2</sub>SO<sub>4</sub> (3.4 mL). The reactional mixture was protected from light and stirred at 100°C under argon. After 48 h, the mixture was cooled down, and NaHCO<sub>3</sub> solution (5% aq) was carefully added. The mixture was extracted with CHCl<sub>3</sub> and organic layer was dried by Na<sub>2</sub>SO<sub>4</sub>. The crude compound was purified by column chromatography (Silica gel, DCM:MeOH = 100:5), giving pure product.

**Yield:** 345 mg (88%)

**<sup>1</sup>H NMR (500 MHz, MeOD-*d*<sub>4</sub>)** δ 9.06 (d, *J* = 4.0 Hz, 2H), 8.57 (d, *J* = 4.5 Hz, 2H), 8.54 (d, *J* = 4.5 Hz, 2H), 8.52 (d, *J* = 4.5 Hz, 2H) 8.28 (d, *J* = 8.0 Hz, 2H), 8.16 (d, *J* = 8.0 Hz, 2H).

**<sup>13</sup>C NMR (125 MHz, MeOD-*d*<sub>4</sub>)** δ 176.1, 148.4, 147.7, 146.7, 142.6, 142.1, 140.0, 137.9, 137.2, 135.3, 134.0, 128.6, 127.0, 125.1, 122.1, 118.3, 117.4, 111.3, 95.4.

**<sup>19</sup>F NMR (470 MHz, MeOD-*d*<sub>4</sub>)** δ -140.34 (m, 4F), -159.04 (t, *J* = 20.0 Hz, 2F), -166.47 (m, 4F).

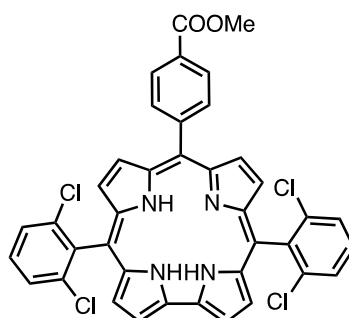
**MS (MALDI-TOF):** *m/z* = 751.41 [M+H]<sup>+</sup>, 751.12 calcd for C<sub>38</sub>H<sub>17</sub>F<sub>10</sub>N<sub>4</sub>O<sub>2</sub>.

**HR-MS (ESI):** *m/z* = 751.1185 [M+H]<sup>+</sup>, 751.1186 calcd for C<sub>38</sub>H<sub>17</sub>F<sub>10</sub>N<sub>4</sub>O<sub>2</sub>.

**UV-vis (DCM):** λ<sub>max</sub> (nm) (ε × 10<sup>-3</sup> L mol<sup>-1</sup> cm<sup>-1</sup>) 411 (113.9), 424 (101.6), 566 (18.7), 612 (11.4), 642 (4.8).

**FTIR (KBr, cm<sup>-1</sup>):** 2923 (broad peak, OH carboxyl), 1685 (C=O carboxyl).

## 5,15-Di(2,6-dichlorophenyl)-10-(4-carboxymethylphenyl)corrole (**26**)<sup>19</sup>



Chemical Formula: C<sub>39</sub>H<sub>24</sub>Cl<sub>4</sub>N<sub>4</sub>O<sub>2</sub>  
Exact Mass: 720.0653  
Molecular Weight: 722.4470

Corrole **26** was obtained according to general procedure **A** described above. For the reaction, dipyrromethane **10** (2.91 g, 10 mmol, 1 eq) and 4-carboxymethylbenzaldehyde (821 mg, 5 mmol, 0.5 eq) were used. The crude compound was collected and recrystallized from CHCl<sub>3</sub>/MeOH, giving purple solid.

**Yield:** 1.20 g (33%)

**<sup>1</sup>H NMR (400 MHz, DMSO-*d*<sub>6</sub>, 10 μL Hydrazine)** δ 8.86 (d, *J* = 5.0 Hz, 2H), 8.29 (m, 2H), 8.25-8.23 (m, 4H), 8.20 (d, *J* = 4.5 Hz, 2H), 8.17 (d, *J* = 4.0 Hz, 2H), 7.86 (m, 4H), 7.75 (m, 2H), 4.01 (s, 3H).

**<sup>13</sup>C NMR (100 MHz, DMSO-*d*<sub>6</sub>, 10 μL Hydrazine)** δ 167.1, 149.8, 140.6, 140.4, 139.4, 137.8, 135.5, 134.8, 132.2, 130.4, 127.9, 127.5, 127.4, 124.2, 124.0, 120.2, 115.3, 107.3, 106.5, 52.4.

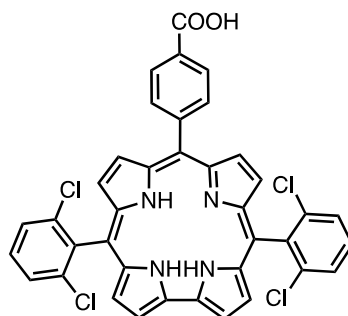
**MS (MALDI-TOF):** *m/z* = 721.79 [M+H]<sup>+</sup>, 721.07 calcd for C<sub>39</sub>H<sub>25</sub>Cl<sub>4</sub>N<sub>4</sub>O<sub>2</sub>.

**HR-MS (ESI):** *m/z* = 721.0739 [M+H]<sup>+</sup>, 721.0732 calcd for C<sub>39</sub>H<sub>25</sub>Cl<sub>4</sub>N<sub>4</sub>O<sub>2</sub>.

**UV-vis (DCM):** λ<sub>max</sub> (nm) (ε × 10<sup>-3</sup> L mol<sup>-1</sup> cm<sup>-1</sup>) 410 (138.8), 427 (114.8), 569 (22.6), 608 (14.0), 638 (4.9).

**FTIR (KBr, cm<sup>-1</sup>):** 1702 (C=O ester).

## 5,15-Di(2,6-dichlorophenyl)-10-(4-carboxylphenyl)corrole (**27**)<sup>19</sup>



Chemical Formula: C<sub>38</sub>H<sub>22</sub>Cl<sub>4</sub>N<sub>4</sub>O<sub>2</sub>  
Exact Mass: 706.0497  
Molecular Weight: 708.4200

Corrole **27** was obtained according to general procedure **C** described above. For the reaction, corrole **26** (200 mg, 0.28 mmol, 1 eq) and NaOH (332 mg, 8.31 mmol, 30 eq) were used. The crude compound was collected and purified by column chromatography (Silica, DCM:MeOH = 100:5), giving purple solid.

**Yield:** 195 mg (99%)

**<sup>1</sup>H NMR (500 MHz, DMSO-*d*<sub>6</sub>, 10 μL Hydrazine)** δ 8.84 (d, *J* = 4.0 Hz, 2H), 8.25 (d, *J* = 4.5 Hz, 2H), 8.20 (d, *J* = 8.0 Hz, 2H), 8.17 (d, *J* = 4.0 Hz, 2H), 8.15 (d, *J* = 4.0 Hz, 2H), 8.02 (d, *J* = 8.0 Hz, 2H), 7.86 (d, *J* = 8.5 Hz, 4H), 7.74 (m, 2H).

**<sup>13</sup>C NMR (125 MHz, DMSO-*d*<sub>6</sub>, 10 μL Hydrazine)** δ 171.40, 145.48, 140.78, 139.57, 139.46, 137.80, 136.83, 135.38, 133.61, 131.95, 130.33, 127.90, 127.37, 124.65, 123.60, 119.90, 115.06, 107.88, 106.82.

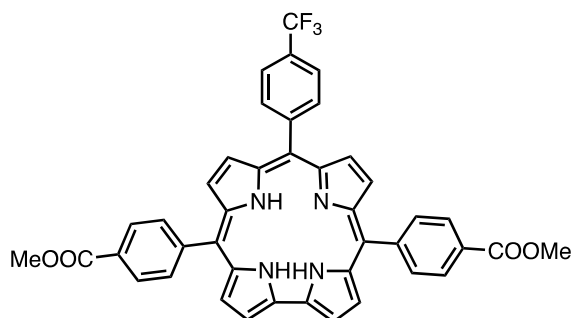
**MS (MALDI-TOF):** *m/z* = 707.82 [M+H]<sup>+</sup>, 707.05 calcd for C<sub>38</sub>H<sub>23</sub>Cl<sub>4</sub>N<sub>4</sub>O<sub>2</sub>.

**HR-MS (ESI):** *m/z* = 707.0565 [M+H]<sup>+</sup>, 707.0570 calcd for C<sub>38</sub>H<sub>23</sub>Cl<sub>4</sub>N<sub>4</sub>O<sub>2</sub>.

**UV-vis (DCM):** λ<sub>max</sub> (nm) (ε × 10<sup>-3</sup> L mol<sup>-1</sup> cm<sup>-1</sup>) 410 (127.0), 427 (104.5), 569 (20.6), 608 (13.0), 638 (5.0).

**FTIR (KBr, cm<sup>-1</sup>):** 3068 (broad peak, OH carboxyl), 1687 (C=O carboxyl).

## 5,15-Di(4-carboxymethylphenyl)-10-(4-trifluoromethylphenyl)corrole (28)



Chemical Formula: C<sub>42</sub>H<sub>29</sub>F<sub>3</sub>N<sub>4</sub>O<sub>4</sub>  
Exact Mass: 710.2141  
Molecular Weight: 710.7132

Corrole **28** was synthesized according to general procedure **A** described above. For the reaction, dipyrromethane **7** (2.80 g, 10 mmol, 1 eq) and 4-trifluoromethylbenzaldehyde (870 mg, 5 mmol, 0.5eq) were used. The crude compound was collected and recrystallized from THF/MeOH/heptane, giving purple solid.

**Yield:** 573 mg (16%)

**<sup>1</sup>H NMR (500 MHz, DMSO-*d*<sub>6</sub>, 10 μL Hydrazine)** δ 8.99 (d, *J* = 4.0 Hz, 2H), 8.67 (d, *J* = 4.5 Hz, 2H), 8.55 (d, *J* = 4.0 Hz, 2H), 8.41-8.37 (m, 8H), 8.32-8.30 (m, 4H), 8.07 (d, *J* = 8.0 Hz, 2H), 4.02 (s, 6H).

**<sup>13</sup>C NMR (125 MHz, DMSO-*d*<sub>6</sub>, 10 μL Hydrazine)** δ 167.0, 166.9, 149.0, 147.1, 140.2, 139.8, 135.9, 135.0, 134.9, 132.2, 128.5, 126.9, 125.2, 124.5, 123.4, 123.4, 121.7, 115.6, 112.2, 106.1, 52.3.

**<sup>19</sup>F NMR (470 MHz, DMSO-*d*<sub>6</sub>, 10 μL Hydrazine)** δ -60.19 (s, 3F).

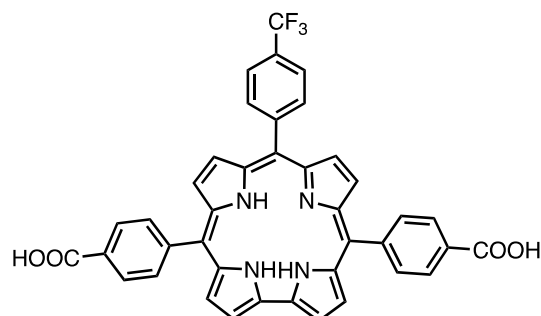
**MS (MALDI-TOF):** *m/z* = 709.95 [M]<sup>+</sup>, 710.21 calcd for C<sub>42</sub>H<sub>29</sub>F<sub>3</sub>N<sub>4</sub>O<sub>4</sub>.

**HR-MS (ESI):** *m/z* = 711.2205 [M+H]<sup>+</sup>, 711.2214 calcd for C<sub>42</sub>H<sub>30</sub>F<sub>3</sub>N<sub>4</sub>O<sub>4</sub>.

**UV-vis (DCM):** λ<sub>max</sub> (nm) (ε × 10<sup>-3</sup> L mol<sup>-1</sup> cm<sup>-1</sup>) 424 (123.0), 583 (21.2), 622 (15.8), 653 (10.2).

**FTIR (KBr, cm<sup>-1</sup>):** 1716 (C=O ester).

## 5,15-Di(4-carboxylphenyl)-10-(4-trifluoromethylphenyl)corrole (**29**)



Chemical Formula: C<sub>40</sub>H<sub>25</sub>F<sub>3</sub>N<sub>4</sub>O<sub>4</sub>  
Exact Mass: 682.1828  
Molecular Weight: 682.6592

Corrole **29** was obtained according to general procedure **C** described above. For the reaction, corrole **28** (500 mg, 0.70 mmol, 1 eq) and NaOH (1.69 g, 42.0 mmol, 60 eq) were used. The crude compound was collected and purified by column chromatography (Silica, DCM:MeOH = 100:5), giving purple solid.

**Yield:** 436 mg (91%)

**<sup>1</sup>H NMR (500 MHz, DMSO-*d*<sub>6</sub>, 10 μL Hydrazine)** δ 8.92 (d, *J* = 4.0 Hz, 2H), 8.66 (d, *J* = 4.5 Hz, 2H), 8.51 (d, *J* = 4.0 Hz, 2H), 8.31 (d, *J* = 8.0 Hz, 2H), 8.29 (d, *J* = 8.0 Hz, 4H), 8.26 (d, *J* = 8.0 Hz, 2H), 8.19 (d, *J* = 8.0 Hz, 4H), 8.06 (d, *J* = 8.0 Hz, 2H).

**<sup>13</sup>C NMR (125 MHz, DMSO-*d*<sub>6</sub>, 10 μL Hydrazine)** δ 149.3, 143.1, 140.5, 140.0, 136.1, 135.1, 133.9, 132.1, 128.5, 126.8, 126.3, 125.7, 124.1, 123.9, 123.5, 123.5, 121.6, 114.9, 113.8, 105.0.

**<sup>19</sup>F NMR (470 MHz, DMSO-*d*<sub>6</sub>, 10 μL Hydrazine)** δ -60.16 (s, 3F).

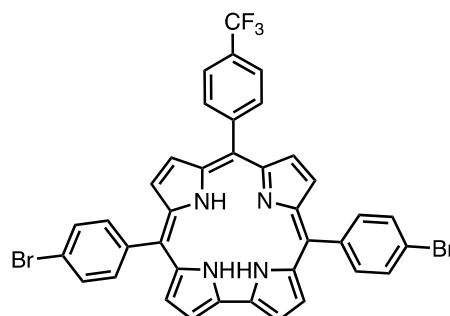
**MS (MALDI-TOF):** *m/z* = 683.29 [M+H]<sup>+</sup>, 683.19 calcd for C<sub>40</sub>H<sub>26</sub>F<sub>3</sub>N<sub>4</sub>O<sub>4</sub>.

**HR-MS (ESI):** *m/z* = 683.1901 [M+H]<sup>+</sup>, 683.1901 calcd for C<sub>40</sub>H<sub>26</sub>F<sub>3</sub>N<sub>4</sub>O<sub>4</sub>.

**UV-vis (DCM):** λ<sub>max</sub> (nm) (ε × 10<sup>-3</sup> L mol<sup>-1</sup> cm<sup>-1</sup>) 435 (100.7), 468 (41.4), 560 (7.4), 589 (7.4), 645 (13.2), 699 (24.1).

**FTIR (KBr, cm<sup>-1</sup>):** 2962 (broad peak, OH carboxyl), 1689 (C=O carboxyl).

### 5,15-Di(4-bromophenyl)-10-(4-trifluoromethylphenyl)corrole (30)



Chemical Formula:  $C_{38}H_{23}Br_2F_3N_4$   
Exact Mass: 750.0242  
Molecular Weight: 752.4332

Corrole **30** was synthesized according to general procedure **A** described above. For the reaction, dipyrromethane **11** (3.00 g, 10 mmol, 1 eq) and 4-trifluoromethylbenzaldehyde (870 mg, 5 mmol, 0.5 eq) were used. The crude compound was collected and recrystallized from DCM/heptane, giving purple solid.

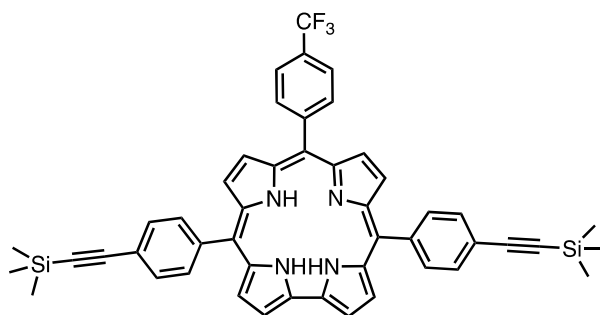
**Yield:** 1.23 g (33%)

**$^1H$  NMR (500 MHz, DMSO- $d_6$ , 10  $\mu$ L Hydrazine)**  $\delta$  8.97 (d,  $J$  = 4.0 Hz, 2H), 8.65 (d,  $J$  = 4.5 Hz, 2H), 8.52 (d,  $J$  = 4.0 Hz, 2H), 8.33-8.30 (m, 4H), 8.20 (d,  $J$  = 8.0 Hz, 4H), 8.07 (d,  $J$  = 8.0 Hz, 2H), 7.98 (d,  $J$  = 8.0 Hz, 4H).

**$^{13}C$  NMR (125 MHz, DMSO- $d_6$ , 10  $\mu$ L Hydrazine)**  $\delta$  149.1, 141.2, 140.4, 139.7, 136.3, 135.8, 135.0, 132.1, 130.6, 125.2, 124.2, 123.4, 123.4, 121.3, 120.1, 115.2, 112.1, 105.3, 79.2.

**MS (MALDI-TOF):**  $m/z$  = 753.079  $[M+H]^+$ , 751.032 calcd for  $C_{38}H_{24}Br_2F_3N_4$ .

## 5,15-Di(4-(trimethylsilylethynyl)phenyl)-10-(4-trifluoromethylphenyl)corrole (31)



Chemical Formula:  $C_{48}H_{41}F_3N_4Si_2$   
Exact Mass: 786.2822  
Molecular Weight: 787.0492

Corrole **31** was synthesized through two synthetic pathways.

### A. Sonogashira cross-coupling reaction

Corrole **30** (1.00 g, 1.33 mmol, 1 eq) and  $PdCl_2(PPh_3)_2$  (382 mg, 0.544 mmol, 0.4 eq) were placed in a round bottom flask, followed by vacuum and argon cycles. Dry THF (100 mL), TEA (37.5 mL) and (trimethylsilyl)acetylene (756  $\mu$ L, 5.32 mmol, 4 eq) were added under argon. The mixture was heated and stirred at 70°C for 12 h. The solvents were removed and residues were purified by column chromatography (Silica, DCM: heptane = 3:7), recrystallized from DCM/heptane, giving pure compound.

**Yield:** 397 mg (38%)

### B. General procedure A from dipyrromethane

Corrole **31** was synthesized according to general procedure A described above. For the reaction, dipyrromethane **12** (3.18 g, 10 mmol, 1 eq) and 4-trifluoromethylbenzaldehyde (870 mg, 5 mmol, 0.5 eq) were used. The crude compound was collected and recrystallized from DCM/heptane, giving purple solid.

**Yield:** 408 mg (33%)

**$^1H$  NMR (500 MHz, DMSO- $d_6$ , 10  $\mu$ L Hydrazine)**  $\delta$  8.96 (d,  $J$  = 4.0 Hz, 2H), 8.65 (d,  $J$  = 4.5 Hz, 2H), 8.52 (d,  $J$  = 4.0 Hz, 2H), 8.31-8.28 (m, 4H), 8.25 (d,  $J$  = 8.0 Hz, 4H), 8.06 (d,  $J$  = 8.0 Hz, 2H), 7.86 (d,  $J$  = 8.0 Hz, 4H), 0.34 (s, 18H).

**$^{13}C$  NMR (125 MHz, DMSO- $d_6$ , 10  $\mu$ L Hydrazine)**  $\delta$  149.1, 142.8, 140.5, 140.3, 139.8, 135.9, 135.0, 134.8, 132.1, 131.1, 127.2, 125.3, 124.3, 123.5, 121.6, 119.3, 115.4, 112.7, 105.7, 84.2, 81.3, 1.9.

**<sup>19</sup>F NMR (470 MHz, DMSO-*d*<sub>6</sub>, 10 μL Hydrazine)** δ -60.19 (s, 3F).

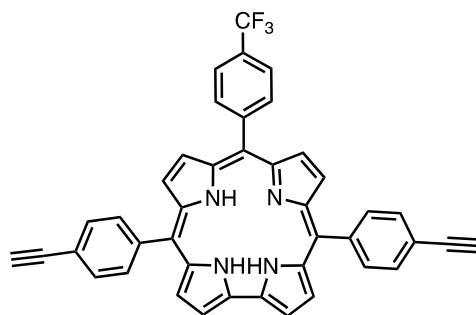
**MS (MALDI-TOF):**  $m/z = 786.28 [M]^+$ , 786.28 calcd for C<sub>48</sub>H<sub>41</sub>F<sub>3</sub>N<sub>4</sub>Si<sub>2</sub>.

**HR-MS (ESI):**  $m/z = 786.2809 [M]^+$ , 786.2816 calcd for C<sub>48</sub>H<sub>41</sub>F<sub>3</sub>N<sub>4</sub>Si<sub>2</sub>.

**UV-vis (DCM):** λ<sub>max</sub> (nm) (ε × 10<sup>-3</sup> L mol<sup>-1</sup> cm<sup>-1</sup>) 424 (136.2), 584 (22.8), 624 (20.4), 652 (12.9).

**FTIR (KBr, cm<sup>-1</sup>):** 2158 (C≡C), 838 (Si-C).

### 5,15-Di(4-ethynylphenyl)-10-(4-trifluoromethylphenyl)corrole (32)



Chemical Formula: C<sub>42</sub>H<sub>25</sub>F<sub>3</sub>N<sub>4</sub>  
Exact Mass: 642.2031  
Molecular Weight: 642.6852

Corrole **31** (600 mg, 0.762 mmol, 1 eq) was placed in a round bottom flask followed by vacuum and argon cycles. 50 mL of dry DCM was added under argon and the mixture was stirred for 5 min to dissolve all the corrole. The mixture was cooled to 0°C by ice bath and TBAF (1M in THF, 1.68 mmol, 2.2 eq) was added slowly. After addition, the reaction was allowed to come back to room temperature and stirred for 12 h. The solvent was removed and the crude compound was purified by column chromatography (Silica, DCM:heptane = 1:1), giving pure compound.

**Yield:** 343 mg (70%)

**<sup>1</sup>H NMR (500 MHz, DMSO-*d*<sub>6</sub>, 10 μL Hydrazine)** δ 8.95 (d, *J* = 4.0 Hz, 2H), 8.64 (d, *J* = 4.5 Hz, 2H), 8.51 (d, *J* = 4.0 Hz, 2H), 8.29 (d, *J* = 8.0 Hz, 2H), 8.27 (d, *J* = 4.5 Hz, 2H), 8.25 (d, *J* = 8.0 Hz, 4H), 8.05 (d, *J* = 8.0 Hz, 2H), 7.88 (d, *J* = 8.0 Hz, 4H), 4.33 (s, 2H).

**<sup>13</sup>C NMR (125 MHz, DMSO-*d*<sub>6</sub>, 10 μL Hydrazine)** δ 149.2, 142.9, 140.5, 140.0, 136.1, 135.2, 135.0, 132.3, 131.3, 126.4, 125.5, 124.4, 123.7, 123.6, 121.7, 119.4, 115.5, 112.9, 105.8, 84.4, 81.4.

**<sup>19</sup>F NMR (470 MHz, DMSO-*d*<sub>6</sub>, 10 μL Hydrazine)** δ -60.0 (s, 3F).

**MS (MALDI-TOF):** *m/z* = 642.09 [M]<sup>+</sup>, 642.20 calcd for C<sub>42</sub>H<sub>25</sub>F<sub>3</sub>N<sub>4</sub>.

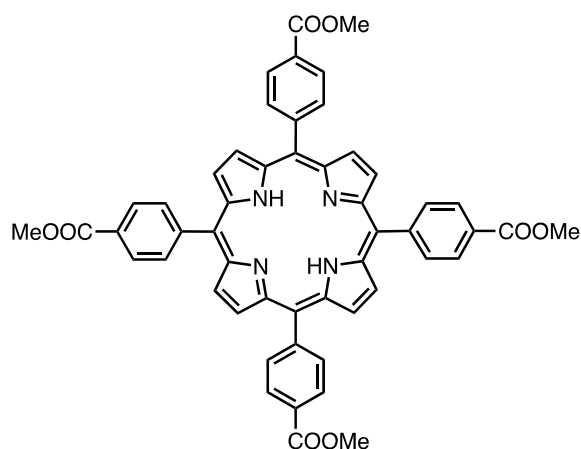
**HR-MS (ESI):** *m/z* = 643.2091 [M+H]<sup>+</sup>, 643.2104 calcd for C<sub>42</sub>H<sub>26</sub>F<sub>3</sub>N<sub>4</sub>.

**UV-vis (DCM):** λ<sub>max</sub> (nm) (ε × 10<sup>-3</sup> L mol<sup>-1</sup> cm<sup>-1</sup>) 421 (130.4), 582 (21.9), 621 (17.7), 652 (11.3).

**FTIR (KBr, cm<sup>-1</sup>):** 2107 (C≡C).

#### 4. Synthesis of porphyrins

##### 5,10,15,20-Tetrakis(4-methoxycarbonylphenyl)porphyrin (**33**)<sup>20</sup>



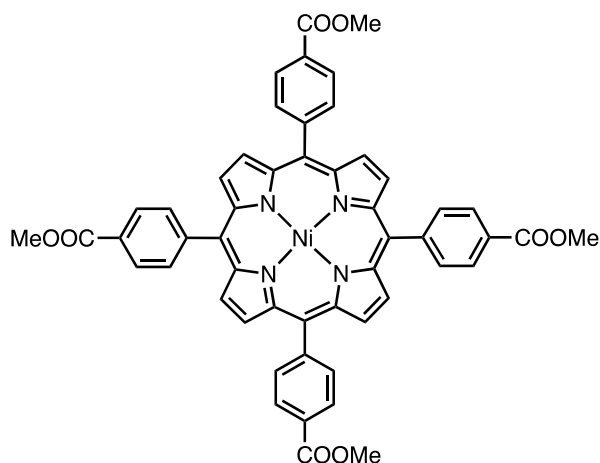
Chemical Formula: C<sub>52</sub>H<sub>38</sub>N<sub>4</sub>O<sub>8</sub>  
Exact Mass: 846.2690  
Molecular Weight: 846.8960

In a 500-mL three necked flask, methyl *p*-formylbenzoate (13.8 g, 0.084 mol, 1 eq) was dissolved in propionic acid (200 mL). Pyrrole was then added dropwise (6.0 mL, 0.086 mol, 1.02 eq) and the solution was refluxed for 12 h. After the reaction, the mixture was cooled to room temperature, and the precipitate was collected by suction-filtration and washed with methanol, ethyl acetate and THF, respectively. After being dried in an oven for 12 h, compound **33** was obtained as pure product.

**Yield:** 7.0 g (39%)

**<sup>1</sup>H NMR (500 MHz, CDCl<sub>3</sub>)** δ 8.82 (s, 8H), 8.45 (d, *J* = 8.0 Hz, 8H), 8.30 (d, *J* = 8.0 Hz, 8H), 4.12 (s, 12H), -2.81 (s, 2H).

**[5,10,15,20-Tetrakis(4-methoxycarbonylphenyl)porphyrinato]-Ni(II) (34)** <sup>21</sup>



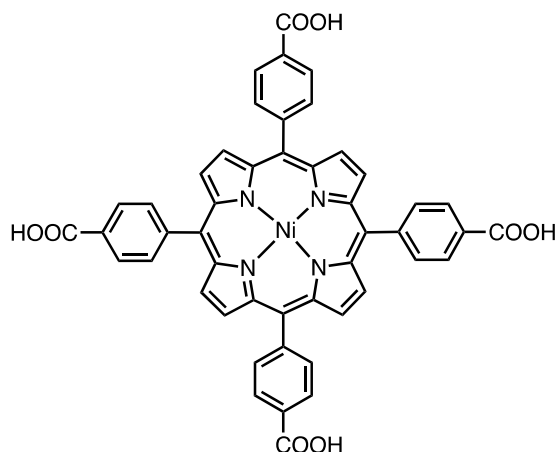
Chemical Formula:  $C_{52}H_{36}N_4NiO_8$   
Exact Mass: 902.1887  
Molecular Weight: 903.5734

A solution of porphyrin **33** (7.00 g, 8.27 mmol, 1 eq) and  $NiCl_2 \cdot 6H_2O$  (29.5 g, 124 mmol, 15 eq) in 500 mL of DMF was refluxed overnight. After the mixture was cooled to room temperature, 500 mL of  $H_2O$  was added. The resultant precipitate was filtered and washed with 150 mL of  $H_2O$  for two times. The obtained solid was dissolved in  $CHCl_3$ , followed by three times of washing with 1 M HCl and twice with water. The organic layer was dried over anhydrous sodium sulfate and evaporated to afford crude compound. Then the crude compound was purified by chromatography (silica gel) with  $CHCl_3$  as eluent to afford red powder.

**Yield:** 5.85 g (78%).

**$^1H$  NMR (500 MHz,  $CDCl_3$ )**  $\delta$  8.71 (s, 8H), 8.37 (d,  $J = 8.5$  Hz, 8H), 8.09 (d,  $J = 8$  Hz, 8H), 4.08 (s, 12H)

**[5,10,15,20-Tetrakis(4-carboxyphenyl)porphyrinato]-Ni(II) (35)** <sup>22</sup>



Chemical Formula: C<sub>48</sub>H<sub>28</sub>N<sub>4</sub>NiO<sub>8</sub>  
Exact Mass: 846.1261  
Molecular Weight: 847.4654

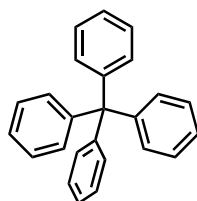
Nickel porphyrin **34** (5.85 g, 6.47 mmol, 1 eq) was stirred in THF (200 mL) and MeOH (200 mL), to which a solution of KOH (17.4 g, 310 mmol, 48 eq) in H<sub>2</sub>O (200 mL) was introduced. This mixture was refluxed for 12 h. After cooling down to room temperature, THF and MeOH were evaporated. Additional water was added to the resulting water phase and the mixture was heated until the solid was fully dissolved, then the homogeneous solution was acidified with 1M HCl until no further precipitate was detected. The solid was collected by filtration, washed with water and dried in vacuum.

**Yield:** 5.68 g (91%)

**<sup>1</sup>H NMR (500 MHz, DMSO-*d*<sub>6</sub>)** δ 13.27 (s, 4H), 8.71 (s, 8H), 8.29 (d, *J* = 8.0 Hz, 8H), 8.12 (d, *J* = 8.0 Hz, 8H).

## 5. Synthesis of platform precursors

### Tetraphenylmethane (36)<sup>23</sup>



Chemical Formula: C<sub>25</sub>H<sub>20</sub>  
Exact Mass: 320.1565  
Molecular Weight: 320.4350

The compound was synthesized according to the literature with a slight modification.<sup>23</sup> In a 500 mL round bottom flask, chlorotriphenylmethane (25.0 g, 89.7 mmol, 1 eq) and aniline (22.0 mL, 22.5 g, 232 mmol, 2.6 eq) were added. The mixture was stirred vigorously and slowly heated to 190°C. The mixture was stirred at 190°C for 1 h, until all residues became solid. After grinding all the solid into powder, a solution of aqueous HCl (2 M, 100 mL) and methanol (150 mL) were added to the purple powder and the reaction mixture was heated to 80°C for more than 2 h. After cooling, the resulting solid was filtered off, washed with water and methanol and dried under vacuum, giving pink powder.

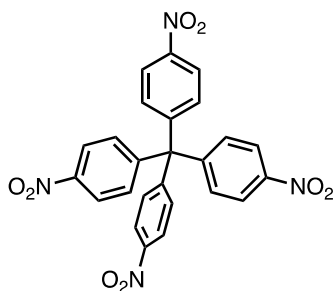
The dry solid was then suspended in DMF (250 mL) and the mixture was cooled to -15°C. Sulfuric acid (96%, 27.5 mL) and isoamyl nitrite (19.9 mL, 17.3 g, 148 mmol, 1.7 eq) were added slowly and the resulting suspension was stirred for 1 h. The reaction mixture was allowed to warm up to room temperature. Then hypophosphoric acid (50%, 45 mL) was added dropwise. After the addition, the mixture was heated at 50°C until the evolution of gas has ceased. Then, the solid was filtered off and washed subsequently with DMF, water, and ethanol and the washing procedure was repeated twice. After drying under vacuum, the pure product was obtained.

**Yield:** 15.0 g (52%)

**<sup>1</sup>H NMR (500 MHz, CDCl<sub>3</sub>)** δ 7.22-7.09 (m, 20H).

**<sup>13</sup>C NMR (125 MHz, CDCl<sub>3</sub>)** δ 146.9, 131.3, 127.6, 126.0, 65.1.

### Tetrakis(4-nitrophenyl)methane (37)



Chemical Formula: C<sub>25</sub>H<sub>16</sub>N<sub>4</sub>O<sub>8</sub>

Exact Mass: 500.0968

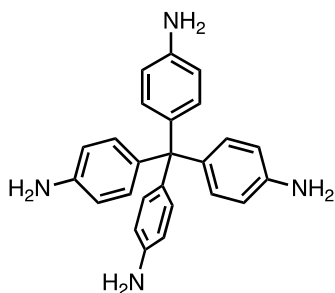
Molecular Weight: 500.4230

This compound was synthesized according to the literature with a slight modification.<sup>24</sup> In a round bottom flask, compound **36** (4.00 g, 12.5 mmol, 1 eq) was slowly added to fuming nitric acid (22 mL) at 0°C. Then, glacial acetic acid (13.6 mL) and acetic anhydride (7.6 mL) were added. The mixture was stirred for 5 h and then filtered to give yellow-brown solid which was further washed with water, then dried and recrystallized from THF to give pure compound.

**Yield:** 4.38 g (70%)

**<sup>1</sup>H NMR (500 MHz, CDCl<sub>3</sub>)** δ 8.23 (d, *J* = 9.0 Hz, 8H), 7.41 (d, *J* = 9.0 Hz, 8H).

### Tetrakis(4-aminophenyl)methane (38)



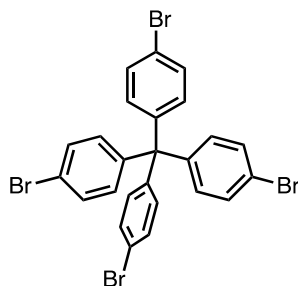
Chemical Formula: C<sub>25</sub>H<sub>24</sub>N<sub>4</sub>  
Exact Mass: 380.2001  
Molecular Weight: 380.4950

Compound **38** was synthesized according to the literature with a slight modification.<sup>24</sup> The Pd/C catalyst (500 mg, 5% palladium on carbon, 50% water) was activated by heating at 100°C and vacuum for 3 h. A solution of compound **37** (1.90 g, 3.80 mmol, 1 eq) in dry THF (100 mL) was added to the Pd/C catalyst. The reaction mixture was purged with nitrogen followed by dihydrogen and stirred for 12 h. Pd/C powder was filtered over celite. The filtrate was dried to give white compound.

**Yield:** 1.47 g (91%)

**<sup>1</sup>H NMR (500 MHz, DMSO-*d*<sub>6</sub>)** δ 6.67 (d, *J* = 8.5 Hz, 8H), 6.39 (d, *J* = 8.5 Hz, 8H), 4.84 (s, 8H).

### Tetrakis(4-bromophenyl)methane (39)



Chemical Formula: C<sub>25</sub>H<sub>16</sub>Br<sub>4</sub>  
Exact Mass: 631.7986  
Molecular Weight: 636.0190

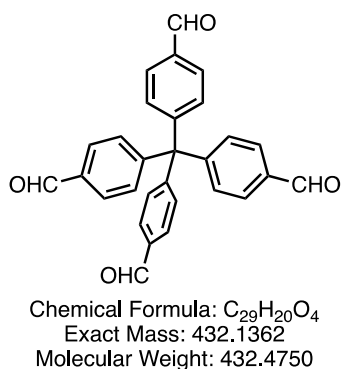
Compound **39** was synthesized according to the literature with a slight modification.<sup>23</sup> To a round bottom flask containing bromine (30 mL, 93.4 g, 0.59 mol, 24 eq), tetraphenylmethane **36** (8.00 g, 25.0 mmol, 1 eq) was added in small portions under vigorous stirring at room temperature. After the addition was completed, the resulting solution was stirred for 20 min and then cooled to -78°C. At this temperature, ethanol (150 mL) was added slowly and the reaction mixture was allowed to warm to room temperature overnight. After, the precipitate was filtered off and washed subsequently with saturated aqueous NaHSO<sub>3</sub> solution and water, dried under vacuum. The crude compound was recrystallized with CHCl<sub>3</sub>/EtOH to afford yellow crystals.

**Yield:** 13.5 g (85%)

<sup>1</sup>H NMR (500 MHz, CDCl<sub>3</sub>) δ 7.39 (d, *J* = 8.5 Hz, 8H), 7.01 (d, *J* = 8.5 Hz, 8H).

<sup>13</sup>C NMR (125 MHz, CDCl<sub>3</sub>) δ 144.6, 132.5, 131.2, 121.0, 63.8.

## Tetrakis(4-formylphenyl)methane (**40**)

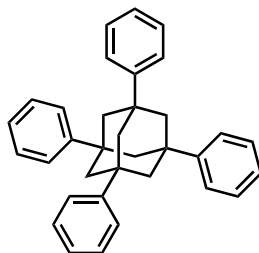


Compound **40** was synthesized according to the literature with a slight modification.<sup>25</sup> A solution of compound **39** (8.00 g, 12.6 mmol, 1 eq) in dry THF (250 mL) was stirred at -78 °C under nitrogen and treated dropwise with a solution of *n*-butyllithium (50.0 mL, 2.5 M in hexane, 125 mmol). The resulting mixture was kept at -78 °C for 1 h, and then DMF (20.2 mL, 250 mmol) was added dropwise. The mixture was stirred overnight while the temperature was allowed to rise to room temperature. To the solution was added 1.0 M aqueous HCl (100 mL), and solvents were partially removed by evaporation under reduced pressure. The remaining aqueous concentrate was extracted with ethyl acetate, and the combined organic extracts were washed with water and brine, dried over MgSO<sub>4</sub>, and filtered. Solvents were removed by evaporation under reduced pressure, and the residue purified through column chromatography (Silica, toluene:acetone = 95:5), giving colorless compound.

**Yield:** 1.5 g (28%)

**<sup>1</sup>H NMR (500 MHz, CDCl<sub>3</sub>)** δ 10.02 (s, 4H), 7.84 (d, *J* = 8.5 Hz, 8H), 7.43 (d, *J* = 8.5 Hz, 8H).

### 1,3,5,7-Tetrakisphenyladamantane (41)



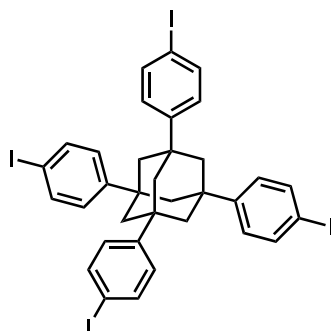
Chemical Formula: C<sub>34</sub>H<sub>32</sub>  
Exact Mass: 440.2504  
Molecular Weight: 440.6300

The compound was synthesized according to the literature with a slight modification.<sup>23</sup> 1-Bromoadamantane (14.0 g, 65.1 mmol, 1 eq) was dissolved in benzene (120 mL) under an argon atmosphere. *t*-Butylbromide (14.7 mL, 130 mmol, 2 eq) and aluminum chloride (0.75 g, 5.60 mmol, 0.1 eq) were added to the solution, which was then refluxed overnight. The reaction mixture was cooled to room temperature and the formed precipitate was filtered off and washed with chloroform, water, and again chloroform. The product was dried under reduced pressure overnight.

**Yield:** 18.0 g (64%)

**<sup>1</sup>H NMR (500 MHz, DMSO-*d*<sub>6</sub>)** Insoluble in common organic solvents

### 1,3,5,7-Tetrakis(4-iodophenyl)adamantane (42)



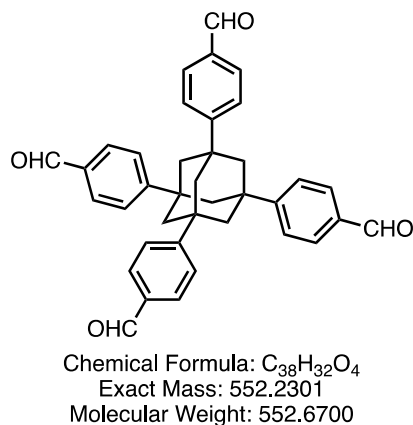
Chemical Formula: C<sub>34</sub>H<sub>28</sub>I<sub>4</sub>  
Exact Mass: 943.8370  
Molecular Weight: 944.2159

Compound **42** was synthesized according to the literature with a slight modification.<sup>23</sup> Iodine (2.36 g, 9.06 mmol, 2 eq) was added to a suspension of 1,3,5,7-tetraphenyladamantane **41** (2.00 g, 4.54 mmol, 1 eq) in chloroform (50 mL) and the mixture was stirred until the iodine had dissolved. Then, (bis(trifluoroacetoxy)iodo)benzene (3.90 g, 9.06 mmol, 2 eq) was added and the suspension was stirred for 24 h at room temperature. The mixture was filtered to remove a purple solid. The organic layer was washed with saturated aqueous sodium bisulfite solution (5%, 50 mL), water (50 mL), and brine (50 mL), and dried over magnesium sulfate. The product was recrystallized in a chloroform/methanol mixture (9:1, v:v) to isolate colorless crystals of 1,3,5,7-tetrakis(4-iodophenyl)adamantane.

**Yield:** 1.9 g (44%)

**<sup>1</sup>H NMR (400 MHz, CDCl<sub>3</sub>)** δ 7.67 (d, *J* = 8.5 Hz, 8H), 7.18 (d, *J* = 8.5 Hz, 8H), 2.05 (s, 12H).

### 1,3,5,7-Tetrakis-4-formylphenyladamantane (43)



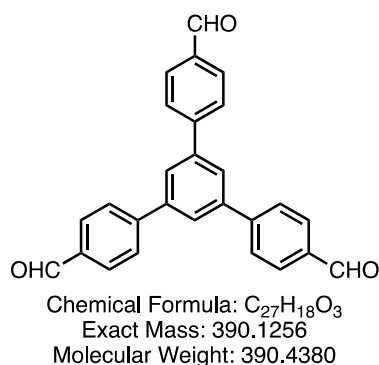
The compound was synthesized according to the literature.<sup>26</sup>

To a 250 mL round bottom flask, adamantane **41** (1.20 g, 2.72 mmol, 1 eq) and 150 mL dry dichloromethane was added under argon. The mixture was stirred and cooled to -10°C. TiCl<sub>4</sub> (6.00 mL, 54.4 mmol, 20 eq) was slowly added to the mixture and stirred at -10°C for 30 min. Then, dichloromethyl methylether (3.90 mL, 43.5 mmol, 16 eq) was subsequently added dropwise to the mixture. The reaction was kept at -10°C for 3 h and then allowed to warm to room temperature and stirred overnight. The mixture was poured into 100 mL ice-water, and 33 mL of 1 M HCl was added and allowed to stir for 30 minutes. The two-phase mixture was separated, and the aqueous phase was washed twice with DCM. The combined organic phases were successively washed with saturated aqueous NaHCO<sub>3</sub> and saturated NaCl and then dried with Na<sub>2</sub>SO<sub>4</sub>. Solvents were removed and the resultant was purified by column chromatography (Silica, DCM:MeOH = 98:2), giving pure compound.

**Yield:** 1.0 g (67%)

**<sup>1</sup>H NMR (500 MHz, CDCl<sub>3</sub>)** δ 10.02 (s, 4H), 7.90 (d, *J* = 8.5 Hz, 8H), 7.65 (d, *J* = 8.5 Hz, 8H), 2.25 (s, 12H).

### 1,3,5-Tris(4-formylphenyl)benzene (44)

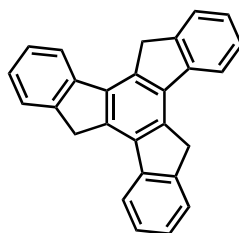


Compound **44** was synthesized according to the literature with a slight modification.<sup>27</sup> 1,3,5-tribromobenzene (2.00 g, 6.36 mmol, 1 eq) and 4-formylphenylboronic acid (2.90 g, 19.4 mmol, 3.05 eq) were dissolved in 100 mL of tetrahydrofuran. Aqueous solution of potassium carbonate (10.0 mL, 2.0 M) was added to the solution under nitrogen atmosphere. The resulting suspension was subjected to the freeze-pump-thaw cycles. After the addition of bis(triphenylphosphine)palladium(II) dichloride (0.602 g, 0.858 mmol, 0.27 eq), the mixture was refluxed for 24 h. After cooling to room temperature, the mixture was extracted twice with dichloromethane (2 × 100 mL). The obtained organic layer was collected and dried with anhydrous sodium sulfate. After that, the solvent was removed under reduced pressure. The crude product was purified by column chromatography (Silica, DCM), giving yellow powder.

**Yield:** 1.64 g (66%)

**<sup>1</sup>H NMR (500 MHz, CDCl<sub>3</sub>)** δ 10.11 (s, 3H), 8.03 (d, *J* = 8.0 Hz, 6H), 7.91 (s, 3H), 7.88 (d, *J* = 8.0 Hz, 6H).

## Truxene (45)



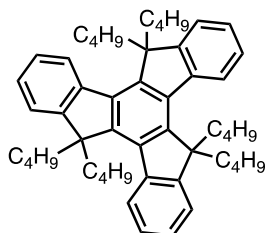
Chemical Formula: C<sub>27</sub>H<sub>18</sub>  
Exact Mass: 342.1409  
Molecular Weight: 342.4410

Compound **45** was synthesized according to the literature with a slight modification.<sup>28</sup> 1-Indanone (8.90 g, 67.3 mmol, 1 eq) was dissolved in 40 mL of acetic acid, and then 20 mL of concentrated hydrochloric acid was added. The solution was heated to 100 °C and stirred for 16 h, until it turned into yellow colored suspension. The hot mixture was poured into 500 ml of saturated sodium carbonate aqueous solution with ice, and stirred for 1 h. The yellow precipitate was filtered, and washed with water, acetone and dichloromethane to give a white powder.

**Yield:** 6.00 g (80%).

**<sup>1</sup>H NMR (300 MHz, CDCl<sub>3</sub>)** δ 7.97 (d, *J* = 7.5 Hz, 3H), 7.71 (d, *J* = 7.5 Hz, 3H), 7.51 (t, *J* = 7.5 Hz, 3H), 7.40 (t, *J* = 7.5 Hz, 3H), 4.30 (s, 6H).

### 5,5,10,10,15,15-Hexabutyl-truxene (46)



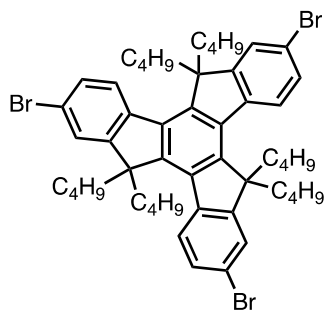
Chemical Formula: C<sub>51</sub>H<sub>66</sub>  
Exact Mass: 678.5165  
Molecular Weight: 679.0890

Compound **46** was synthesized according to the literature with a slight modification.<sup>29</sup> With vigorous stirring, 44.0 mL of *n*-BuLi (1.6 M in hexane, 70.4 mmol, 3.78 eq) was added to a suspension of truxene **45** (6.36 g, 18.6 mmol, 1 eq) in 100 mL of anhydrous THF at 0°C and the mixture was allowed to warm up to room temperature, stirred at rt for 1 h. 1-Bromobutane (7.70 mL, 71.2 mmol, 3.84 eq) was added to the mixture at 0°C. After addition, the reaction mixture was stirred at room temperature for 4 h. A second portion of *n*-BuLi (1.6 M in hexane, 70.4 mmol, 3.78 eq) was added at 0°C and the mixture was stirred at RT for 1 h. 1-Bromobutane (7.70 mL, 71.2 mmol, 3.84 eq) was followed at 0°C. The reaction was stirred overnight. The mixture was quenched with NH<sub>4</sub>Cl solution, extracted with DCM and then the combined organic phase was dried over MgSO<sub>4</sub>. After the solvent was removed, the residue was purified by flash column chromatography (Silica, heptane), giving a light-yellow solid.

**Yield:** 12.2 g (96%)

**<sup>1</sup>H NMR (300 MHz, CDCl<sub>3</sub>)** δ 8.40-8.37 (m, 3H), 7.48-7.45 (m, 3H), 7.43-7.33 (m, 6H), 3.03-2.94 (m, 6H), 2.15-2.05 (m, 6H), 0.94-0.83 (m, 12H), 0.57-0.42 (m, 30H).

### 5,5,10,10,15,15-Hexabutyl-2,7,12-tribromotruxene (47)



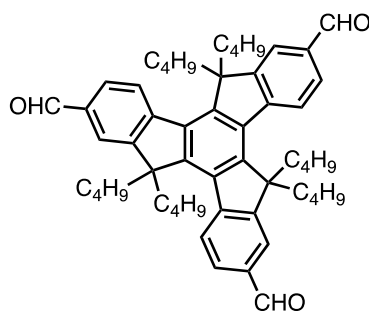
Chemical Formula:  $C_{51}H_{63}Br_3$   
Exact Mass: 912.2480  
Molecular Weight: 915.7770

The compound was synthesized according to the literature with a slight modification.<sup>29</sup> To a solution of **46** (3.40 g, 5.00 mmol, 1 eq) in DCM (50 mL), bromine (1.8 mL, 35.1 mmol, 7 eq) was added slowly at 0°C, covered from light. After 12 h, the reaction was quenched with saturated sodium thiosulfate solution and brine to remove excess bromine. The mixture was extracted with DCM, and organic layer was washed with  $Na_2CO_3$  solution and dried with  $MgSO_4$ . After removal of the solvent, a solid residue was afforded. The crude product was purified by flash column chromatography (Silica, heptane), giving a yellow solid.

**Yield:** 4.38 g (93%)

**$^1H$  NMR (300 MHz,  $CDCl_3$ )**  $\delta$  8.19 (d,  $J = 8.5$  Hz, 3H), 7.57 (d,  $J = 2.0$  Hz, 3H), 7.52 (dd,  $J = 8.5$  Hz,  $J = 2.0$  Hz, 3H), 2.91-2.81 (m, 6H), 2.09-1.99 (m, 6H), 1.0-0.80 (m, 12H), 0.59-0.34 (m, 30H).

### 5,5,10,10,15,15-Hexabutyl-2,7,12-triformyltruxene (48)



Chemical Formula: C<sub>54</sub>H<sub>66</sub>O<sub>3</sub>  
Exact Mass: 762.5012  
Molecular Weight: 763.1190

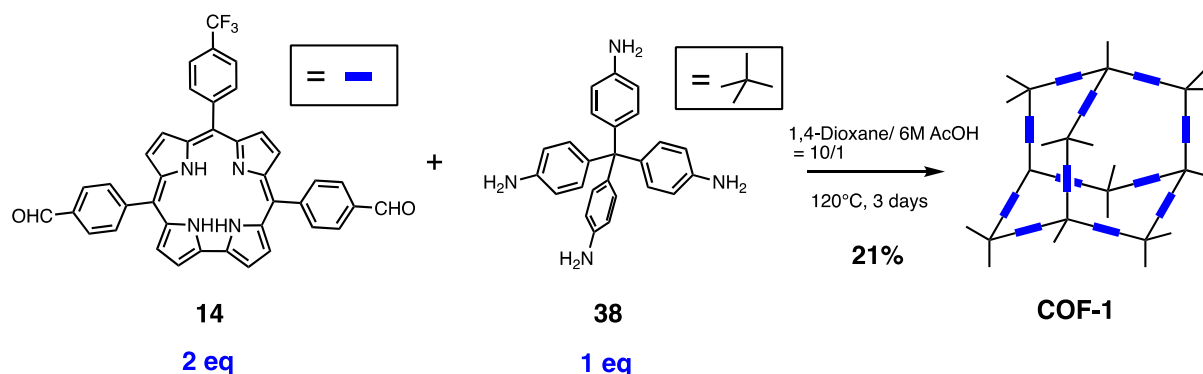
Compound **48** was synthesized according to the literature with a slight modification.<sup>30</sup> Truxene **47** (1.83 g, 2.0 mmol, 1 eq) and anhydrous ethyl ether (80 mL) were added to a flask under nitrogen. The mixture was cooled to -78°C and *n*-BuLi (7.30 mL, 18.3 mmol, 2.4 M in hexane) was dropwise under nitrogen. After addition, the reaction was stirred for 30 min at -78°C then allowed to warm up to room temperature and stirred for 30 min. The reaction was cooled to -78 °C again and DMF (1.42 g, 19.5 mmol) was slowly added to the flask. The reaction was stirred overnight and quenched with aqueous hydrochloric acid (2 M, 100 mL). The organic layer was washed with aqueous sodium chloride solution (20 mL × 3) and dried over sodium sulfate. The solvent was evaporated under vacuum and the solid was purified by column chromatography (Silica, DCM:heptane = 6:4), giving yellow powder.

**Yield:** 1.23 g (81%)

**<sup>1</sup>H NMR (500 MHz, CDCl<sub>3</sub>)** δ 10.16 (s, 3H), 8.57 (d, *J* = 8.0 Hz, 3H), 8.03 (d, *J* = 1.5 Hz, 3H), 7.79 (dd, *J* = 8.0 Hz, *J* = 1.5 Hz, 3H), 3.03-2.94 (m, 6H), 2.29-2.19 (m, 6H), 1.00-0.80 (m, 12H), 0.58-0.36 (m, 30H).

## 6. Synthesis of COFS based on cobalt corroles

### COF-1

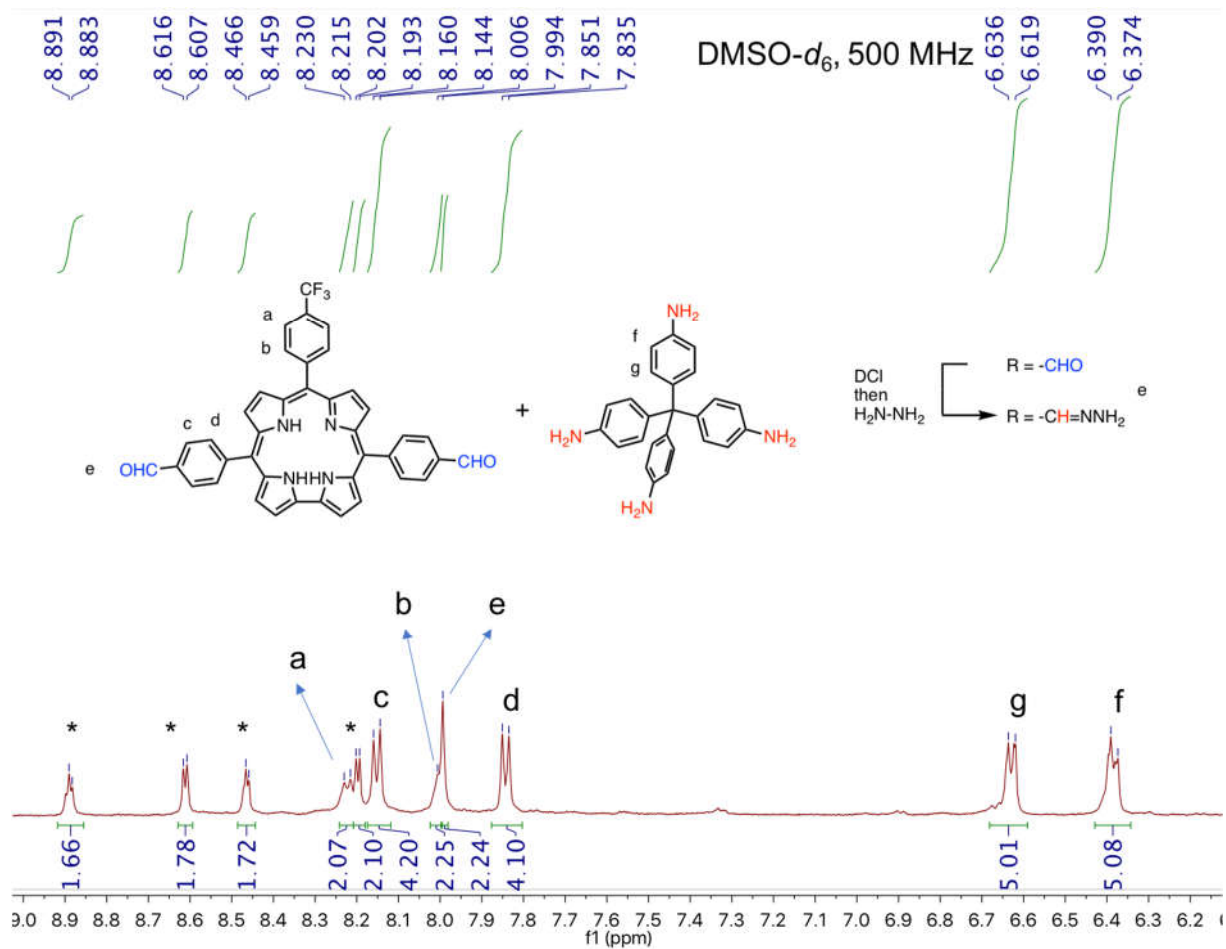


A Schlenk tube was charged with aldehyde corrole **14** (72.8 mg, 0.11 mmol, 2 eq) and platform **38** (21.3 mg, 0.055 mmol, 1 eq) in a mixed solution of 1,4-Dioxane (5.6 mL) and 6 M aqueous acetic acid (0.56 mL). The mixture was sonicated for 10 min to completely solubilize the starting materials. Then the Schlenk tube was sealed and the mixture was flash frozen at 77 K (liquid N<sub>2</sub> bath), followed by three freeze-pump-thaw cycles and sealed under vacuum. The reaction mixture was heated at 120 °C for 3 days to afford a dark precipitate which was isolated by centrifugation and washed by THF several times. The product was dried under vacuum for 24 hours to afford dark powder.

**Yield:** 20 mg (21%).

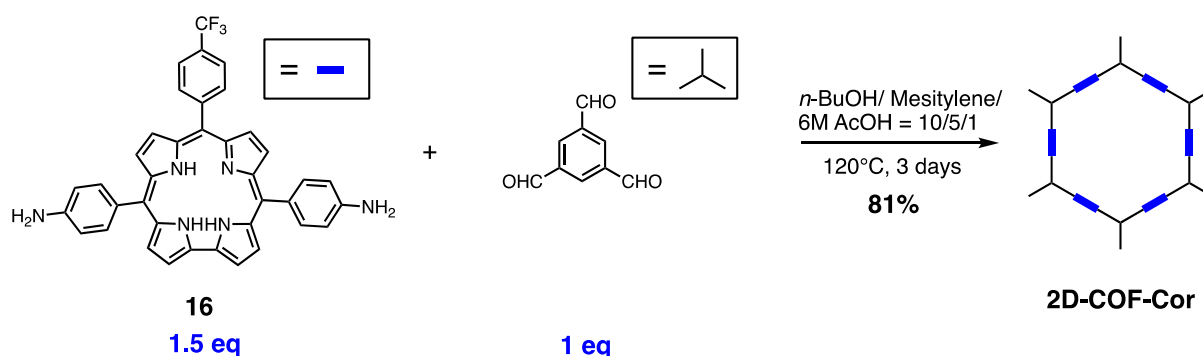
**<sup>1</sup>H NMR (500 MHz, DMSO-*d*<sub>6</sub>, 5 μL DCl (7M), then 50 μL Hydrazine)** δ 8.88 (d, *J* = 4.0 Hz, 2H), 8.61 (d, *J* = 4.5 Hz, 2H), 8.46 (d, *J* = 4.0 Hz, 2H), 8.22 (d, *J* = 8.0 Hz, 2H), 8.19 (d, *J* = 4.5 Hz, 2H), 8.15 (d, *J* = 8.0 Hz, 4H), 8.01 (d, *J* = 8.0 Hz, 2H), 8.0 (s, 2H), 7.84 (d, *J* = 8.0 Hz, 4H), 6.62 (d, *J* = 8.0 Hz, 4H), 6.38 (d, *J* = 8.0 Hz, 4H).

**FTIR (KBr, cm<sup>-1</sup>):** 1616 (C=N imine bond).



<sup>1</sup>H NMR spectrum of COF-1 decomposed by DCI in DMSO-*d*<sub>6</sub>.

## 2D-COF-Cor



A Schlenk tube was charged with amino corrole **16** (462 mg, 0.74 mmol, 1.5 equiv.) and 1,3,5-triformylbenzene (80.0 mg, 0.49 mmol, 1 equiv.) in a mixed solution of *n*-butanol (32.0 mL), mesitylene (16.0 mL) and 6 M aqueous acetic acid (3.2 mL). The mixture was sonicated for 10 min to completely solubilize the starting materials. Then the Schlenk tube was sealed and the mixture was flash frozen at 77 K (liquid N<sub>2</sub> bath), followed by three freeze-pump-thaw cycles and sealed under vacuum. The reaction mixture was heated at 120 °C for 3 days to afford a dark precipitate which was isolated by centrifugation and washed by THF several times. The product was dried under vacuum for 24 hours to afford dark powder.

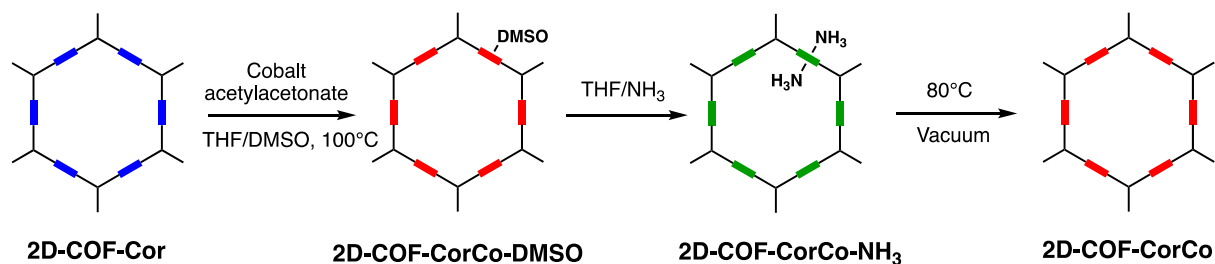
**Yield:** 420 mg (81%).

**<sup>1</sup>H NMR (500 MHz, DMSO-*d*<sub>6</sub>, 5 μL DCl (7M), then 50 μL Hydrazine)** δ 8.77 (d, *J* = 4.0 Hz, 2H), 8.58 (d, *J* = 4.5 Hz, 2H), 8.39 (d, *J* = 4.0 Hz, 2H), 8.23 (d, *J* = 8.0 Hz, 2H), 8.12 (d, *J* = 4.5 Hz, 2H), 8.01 (d, *J* = 8.0 Hz, 2H), 7.87 (d, *J* = 8.0 Hz, 4H), 7.68 (s, 3H), 7.42 (s, 3H), 6.99 (d, *J* = 8.0 Hz, 4H).

**Elementary analysis (%):** calculated for C<sub>47</sub>H<sub>29</sub>F<sub>3</sub>N<sub>6</sub>: C 76.83, H 3.98, N 11.44; found: C 73.67, H 3.78, N 11.32.

**FTIR (KBr, cm<sup>-1</sup>):** 3368 (NH<sub>2</sub>, corrole), 1699 (C=O, platform), 1614 (C=N imine bond).

## 2D-COF-CorCo



In a flask was added 2D COF (100 mg), followed by a solution of cobalt acetylacetonate (70.5 mg, 0.274 mmol, 2.00 eq for corrole) in the mixture of DMSO (8.00 mL) and THF (2.00 mL). The mixture was heated at 100 °C for 5 h under argon without stirring. After cooling down the solution, the suspension was centrifugated. After removing the supernatant, the solid was washed with THF several times to afford 2D-COF-CorCo-DMSO. Part of 2D-COF-CorCo-DMSO was further washed with a solution of THF saturated with NH<sub>3(g)</sub> to afford 2D-COF-CorCo-NH<sub>3</sub>. The solids were then dried under vacuum. The 2D-COF-CorCo-NH<sub>3</sub> was degassed under vacuum at 80°C to afford 2D-COF-Cor-Co which is used for CO sorption test.

## 2D-COF-CorCo-DMSO

**Yield:** 90 mg (79%).

**Elementary analysis (%):** calculated for C<sub>47</sub>H<sub>26.67</sub>F<sub>3</sub>N<sub>6</sub>Co<sub>0.776</sub> (DMSO)<sub>0.7·3</sub> THF: C 69.15, H 5.27, N 8.01, S 2.14; found: C 63.77, H 3.65, N 9.06, S 2.15.

**FTIR (cm<sup>-1</sup>):** 3368 (NH<sub>2</sub>, corrole), 1614 (C=N imine bond), 1014 (S=O, DMSO ligand).

## 2D-COF-CorCo-NH<sub>3</sub>

**Yield:** 93 mg (95%).

**Elementary analysis (%):** calculated for C<sub>47</sub>H<sub>26.67</sub>F<sub>3</sub>N<sub>6</sub>Co<sub>0.776</sub> (NH<sub>3</sub>)<sub>1.3·4.5</sub>THF: C 69.41, H 5.97, N 9.09; found: C 68.63, H 3.51, N 9.07.

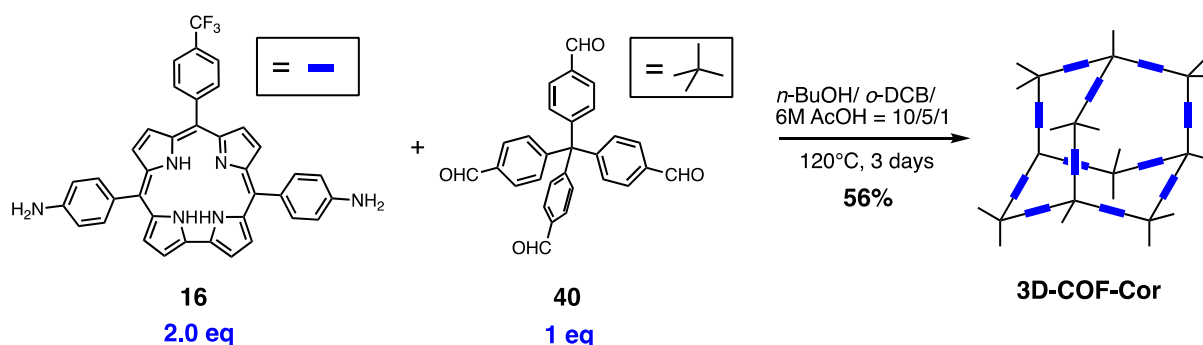
**FTIR (cm<sup>-1</sup>):** 3352 (NH<sub>2</sub>, corrole and NH<sub>3</sub> ligand), 1614 (C=N imine bond).

## 2D-COF-CorCo

**Elementary analysis (%):** calculated for C<sub>47</sub>H<sub>26.67</sub>F<sub>3</sub>N<sub>6</sub>Co<sub>0.776</sub> : C 72.54, H 3.45, N 10.80; found: C 69.30, H 3.28, N 9.68.

**ICP:** Calc %Co : 7.45, found : 5.88 (77.6% metalation).

### 3D-COF-Cor



A Schlenk tube was charged with amino corrole **16** (404 mg, 0.65 mmol, 2 equiv.) and tetrakis(4-formylphenyl)methane **40** (140 mg, 0.32 mmol, 1 equiv.) in a mixed solution of *n*-butanol (28.0 mL), *o*-DCB (14 mL) and 6 M aqueous acetic acid (2.8 mL). The mixture was sonicated for 10 min to make the starting materials dissolve completely. Then the tube was sealed, frozen at 77 K (liquid N<sub>2</sub> bath) and set under vacuum. The reaction mixture was heated at 120 °C for 3 days to afford a dark precipitate which was isolated by centrifugation and washed by THF several times. The product was dried under vacuum for 24 hours to afford dark powder.

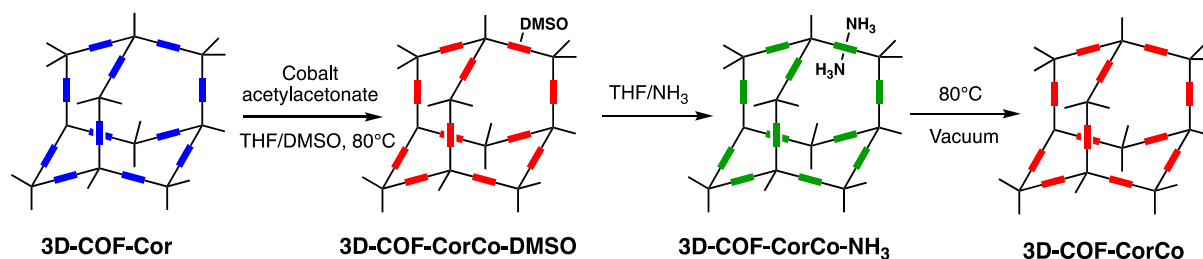
**Yield:** 300 mg (56%).

**<sup>1</sup>H NMR (500 MHz, DMSO-*d*<sub>6</sub>, 5 μL DCI (7M), then 50 μL Hydrazine)** δ 8.77 (d, *J* = 4.0 Hz, 2H), 8.59 (d, *J* = 4.5 Hz, 2H), 8.40 (d, *J* = 4.0 Hz, 2H), 8.26 (d, *J* = 8.0 Hz, 2H), 8.14 (d, *J* = 4.5 Hz, 2H), 8.02 (d, *J* = 7.5 Hz, 2H), 7.88 (d, *J* = 8.0 Hz, 4H), 7.65 (s, 3.6 H), 7.36 (d, *J* = 8.5 Hz, 7.2 H), 7.08 (d, *J* = 8.0 Hz, 7.2 H), 6.99 (d, *J* = 8.0 Hz, 4H).

**Elementary analysis (%)**: calculated for C<sub>58.7</sub>H<sub>37.3</sub>F<sub>3</sub>N<sub>6</sub> · 0.4THF: C 79.01, H 4.51, N 9.10; found: C 78.06, H 4.70, N 9.05.

**FTIR (cm<sup>-1</sup>)**: 3367 (NH<sub>2</sub>, corrole), 1610 (C=N imine bond).

### 3D-COF-CorCo



In a flask was added 3D COF (100 mg), followed by a solution of cobalt acetylacetonate (51.4 mg, 0.200 mmol, 2.00 eq for corrole) in the mixture of DMSO (8.00 mL) and THF (2.00 mL). The mixture was heated at 80 °C for 5 h under argon without stirring. After cooling down the solution, the suspension was centrifugated. After removing the supernatant, a few grains of solid were washed with THF several times to afford 3D-COF-CorCo-DMSO. Then 3D-COF-CorCo-DMSO was further washed with a solution of THF saturated with NH<sub>3(g)</sub> to afford 3D-COF-CorCo-NH<sub>3</sub>. The solids were then dried under vacuum. The 3D-COF-CorCo-NH<sub>3</sub> was degassed under vacuum at 80°C to afford 3D-COF-Cor-Co which is used for CO sorption test.

### 3D-COF-CorCo-DMSO

**Yield:** 90 mg (79%).

**Elementary analysis (%):** calculated for C<sub>58.7</sub>H<sub>35.1</sub>F<sub>3</sub>N<sub>6</sub>Co<sub>0.72</sub> (DMSO)<sub>0.69</sub>·2.3THF: C 72.76, H 5.08, N 7.35, S 1.93; found: C 72.7, H 4.67, N 7.42, S 1.95.

**FTIR (cm<sup>-1</sup>):** 3369 (NH<sub>2</sub>, corrole), 1610 (C=N imine bond), 1014 (S=O, DMSO ligand).

### 3D-COF-CorCo-NH<sub>3</sub>

**Yield:** 93 mg (95 %).

**Elementary analysis (%):** calculated for C<sub>58.7</sub>H<sub>35.1</sub>F<sub>3</sub>N<sub>6</sub>Co<sub>0.72</sub> (NH<sub>3</sub>)<sub>1.2</sub>·1.1THF: C 74.04, H 4.68, N 9.85; found: C 71.90, H 4.61, N 9.42.

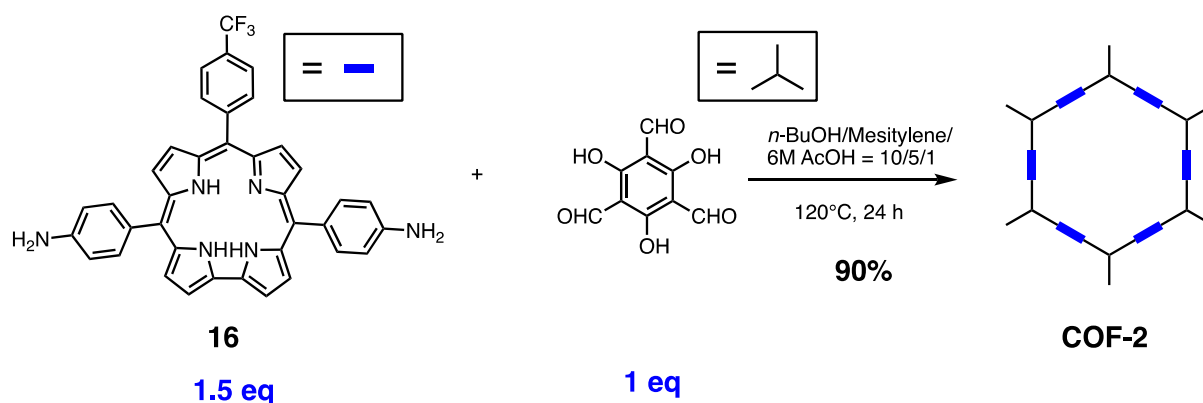
**FTIR (cm<sup>-1</sup>):** 3355 (NH<sub>2</sub>, corrole and NH<sub>3</sub> ligand), 1610 (C=N imine bond).

### 3D-COF-CorCo

**Elementary analysis (%):** calculated for C<sub>58.7</sub>H<sub>35.1</sub>F<sub>3</sub>N<sub>6</sub>Co<sub>0.72</sub>: C 76.31, H 3.83, N 9.10; found: C 75.06, H 4.07, N 8.79.

**ICP:** Calc %Co : 6.25, found : 4.59 (72.0% metalation).

## COF-2

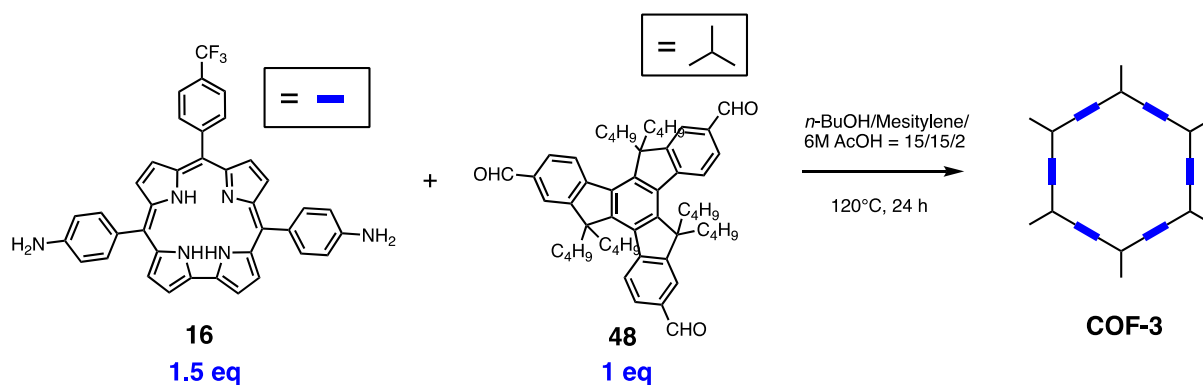


A Schlenk tube was charged with aldehyde corrole **16** (22.3 mg, 0.036 mmol, 1.5 eq) and platform (5 mg, 0.024 mmol, 1 eq) in a mixed solution of *n*-BuOH (2 mL), mesitylene (1 mL) and 6 M aqueous acetic acid (0.2 mL). The mixture was sonicated for 10 min to completely solubilize the starting materials. Then the Schlenk tube was sealed and the mixture was flash frozen at 77 K (liquid N<sub>2</sub> bath), followed by three freeze-pump-thaw cycles and sealed under vacuum. The reaction mixture was heated at 120 °C for 24 h to afford a dark precipitate which was isolated by centrifugation and washed by THF several times. The product was dried under vacuum for 24 hours to afford dark powder.

**Yield:** 24.6 mg (90%).

**FTIR (KBr, cm<sup>-1</sup>):** 1631 (C=O keto stretch), 1600 (C=C keto stretch), 1278 (C-N keto form).

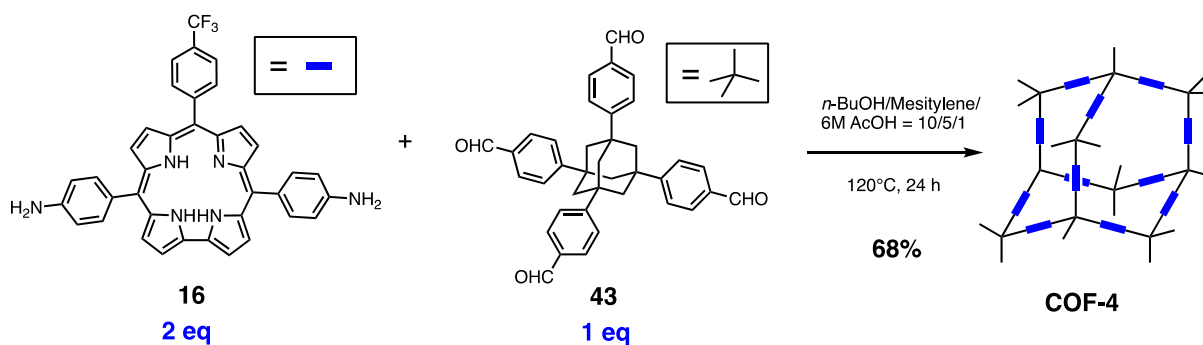
## COF-3



A Schlenk tube was charged with aldehyde corrole **16** (16.6 mg, 0.027 mmol, 1.5 eq) and platform (13.7 mg, 0.018 mmol, 1 eq) in a mixed solution of  $n$ -BuOH (1.5 mL), mesitylene (1.5 mL) and 6 M aqueous acetic acid (0.2 mL). The mixture was sonicated for 10 min to completely solubilize the starting materials. Then the Schlenk tube was sealed and the mixture was flash frozen at 77 K (liquid N<sub>2</sub> bath), followed by three freeze-pump-thaw cycles and sealed under vacuum. The reaction mixture was heated at 120 °C for 24 h to afford a dark precipitate which was isolated by centrifugation and washed by THF several times. The product was dried under vacuum for 24 hours to afford dark powder.

**FTIR (KBr, cm<sup>-1</sup>):** 1618 (C=N imine bond).

## COF-4



A Schlenk tube was charged with aldehyde corrole **16** (22.6 mg, 0.036 mmol, 2 eq) and platform (10 mg, 0.018 mmol, 1 eq) in a mixed solution of *n*-BuOH (2 mL), mesitylene (1 mL) and 6 M aqueous acetic acid (0.2 mL). The mixture was sonicated for 10 min to completely solubilize the starting materials. Then the Schlenk tube was sealed and the mixture was flash frozen at 77 K (liquid N<sub>2</sub> bath), followed by three freeze-pump-thaw cycles and sealed under vacuum. The reaction mixture was heated at 120 °C for 24 h to afford a dark precipitate which was isolated by centrifugation and washed by THF several times. The product was dried under vacuum for 24 hours to afford dark powder.

**Yield:** 22.2mg (68%).

**FTIR (KBr, cm<sup>-1</sup>):** 1616 (C=N imine bond).

## Reference

1. Walton, K. S.; Snurr, R. Q., Applicability of the BET Method for Determining Surface Areas of Microporous Metal–Organic Frameworks. *J. Am. Chem. Soc.* **2007**, *129* (27), 8552-8556.
2. Rouquerol, J.; Llewellyn, P.; Rouquerol, F., Is the bet equation applicable to microporous adsorbents? In *Studies in Surface Science and Catalysis*, Llewellyn, P. L.; Rodriguez-Reinoso, F.; Rouquerol, J.; Seaton, N., Eds. Elsevier: 2007; Vol. 160, pp 49-56.
3. Eckert, J.-F.; Nicoud, J.-F.; Nierengarten, J.-F.; Liu, S.-G.; Echegoyen, L.; Barigelletti, F.; Armaroli, N.; Ouali, L.; Krasnikov, V.; Hadziioannou, G., Fullerene-Oligophenylenevinylene Hybrids: Synthesis, Electronic Properties, and Incorporation in Photovoltaic Devices. *J. Am. Chem. Soc.* **2000**, *122* (31), 7467-7479.
4. Mao, Y.; Liu, Y.; Hu, Y.; Wang, L.; Zhang, S.; Wang, W., Pd-Catalyzed Debenzylation and Deallylation of Ethers and Esters with Sodium Hydride. *ACS Catal.* **2018**, *8* (4), 3016-3020.
5. Eisterhold, A. M.; Puangsamlee, T.; Otterbach, S.; Bräse, S.; Weis, P.; Wang, X.; Kutonova, K. V.; Miljanić, O. Š., Expanded Cyclotetrabenzoin. *Org. Lett.* **2021**, *23* (3), 781-785.
6. Laha, J. K.; Dhanalekshmi, S.; Taniguchi, M.; Ambroise, A.; Lindsey, J. S., A Scalable Synthesis of Meso-Substituted Dipyrromethanes. *Org. Process Res. Dev.* **2003**, *7* (6), 799-812.
7. Thamyongkit, P.; Yu, L.; Padmaja, K.; Jiao, J.; Bocian, D. F.; Lindsey, J. S., Porphyrin Dyads Bearing Carbon Tethers for Studies of High-Density Molecular Charge Storage on Silicon Surfaces. *J. Org. Chem.* **2006**, *71* (3), 1156-1171.
8. Yadav, O.; Varshney, A.; Kumar, A.; Ratnesh, R. K.; Mehata, M. S., A<sub>2</sub>B corroles: Fluorescence signaling systems for sensing fluoride ions. *Spectrochim. Acta A Mol. Biomol. Spectrosc.* **2018**, *202*, 207-213.
9. Shin, J.-Y.; Nguyen, A. Q., Exquisite chemistries of meso-pentafluorophenyl and meso-(2,6-dichlorophenyl) dipyrromethanes. *J. Porphyr. Phthalocyanines* **2021**, *25* (10n12), 885-896.
10. Trestsova, M. A.; Utepova, I. A.; Chupakhin, O. N.; Semenov, M. V.; Pevtsov, D. N.; Nikolenko, L. M.; Tovstun, S. A.; Gadomska, A. V.; Shchepochkin, A. V.; Kim, G. A.; Razumov, V. F.; Dorosheva, I. B.; Rempel, A. A., Oxidative C-H/C-H Coupling of Dipyrromethanes with Azines by TiO<sub>2</sub>-Based Photocatalytic System. Synthesis of New

- BODIPY Dyes and Their Photophysical and Electrochemical Properties. *Molecules* **2021**, *26* (18).
11. Muthukumar, K.; Ptaszek, M.; Noll, B.; Scheidt, W. R.; Lindsey, J. S., Boron-Complexation Strategy for Use with 1-Acyldipyrromethanes. *J. Org. Chem.* **2004**, *69* (16), 5354-5364.
  12. Gryko, D. T.; Koszarna, B., Refined methods for the synthesis of meso-substituted A<sub>3</sub>- and trans-A<sub>2</sub>B-corroles. *Org. Biomol. Chem.* **2003**, *1* (2), 350-357.
  13. Yadav, P.; Rath, P.; Sankar, M., Facile Generation of A<sub>2</sub>B Corrole Radical Using Fe(III) Salts and Its Spectroscopic Properties. *ACS Omega* **2017**, *2* (3), 959-965.
  14. Jyoti; Fridman, N.; Kumar, A.; Warkar, S. G., Synthesis, structural characterization and binding ability of A<sub>2</sub>B cobalt(III) corroles with pyridine. *Inorganica Chim. Acta* **2021**, *527*, 120580.
  15. Gros, C. P.; Desbois, N.; Michelin, C.; Demilly, E.; Tilkin-Mariamé, A.-F.; Mariamé, B.; Gallardo, F., Synthesis and Antiviral Activity Evaluation of Nitroporphyrins and Nitrocorroles as Potential Agents against Human Cytomegalovirus Infection. *ACS Infect. Dis.* **2015**, *1* (8), 350-356.
  16. Zhao, Y.; Qi, S.; Niu, Z.; Peng, Y.; Shan, C.; Verma, G.; Wojtas, L.; Zhang, Z.; Zhang, B.; Feng, Y.; Chen, Y.-S.; Ma, S., Robust Corrole-Based Metal–Organic Frameworks with Rare 9-Connected Zr/Hf-Oxo Clusters. *J. Am. Chem. Soc.* **2019**, *141* (36), 14443-14450.
  17. Manuela S.; Donato M.; Mariano V. and Roberto P., Kinetic and spectroscopic studies on the self-aggregation of a meso-substituted amphiphilic corrole derivative. *New J. Chem.*, **2007**, *31*, 1722-1725.
  18. Honig, H. C.; Krishnamurthy, C. B.; Borge-Durán, I.; Tasior, M.; Gryko, D. T.; Grinberg, I.; Elbaz, L., Structural and Physical Parameters Controlling the Oxygen Reduction Reaction Selectivity with Carboxylic Acid-Substituted Cobalt Corroles Incorporated in a Porous Carbon Support. *J. Phys. Chem. C* **2019**, *123* (43), 26351-26357.
  19. Rohand, T.; Dolusic, E.; Ngo, T. H.; Maes, W.; Dehaen, W., Efficient synthesis of aryldipyrromethanes in water and their application in the synthesis of corroles and dipyrromethenes. *ARKIVOC* **2007**, *2007* (10), 307-324.
  20. Keum, Y.; Park, S.; Chen, Y.-P.; Park, J., Titanium-Carboxylate Metal-Organic Framework Based on an Unprecedented Ti-Oxo Chain Cluster. *Angew. Chem. Int. Ed.* **2018**, *57* (45), 14852-14856.

21. Cichocka, M. O.; Liang, Z.; Feng, D.; Back, S.; Siahrostami, S.; Wang, X.; Samperisi, L.; Sun, Y.; Xu, H.; Hedin, N.; Zheng, H.; Zou, X.; Zhou, H.-C.; Huang, Z., A Porphyrinic Zirconium Metal–Organic Framework for Oxygen Reduction Reaction: Tailoring the Spacing between Active-Sites through Chain-Based Inorganic Building Units. *J. Am. Chem. Soc.* **2020**, *142* (36), 15386-15395.
22. Feng, L.; Wang, Y.; Yuan, S.; Wang, K.-Y.; Li, J.-L.; Day, G. S.; Qiu, D.; Cheng, L.; Chen, W.-M.; Madrahimov, S. T.; Zhou, H.-C., Porphyrinic Metal–Organic Frameworks Installed with Bronsted Acid Sites for Efficient Tandem Semisynthesis of Artemisinin. *ACS Catal.* **2019**, *9* (6), 5111-5118.
23. Lu, W.; Yuan, D.; Zhao, D.; Schilling, C. I.; Plietzsch, O.; Muller, T.; Bräse, S.; Guenther, J.; Blümel, J.; Krishna, R.; Li, Z.; Zhou, H.-C., Porous Polymer Networks: Synthesis, Porosity, and Applications in Gas Storage/Separation. *Chem. Mater.* **2010**, *22* (21), 5964-5972.
24. Ganesan, P.; Yang, X.; Loos, J.; Savenije, T. J.; Abellon, R. D.; Zuilhof, H.; Sudhölter, E. J. R., Tetrahedral n-Type Materials: Efficient Quenching of the Excitation of p-Type Polymers in Amorphous Films. *J. Am. Chem. Soc.* **2005**, *127* (42), 14530-14531.
25. Lu, Q.; Ma, Y.; Li, H.; Guan, X.; Yusran, Y.; Xue, M.; Fang, Q.; Yan, Y.; Qiu, S.; Valtchev, V., Postsynthetic Functionalization of Three-Dimensional Covalent Organic Frameworks for Selective Extraction of Lanthanide Ions. *Angew. Chem. Int. Ed.* **2018**, *57* (21), 6042-6048.
26. Zhu, D. Y.; Landis, R. F.; Li, C.-H.; Gupta, A.; Wang, L.-S.; Geng, Y.; Gopalakrishnan, S.; Guo, J. W.; Rotello, V. M., Dynamically crosslinked polymer nanocomposites to treat multidrug-resistant bacterial biofilms. *Nanoscale* **2018**, *10* (39), 18651-18656.
27. Janeta, M.; Bury, W.; Szafert, S., Porous Silsesquioxane–Imine Frameworks as Highly Efficient Adsorbents for Cooperative Iodine Capture. *ACS Appl. Mater. Interfaces* **2018**, *10* (23), 19964-19973.
28. Dehmlow, E. V.; Kelle, T., Synthesis of New Truxene Derivatives: Possible Precursors of Fullerene Partial Structures? *Synth. Commun.* **1997**, *27* (11), 2021-2031.
29. Zhou, H.; Zhao, X.; Huang, T.; Lu, R.; Zhang, H.; Qi, X.; Xue, P.; Liu, X.; Zhang, X., Synthesis of star-shaped monodisperse oligo(9,9-di-n-octylfluorene-2,7-vinylene)s functionalized truxenes with two-photon absorption properties. *Org. Biomol. Chem.* **2011**, *9* (5), 1600-1607.

30. Wang, X.; Wang, Y.; Yang, H.; Fang, H.; Chen, R.; Sun, Y.; Zheng, N.; Tan, K.; Lu, X.; Tian, Z.; Cao, X., Assembled molecular face-rotating polyhedra to transfer chirality from two to three dimensions. *Nat. Comm.* **2016**, 7 (1), 12469.

# Communications

## Publications

1. **Jian Yang**, Laurie André, Nicolas Desbois, Claude P. Gros and Stéphane Brandès, 2D/3D Covalent Organic Frameworks based on cobalt corroles for CO binding, submitted to *Chemistry – A European Journal*.
2. Meddy Vanotti, Sacha Poisson, Valérie Soumann, Valentin Quesneau, Stéphane Brandès, Nicolas Desbois, **Jian Yang**, Laurie André, Claude P. Gros, Virginie Blondeau-Patissier, Influence of interfering gases on a carbon monoxide differential sensor based on SAW devices functionalized with cobalt and copper corroles. *Sens. Actuators B: Chem.* **2021**, 332, 129507.

## Communication orals

1. **Jian Yang**, Laurie André, Nicolas Desbois, Stéphane Brandès, Claude P. Gros, Meddy Vanotti, Sacha Poisson, and Virginie Blondeau-Patissier, Synthesis of Covalent Organic Frameworks based on Cobalt Corrole for Carbon Monoxide Detection. *XXI<sup>ème</sup> Journée de l'Ecole Doctorale Carnot-Pasteur*, **June 24 2022**, Besançon.
2. **Jian Yang**, Laurie André, Nicolas Desbois, Stéphane Brandès, Claude P. Gros, Synthesis of Porous Materials based on Metallated Corroles for Carbon Monoxide Detection. *GDR-Mapyro Virtual Meeting*, **May 27 2021**.
3. Claude Gros, Stéphane Brandès, **Jian Yang**, Camille Monot, Dimitri Sabat, Sandrine Pacquelet, Nicolas Desbois, Laurie André, François Estour, and Rachid Baati, Corroles As Precursors of Porous Organic Polymers (POPs) and Molecularly Imprinted Polymers (MIPs) - Application to the Detection of CO and the Decontamination of Chemical Nerve Agents. *241<sup>st</sup> ECST Meeting*, **May 29 - June 3 2022**, Vancouver, Canada.
4. Stéphane Brandès, Valentin Quesneau, **Jian Yang**, Nicolas Desbois, Meddy Vanotti, Virginie Blondeau-Patissier and Claude P. Gros, Porous Organic Polymers (POPs) based on cobalt corroles for the detection of carbon monoxide. *11<sup>th</sup> International Conference on Porphyrins and Phthalocyanines, ICPP-11 - Virtual meeting*, **June 26 - July 3 2021**.

Communication posters

1. **Jian Yang**, Claude P. Gros, Léo Bucher, Nicolas Desbois, Yoann Rousselin, Frédéric Bolze, Hai-Jun Xu, Two Photon Absorption Properties and Structures of BODIPY and Its Dyad, Triad and Tetrad. *XX<sup>èmes</sup> Journée de l'Ecole Doctorale Carnot-Pasteur*, **June 11-12 2019**, Dijon.
2. Claude P. Gros, **Jian Yang**, Léo Bucher, Nicolas Desbois, Yoann Rousselin, Frédéric Bolze, Hai-Jun Xu, BODIPYs from 1 to 4: the more, the better? *10<sup>th</sup> International Conference on Porphyrins and Phthalocyanines, ICPP-10*. **July 1-6 2018**, Munich, Germany.
3. Stéphane Brandès, Laurie André, **Jian Yang**, Nicolas Desbois, Meddy Vanotti, Virginie Blondeau-Patissier, and Claude P. Gros, Covalent Organic Frameworks for the detection of CO. *11<sup>th</sup> International Conference on Porphyrins and Phthalocyanines, ICPP-11 -Virtual meeting*, **June 26 - July 3 2021**.
4. **Jian Yang**, Laurie André, Nicolas Desbois, Stéphane Brandès, and Claude P. Gros, 2D/3D Covalent Organic Frameworks Based on Cobalt Corroles for CO Binding. *12<sup>th</sup> International Conference on Porphyrins and Phthalocyanines, ICPP-12*, **July 10-15 2022**. Madrid, Spain.
5. **Jian Yang**, Laurie André, Nicolas Desbois, Stéphane Brandès, Claude P. Gros, Meddy Vanotti, Sacha Poisson, Virginie Blondeau-Patissier, *11<sup>th</sup> Barrande-Vltava French-Czech Chemistry Meeting*, **August 28-30 2022**, Dijon, France.
6. **Jian Yang**, Laurie André, Nicolas Desbois, Stéphane Brandès, Meddy Vanotti, Sacha Poisson, Virginie Blondeau-Patissier and Claude P. Gros, Synthesis of Porous Materials based on Metallated Corroles for Carbon Monoxide Detection. *8<sup>th</sup> International Conference on Metal-Organic Frameworks and Open Framework Compounds*, **September 4-7 2022**, Dresden, Germany.
7. Meddy Vanotti, Sacha Poisson, Valérie Soumann, Stéphane Brandès, Nicolas Desbois, **Jian Yang**, Laurie André, Claude P. Gros, Virginie Blondeau-Patissier, Selective measurement of CO and CO<sub>2</sub> with SAW sensors functionalized with metallo-corroles and Metal-Organic Frameworks. *Euroensors*, **September 11-14 2022**, Lecce, Italy.



**Titre :** Synthèse de matériaux poreux à base de corroles de cobalt pour la détection du monoxyde de carbone

**Mots clés :** matériaux poreux, corroles de cobalt, monoxyde de carbone

**Résumé :** Le monoxyde de carbone (CO), connu sous le nom de "tueur silencieux", est un gaz dangereux, incolore et hautement inflammable dont la limite d'exposition admissible recommandée est de 50 ppm. Il coûte chaque année la vie à un grand nombre d'individus dans le monde entier. Des matériaux poreux prometteurs, tels que les structures organiques covalentes (COF), les réseaux de type métal-organique (MOF) et les polymères organiques poreux et amorphes (POP), ont attiré l'attention en raison de leurs structures adaptées à la sorption et à la capture des gaz. Des matériaux poreux à base de corroles ont été développés au cours de ce travail dans le but de répondre au besoin urgent de prévention à l'empoisonnement au CO avec des capteurs de CO hautement sensibles et sélectifs.

En effet, les complexes de corroles de cobalt sont connus pour leur sélectivité unique de sorption du CO. Plusieurs corroles et leurs analogues de complexes de cobalt ont été synthétisés au cours de ce travail de thèse puis utilisés pour construire de nouveaux matériaux poreux (COFs, MOFs et POPs). Des COF 2D et des COF 3D à base de corroles ont été obtenus et caractérisés. Nous avons constaté que le COF 3D ne présente aucune cristallinité alors que le COF 2D est hautement cristallin. Pour la sorption du CO, le COF 2D a montré une plus grande affinité et sélectivité pour le CO que le COF 3D. De plus, le COF 2D a montré une plus grande sélectivité pour le CO par rapport au CO<sub>2</sub>, O<sub>2</sub>, N<sub>2</sub> qui sont des gaz interférents pour les capteurs.

**Title:** Synthesis of porous materials based on cobalt corroles for carbon monoxide detection

**Keywords:** porous materials, cobalt corroles, carbon monoxide

**Abstract:** Carbon monoxide (CO), known as the "silent killer", is a dangerous, colorless, and highly flammable gas whose permissible exposure limit is recommended to be as low as 50 ppm. It costs the life of a large number of individuals all over the world each year. Promising porous materials, such as Covalent Organic Frameworks (COFs), Metal–Organic Frameworks (MOFs), and amorphous Porous Organic Polymers (POPs), have gained attention due to their distinctive attributes adapted for gas sorption and capture. Corrole-based porous materials have thus been developed in this work with the aim to answer the urgent need for CO poisoning prevention with highly sensitive and

selective CO sensors. Indeed, cobalt corrole complexes are known for their unique CO sorption selectivity. Several corroles and their cobalt complex analogues were synthesized during the PhD work, and further used to build new porous materials (COFs, MOFs et POPs). 2D-COF and 3D-COF based on corroles were obtained and characterized We found that 3D COF showed no crystallinity while 2D COF is highly crystalline. For CO sorption, 2D COF showed higher affinity and selectivity for CO than 3D COF. What's more, 2D COF showed higher selectivity for CO vs CO<sub>2</sub>, O<sub>2</sub>, N<sub>2</sub> which are interference gas for sensors.